ASSESSING THE RISK AND CONSEQUENCE OF ENGINEERED NANO-SCALE ZINC OXIDE IN PHYTOLOGICAL AND BACTERIAL SYSTEMS



Dissertation submitted for the degree of

DOCTOR OF PHILOSOPHY

Department of Engineering Science

UNIVERSITY OF OXFORD

CORDELIA PETRA NADINE RAMPLEY

Supervisors: Professor Ian P. Thompson and Professor Andrew Smith

St Hugh's College
Hilary Term 2015

Assessing the Risk and Consequence of engineered Nano-Scale Zinc Oxide in Phytological and Bacterial Systems

Cordelia Rampley, St Hugh's College, University of Oxford

A thesis submitted for the degree of Doctor of Philosophy, Hilary term 2015

ABSTRACT

With the increased usage and production of engineered nanoparticles (ENPs), entry into the environment and hence contact with plant root systems is inevitable. Nano zinc oxide (nZnO) is widely used in commercial products, such as sunscreens, paints and coatings due to its high antimicrobial properties and wide electrical band-gap. Disposal down drains and into greywater leads to particle entry into the environment via waste water systems. Here, ENPs could potentially interact with plant root systems, which may lead to uptake, translocation and accumulation within plant tissues, and in the case of edible crops have consequences on human health. This study aimed to identify mechanisms of toxicity by employing whole-cell biosensors in conjunction with model bacteria and plant species. Furthermore, zeta potential (ZP), particle size, reactive oxygen species (ROS) release and solubility of the particles were determined and linked to both plant and bacterial toxicity. In *Escherichia coli* bacteria, it was demonstrated that growth inhibition from nano-scale ZnO treatment was similar to that from the bulk-scale ZnO and ionic zinc treatments, with the concentrations leading to 50 % inhibition (IC_{50}) demonstrated to be 251, 282 and 298 mg/L for bulk, nano-scale and $ZnSO_4$, respectively. It was demonstrated that the mode of nZnO toxicity in *E. coli* was bacteriostatic rather than bacteriotoxic. In barley plants, biomass was negatively impacted by up to 50 %, and significantly more zinc was able to enter root tissues as a result of hydroponic nZnO treatment, with 47 mg/L zinc detected in root tissues after 7 days treatment with 500 mg/L nZnO. Comparison of particle characteristics revealed that ROS, solubility, ZP, size and concentration were involved in toxicity, with ZP (charge) identified as a key parameter in both plant and bacterial toxicity.

ACKNOWLEDGMENTS

To my supervisor, Professor Ian Thompson, thank you for being my mentor and giving me the confidence to pursue a project off the beaten tracks and into the unknown. You have offered me so many opportunities throughout and I am incredibly grateful. Dr. Duane Ager, we desperately needed your expertise, intelligence and ingenuity, and I honestly can't remember what the lab was like before you joined us!

I have been lucky to work among some wonderful people; Naomi W., Meg U., Lakshmi A., Licheng S., Assia K., Rachel M., Ana C., Andrew S., Yaldah A., Helen T., Andrea C., Patrick T., Shiv S., Gabi G., Lucy T., Giulia S., Cindy H., Malgorzata R-S., Fazriz F., and Dan B.; thank you all for your friendship, support and encouragement. I would especially like to thank Leo B. for everything he has done.

To Andrée and Graham; it's hard to articulate how thankful I am. Our family may be few in number but you make up for it with an unwavering amount of belief in me.

Finally, I would like to express my gratitude to my funding body SCAST who have kindly supported me through my D.Phil. I have thoroughly enjoyed the November meetings where we all met and exchanged our ideas and inspirations. I am incredibly grateful that you selected me as one of the lucky candidates, and I hope you enjoy reading the results.

TABLE OF CONTENTS

ASSESSING THE RISK AND CONSEQUENCE OF ENGINEERED NANO-SCALE ZINC OXIDE IN PHYTOLOGICAL AND BACTERIAL SYSTEMS 1
ABSTRACT 2
ACKNOWLEDGMENTS 3
TABLE OF CONTENTS 4
TABLE OF FIGURES 11
LIST OF TABLES 13
ABBREVIATIONS 14
1. INTRODUCTION 15
1.1. Nanotechnology: An Overview 15
1.1.1. Engineered Nanoparticles 15
1.1.2. Metal Oxide ENPs 17
1.1.3. Nano-Scale ZnO 17
1.1.4. Nano-Scale ZnO in Sunscreens 18
1.1.5. Solutions, Colloids and Suspensions 19
1.1.6. Aggregation and Agglomeration 21
1.1.7. Reactive Oxygen Species 22
1.1.8. Entry into the Environment 23
1.2. Plants: An Introduction 25
1.2.1. Plant Physiology 26
1.2.2. Plant Germination 28
1.2.3. *Hordeum vulgare* (Barley) 29
1.2.4. Growth and Development 30
1.2.5. Plant Zinc Requirement 30
1.2.6. Roots and Root Exudates 32
1.2.7. Plant Pathogen Response 33
1.2.8. Nanoparticles & Plants 34
1.3. Bacteria: An Introduction 38
1.3.1. Bacterial membrane structure 38
1.3.2. Bacteria and Nanoparticles 40
1.3.3. Bacteria and Plants 42

1.3.4. Bacterial zinc nutrition and requirement 42
1.3.5. Antibacterial effects of Zinc Oxide 42
1.4. Aim of Research 43
1.5. Significance of Research 44
2. MATERIALS CHARACTERISATION OF ENGINEERED NANO-SCALE AND BULK-SIZED ZINC OXIDE PARTICLES 46
2.1 Introduction 46
2.1.1 Particle Size Determination 46
2.1.2 Zeta Potential 49
2.1.3 Reactive Oxygen Species 50
2.1.4 Zinc Dissolution 51
2.1.5 Atomic Absorbance Spectrophotometry 52
2.1.6 UV-Visible Absorbance 53
2.2 Materials and Methods 54
2.2.1 Nanoparticles 54
2.2.2 CPS Size Distribution Analysis 54
2.2.3 Dynamic Light Scattering Size Distribution Analysis 55
2.2.4 Zeta Potential of Particles Over a pH Range 55
2.2.5 Scanning Electron Microscopy 55
2.2.6 Reactive Oxygen Species 56
2.2.7 Zinc Dissolution Assay 56
2.2.8 UV-Visible Absorbance 57
2.2.9 Statistical Analysis 58
2.3 Results and Discussion 59
2.3.1 Zeta Potential of nZnO over a pH range 59
2.3.2 DLS Size Measurements 61
2.3.3 CPS Disc Centrifuge™ 62
2.3.4 Scanning Electron Microscopy 64
2.3.5 Reactive Oxygen Species 66
2.3.6 Zinc Dissolution Assay 67
2.3.7 UV Visible Absorbance 69
2.4. Discussion 70
2.4.1. Zeta Potential Results Demonstrated Different Stabilities of Bulk and 50 nm nZnO Particles in Suspension 71

2.4.2. Particle Size for Both Particles was Defined using Complementary Methods 71
2.4.3. nZnO Dissolved Significantly Faster than Bulk ZnO in DI Water 72
2.4.4. Bulk ZnO Dissolved at a Greater Rate than nZnO in Hoagland Solution.....73
2.4.5. Mathematical Calculation of Particle Number Relative to Bacterial Cell Number 73
3. EXAMINING THE TOXICITY OF NANO-SCALE ZINC OXIDE IN COMPARISON TO THE BULK SIZED AND IONIC FORMS TO *ESCHERICHIA COLI* 75
3.1. Introduction.....75
3.1.1. *E. coli* as a Model Organism 75
3.1.2. Biosensors.....77
3.1.3. Al_2O_3 Dopant.....79
3.1.4. Flow Cytometry.....80
3.1.5. Statistical Analysis 80
3.1.6. Chapter Aims.....81
3.2. Materials and Methods.....81
3.2.1. Acute Toxicity ATP-Linked Biosensor *E. coli* 81
3.2.2. Genotoxic Assay with *A. baylyi* 83
3.2.3. *E. coli* Growth inhibition.....83
3.2.4. Live-Dead Flow Cytometry Assay.....84
3.3. Results and Discussion.....85
3.3.1. *Escherichia coli* Growth Inhibition.....85
3.3.2. Acute Toxicity to *E. coli* HB101 87
3.3.3. Genotoxicity to *A. baylyi* 91
3.3.4. Flow Cytometry.....93
3.4. Discussion 95
3.4.1. The Nano-Form of ZnO Did Not Cause Greater Inhibition or Cell Death than the Bulk Form.....96
3.4.2. Evidence for a Large Role of Zn^{2+} Liberation in Acute Toxicity 97
3.4.3. ROS as a Proposed Mechanism for Genotoxicity 97
3.4.4. Importance of Understanding the Mode of Action of Antimicrobial Agents ..98
4. EXAMINING THE TOXICITY OF NANO-SCALE ZINC OXIDE IN COMPARISON TO THE BULK SIZED AND IONIC FORMS IN SEVERAL IMPORTANT FOOD PLANTS 100
4.1. Introduction.....100
4.1.1. Early Developmental Phytotoxicity.....101

4.1.2. Need for a More Reliable Medium than Damp Filter Paper 102
4.1.3. Al_2O_3 as a Dopant.....103
4.1.4. Plant Rhizosphere.....103
4.1.5. Chapter Aims.....103
4.2. Materials and Methods.....104
4.2.1. Particles 104
4.2.2. Seeds.....105
4.2.3. Seed Surface Sterilisation.....105
4.2.4. Early Developmental Phytotoxicity Assay.....105
4.2.5. Visualisation Agars 106
4.2.6. Light Microscopy 108
4.2.7. Solubilisation of ZnO Particles with EDTA.....108
4.2.8. Statistical Analysis 109
4.3. Results and discussion 110
4.3.1. Early Developmental Phytotoxicity Assays 110
4.3.2. Microscopy of Roots 117
4.3.3. Agar Visualisation.....119
4.3.4. UV-Visible Absorbance with the Chelator EDTA.....124
4.4. Discussion 126
4.4.1. Significant Reduction in Root Elongation Detected in Four Species as a Result of Zinc-Containing Treatments 126
4.4.2. Trends in Toxicity Between Monocotyledons and Dicotyledons 128
4.4.3. Nanoparticle Agar Matrix Maintained Particle Dispersion Throughout Toxicity Assay 129
4.4.4. Agar Visualisation Methods Indicated that Root Exudate influenced Particle Dissolution.....130
4.4.5. Particulate Versus Ionic Effect of Treatments.....131
5. DETERMINING IMPACT OF PLANT TREATMENT WITH ENGINEERED NANO-SCALE ZINC OXIDE IN HYDROPONICS 133
5.1. Introduction.....133
5.1.1. Determining Barley-Zn Toxicity and Uptake.....134
5.1.2. Hydroponic Barley Growth 135
5.1.3. Zeta Potential of Particles in Different Media.....135
5.1.4. Investigation into the Long-Term Effects of Zinc-Containing Treatments in Hydroponically Grown Tomato Plants.....137

5.1.5. Chapter Aims 137
5.2. Materials and Methods 138
5.2.1. Zinc-Containing Treatments 138
5.2.2. Hydroponic Solution 138
5.2.3. Barley for Hydroponics 138
5.2.4. Collection of Barley Root Exudates 140
5.2.5. Dry Biomass Assessment of Barley 140
5.2.6. Zinc Quantification of Barley Tissues 141
5.2.7. Zeta Potential of Particles in Different Media 141
5.2.8. Barley Seed Surface Sterilization 142
5.2.9. Barley Seed Soak Assay 142
5.2.10. Hydroponic Growth of MicroTom Tomato Plants 143
5.2.11. Statistical Analysis 144
5.3. Results and Discussion 144
5.3.1. Barley Seed Soak Assay 145
5.3.2. Toxicity of nZnO, Bulk ZnO and Zn^{2+} to Barley in Hydroponics 147
5.3.3. Uptake of Zinc by Barley 150
5.3.4. Translocation of Zinc from Root to Shoot 152
5.3.5. Physiological Response to Treatment in MicroTom Tomato Plants 153
5.3.6. Ripening and Quantities of Tomatoes Produced 154
5.3.7. Dry Mass Assessment of Ripe Tomato Fruit 155
5.3.8. Zeta Potential of Particles in Different Media 156
5.4. Discussion 158
5.4.1. Plant Toxicity Response was Different for Nanoscale ZnO 159
5.4.2. Translocation of Zinc from Root to Shoot was Lower for Nanoparticulate than Bulk or Ionic Treatments 159
5.4.3. Plant Root Exudates Modified ZnO 160
5.4.4. Zeta Potential of Particles Changed as a Result of Root Exudate Influence 162
5.4.5. Tomato Plants Flowered Early as a Result of nZnO Treatment 163
6. MATERIAL PROPERTIES OF AN AGED FORM OF NANO-SCALE ZINC OXIDE AS COMPARED WITH A NON-AGED FORM 165
6.1. Introduction 165
6.1.1. Nanoparticle Ageing 165
6.1.2. Nanoparticles Used in Study 166

6.1.3. Zeta Potential 166
6.1.4. Zinc Solubility of Particles 167
6.1.5. Hydrodynamic Diameter 167
6.1.6. Fourier Transform Infrared Spectroscopy (FTIR) 168
6.1.7. UV Visible Spectroscopy 169
6.2. Materials and Methods 169
6.2.1. Nanoparticles 169
6.2.2. Material Characterisation 169
6.3. Results and Conclusions 172
6.3.1. Zeta Potential 172
6.3.2. Hydrodynamic Diameter of Particles 174
6.3.3. FTIR Spectroscopy 175
6.3.4. UV-Visible Absorbance 176
6.3.5. Reactive Oxygen Species Release 177
6.3.6. Zinc Dissolution Assay 179
6.4. Discussion and Conclusions 181
6.4.1. Particle Size Differs Between Old and New nZnO Particles 181
6.4.2. Zeta Potential of Old and New nZnO Particles Differs Only in Water 182
6.4.3. UV Visible Absorption Greater for Old than New nZnO Particles 183
6.4.4. FTIR Spectra Showed More Hydroxyl Groups on Old nZnO Surface than New nZnO. 184
6.4.5. Dissolution of Old and New nZnO Not Significantly Different in DI Water 184
6.4.6. Limitations of Research 185
6.4.7. Importance of Study 186
7. EXAMINING THE TOXICITY OF ENGINEERED NANO-SCALE ZINC OXIDE IN PLANT AND BACTERIAL SYSTEMS AFTER AGEING IN AMBIENT CONDITIONS 187
7.1. Introduction 187
7.1.1. Bacterial Toxicity 188
7.1.2. Plant toxicity 189
7.1.3. Barley Root Exudates 189
7.1.4. Chapter Aims 192
7.2. Materials and Methods 192
7.2.1. Bacterial Toxicity Assays 192

7.2.2. Barley Assays 195
7.2.3. Statistical Analyses 195
7.3. Results and Discussion 196
7.3.1. Bacterial Assays 196
7.3.2. Plant Assays 205
7.4. Discussion and Conclusions 209
7.4.1. Acute Toxicity to *E. coli* lux Depended on Dispersal Media 209
7.4.2. *E. coli* Growth Inhibition was Similar for New and Old nZnO 210
7.4.3. Growth Inhibition of *E. coli* by nZnO was Affected by Root Exudate Solution 212
7.4.4. Zinc Uptake in Barley was Greater as a Result of New nZnO than of Old nZnO Treatment 213
7.4.5. Conclusions 214
8. DISCUSSION AND CONCLUSIONS 216
8.1. Discussion 216
8.2. Bacterial Toxicity 217
8.2.1. Whole-Cell Biosensors in Combination with *E. coli* cells Suggested the Mechanisms of nZnO Toxicity 217
8.2.2. Plant Root Exudates May Reduce nZnO Toxicity 218
8.3. Plant Toxicity 220
8.3.1. A Novel Agar-Based Phytotoxicity Method Suggested Particle Contact was a Key Parameter in Root Inhibition; Not Solubility 220
8.3.2. Greater Quantities of Zinc were able to be Taken-Up by Barley Plants from nZnO than from Bulk or Ionic Treatments. 221
8.4. Overall Biological Toxicity 222
8.4.1. Key Parameters Identified Could be Used to Aid Engineered Nanoparticle Design to Modify Toxicity in Biological Systems 222
8.5. Future Work 224
8.6. Conclusion 225
REFERENCES 227
SUPPLEMENTARY INFORMATION 243

TABLE OF FIGURES

Figure 1. 1: Demonstration of the increase in surface area to volume ratio of a particle. 16

Figure 1. 2: Simplified diagram of the life cycle and potential release pathways of ENPs 24

Figure 1. 3: Diagram of plant cell components & structure 25

Figure 1. 4: Comparison of Plant Stem Structure 27

Figure 1. 5: Root network of hydroponically grown *Hordeum vulgare* 36

Figure 1. 6: Comparison of Bacterial Cell Envelope Types. 39

Figure 1. 7: Relative Sizes of Bacteria and Nanoparticles Used 40

Figure 2. 1: Diagram showing how the electrical double layer relates to zeta potential 49

Figure 2. 2: Zeta potential of 50nm and bulk-sized ZnO particles over a pH range 59

Figures 2. 3 A & B: Hydrodynamic particle size of nZnO and bulk ZnO 61

Figures 2. 4 A & B: Size distribution curves of nZnO and bulk ZnO 62

Figures 2. 5 A & B: SEM images of bulk ZnO and 50nm nZnO particles 65

Figure 2. 6: Relative fluorescence of 7-hydroxycoumarin after 72 h of exposure of coumarin to 50nm and bulk-sized ZnO particles as a result of ROS release 66

Figure 2. 7: Dissolution of Zn^{2+} from 50nm nZnO and bulk-sized ZnO particles 67

Figures 2. 8 A & B: UV visible absorbance at 630 nm and 405 nm of bulk and nZnO 69

Figure 3. 1: Optical density of E. coli bacteria in the presence of three treatments 86

Figure 3. 2: Relative luminescent output of *E. coli* HB101 over 24 hours 87

Figures 3. 3 A& B: Bioluminescent output depicting acute toxicity after exposure to nZnO, bulk ZnO and ZnSO4 at 4 concentrations 88

Figures 3. 4 A & B: Bioluminescence of genotoxicity biosensor *A. baylyi* after exposure to three treatments, nanoscale and bulk ZnO particles and $ZnSO_4$ over time 92

Figure 3. 5: Proportion of dead, moribund and live *E. coli* cells using flow cytometry 94

Figure 4. 1: Three graphs detailing the change in root length of four species of plant with increasing concentrations of bulk ZnO, 50 nm $ZnSO_4$ and nZnO 111

Figure 4. 2: Three graphs detailing the change in stem length of four species of plant with increasing concentrations of bulk ZnO, 50 nm $ZnSO_4$ and nZnO 113

Figure 4. 3: Photograph of cress seedlings germinated on nZnO containing agar 115

Figure 4. 4: Photographs of the 'clearing' of nano ZnO from around the roots of the monocotyledon, Rye 116

Figures 4. 5 A to C: Light micrographs of representative roots after 7 days growth 117

Figure 4. 6: Technical agar with 100 mg/L dispersed 50 nm nZnO particles 120

Figure 4. 7: Technical agar with bromocresol Purple indicator to visualise pH change from root exudates 121

Figure 4. 8: Technical agar with Patent Blue indicator to visualise pH change from root exudates 122

Figure 4. 9: Technical agar dispersed with 100 mg/L 50 nm nZnO with 0.1M EDTA 123

Figure 4. 10: Absorbance of bulk and 50 nm nZnO particles with 0.1M EDTA 125

Figure 5. 1: Potential transformations of nanomaterials (NMs) in the environment 136

Figures 5. 2 A & B: Root lengths and stem lengths of 7 day old *Hordeum vulgare* after the seeds were soaked in zinc-containing treatments for 90 minutes 145

Figure 5. 3: Dry shoot and root biomasses of *H. vulgare* per plant after treatment with 3 different concentrations of 50 nm nZnO, bulk ZnO and $ZnSO_4$ 148

Figure 5. 4: Zinc content of root tissues of *H. vulgare* after treatment with 3 different concentrations of 50 nm nZnO, bulk ZnO and $ZnSO_4$ 150

Figure 5. 5: Zinc content of root tissues of *H. vulgare* after treatment with 3 different concentrations of 50 nm nZnO, bulk ZnO and $ZnSO_4$ 151

Figure 5. 6: Number of red, orange and green tomatoes produced by MicroTom plants 154

Figure 5. 7: Dry mass of individual ripe tomatoes post-treatment 155

Figure 5. 8: Zeta potential (mV) of 100 mg/L dispersions of 50 nm and bulk-sized ZnO particles in 6 different biologically relevant media 156

Figure 5. 9: Photo of cuvettes containing 100 mg/ L of 50 nm nZnO 157

Figure 6. 1: Zeta potential of two differently aged 50 nm nZnO particles 'New' and 'Old' in 6 biologically relevant media 173

Figures 6. 2 A & B: Hydrodynamic Particle size of 'Old' and 'New' 50 nm nZnO as measured by dynamic light scattering (DLS) 174

Figure 6. 3: FTIR absorbance spectrum of Old 50 nm nZnO and New 50 nm nZnO particles, plotted against wavenumber (cm^{-1}) 175

Figures 6. 4 A & B: UV-visible absorbance at 630 nm (A) and 405 nm (B) of Old and New 50 nm nZnO particles 177

Figure 6. 5: Reactive Oxygen Species release from Old and New nZnO particles 178

Figures 6. 6 A & B: Dissolution of Zn^{2+} from 50 nm nZnO and bulk-sized ZnO particles 179

Figures 7. 1 A & B: Bioluminescence of *E. coli* HB101_pUCD607_*lux* after 30 minutes treatment in DI water (A) and 20% Hoagland Solution (B) 197

Figure 7. 2: Optical density of *E. coli* bacteria demonstrating 24 h growth in the presence of Old and New nZnO 199

Figures 7. 3 A & B: Growth curves of *E. coli* challenged with A) Old & B) New nZnO 200

Figure 7. 4: Optical density of *E. coli* at 630 nm after exposure to 100 mg/L of Old and New 50 nm nZnO in water, Hoagland solution and root exudates 202

Figure 7. 5: Bioluminescence of genotoxicity biosensor *A. baylyi* after Old and New nZnO treatment at 50 mg/L and 250 mg/L 205

Figure 7. 6: Total dry biomass of 27 day old barley treated with Old and New nZnO 206

Figure 7. 7: Zinc uptake into root tissues from barley treated with Old and New nZnO 207

Figure 7. 8: Zinc uptake into shoot tissues from barley treated with Old and New nZnO 209

Figure 8. 1: Illustration of the potential dispersion and solubility states of ZnO particles 223

LIST OF TABLES

Table 1. 1: Differences between Monocotyledon and Dicotyledon plant morphology 28

Table 1. 2: Organic compounds and enzymes present in plant root exudates 33

Table 2. 1: Lifetimes and diffusion distances of different reactive oxygen species 51

Table 2. 2: Summary of particle sizes determined using disc sedimentation and DLS 63

Table 2. 3: Summary of results from Zn dissolution assay of nZnO and bulk ZnO 68

Table 4. 1: Approximate IC_{50} values (mg/L) interpolated from root elongation graphs 110

Table 5. 1: Percentage (%) of total plant zinc found in aerial plant 153

Table 6. 1: Summary of Zn dissolution from New and Old nZnO particles in DI water and Hoagland solution over time 180

ABBREVIATIONS

AAS	Atomic Absorption Spectrophotometry
ATP	Adenosine triphosphate
DI water	De-ionized Water
DLS	Dynamic Light Scatter
DLVO	Derjaguin, Verwey, Landau & Overbeek Theory
EDDHA	Ethylenediamine-N,N'-bis(2-hydroxyphenylacetic acid)
EDTA	Ethylenediaminetetraacetic acid
ENP	Engineered Nanoparticle
IC_{50}	Concentration at which 50% growth is inhibited
ICP-MS	Inductively Coupled Mass Spectroscopy
IEP	Isoelectric Point
NCIMB	National Collection of Industrial, Food and Marine Bacteria
nZnO	Nano-scale ZnO
ROS	Reactive Oxygen Species
SEM	Scanning Electron Microscopy
TEM	Transmission Electron Microscopy
ZP	Zeta Potential

1. INTRODUCTION

1.1. Nanotechnology: An Overview

Nanotechnology as a blanket term encompasses one of the most exciting recent scientific technologies, with a diverse number of applications in current and vital areas. These uses include healthcare, energy production and storage, and water treatments; areas which are particularly important today as a result of our rapidly expanding population. This only heightens the importance of understanding the impact of these new technologies, as previously promising technologies have had to be stopped in their tracks as a result of delayed environmental impact studies. Public perception of novel methods is also of crucial importance, as seen before with genetic modification; once fear of new technologies is instilled it is very difficult to "move past" the issues, and the enormous potential may never be realised (Berube *et. al.*, 2011). Information on the environmental effects is highly valuable for technological progress, public understanding and acceptance. The industry of nanotechnology is estimated to reach a market value of $1 trillion by 2015 so it is important that the environmental research keeps up with growth and demand (Zhang and Karn, 2005).

1.1.1. Engineered Nanoparticles

Engineered nanoparticles (ENPs) are particles with at least one dimension of 100 nm or less, and that have been designed and manufactured for specific uses (Li *et. al.* 2003). Nanoparticles are not a modern phenomenon; colloidal metal nanoparticles were used in the Roman Empire to create colours in glass, such as gold to produce a vibrant red hue. It is only recently however that they are becoming increasingly studied and we are engineering them with specific desirable properties (Buzea *et. al.*, 2007). As the surface area to volume ratio of ENPs is so large, exposure of individual atoms on the surface become significant, altering the physico-chemical behaviour when compared to the same bulk material (Chen *et. al.*,

2008). Properties of metals can change once scaled down to the nano-range, such as with copper (Cu). On the macro scale Cu is a malleable, ductile metal; these properties occur due to the movement between Cu atom clusters of approximately 50 nm size within the metal. If Cu is reduced down to 50 nm or smaller particles, they are no longer malleable or ductile, and so become extremely hard particles. Novel properties can arise, such as quantum confinement; the phenomenon behind the increased difference in energy states and band gap, and hence the changed optical-electronic properties of the material. It also allows the use of smaller quantities than of bulk material in reactions, as the surface area is vastly greater on which reactions can occur (Gnanasangeetha *et. al.*, 2013). The smaller the particle, the larger the surface area to volume ratio (**Figure 1.1**), and hence the surface chemistry becomes more important in predicting particle behavior. The proportion of atoms at the particle surface relative to the interior of the particle is greater and hence becomes significant.

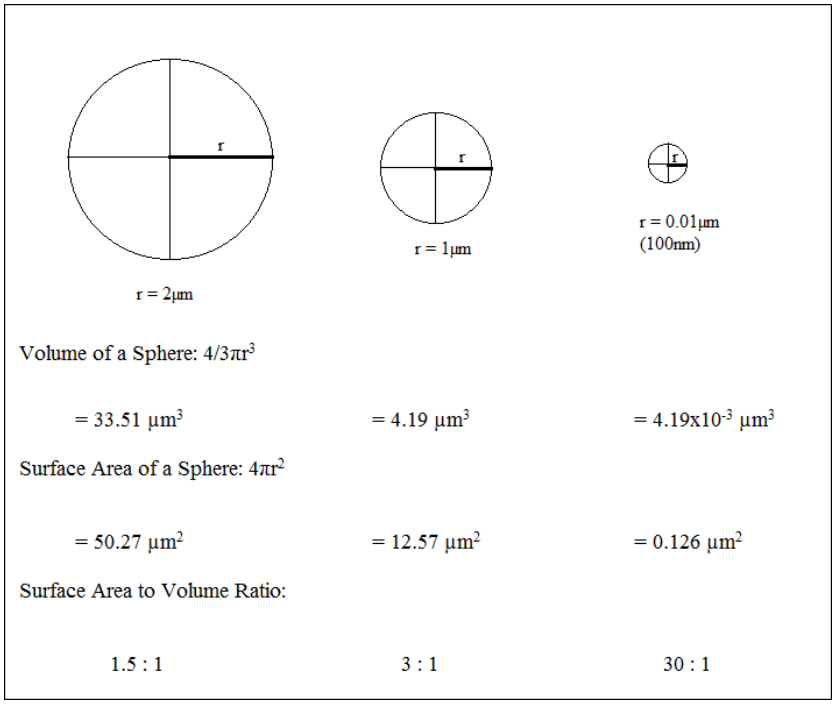


Figure 1.1: Demonstration of the increase in surface area to volume ratio of a particle as its radius (r) decreases.

1.1.2. Metal Oxide ENPs

Metal oxide ENPs represent an important category of nanomaterials well known for their semi-conducting and catalytic properties. They can exhibit metallic, semi-conductor and insulator properties, and have a wide range of uses (Fernandez-Garcia, 2009). Their nano-sized properties allow them altered chemistry compared to the bulk (standard) material, enabling them to be used in a vast number of applications such as paints, coatings, optoelectronics and sun creams (Buzea *et. al.*, 2007). Nano-sized metal oxides can be engineered to have desirable properties, and increasingly treatments such as doping are employed to reduce aggregation and facilitate dispersion in colloidal suspensions (Koskin & Slezov, 2004). Reducing these self-adhesive tendencies is important, both in industry, and when examining uptake and toxicity of particles to biological organisms (Skebo *et. al.*, 2007).

1.1.3. Nano-Scale ZnO

Zinc oxide is an inorganic white solid with a very low water solubility of 0.16 mg/100 mL which is amphoteric (can act as an acid or a base) (Smart *et. al.*, 2005). It has a high band gap, i.e. energy required for an electron to become excited, of around 3.3 eV at room temperature. This enables it to withstand large electric fields. It is an N-type semiconductor due to natural imperfections called vacancies and interstitials in the crystal lattice structure, and as such has important and unique electric conductive behaviour widely valued in industry (Pouran *et. al.*, 2014; Smart *et. al.*, 2005). Zinc oxide is frequently doped i.e. mixed during synthesis with metal oxides such as Al_2O_3 in order to improve consistency of conductivity over a range of temperatures. Metal oxides containing group III ions are mostly used as dopants in order to generate additional electrons and improve material properties, and in particular Al^{3+} is often chosen due to its low cost and comparatively diminutive ionic radius (Alkahlout *et. al.*, 2014). Nano Zinc Oxide (nZnO) is widely used in

commercial products due to its high antimicrobial characteristics and UV filtering properties (Dhas *et. al.,* 2014). It offers photostable broad-spectrum UV absorption, and hence it is produced in large quantities for use in sunscreens, paints and coatings, and as an antimicrobial treatment of waste water (Threes & Stanislav, 2011; Mitchnick *et. al.,* 1999). In 2011, it was estimated that more than 1.4 million tonnes of nano-scale ZnO was synthesized globally (Xu *et. al.,* 2014). As a result, significant quantities of the particles are highly likely to enter the environment, in particular via waste water systems (Bojeong *et. al.*, 2010). As such large quantities of nZnO are synthesized each year, nZnO was designated a priority nanoparticle by the Organisation for Economic Co-Operation and Development (OECD) in their 2008 report (OECD, 2008). It was more recently highlighted in their sponsorship programme in a report published in 2011, which calls for OECD member countries to fund testing of engineered nZnO with a focus on environmental and human health safety (OECD, 2011). The report specifically mentioned the need for scientific testing of environmental toxicology of nZnO particles, hence the focus of this study was to examine nZnO toxicity in plant and bacterial systems.

1.1.4. Nano-Scale ZnO in Sunscreens

Health professionals recommend the use of sunscreen to prevent over exposure to UV radiation, in particular UVA and UVB, and these products are widely used. Many sunscreens contain chemical, physical or both active ingredients in order to prevent ionising damage from UV rays, with the physical fraction involving a physical barrier to radiation (Cayrol *et. al.,* 1999). These are mainly comprised of metal oxides, typically TiO_2 and ZnO, which have excellent UV absorbing and scattering capabilities. Although they are effective at bulk size (> 100 nm), they produce a cosmetically undesirable white appearance when used in creams, and so nanosized particles are used instead, which for TiO_2 are in the range of 20 to 150 nm, and for ZnO are in the range of 40 to 100nm. By using smaller particles,

user experience is improved, making it more likely that individuals will use sun protection, while in addition the reduced size may offer enhanced protection to UVB radiation (Popov *et. al.*, 2005). The nZnO particles used in this study are 50 nm and therefore in the size range employed in sunscreens and hence will provide relevant information for nZnO environmental release from sunscreen usage.

In suncreams, zinc oxide does not pose an inhalation risk as it is suspended in the cream or liquid, however it can be ingested and is in contact with the dermis. Ingestion experiments using 20 to 120 nm nZnO on mice demonstrated toxicity at low doses (1 g/Kg body weight) but little difference between size effects on toxicity (Wang *et. al.*, 2008). Highest toxicity was observed at the lowest dose of 1 g/Kg of 20 nm particles, suggesting a concentration-specific toxic effect. Several studies involving dermal contact have been conducted, with results consistently indicating negligible penetration of nZnO through the stratum corneum when samples containing particulate sizes ranging from 10 to 117 nm were tested on human abdominal skin sections (Dussert *et. al.*, 1997; Gamer *et. al.*, 2006; Zvyagin *et. al.*, 2008; Kuo *et. al.*, 2009). Although the lack of penetration is good news for humans externally applying nZnO, use of products which contain such particles allows uncontrolled release of particles into the environment, such as via showers and swimming pools which then enter water treatment plants and sewage plants and receiving rivers, lakes and oceans, which allows direct release into the natural environment. It is here that exposure to plants and bacteria occurs, and hence why toxicity and impact studies on both plants and bacteria are vital.

1.1.5. Solutions, Colloids and Suspensions

Different phases of substances can exist, the three fundamental ones being solids, liquids and gases. When two are combined it can result in a solution, suspension or colloid,

depending on the physicochemical properties of each material (Marczac *et. al.*, 2010). A solution is a homogenous mixture, comprising a solute and a solvent, resulting in only one phase. The components of solutions are atoms, molecules or ions, and when the concentration is below the saturation point of the solution, it is stable (Wilkinson *et. al.*, 2007).

A suspension involves the mixture of larger solid particles into a liquid or gas, and is unstable so over time particles may not remain dispersed. A colloid is similar to a suspension, however the particles are below 1000 nm in size and so are small enough to be finely dispersed (dispersed phase) into the medium (continuous phase). Colloidal suspensions have the ability to remain stable over time, with stability depending on factors such as electrical charge, surface chemistry, particle size and dispersion medium. Out of colloidal equilibrium, particles may floc or aggregate and eventually settle due to gravity (Everett, 1994). A theorem devised by the scientists Derjaguin, Landau, Verwey and Overbeek (DLVO) describes colloidal stability as being dependent on its total potential energy function (V_T), which is a sum of the components V_A (attractive force due to Van der Waals), V_R (repulsive force as a result of electrical double layer) and V_S (potential energy from solvent) as described in the following equation:

$$V_T = V_A + V_R + V_S$$

There is an energy barrier as a result of repulsion between particles, so if this energy barrier is overcome as a result of sufficient energy in a collision, the Van der Waals force pulls the particles together and forms an irreversibly bonded aggregate. The greater the repulsion the lower the chance of flocculation and hence the more stable the colloidal system will be. If there is little or no repulsive force, the system will be unstable and flocculation/aggregation will occur (Shaw, 1992). The DLVO theory is not inclusive of the

effects of particle shape however, which may alter the efficiency of particle collisions (Grasso *et. al.*, 2002).

Nanoparticles are a branch of colloids i.e. well dispersed particles, but are characterised as being specifically designed and manufactured, as well as having a diameter of less than 100 nm. Nanoparticles can be considered not to be colloids when the surface interactions are not sufficient to maintain dispersion in a suspension. In conclusion not all colloids are composed of nanoparticles, nor are all nanoparticles colloids.

Nano-scale particle solubility was often assumed to be similar to that of the bulk-sized material, which for ZnO is extremely low (Reed *et. al.*, 2012). However, nano-scale ZnO particles are able to release Zn^{2+} ions in solution, a process resulting from crystalline imperfections in their structure (Yang & Xie, 2006). ENPs are structurally more disordered than bulk-sized material, i.e. have a higher entropy, and this results in increased levels of zinc ion dissolution (Hanley *et. al.*, 2009). Release of Zn^{2+} ions from different sized ZnO particles was investigated, with several studies finding greater release ratios of Zn^{2+} from ZnO nanoparticles than standard ZnO particles (Xiong *et. al.*, 2011 and Kasemets *et. al.*, 2009). In a study by Reed *et. al.*, 2012, it was demonstrated that 70 nm nZnO particles released 7.14 to 7.40 mg/L Zn^{2+} as measured after 810 hours in ultrapure water. This was slightly greater than the bulk particles which released around 5.70 mg/L at 20 °C. The method used was ultrafiltration through a 0.02 µm syringe filter, which was demonstrated to be as effective at distinguishing particulates from Zn^{2+} species as the commonly used centrifugal filtration method, and hence was used later in this project.

1.1.6. Aggregation and Agglomeration

Engineered Nanoparticles are prone to agglomeration and aggregation in liquid media, whereby particles clump or attach together due to electrostatic interaction and van der

Waals force. While agglomeration is less permanent than aggregation, both can cause flocculation and settling of particles out of colloidal suspension (Marczak *et. al.*, 2010). This obviously affects the behaviour of the nanomaterial, as with aggregation, the overall physical size is increased when particles are bound together, and there are fewer individual particles left in suspension, if any. This also results in significant portions of the particle surfaces being 'locked away' within an aggregate, reducing the effective surface area. Adsorption to soil particles and organics, agglomeration, and aggregation have been demonstrated to limit the environmental toxicity of nanoparticles (Navarro *et. al.*, 2008; Horst, 2009).

Agglomeration, where particles are loosely coherent, occurs as a result of electrostatic attraction, at a time where the zeta potential approaches zero. Zeta potential is the electrokinetic potential in a colloidal system measured in mV. It is the electrical potential between the dispersion medium and the interfacial double layer. Low zeta potential values below ± 10 mV signify instability, and particle flocculation is likely to occur. Values above ± 30 mV suggest greater stability and reduced tendency to agglomerate. Zeta potential values vary according to medium, and they enable predictions to be made about future potential stability of the suspension. Colloidal stability of nZnO increases with decreasing pH of dispersion medium.

1.1.7. Reactive Oxygen Species

Nano-scale ZnO is able to release reactive oxygen species (ROS) during the dissociation reaction, which is a proposed mechanism of toxicity (Rothen-Rutishauser *et. al.*, 2007). ROS are oxygen-containing, highly reactive molecules able to damage cell structures and generate oxidative stress. Atomic oxygen has two unpaired electrons in its outer electron shell, making it particularly susceptible to radical formation whereby reduction (addition of electrons) forms a number of reactive species such as superoxide anions, peroxide and

hydroxyl radicals (Li *et. al.,* 2012). All types of aerobic life have evolved mechanisms for coping with oxidative stress through ROS, an example of which is by producing the enzyme superoxide dismutase (SOD) which is able to catalyse the conversion of superoxide anions into hydrogen peroxide, which is then safely converted to water and oxygen by catalase enzyme. This prevents cellular damage caused by the free radicals, however the efficacy of such detoxification methods is determined by the duration and magnitude of exposure, so should ENPs generate ROS continuously or in large quantity cellular damage may be irreparable (Held, 2010).

In addition to ROS, ZnO particles release ionic Zn^{2+} which may also have an impact on toxicity. In studies involving mammalian cells, Zn^{2+} ions have been shown to have a propensity to bind to cell membranes due to their affinity for phospholipids (Marin *et. al.*, 2000). The phospholipid bilayer is a feature that both mammalian and plant cells share, suggesting a possible mechanism of phytotoxicity. Characterising the bulk and nZnO particles used in toxicity experiments is essential in understanding the mechanisms of toxicity, as it could be a result of many factors, including metal ion release, ROS generation, physical particle contact, size and surface charge, stability, or most likely a combination.

1.1.8. Entry into the Environment

Vast quantities of nanomaterials are produced each year, with little research into their environmental fate having been conducted as their production is not always regulated (Eisenberger *et. al.*, 2010). Currently, both the potential risk and the quantity involved in nanomaterial entry into the environment have not been well examined. Due to their size, they are highly mobile and hence can disperse widely, making it essential that we begin to understand their environmental impact (Buzea *et. al.* 2007).

It is important to ascertain the implications of nanoparticle entry into the environment as the behaviour and fate of such particles are not able to be predicted based on known chemistry of bulk-sized versions of the same compounds. The Royal Society and the Royal Academy of Engineering were commissioned in 2004 by the UK government to gather information on current nanotechnology studies and their potential negative consequences. The report entitled 'Nanoscience and Nanotechnologies: Opportunities and Uncertainties' concluded that nanoscience offers great benefits in current and future technologies, but that there is an immediate need for research into health and environmental effects of nanoparticles, in particular their exposure pathways and safety (Royal Society, 2004). More recently, the Royal Commission on Environmental Pollution (RCEP, 2008) has called for urgent investigation into how nanomaterials affect health and the environment in its 27th report, stating the importance of life cycle evaluation and eco-toxicity studies. Entry into the environment can happen at a number of different stages during the life cycle of nanomaterials (**Figure 1.2**).

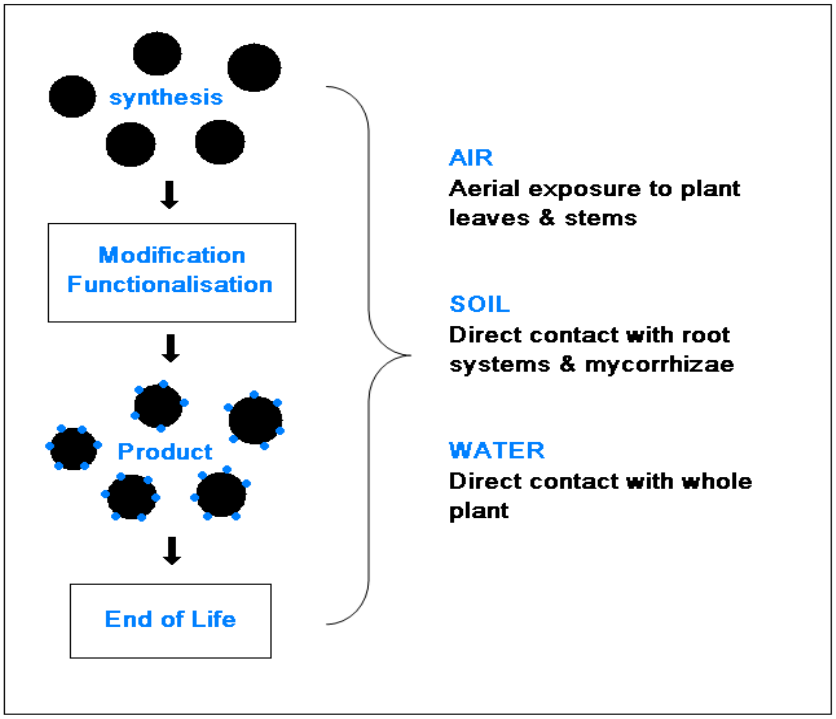


Figure 1.2: Simplified diagram of the life cycle and potential release pathways of ENPs with respect to plant exposure (Adapted from Helland *et. al.*, 2007).

From synthesis to end of life, entry into waste water systems can occur in large quantity. For example, much nZnO enters via drains into sewage systems as a result of widespread use in sunscreens and coatings (Osmond & McCall, 2010). Redox reactions, interaction with natural organic matter (NOM), and microbial action may all modify ENPs in a number of ways. Hence, when looking at the impact of ENP release it is essential to adopt a multidisciplinary approach, as it is this combination of chemical, biological and physical methods that will yield the best information on the true behaviour of released ENPs.

1.2. Plants: An Introduction

Plants are living organisms which are comprised of cells; the structural and functional units of all organisms able to carry out specific functions and reproduce. Plant cells have specific features which are different to animal cells, such as large vacuoles, cell walls and plastids such as chloroplasts (**Figure 1.3**).

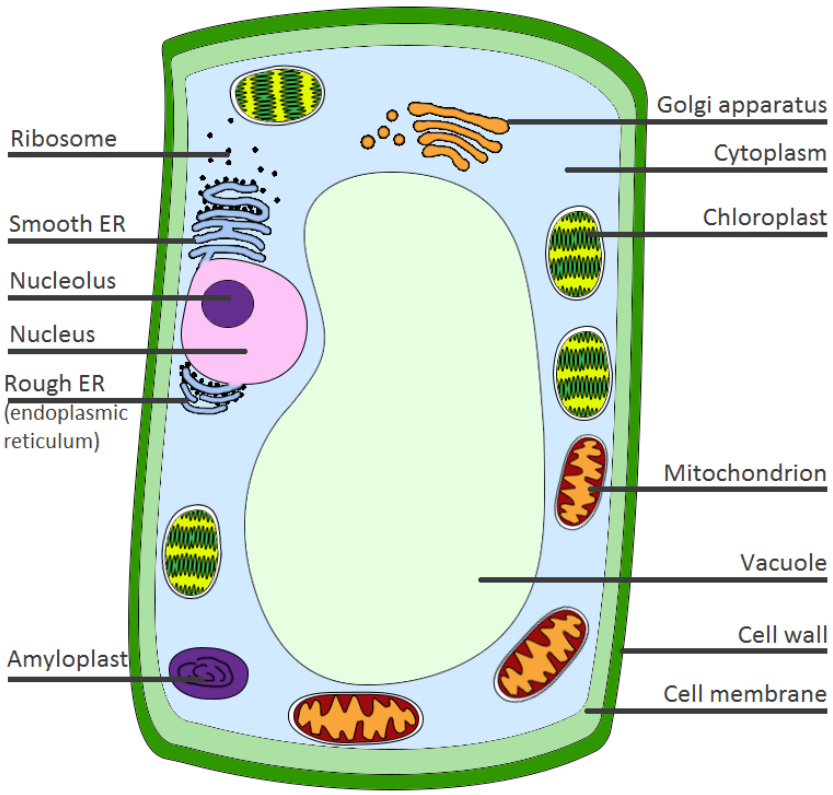


Figure 1.3: Diagram of Plant Cell Components & Structure

Plants are able to photosynthesise, whereby light energy is converted into chemical energy. Plants use atmospheric carbon dioxide (CO_2) and water (H_2O) in the presence of sunlight to produce glucose ($C_6H_{12}O_6$) and oxygen (O_2). This is made possible by plastid organelles called chloroplasts. These contain thylakoids, highly folded cell membrane studded with light-absorbing pigments such as chlorophyll and beta-carotene, surrounded by an enzyme-rich fluid called stroma. In each molecule of pigment, one photon is absorbed and one electron is released. They are then passed down an electron transport chain in a flow of electrons, reducing NADP to NADPH. By doing this, a proton gradient is established across the membrane, which is utilised by ATP synthase in the synthesis of ATP. In a light independent series of reactions, NADPH and ATP are then used to produce glucose, which is then able to be respired by the plant to release energy.

Plants are an essential part of life on earth, evolving from freshwater photosynthetic chlorophyte algae around 500 to 600 million years ago by molecular estimates (Raven, 2001). Cryptospore fossils form the oldest evidence of plants on land from around 470 million years ago, and by the mid-Devonian period approx 390 million years ago land plants would have been recognisable to us as very similar to plants today. As primary producers, they form the basis of all food webs and so are a vital part of life as we know it. Humans depend on land plants, both directly in the human diet as with cereals, vegetables, fruits, and indirectly as food for animals, wood, fibres, resins and medicines to provide just a few examples.

1.2.1. Plant Physiology

Higher plants have vascular systems, whereby photosynthetic products are transported via the phloem, and minerals and water are transported by capillary action through the xylem. Of the flowering plant group of land plants, the angiosperms, there are

two major monophyletic groups known as eudicotyledons and monocotyledons. The physiology of each group differs (**Figure 1.4**).

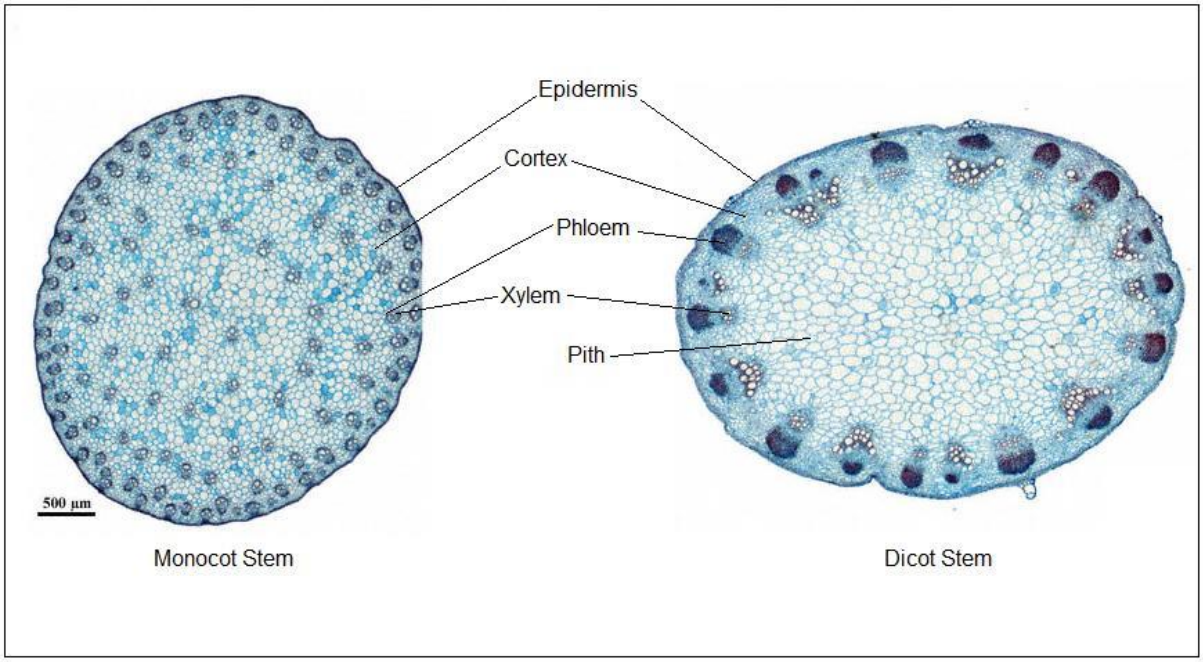


Figure 1.4: Comparison of stem structure between Monocotyledons and Dicotyledons (adapted from Campbell & Reece, 2005)

Vascular tissues allow transport of water, minerals and products of photosynthesis throughout the plant. The largest crop species by mass of production and consumption are monocotylodonous, i.e. grasses such as maize, barley, wheat and rice. Dicotyledon food plants include the families Solanaceae (tomato, aubergine etc.), Brassicaceae (cabbage family) and Fabaceae (beans, peas etc) as examples. Knowledge of the specific plant physiology is required in toxicity studies, as the arrangement of vascular bundles and type of root growth may be able to affect nanoparticle uptake (**Table 1.1**) (Zhu *et. al.*, 2008).

Table 1.1: Differences between Monocotyledon and Dicotyledon plant morphology

	Monocotyledons	**Dicotyledons**
Number of embryonic seed leaves (cotyledons)	One	Two
Vascular Bundle Arrangement	Scattered	Bundled in circles
Root Growth	Adventitious	Radial from the radicle
Major Leaf Vein Arrangement	Parallel	Reticulate

1.2.2. Plant Germination

Early developmental studies are those conducted at the earliest stages of plant life from seed to seedling. Germination occurs whereby a seed sprouts to produce a young plant. The dormant seed contains the embryo and a food reserve within a seed coat, which when activated by the correct external conditions, is able to germinate to produce a seedling. There are several external factors which determine germination, and in the majority of plants the presence of adequate water and oxygen at the correct temperature is sufficient to initiate germination. Water is required to hydrate the cells to enable cellular metabolism to resume from its suspended state. Oxygen is required for aerobic respiration, until the seedling has produced an adequate number of leaves to be able to photosynthesise. Plants require the correct temperature for cellular metabolism, which for most plants falls around room temperature (Mauseth, 2014).

1.2.3. *Hordeum vulgare* (Barley)

Barley is a cereal grain crop plant, a monocotyledon from the *Hordeum* genus. Barley is classed by its need for cold temperatures, with winter barley requiring vernalisation (being subjected to low temperatures to induce competence to flower or ripen) and spring barley not requiring this step. It is an important commercial food crop, acting as a staple grain for many animal feeds in many countries; however it is also culturally important for traditional malt production, particularly for use in malted beverages. Malting involves germination of the barley and then drying to halt the germination process. It results in enzymatic modification of grain starch into sugars (including maltose) able to be respired by yeast in order to make beer, malted drinks and whisky. It is a highly versatile crop with good tolerance to abiotic and biotic factors, however is has a lower yield than wheat, and so is often a secondary crop grown in rotation. In the UK alone it is the second most important crop with over 7 million metric tonnes of barley produced in 2013. It was also the 17th most produced crop in the world with 134 million tonnes produced annually (FAOSTAT data, 2015).

Barley has been chosen as the primary crop for investigation in this project due to its fast growth rate, homogeneity of growth, low variation and importance as a UK crop. This project uses *Hordeum vulgare* of the variety 'Westminster' to examine and compare the effects of various zinc treatments. It is a well-documented variety of barley, however there has been no published data on the effect of ZnO nanoparticles in this variety, or indeed in barley as a whole. Westminster is a feed variety spring barley, bred specifically for a high yield and to produce a long stiff straw. It also has broad-spectrum disease resistance, most notably to mildew, yellow & brown rusts, and rhynchosporium (HGCA Recommended Lists database, 2012). This combined with its high specific weight of 70.0 Kg/hl makes it a very popular choice for British farmers.

1.2.4. Growth and Development

Barley growth can be described by the following stages: germination, root establishment, leaf production, tillering, elongation, pollination and development and maturation of a kernel (Bauer *et. al.*, 1984). For germination, spring barley requires moisture and a minimum temperature of 1 to 2 ºC, and the time required to germinate provides useful information on the effect of different treatments at the early developmental phase. Factors affecting plant growth include available light, water, temperature and nutrients, so that when different treatments between plants are compared it is essential that identical photoperiods and nutrient conditions are maintained for the duration of growth. This is made possible with stock nutrient solutions; an example of which is the medium Hoagland solution; a fully comprehensive nutrient solution containing a known quantity of trace elements sufficient for plant growth. Greenhouses provide a temperature controlled environment and often a known or controlled photoperiod.

When conducting phytotoxicity assays, young plants early in their development are desirable as they can remain in reasonably good health for the duration of the assay. The whole plant can then be harvested and analysed by acid digestion and atomic absorption spectroscopy (AAS), providing information on the concentration of metal ions within the plant. This can be broken down into roots and shoots to provide an insight into location of metal ion accumulation and transport within the plant structure.

1.2.5. Plant Zinc Requirement

Zinc is required in plants for optimum growth, and is taken up in its divalent form (Fang *et. al.*, 2008). Zn^{2+} uptake requires a certain level of growth-medium moisture, and as a result, zinc deficiency is mainly observed in arid areas. Optimum zinc uptake occurs in acidic soils < pH 7, as acidic conditions improve solubility (Korayem, 1993). Physical

uptake of zinc occurs via both passive diffusion and specific active zinc transporters (Grotz *et. al.*, 1998).

Many plants are able to produce chelating agents such as phenolics, organic acids and phytosiderophores (Dakora *et. al.*, 2002). Chelators are metal ion binding molecules which have a high affinity for a metal ion such as Fe^{2+} or Zn^{2+}, and bind to form a metal-ligand complex. Barley releases hexadentate metal chelators (mugineic acid family organic acids), which are described as phytometallophores when they bind with metals. They are called phytosiderophores if bound exclusively to iron (Kochian 1993). The organic acids exuded from plant roots, like citric and succinic acids, are multipurpose and while acting as chelators can also act as a chemoattractant to microbes. The plant promotes microbial warfare as these exudates attract microbes antagonistic to plant-pathogenic microbial species, helping reduce the number of pathogenic microbes that would otherwise threaten the plant's health.

Zn^{2+} is able to migrate in the xylem as well as the phloem, and is also a component in natural plant antioxidants such as superoxide dismutase and catalase (Sunkar *et. al.*, 2006). These enzymes catalyse the dismutation of superoxide, O_2^-, into hydrogen peroxide, in order to protect cells from oxidative damage due to reactive oxygen species (ROS) (Smirnoff *et. al.*, 1993). ROS are formed in plant metabolism, UV radiation and as a result of nutrient deficiency, and as such the plant is constantly under oxidative stress and need of such antioxidants (Alscher *et. al.*, 2002). Zinc is also required in the production of the growth hormone auxin (Heisler *et. al.*, 2005). Zn regulates root development, aids in chlorophyll synthesis and facilitates cytochrome pigment synthesis (Raychaudhuri *et. al.*, 2008). Zinc may be a limiting factor in wild plant growth depending on the type of soil, pH and its natural organic matter (NOM) content. Higher pH values are correlated to lower levels of free Zn^{2+}, and higher NOM levels with greater levels of Zn cations. In general with metal ions, the higher the charge of the cation, the more strongly it is attracted to the negative

charge of soil particles, and hence divalent cations like Zn^{2+} are harder to leach from soil than monovalent cations such as K^{+}.

1.2.6. Roots and Root Exudates

Plants obtain minerals and water via their root systems, organised structures which typically lie below the ground in contact with soil. Roots have several key functions including anchorage, absorption of nutrients and water, synthesis and secretion of important compounds and, for certain species, storage of food such as in potatoes and cassava.

Plant roots exude a cocktail of chemicals in order to interact with their surroundings, for example by affecting bacterial chemotaxis, inducing fungal mutualism, and protecting themselves from pathogens. The area immediately around the roots is known as the rhizosphere, a complicated area able both to influence and be influenced by the plant (Walker *et. al.*, 2003). The rhizosphere contains microorganisms such as bacteria, fungi and protozoa. Plants allocate energy into producing both high and low molecular weight root secretions such as glucose, saponins and organic acids to influence the local microbes, able to act as either as attractants, neutral signalling molecules or antimicrobials (Lines-Kelly, 2005) (**Table 1.2**). Root exudate composition is dynamic in content and quantity, and hence is a difficult medium to characterise.The rhizosphere characteristically has a low pH as a result of acids released by plants in order to liberate trace metal ions to facilitate uptake. Typically, trace elements are limiting factors in plant growth especially in impoverished soils and so mechanisms such as this exist to mediate mineral uptake (Dakora, & Phillips, 2002).

These exudates are able to alter the pH and chemistry of the rhizosphere, and as a result may be able to influence ENP behaviour when the two come into contact with one another (Handy *et. al.*, 2008). Particle behaviour may be modified as a result of increased

dispersion, or induced agglomeration by changes in surface charge. Understanding the net effect of these exudates on nanoparticles may elucidate mechanisms of uptake and translocation of particles within plants. As the pH changes, nanoparticle stability also changes, which is able to be measured by determining the zeta potential. Typically low pH corresponds to an increase in ENP stability (Sauve *et. al.*, 2000), hence it is hypothesized that ENP mobility should be greater in the rhizosphere, which may facilitate uptake into the plant via root systems.

Table 1.2: Organic compounds and enzymes present in root exudates of various different plant species, compiled from literature (Dakora & Phillips, 2002)

Amino acids	Organic acids	Sugars	Vitamins	Purines/ nucleoside	Enzymes	Inorganic ions and gases
α-alanine β-alanine asparagine aspartate cysteine cystine glutamate glycine isoleucine leucine lysine methionine serine threonine proline valine tryptophan ornithine histidine arginine homoserine phenylalanine γ-aminobutyric acid α-aminoadipic acid	citric oxalic malic fumaric succinic acetic butyric valeric glycolic piscidic formic aconitic lactic pyruvic glutaric malonic aldonic erythronic tetronic	glucose fructose galactose maltose ribose xylose rhamnose arabinose raffinose desoxyribose oligosaccharides	biotin thiamine niacin pantothenate riboflavin	adenine guanine cytidine uridine	acid/alkaline phosphatase invertase amylase protease	HCO_3- OH- H+ CO_2 H_2

1.2.7. Plant Pathogen Response

Plants have an elaborate defense system, relying on their intrinsic ability to detect pathogens and trigger local and systemic responses (Wasternack & Hausem, 2013). Their innate immune system is based on recognition of non-self. This occurs both directly, via receptor-ligand interaction, and indirectly by host-produced intermediates (Atkinson *et. al.*, 2012). This is essential in the sessile, non-sterile environment which plants occupy. Plant cells have an advantage over animal cells as they have cell walls; physical barriers to attack by pathogens. Suberin and cutin reinforce the exposed exterior of the plant, and lignin, an organic polymer, maintains strength in the secondary cell wall. This not only protects against abrasion and initial infection, but also responds to invasion (Luna *et. al.*, 2011).

In addition to physical barriers, plants also produce low molecular weight antimicrobial compounds called phytoanticipins even prior to pathogenic challenges. Other innate antimicrobials include saponins; potent antifungals which act by lysing sterol-containing membranes, terpenes; which act as insect deterrents, and flavonoids; which can inhibit fungal pathogens. Tannins also serve to defend against attack, as they are astringent, bitter polyphenols which have the ability to bind to or shrink proteins (Moghaddam, 2012).

1.2.8. Nanoparticles & Plants

Plants have a large role in nanoparticle uptake and accumulation, influencing the environmental fate of such particles (Birbaum *et. al.*, 2010). Soil is a bulk sink of ENPs in the environment, which will inevitably result in contact with plant roots (Kurepa *et. al.*, 2011). ENPs could potentially interact with plant root systems, which may lead to uptake, translocation and accumulation within plant tissues (Lin & Xing, 2008).

There have been limited and dispersed studies investigating the phytotoxicity of nanomaterials, with reports of both positive and negative effects on plant growth (Molina *et.*

al., 2011; Birbaum *et. al.*, 2010; Ma *et. al.*, 2010; Zhu *et. al.*, 2008; Lin & Xing 2007 & 2008). Titanium dioxide nanoparticles have been reported to improve photosynthesis and growth as a result, in spinach (Hong *et. al.*, 2005), whereas ZnO has been seen to inhibit root elongation of ryegrass, radish and rape (Lin & Xing, 2007).

It is hypothesised that the effect of ENPs on plants is specific to the type of species exposed, particle character and environmental conditions. Some plant species are more sensitive to metal ions than others, and as of yet it is unknown whether there is a pattern to toxicity relating to physiology (Zang & Karn, 2005). An improved understanding of the mechanism of phytotoxicty would allow predictions to be made about particle toxicity to important plant species. It would also allow considerations to be made about the environmental implications of particle properties during future particle design (Shi *et. al.*, 2011). It is this kind of information that can be used in pre-emptive design of nanoparticles, in order to reduce the negative environmental impact of current and future particles.

Root exudates alter the environmental conditions, affecting dissolution of metal ions and hence toxicity. Combined with the antibacterial effect of many metal oxide NPs, in particular nZnO, the rhizosphere may be altered (Huang, 2008). The net effect of root exudates on particle behaviour would vary between plant species, as a result of different combinations of sugars and organic acids in particular, as well as effective root surface area (**Figure 1.5**). Numerous interactions occur at the soil-root-biota interface, where organic acids may facilitate particle dispersion by increasing electrostatic repulsion, and sugars may coat NPs and encourage agglomeration. The differently charged amino acids histidine, glycine, aspartic acid and glutamic acid were reported to affect zeta potential of nZnO, change hydrodynamic size, and lead to decreased agglomeration of NPs (Molina *et. al.*, 2011). Nanoparticles may also affect plant-microbial mutualistic relationships, as nZnO in

particular is known to be an antimicrobial agent it may be able to indirectly as well as directly affect the plant (Ma *et. al.*, 2010).



Figure 1.5: Root network of hydroponically grown *Hordeum vulgare* v. Westminster showing large surface area to volume ratio of roots.

Nanoparticles may also be able to influence plants by direct entry through the cell wall. Cell walls are rigid structures comprised of cellulose, hemicellulose and pectins and serve to provide structural support and protection, whilst acting as selective molecular filters. Historically, it was demonstrated that the maximum pore size of cell walls was usually below 4 nm for root hair cells and below 6 nm in palisade parenchyma cells (Fleischer *et. al.*, 1999; Carpita *et. al.*, 1979). However, more recently single-walled carbon nanotubes were found to be able to penetrate tobacco cell walls and membranes (Liu *et. al.*, 2009). Internalisation via endocytosis can then occur, whereby invagination of the cell membrane compartmentalises particles in vesicles. These vesicles were seen to range from 0.2 to 2 µm

in diameter in tobacco mesophyll cells treated with 100 to 200 nm diameter mesoporous silica nanoparticles (Torney *et. al.*, 2007). Hence there is a possible size-dependent mechanism for internalization of particles.

With the increased usage and availability of engineered nanoparticles (ENPs) and their entry into the environment, it is becoming increasingly important to understand the mechanisms of plant uptake and which species are most susceptible (Lin, D. & Xing, B., 2007). The importance of plants is often overlooked, as shown by the overwhelming disparity between the amounts of research into the effects of nanoparticles on animals when compared with plants. However, we rely on plants as primary producers of energy in the food chain; which stresses the importance of understanding the impact of new technologies and their knock on effects.

The effect of ENPs on barley has not included zinc oxide, and has predominantly been limited to work on palladium (Battke *et. al.*, 2009), zero-valent iron (nZVI), silver (El-Temsah and Joner, 2012) and titanium dioxide (TiO_2) (Mandeh *et. al.*, 2012, Moaveni *et. al.*, 2001). Due to the economic importance of both nZnO in the 40 nm to 100 nm range for sunscreen use and barley in the UK this combination will provide valuable data

Zinc oxide has predominately been examined in *Glycine max* (Lopez-Moreno *et. al.*, 2010), *Alium cepa* (Ghodake *et. al.*, 2011, Khumari *et. al.*, 2011), *Arabidopsis thaliana* (Lee *et. al.*, 2010) and *Zea mais (*Lin & Xing, 2007) as well as numerous lower economic value food plant species such as lettuce, cucumber, radish and zucchini (Stampoulis *et. al.*, 2009, Lin & Xing, 2007 & 2008). One of the limitations that has been noted is that although comparisons of ionic versus nanoparticulate treatments have been made, few studies combine ionic, nano-scale and bulk-sized comparisons.

1.3. Bacteria: An Introduction

Bacteria are ubiquitous single-celled prokaryotic microorganisms. Despite being the smallest form of life, bacteria form the majority of all biomass on the planet (Brock, 1999). Microbial degradation and nutrient recycling activity is vital to the maintenance of life. They are prokaryotes as opposed to plants which are eukaryotes, defined by whether their DNA is enclosed within a nuclear envelope. The individual bacterial cell is a highly structured and organised unit, a compartmentalised structure with the ability to replicate, move, communicate and evolve.

1.3.1. Bacterial Membrane Structure

Bacteria have differences in their cell membrane structure, with Gram-negative bacteria containing just a thin layer of peptidoglycan between the inner and outer membranes, and Gram-positive bacteria having a thick peptidoglycan layer with no outer membrane (**Figure 1.6**). The name 'Gram' is derived from Hans Christian Gram, who devised the staining method of differentiating between bacterial types using crystal violet dye, followed by a counterstain of safranin and an alcohol wash. Gram-positive organisms retain the crystal violet dye as a result of their outer peptidoglycan layer and appear purple, and Gram negative bacteria do not and hence show the pink stain of the safranin (Brock, 1999). A noticeable difference between the two is that Gram-negative bacteria have a periplasm (a space between two semi-permeable membranes) and Gram-positive bacteria do not, increasing selectivity in transport of molecules across the membranes (Merchante *et. al.*, 1995). The differences between the cell envelope structures of the two classes of bacteria are important in bacterial susceptibility to toxic compounds. The cell wall composition of Gram-negative bacteria is high in lipids and low in murein (peptidoglycan), whereas in Gram-positive bacteria the reverse is true, with a significantly higher murein content and low lipid content. This structural difference leads to different susceptibilities to antibiotics, with

greater antibiotic resistance observed with Gram-negative bacteria as a result of their additional external membrane.

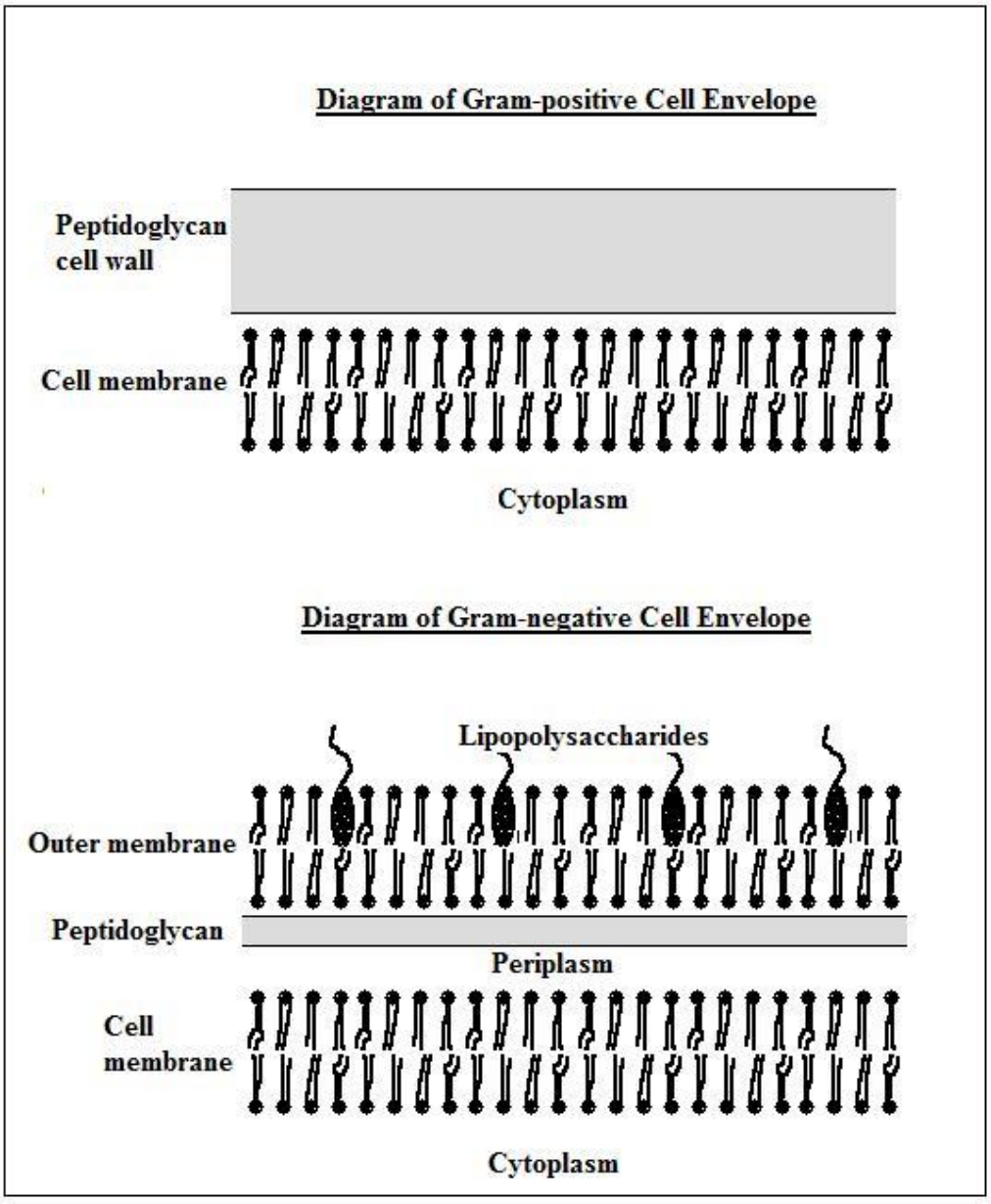


Figure 1.6: Comparison of cell envelope types. **(Top) Gram-positive envelope contains an external peptidoglycan cell wall and internal cell membrane. (Bottom) Gram-negative envelope contains an outer membrane and periplasm in addition to the thinner cell wall and inner cell membrane (adapted from Madigan *et. al.*, 2011).**

1.3.2. Bacteria and Nanoparticles

The nanoparticles are small relative to bacteria, and their size relative to *E. coli* and *B. subtilis* is depicted in **Figure 1.7**. This allows them to surround and interact physically with the cells. The smaller the particle, the more particles are able to surround the cell and hence the greater potential for interaction. Zinc oxide was chosen as the primary nanoparticle in this investigation as it is so widely used and as such has a high potential for environmental release.

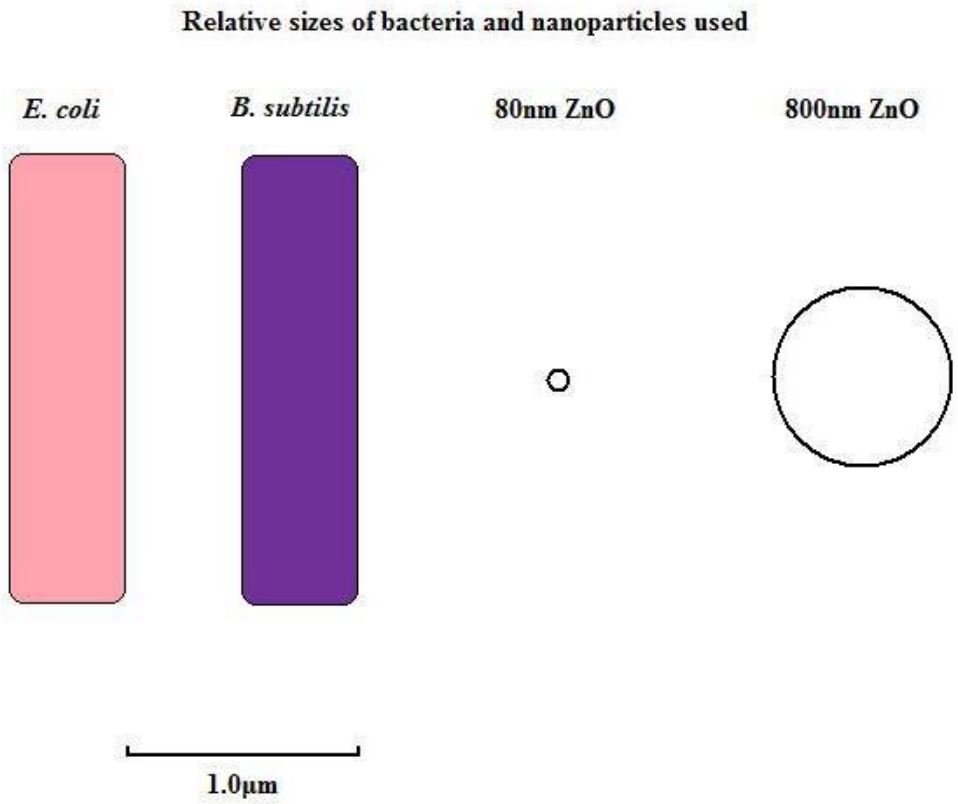


Figure 1.7: Relative sizes of bacteria and nanoparticles used. Diagram showing approximate relative sizes of 2 different bacteria used in this study compared with the smallest and largest size of nanoparticles they encountered

Toxicity in bacteria can be categorized into 2 general modes of action. The term bactericidal is used when the compound kills bacteria i.e. they are no longer able to grow or

reproduce. The term bacteriostatic is used when a compound inhibits growth or cell division (Rendueles *et. al.,* 2014). In addition, acute toxicity describes harm caused as a result of short-term exposure to a substance. Differentiating between different types of toxicity is an important step in characterizing an antimicrobial agent (Guzman *et. al.,* 2012; Brudzynski *et. al.,* 2011).

An experiment with ZnO particles sized 0.1 μm to 0.8 μm demonstrated that a decrease in particle size and an increase in concentration of suspension lead to increased antimicrobial activity in *E. coli* and *S. aureus* (Yamamoto, 2001). This led to the idea that cytotoxicity is proportional to nanoparticle size and concentration. In another study using silver nanoparticles, cytotoxicity of silver nanoparticles was shown to be likely to occur through oxidative stress damage, as an increase from 10 mg/L to 50 mg/L of Ag-15nm particles added to bacteria led to a more than 10-fold increase in ROS levels in the cells (Carson *et. al.*, 2008). In order to compare and understand nanoparticle toxicities; solubility, size, aggregation state and ROS release must also be examined and compared with the bulk and ionic forms in multiple organisms, a combination which, to date, is not known to have been undertaken. This more thorough characterization of the particles will allow a better understanding of the mechanisms of toxicity as detailed in the following chapters.

This study is novel and makes a unique contribution to the field as it thoroughly characterizes nano-scale and bulk ZnO particles which are then tested for toxicity against multiple organisms. By examining the effects of the same nZnO particles on both plants and bacteria, commonality in toxicity can be identified and related to the particle characteristics in order to identify the mechanisms behind toxicity.

1.3.3. Bacteria and Plants

Microbial activity is intrinsically linked to plants, such as in the degradation of organic matter and liberation and sequestration of key elements into nutrient cycles (Madigan *et. al.,* 2011). Bacteria can act beneficially, pathogenically, neutrally or some combination to plants, and vice versa. It is this form of interaction between plant and bacteria that is ubiquitous across all plant species and acts as a communication tool for plants in their sessile state. The microbes associated with the plant form its microbiome; a complex community that is influenced by the plants in the rhizosphere. Root secreted metabolites and physical root architecture manipulates bacterial communities by providing dead root cells and carbon-containing exudates as energy sources (Taylor *et. al.,* 2009). Plants are able to produce substances that mimic quorum sensing compounds as well as antimicrobials in order to manipulate microbial communities, and it has been demonstrated that the structure of these communities can change under metal toxicity stress (Mariano *et. al.,* 2005).

1.3.4. Bacterial Zinc Nutrition and Requirement

Bacteria require very small but essential quantities of zinc in order to form various key enzymes such as carbonic anhydrase, alcohol dehydrogenase, and RNA and DNA polymerases. Zinc is an essential nutrient, though the cellular concentrations involved are so low as to be very difficult to quantify, and hence are described as trace micronutrients. Bacteria in the environment are often subject to only low concentrations of zinc, leading to the evolution of complex zinc scavenging molecules.

1.3.5. Antibacterial Effects of Zinc Oxide

Zinc oxide has previously been demonstrated to have antimicrobial properties (Jain *et. al.,* 2013). The antibacterial nature of ZnO is considered to be a result of particle size, shape, ROS or Zn^{2+} release, or a combination of both (Juang *et. al.,* 2009). In a study by

Yamamoto, 2001, the size of ZnO was shown to be important, as a decrease in size lead to an increase in toxicity to *E. coli*. However, the smallest particle tested was 100 nm and the other particles were not in the nanoscale range. Fifty nm sized ZnO is more widely used in sunscreens and UV protective coatings and hence was chosen for this study, as it has a large potential to enter the environment. The wide use of ZnO means that many particles find their way into water and soil, and may kill indigenous bacteria. However, since ZnO particles are generally regarded as safe (GRAS) for humans (Federal Register, 1998) there is interest in using ZnO in food technology applications to prevent spoilage (Das *et. al*., 2009). There is also potential for the antimicrobial properties to be utilised against human bacterial infections (Dhas *et. al.,* 2014).

1.4. Aim of Research

This project had several aims with regards to examining the effect of nZnO in plants and bacteria in order to better understand the consequences of environmental release.

Firstly, the aim was to characterize the particles used in the study thoroughly to gain information on their size, charge, ROS release and stability in order to relate these properties to any biological effects observed. Secondly it aimed to determine whether zinc in any form is able to enter crop plants from 50 nm ZnO nanoparticles. If so, it is vital to understand whether it concentrates in the aerial part of the plant or the roots and in what quantities, and hence whether it is able to enter the food chain in any measurable quantity. In addition, the aim was to determine whether nZnO particles inhibited or killed bacterial cells. This was examined for two reasons; plants are non-sterile entities and hence environmental nZnO release would impact both bacteria and plants directly and indirectly. Finally, antibiotic resistance in bacteria is increasingly becoming a widespread concern and identification of novel antimicrobials is a priority in global research, as recently highlighted in the UK

Department for Health's five-year antimicrobial research strategy (Department of Health, 2013).

The overall aim of this project is, rather than to examine a very narrow combination in depth, to instead look at the possible interactions with an almost holistic approach, traversing domains and identifying areas that require further examination. By using the same nanoparticles tested on plants and bacteria, and then linking the results to particle characteristics, observations which are highly relevant but have not yet been widely considered can be identified and provide direction for future research.

1.5. Significance of Research

The significance of research in this area is seen when the implications of a negative effect of nanomaterial on plants are considered; we are already facing a food shortage because of the rapidly growing global population, so if nanoparticles were to negatively impact on crop growth or food safety this would hamper crop production, and there may be other possible negative consequences due to nanoparticles entering the food chain. Conversely, uptake of nZnO could increase the zinc content in the plant, and in some countries, where zinc is limiting, could have some positive health consequences. As Zn is essential for normal cell function, deprivation leads to decreased function in all tissues, and clinical symptoms are observed in the immune system, reproductive and gastrointestinal systems (Hambidge, 1982). Translocation of zinc to edible sections of the plant such as leaves and seeds could provide a method of biofortification. In an ever expanding population where up to 1/3 of humans are at risk of zinc deficiency, cheap methods of biofortification are increasingly sought after (Hambidge, 2000). If the levels of nZnO release into the environment remains low enough to avoid plant toxicity, but present enough to biofortify crops, there is a potential for a positive consequence of low level environmental release.

To date there has been much greater research on mammalian cells, which show the potential of nanoparticles to enter cells and possibly disrupt cell function. Should nanoparticles accumulate in food plants, we would therefore be ingesting them, which highlights the need for stringent regulations on particle production. This project is highly topical, as currently there is very little data on nanotoxic effects on plants, bacteria, and their combinations, and what little data there is suggests negative implications on growth and plant health. Not only does it examine an important and under researched area of science, it involves multiple scientific disciplines; engineering, materials science and biology. The interdisciplinary nature of this project aimed to provide an overview of the potential environmental effects of engineered nano-scale zinc oxide in order to further current knowledge on the possible impact these nanomaterials have in biological systems.

This thesis is split into 6 experimental chapters which ask the following research questions:

1. What are the material characteristics of nano-scale and bulk scale ZnO?
2. Is nano-scale ZnO differently toxic than the bulk or ionic form to *Escherichia coli*?
3. Is there a trend in toxicity between monocotyledon and dicotyledon plants?
4. How much zinc is able to enter barley from these three particle types, and does nano-scale ZnO affect plant biomass more or less than the bulk sized or ionic form?
5. What are the material characteristics of an aged form of nZnO when compared to a non-aged form?
6. How do these material characteristic differences affect the toxicity of the ENPs?

The results are then discussed in the context of how engineered particle design may impact on phyto- and bacterio-toxicity, and the types of future work that should be done to further knowledge of plant-nanoparticle interactions in order to reduce risk and enhance benefits to industry, the environment and society.

2. MATERIALS CHARACTERISATION OF ENGINEERED NANO-SCALE AND BULK-SIZED ZINC OXIDE PARTICLES

2.1 Introduction

This chapter aimed to describe the various physico-chemical properties of the different zinc-containing particles used in this research, in order to understand and predict behaviour of nanoparticles in phytological and bacterial systems. Any differences observed between the different zinc-containing treatments with plants and bacteria will need to be explained using information on the particle size, chemical state, solubility and stability. Specifically 50 nm ZnO and bulk (standard) sized ZnO will be examined and compared in terms of size distribution, zeta potential, shape, surface chemistry, release of reactive oxygen species (ROS) and solubility. Zinc sulphate is used as an ionic control later in this project, but as it fully dissociates in water at the concentrations used throughout this project (maximum solubility 1 g in 0.6 ml (Merck Index, 12th ed), 2015)), particle-specific analyses were not performed on it (Cronholm *et. al.*, 2011).

2.1.1 Particle Size Determination

When using any form of particulate matter, especially nanoparticles, it is important to know the average size of the particles being used, as well as their size distribution (the range of particle sizes and the way in which they are distributed). The distribution provides vital information, particularly where the quantity is large and sample is non-uniform (Mendes *et. al.*, 2014). Knowledge of particle size allows a better understanding of its properties, for example it allows the comparison between particle and plant or bacterial cells to give a relative size ratio, which can help further understand the measured interactions. The size of spherical and near-spherical particles can be described by their physical and hydrodynamic diameters, whereas non-spherical particles can be sized by volume, mass, surface area or

hydrodynamic diameter (Horiba Scientific, 2014). Particle size can be determined using a number of different methods such as disc centrifugation for physical size analysis, and dynamic light scattering for hydrodynamic size analysis. By using a combination of methods to verify consistency of results, the average particle diameter and size distribution can be quantified.

Prior to analyses, particles were sonicated once dispersed in water, whereby ultrasound was applied to the suspension via an ultrasonic water bath in order to deagglomerate particles by inducing cavitation and microbubbles (Bihari *et. al.*, 2008). Sonication is required to agitate the particles, facilitate dispersion and reduce aggregation (Al-Kaysi *et. al.*, 2005). Sonication also ensured optimum nanoparticle dispersion in the suspension, and is a required step in determining phytotoxicity of individual particles, particularly when preparing dispersions of nanoparticle powders in liquid (Taurozzi & Hackley, 2012).

2.1.1.1 Hydrodynamic Diameter

Hydrodynamic diameter is a measure of the apparent size of a dynamic particle in a hydrated or solvated system. It is determined by the physical size of the particle plus the size influence of the electric dipole layer on the particle surface when in a liquid solvent or dispersal media (Atkins & De Paula, 2010). This layer affects the movement and behaviour of the particle and is always greater than the physical diameter as measured by more direct observation methods such as TEM (Hackley & Clogston, 2011). As a result of the behavioural effect of the dipole layer, it is a highly useful measure for particle behaviour in hydrated systems.

The apparent size of particles can be measured by the dynamic light scattering method, such as by use of a Malvern Zetasizer, which utilises non-invasive backscatter optics (NIBS) to improve detection of aggregates. As particles move under Brownian

motion, light hitting them from a laser is scattered, and the particle hydrodynamic radius can then be determined using the Stokes-Einstein relationship based on the viscosity. The Stokes-Einstein relationship is derived from the Einstein-Smoluchowski relation of kinetic theory:

$$D_t = \mu k_B T$$

where D_t represents the translational diffusion constant in the liquid, μ is the particle mobility, k_B is the Boltzmann constant and T is the absolute temperature. From this is derived the Stokes-Einstein relationship in a form most commonly used for size determination, which calculates hydrodynamic diameter, D_h, by including the dynamic viscosity of the liquid, η:

$$D_h = \frac{k_B T}{3\pi\eta D_t}$$

The calculations for hydrodynamic diameter are performed by the Malvern instrument software. This method has drawbacks as the size calculation is based on the manner by which the particles move, which may be influenced by surface ligands or solvent molecules. In a non-uniformly size distributed sample, scatter from larger particles or aggregates may obfuscate scatter from smaller particles, so samples should always be sonicated thoroughly prior to measurement (Murdock *et. al.*, 2007). It is also important to note that temperature features in the size determination equation, and as such it is vital to maintain the same measurement temperature for each sample for accurate comparison.

2.1.1.2 Disc Centrifugation

Disc centrifugation is a high resolution method which uses centrifugal sedimentation in a liquid medium in order to separate out different sizes of particle. The differential sedimentation rates of different sized particles allow the determination of particle size range

(Provder, 1991). It produces a size distribution graph by using the density and sedimentation rate of particles through a sucrose gradient to calculate the equivalent spherical diameter.

Particles settle due to gravity and the velocity at which this occurs is determined by the particle radius. They are then detected in the optically clear sedimentation medium using a light beam, the intensity of which is affected by the scattering and/or blocking effect of particles. Operational software then calculated the size distribution according to the effect of particles on the light beam. From the average diameter obtained by disc centrifugation, the approximate number of particles in a given concentration can be calculated in order to compare particle numbers with bacterial cell numbers.

2.1.2 Zeta Potential

Zeta potential is a measure of the electrokinetic potential between the charge associated with the surface of a particle and the liquid medium in which it is dispersed (Hunter, 1986). It can also be described as the difference in electric potential between the stern layer (stationary layer of fluid on the outside of the particle) and a point in the bulk dispersion medium (**Figure 2.1**). It is an important measure of particle stability and indicator of how well particles will remain dispersed over time, which is important for toxicity experiments as it affects the bioavailability of particles.

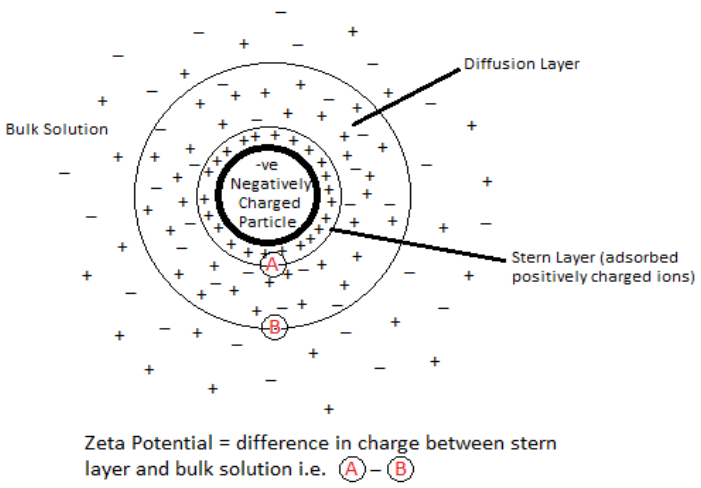


Figure 2.1: Diagram explaining zeta potential, adapted from Chen, (2013).

The zeta potential measured using laser doppler micro-electrophoresis whereby an electric field is applied to a zeta cell containing dispersed particles. Particles then move at different velocities through this electric field, the motion of which is detected by dynamic light scattering (Everett, 1994). A laser is polarized and directed through the sample, where it is scattered by the particles according to Rayleigh scattering (Chu & Liu, 2000). This is the elastic scattering of light radiation in all directions. The scattered light is then photomultiplied and the speckle pattern is interpreted. This is then used to calculate electrophoretic mobility, from which the zeta potential can then be calculated (Malvern, 2013). Zeta potential provides useful information about the stability of a dispersion, with values more negative than −30 mV or more positive than +30 mV resulting in mutual repulsion between particles and hence stability. Values less negative than −14 mV or less positive than +14 mV indicate reduced stability and likely agglomeration (Hussain *et. al.,* 2009). When analysing particle stability over a range of pH values, the isoelectric point (IEP) is the point at which the particle carries no net charge. At this point, particles are particularly unstable and crash out of suspension, significantly reducing bioavailability in toxicity experiments (Lin *et. al.,* 2007).

2.1.3 Reactive Oxygen Species

Reactive Oxygen Species (ROS) are able to be released from particle surfaces and increase particle toxicity either by direct release of ROS or induction of ROS in cells (Ma *et. al.,* 2014; Dutta *et. al.,* 2012). They are very reactive and unstable oxygen-containing molecules, and as a result are incredibly short lived species (**Table 2.1**). As a result, physical contact with particles was demonstrated to be necessary to induce toxicity in human cancer cells (Moos *et. al*., 2010) In order to observe them, therefore, detection relies on their reaction with any molecule or compound that elicits an observable change, such as the fluorescent dye coumarin (Ishibashi *et. al.*, 2000).

Table 2.1: Lifetimes and diffusion distances of different reactive oxygen species (Lesser, 2006)

Reactive Oxygen Species	Lifetime (milliseconds)	Diffusion distances (nanometers)
Singlet oxygen	3.7	82
Superoxide radicals	50	320
Hydroxyl radical	10^{-4}	4.5

Coumarin was chosen for quantification of ROS released by the nanoparticles directly as it rapidly reacts with active oxygen species, forming 7-hydroxycoumarin, a stable, fluorescent molecule with an excitation wavelength of 345 nm and emission of 450 nm. The relationship between concentration of 7-hydroxycoumarin and the fluorescent signal is linear and this, combined with its stability, results in a highly sensitive ROS quantification technique (Townley *et. al.*, 2011).

2.1.4 Zinc Dissolution

To establish the concentration of Zn^{2+} ions released by nZnO and bulk ZnO in water and the plant growth media (20 % Hoagland solution) over time, suspensions of particles were ultrafiltered to remove particulates and the filtrate examined for Zn concentration by Atomic Absorption Spectrophotometry (AAS). Hoagland solution was used for hydroponic growth of barley in Chapter 4, so dissolution of particles in this complex nutritional medium was examined. The experiment was conducted at four time points over 12 days (288 h) to obtain long term dissolution rates. Readings at 1 day (24 h) and 7 days (168 h) were included to relate to the 24 h bacterial growth inhibition assays in Chapter 3, and to 7 days hydroponic treatment of barley with the particles in Chapter 4, respectively. The method used was adapted from Reed *et. al.* (2012), with analyses performed by use of AAS rather than the more expensive method of Inductively Coupled Plasma - Mass Spectroscopy (ICP-MS).

2.1.5 Atomic Absorbance Spectrophotometry

Flame Atomic Absorption Spectrophotometry (AAS) is a sensitive metal quantification technique which uses absorption of optical radiation to measure the concentration of atoms in the gas phase (Welz & Sperling, 1999). Samples are prepared in liquid form before being vaporised in a flame furnace. Flame AAS typically uses a mixture of air and acetylene gas to produce a flame. Samples are aspirated into a nebulising chamber before being injected into the flame, liberating analyte atoms (L'vov *et. al.,* 2005). Electrons within the atoms are temporarily excited to higher orbitals by absorbing ultraviolet or visible light. The amount of energy absorbed, of a given wavelength, is measured, and each wavelength is indicative of only one element which enables the technique its sensitivity (Becker-Ross *et. al.,* 1996). The AAS uses a long, thin slot type burner to maximise the path length and hence maximise absorption readings. The radiation source comprises a hollow cathode lamp, which is fabricated from the element to be quantified. For example with zinc, light from excited zinc atoms in the lamp is emitted at the correct wavelength/s to be absorbed by the liberated zinc atoms in the vapourised sample (Broekaert 1998).

Calibration with known concentrations of each test element is required; hence measured absorbance can be used to calculate element concentration using the Beer-Lambert Law (Welz *et. al.,* 2005).The Beer Lambert Law links the relative light absorption to the physical properties of the material the light is passing through, and states that:

$$A = a_\lambda \times b \times c$$

where A represents measured absorbance, a_λ wavelength-dependent absorptivity coefficient, b path length and c concentration of analyte. The absorbance value is then used to calculate the concentration of the analyte in mg/L. This technique is used throughout this

project to accurately quantify zinc in dissolution experiments and plant zinc uptake experiments in Chapter 4.

2.1.6 UV-Visible Absorbance

The UV absorption of zinc oxide nanoparticles is of interest to manufacturers and consumers due to the frequent use of zinc oxide in optical settings, such as solar cells and sunscreens (Mitchnick *et. al.*, 1999). Absorbance is linked to particle size, with absorbance increasing as particle size increases. Hence, absorption values are widely used to characterise nanomaterials optically (Talam *et. al.*, 2012).

Many studies have examined ZnO of particle size 10 nm or less, to identify quantum-type behaviour and properties such as blue shift and photoluminescence (Madler *et. al.*, 2002). Such measurements have identified that the phenomenon of quantum confinement only manifests itself in particles of 7 nm and smaller, which is associated with the broadening of the electrical bandgap at ultralow particulate size (Lin *et. al.*, 2005). There are surprisingly few measurements of UV absorption of particles greater than 10 nm in size, and even fewer for particles above 40 nm (Goh *et. al.*, 2014). Zinc oxide particles of size 40 to 100 nm are widely used as UV absorbers in sunscreens due to being large enough not to traverse the human epidermal barrier but small enough to have reduced absorbance compared to the bulk-sized material and hence appear translucent on the skin (Popov *et. al.*, 2005). The nZnO used in this study falls within this 10 to 100 nm size range and was chosen for toxicity determination as it is a commonly used size of nZnO, with high potential for environmental release as a consequence (Eisenberger *et. al.*, 2010).

2.2 Materials and Methods

2.2.1 Nanoparticles

All particles were purchased from Sigma Aldrich, (UK). The particles used throughout this study were nZnO 50 nm, < 6 % Al doped, and standard ZnO powder (bulk-sized, undoped). Particles were suspended in sterile de-ionised (DI) water for ease of use and to reduce particulate inhalation risk. Stock solutions of 10 g/L were made by adding 0.3 g of particles to 30 ml of DI water. Different concentrations were achieved by serial dilution from stock solution to give four concentrations of 10 g/L, 1 g/L, 0.1 g/L and 0.01 g/L. Before use, NP suspension vials were placed in a Branson 3510 Ultrasound Bath (Sigma Aldrich, UK) at 40 kHz for 1 hour in order to ensure particles were well dispersed.

2.2.2 CPS Size Distribution Analysis

Subsequent to 1 hour of sonification, 1 g/L nZnO suspensions were tested for particle size distribution using a CPS Disc Centrifuge™ Model DC24000 (CPS Instruments, UK) as per the manufacturer's instructions. Sucrose (≥ 99.5 % purity, Sigma Aldrich, Dorset, UK) solutions in DI water were made at 8 % and 24 % (w/v) concentrations. The rotary speed of 10,000RPM was chosen to allow detection of particles < 2 µm. A sucrose gradient was established through injection of sucrose solutions in decreasing concentration before sealing with 0.5 ml dodecane. A standard of 0.377 µm polyvinyl chloride (Sigma Aldrich, Dorset, UK) particles was used for calibration. Subsequently 0.1 mL of each particle suspension was injected into the machine. The relative size distribution of particles within each solution was automatically assessed by the CPS software. Triplicates were taken to ensure reliability of results and graphs were automatically checked for normality.

2.2.3 Dynamic Light Scattering Size Distribution Analysis

Particle solution concentrations for use in the Malvern ZetaSizer Nano ZS are recommended based on particle size; for 10 to 100 nm, a minimum concentration of 100 mg/L is suggested (Malvern Instruments Ltd., UK). Particle solutions of 100 mg/L concentration in DI water were sonicated for 1 h before being syringed into disposable 1 cm cuvettes with a disposable 5 ml syringe (Fisher, UK). These were then inserted into the Malvern ZetaSizer Nano ZS and size determination software was used as per the manufacturer's instruction. Each sample was run three times with each measurement comprising of five sub runs of 10 s each. Malvern software contains a built-in system to analyse data quality, with ‘good’ to denote a normal distribution of cumulative data and hence good reliability. Each test was confirmed to be ‘good’ before proceeding. Data were presented in two forms; firstly the form of relative intensity at each hydrodynamic diameter and secondly cumulative percentage. This provided information on proportion of hydrodynamic particle sizes and distribution.

2.2.4 Zeta Potential of Particles Over a pH Range

For zeta potential analysis of particles in acidic and alkaline adjusted DI water, suspensions of 1 g/L nZnO and bulk-sized ZnO were adjusted with HCl and NaOH to produce a range of five pH values. Samples were analysed using the Malvern ZetaSizer Nano ZS and triplicates taken. Temperature was maintained by at 25 ºC ± 0.1 ºC by the machine throughout the experiment.

2.2.5 Scanning Electron Microscopy

Samples of particles suspended in a solution of 70 % isopropanol and 30 % MilliQ water at 100 mg/L were sonicated for 1 h before a single drop of suspension was pipetted onto a 1.5 cm x 1.5 cm silicon slide. The particle suspension was allowed to dry in a lidded

Petri dish to prevent dust contamination. Samples were analysed with a Jeol 840 F SEM (MA, USA) at a 15 mm to 16 mm working distance with 5 kV beam energy, by Assia Taferka; D.Phil candidate in Materials Science, University of Oxford. Approximate particle sizes were then ascertained by analysing the micrographs with GIMP 2.8 software.

2.2.6 Reactive Oxygen Species

Stock suspensions of different zinc-containing particles were made at a concentration of 5 mg/ml and 200 µl of each was added to 4.8 ml of a 2 mg/mL solution of coumarin made using MilliQ water. Suspensions of each particle type were tested in independent triplicate. A control containing solely coumarin solution was also prepared in triplicate. Samples were prepared in amber glass vials to prevent light causing photocatalytic release of ROS from the particles. At each sampling time point (1 h, 8 h, 24 h, 48 hr, 72 h) samples were vortexed and a 1 ml aliquot was taken and pipetted into a micro Eppendorf vial. Each vial was centrifuged for 15 minutes at 12,000 RPM to pellet the nanoparticles. Subsequently, 100 µl aliquots were taken from the supernatant and pipetted into a Nunclon 96-well clear-bottomed plate. The plate was then inserted into a BioTek plate reader and fluorescence values recorded (excitation wavelength 345 nm, emission wavelength 450 nm).

2.2.7 Zinc Dissolution Assay

Samples of 100 ml were prepared in triplicate containing around 100 mg/L nZnO or bulk-sized ZnO particles, with exact masses recorded to four decimal places ± 1mg for particles and to two decimal places for either Hoagland solution or water added so the exact concentrations were known. This allowed calculations of the percentage of dissolved zinc relative to the total zinc in solution. Samples of control Hoagland solution and DI water were made as above. All samples were sonicated for 1 h prior to the first reading and subsequently maintained at 25 ºC ± 1 ºC. Samples were shaken for 1 minute daily to simulate the stirring

regime used in the hydroponic barley experiments in Chapter 5. At each time point of 1 h, 24 h, 168 h and 288 h, 5 ml was extracted from each sample using a clean 5 ml syringe which was then prefiltered through a Whatman 0.22 µm syringe filter. This filtrate was then drawn into a new clean 5 ml syringe and passed through an ultrafine 0.02 µm syringe filter into clean 30 ml amber glass vials. This pore size of 0.02 µm (i.e. 20 nm) was chosen to exclude the 50 nm nanoparticles and leave only dissolved Zn. Care was taken not to cross-contaminate any samples or to touch inside the vials to prevent external zinc from entering the samples. Samples were then diluted ten-fold with DI water prior to analysis by AAS.

The AAS was calibrated using $ZnCl_2$ standards from 0.1 to 2.0 mg/L to produce a calibration curve. All samples were diluted ten-fold to fit into this range, as established by preliminary tests indicating required dilution. Background readings of DI water were taken every ten samples and used as a correction.

Graphs of Zn^{2+} concentration (mg/L) over time (hours) were plotted for nZnO and bulk-sized ZnO particles with error bars showing one standard deviation of triplicates. In order to establish the long term dissolution rate, Zn^{2+} concentration values were plotted against time to produce a linear model expressed as:

$$[Zn^{2+}] = Slope \times Time + Intercept$$

with slope describing dissolution rate in mg L^{-1} h^{-1} then multiplied by 10^3 to produce the final dissolution rate expressed in µg L^{-1} h^{-1}.

2.2.8 UV-Visible Absorbance

UV-visible absorbance was measured across a range of particle concentrations at 405 nm and 630 nm wavelengths (Talam *et. al.*, 2012). Stock suspensions of 50 nm and bulk-sized ZnO particles were made at 1000 mg/L in DI water in triplicate and sonicated for 1 h at

40 kHz prior to use. Two hundred µl of 1000 mg/L suspension was pipetted into wells on the left hand side of the plate. A serial dilution from 1000 mg/L to 0.488 mg/L was then made in a Nunclon clear-bottomed 96-well plate using a multichannel pipette to continually halve the concentration of particles by the addition of 100 µl DI water. The plate was then read using a BioTek Synergy HT microplate reader (BioTek Corporation, UK). The wavelength of 405 nm was chosen based on peak values of nZnO particles identified in the literature (Goh *et. al.*, 2014; Talam *et. al.*, 2012), and the value of 630 nm was chosen based on the peak bacterial absorption wavelength, which was used for bacterial growth experiments in this report and is the traditional wavelength used for determining bacterial growth (Stubbings *et. al.*, 2004; Shapiro *et. al.*, 2002,).

2.2.9 Statistical Analysis

Arithmetic means and standard deviations were calculated from the recorded data. Data were analysed using Student's t-test or ANOVA where appropriate with 0.05 as the alpha value.

2.3 Results and Discussion

2.3.1 Zeta Potential of nZnO over a pH range

Zeta potential analyses were performed on both bulk-sized ZnO and 50 nm nZnO over a pH range to determine the change in particle stability in acidic and alkaline conditions (**Figure 2.2**).

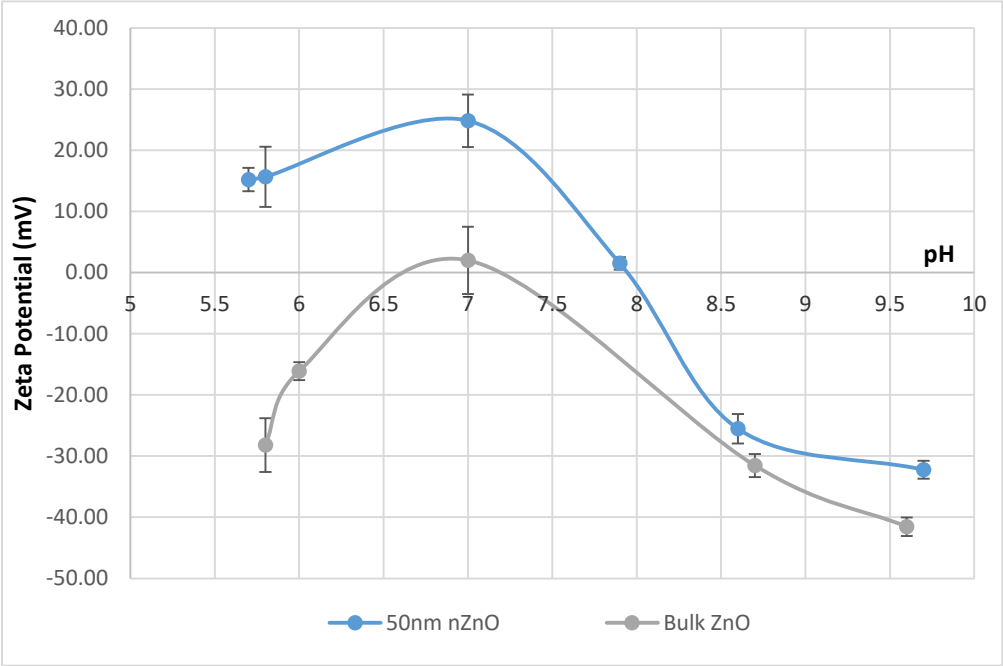


Figure 2.2: Zeta potential of 50 nm and bulk-sized ZnO particles over a pH range (*n* = 3), error bars denote one standard deviation above and below the mean.

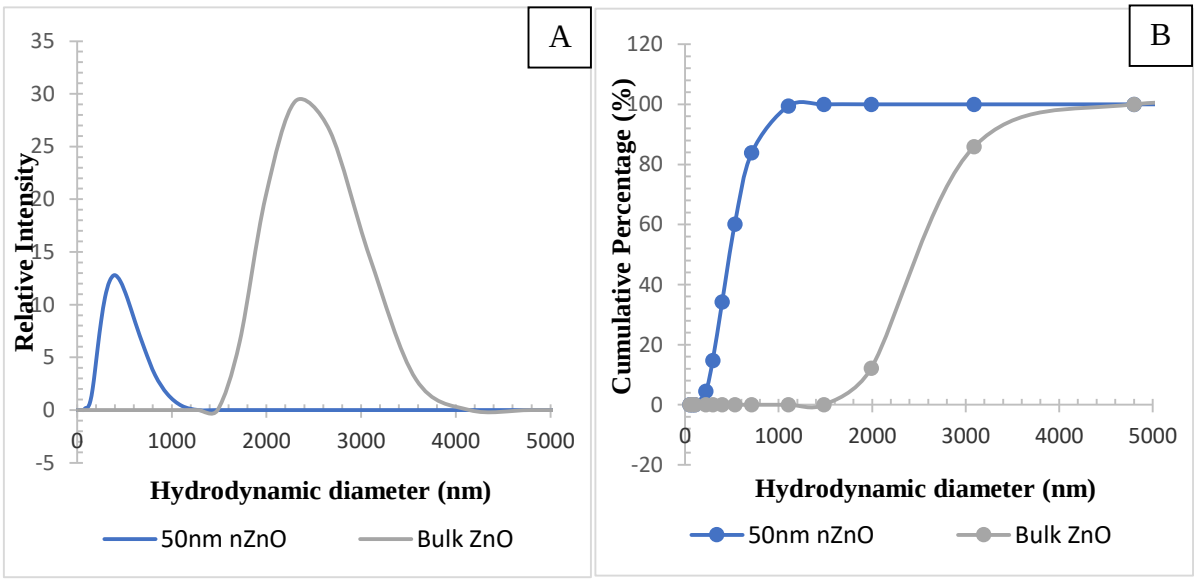
The results demonstrated that the isoelectric point (IEP) of the nZnO particles was higher than that of the bulk ZnO particles, with IEPs of pH 7.93 and 7.21 respectively. With the 50 nm nZnO particles, the zeta potentials were significantly higher than that of the bulk ZnO particles across the entire pH range tested. The lowest pH value of between 5.5 and 6.0 was chosen to approximate the pH of plant root exudates (Bais *et. al.*, 2006), and the difference in zeta potential between the two particles at this pH was highly significant. The bulk particles had a negative surface charge of greater magnitude than the 50 nm particles

which were positively charged. The greater magnitude demonstrated that the bulk particles were more stable than 50 nm nZnO at a pH likely to be found in root exudates, and hence would be more bioavailable due to greater stability and reduced tendency to agglomerate. However, at a natural pH of around 7, the bulk particles had a zeta potential of +2.00 mV ± 5.48 which is very near the isoelectric point of zero charge. The zeta curve for bulk particles crossed the *x* axis at two points between pH 6.5 and 7.5, which indicated that over this pH range the particles were particularly unstable in suspension and would settle quickly. This would likely reduce the bioavailability and hence the toxicity, as fewer individual particles are left free in suspension. This was not the case for the 50 nm nZnO particles, which had a zeta potential of +23.8 mV ± 4.29 at pH 7 and hence were significantly more stable than the bulk particles.

Both particles were most stable at a pH of around 9.5, where both had ZP values of greater than −30 mV. This demonstrated the importance of pH to the stability of nanoparticles and bulk particles alike, and detailed the changes which occur over a pH range relevant to the interaction of particles with plant root exudates.

2.3.2 DLS Size Measurements

The results from the DLS size measurements using the Malvern Zetasizer ZS were displayed graphically in **Figure 2.3**. For the relative intensity plot (**Figure 2.3 A**), a primary peak at 396 nm was recorded for 50 nm nZnO, and at 2305 nm for bulk-sized ZnO, and the average hydrodynamic diameter as ascertained by the software was 400 ± 56.2 nm and 2560 ± 244 nm respectively. This showed that bulk particles were significantly larger in hydrodynamic diameter than the 50 nm nZnO, as anticipated. The hydrodynamic diameter recorded for 50 nm nZnO was much larger than the physical stated size of 50 nm, which demonstrated the larger effective size of these particles including dipole interactions in hydrated systems. From the cumulative percentage distribution in **Figure 2.3 B**, it was determined that 100 % of 50 nm particles were of size 1000 nm or below, whereas for bulk ZnO 100 % of particles had hydrodynamic diameters in the range of 1500 to 4000 nm. This indicated that they each occupied a discrete size range with bulk ZnO having significantly larger hydrodynamic diameter particles than 50 nm nZnO particles



Figures 2.3 A & B: Hydrodynamic particle size of nZnO and bulk ZnO as measured by dynamic light scattering (DLS), displayed as relative intensity (A) and as cumulative percentage of counts from integrated DLS measurements (B).

2.3.3 CPS Disc Centrifuge

The size distributions of the purchased 50 nm and bulk-sized Zinc Oxide particles were measured using a CPS Disc Centrifuge. Results were recorded in triplicate for both bulk-sized ZnO and 50 nm nZnO and graphs overlaid in **Figure 2.4 A** and **B** respectively.

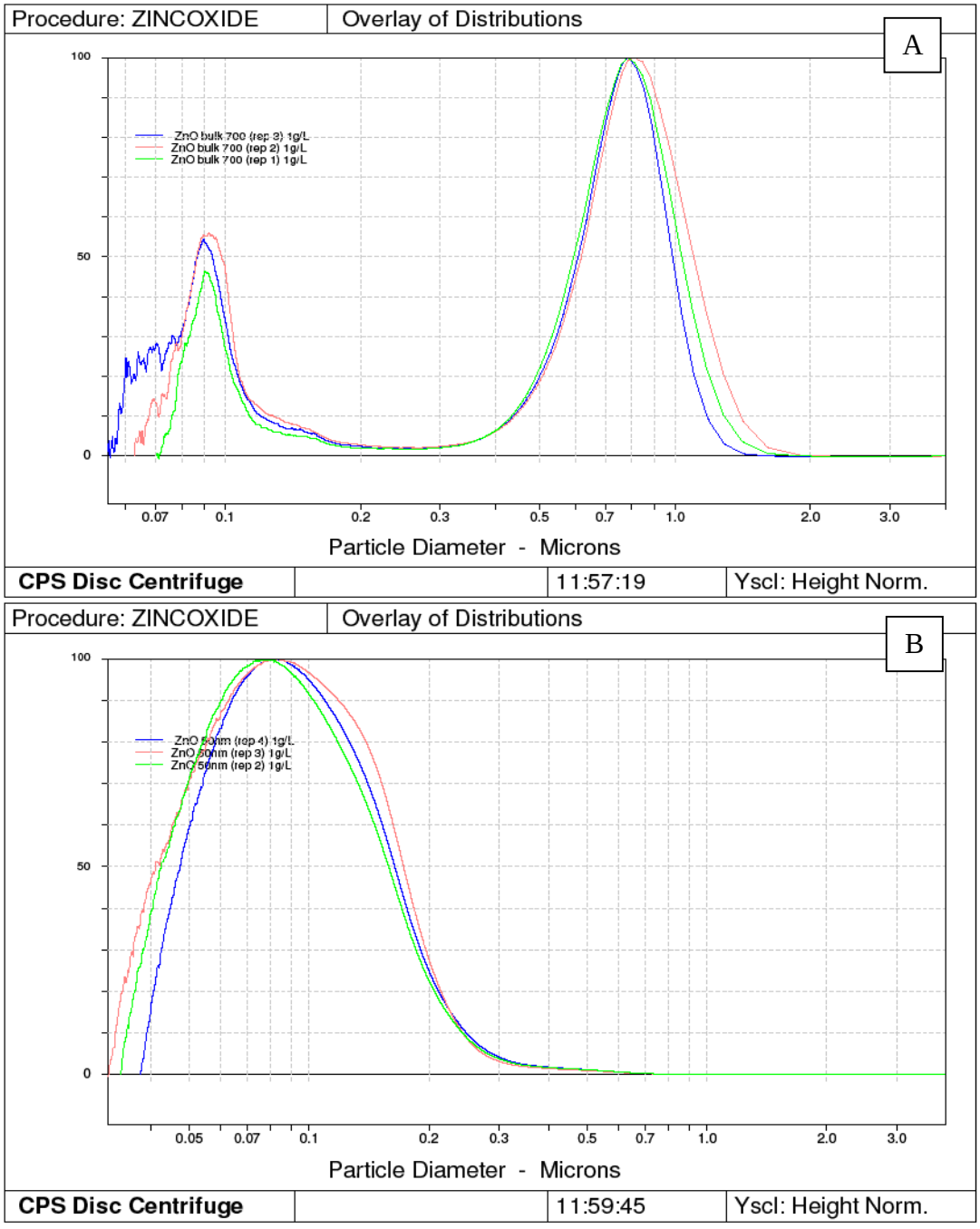


Figure 2.4 A & B: Size distribution curves of bulk-sized ZnO (A) and 50 nm nZnO (B) displayed as overlaid triplicate measurements. Y-axis denotes relative intensity.

For the bulk-sized particles there was a bimodal size distribution with a primary peak at 800 nm in diameter and a secondary peak at 90 nm (**Figure 2.4 A**). This provided an average size of 702 ± 43.9 nm. For the 50 nm nZnO particles, there was a single broad peak at around 80 nm which gave the particles an average size of 84.3 ± 20.2 nm. The manufacturer's stated size of nano-ZnO was 50 nm, but the measured size from the disc centrifuge was larger at approximately 85 nm. This type of discrepancy is not uncommon and is a result of non-sphericity and variations within samples (Heinlaan *et. al.*, 2008; Adams *et. al.,* 2006). As all particle suspensions were sonicated for a minimum of 1 h immediately prior to use, any aggregates that may have formed should have broken down and should not be responsible for the discrepancy.

The photosedimentometric method used by this machine allowed the size distribution of particles without the influence of the electrical dipole layer, as was the case with hydrodynamic diameter as above. The average size values were calculated by the CPS software and displayed along with the hydrodynamic diameters in **Table 2.2** for comparison. The disc centrifuge method provided a more accurate physical particle size, however the combination of both methods provided information on how their size affects particle behaviour.

Table 2.2: **Summary of particle sizes determined using disc sedimentation and dynamic light scatter methods to compare to the manufacturer-stated diameter.**

Particle	CPS mean diameter (nm)	DLS average hydrodynamic diameter (nm)	Manufacturer stated diameter (nm)
50 nm ZnO	84.3 ± 20.2	400.4 ± 56.2	50
Bulk ZnO	701.8 ± 43.9	2305 ± 243.8	Unstated

2.3.4 Scanning Electron Microscopy

SEM imaging showed that particles exhibited the typical shape of wurtzite crystal structure characterised by elongated hexagonal crystals (Guo *et. al.*, 2002) (**Figure 2.5 A** & **B**). The SEM micrograph for bulk ZnO particles explained the bimodal distribution demonstrated after analysis by CPS disc centrifuge (**Figure 2.5 A**). A mixture of different-sized particles was clearly visible from around 50 nm to around 1 µm. The majority of the particles were hexagonal cylinders with varying aspect ratios. For the 50 nm nZnO particles (**Figure 2.5 B**), the particle sizes were near the limit of resolution, although the particle sizes were between approximately 30 nm and 100 nm as measured in GIMP. This was concordant with the CPS disc centrifuge data.

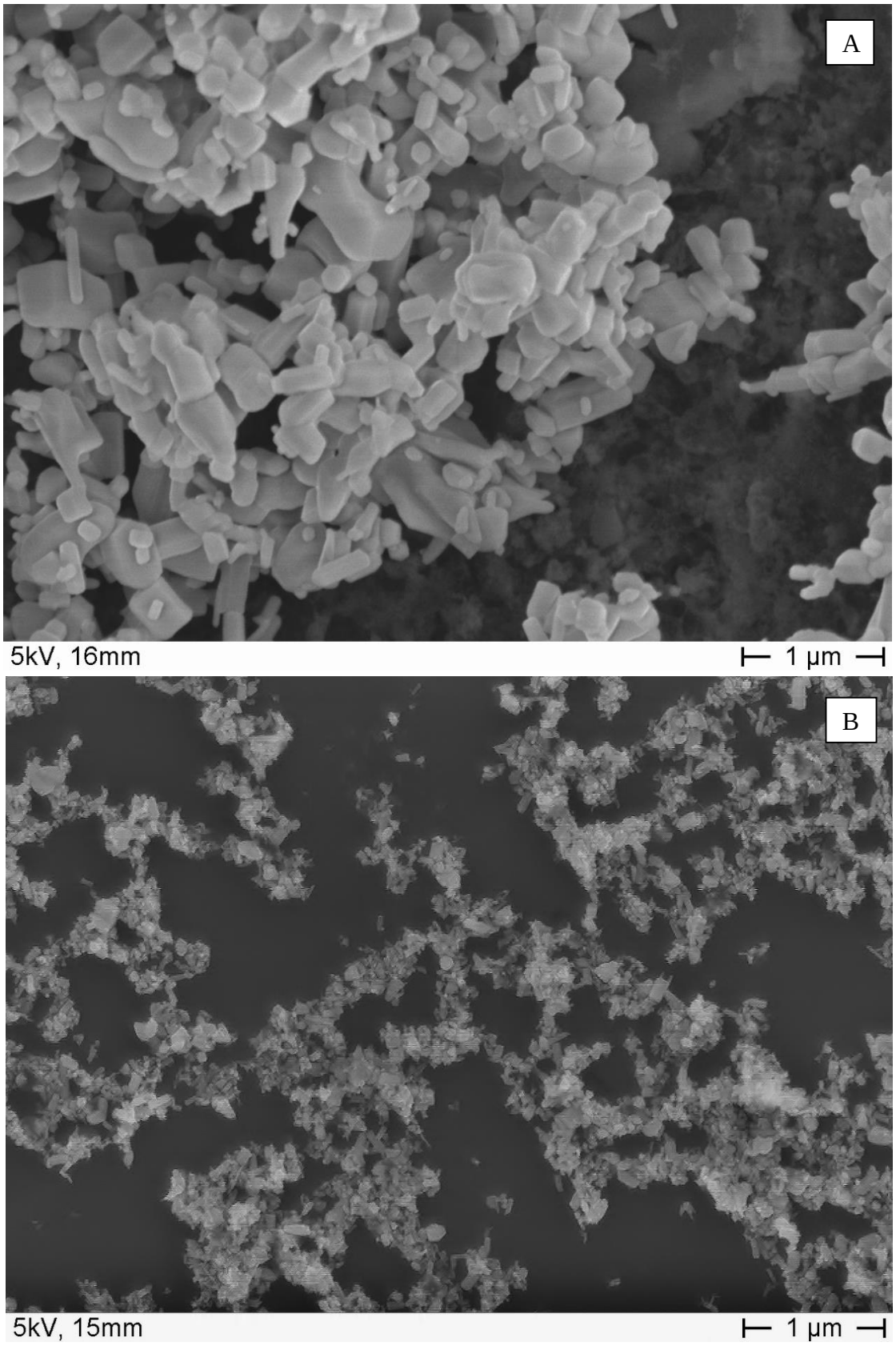


Figure 2.5 A & B: SEM images of bulk-sized ZnO particles (A) and 50 nm nZnO particles (B) taken with a JEOL 840 F SEM at 5 kV. Scale bar represents 1 µm.

2.3.5 Reactive Oxygen Species

Relative reactive oxygen species (ROS) release from ZnO was detected using the fluorescent dye coumarin and results were expressed as a percentage of the control (**Figure 2.6**). Contrary to the hypothesis that smaller sized particles would release greater quantities of ROS as a result of increased surface area to volume ratio, the converse was observed. The greatest fluorescence was measured from the bulk ZnO, and the least fluorescence was detected from the smallest 50 nm ZnO particles. The difference in fluorescence between the bulk particles and 50 nm nZnO particles was significant (p = 0.006), showing that bulk ZnO particles released statistically greater quantities of ROS than 50 nm nZnO particles.

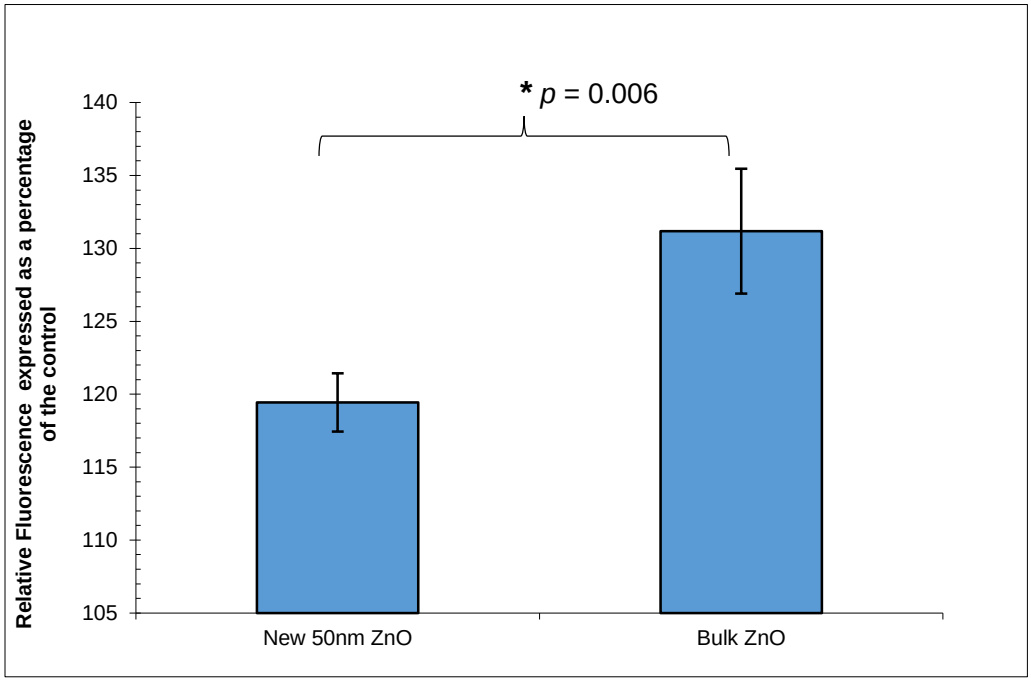


Figure 2.6: Relative fluorescence of 7-hydroxycoumarin produced after 72 h of exposure of coumarin to 50 nm and bulk-sized ZnO particles as a result of ROS release, displayed as a percentage of the negative control (DI water).

2.3.6 Zinc Dissolution Assay

The liberation of Zn^{2+} ions from 50 nm and bulk ZnO particles was examined by ultrafiltration and AAS quantification over time to determine the rate of dissolution. Graphs of concentration of Zn^{2+} in solution over time were plotted and displayed for 50 nm nZnO and bulk-sized ZnO in water (**Figure 2.7 A**) and in Hoagland solution (**Figure 2.7 B**).

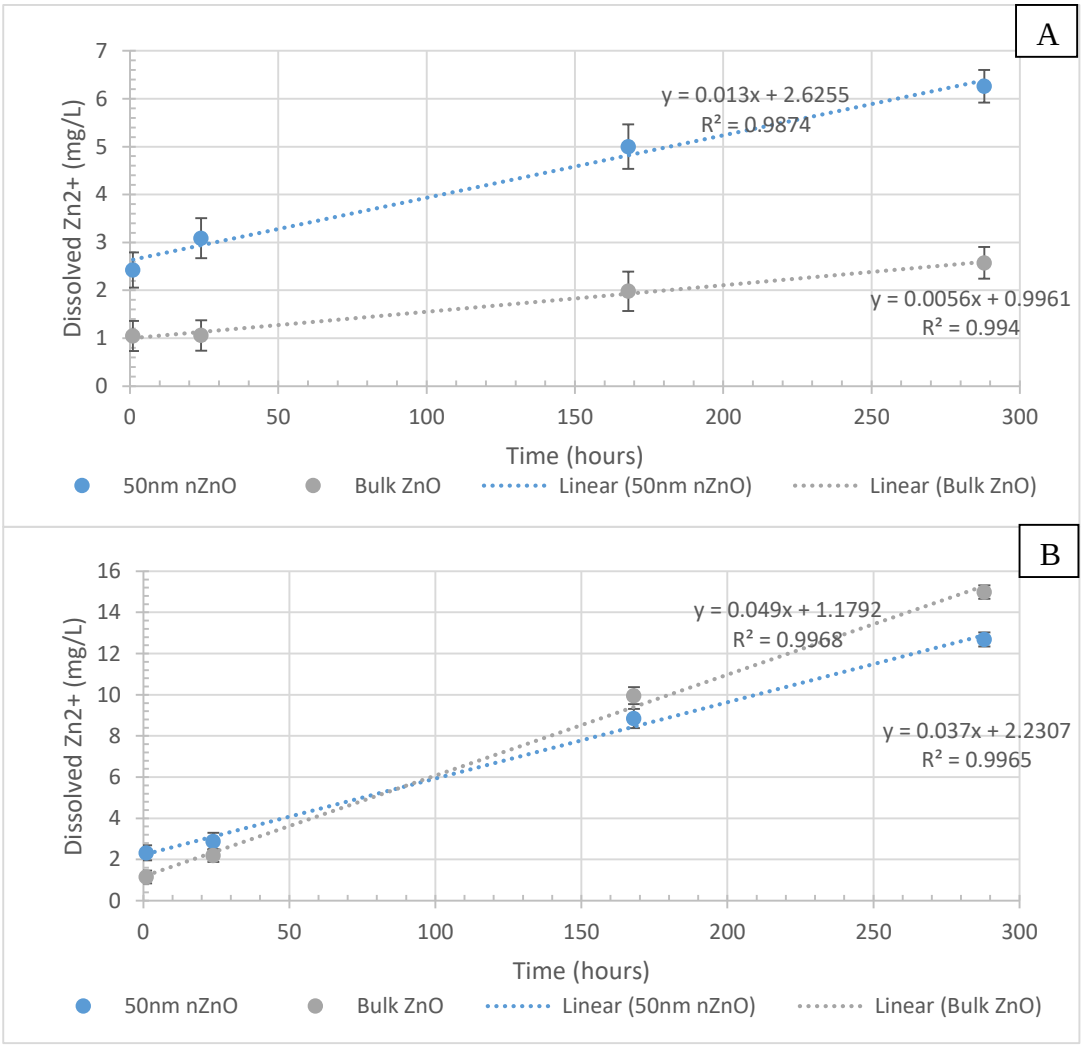


Figure 2.7 A & B: Dissolution of Zn^{2+} from 50 nm nZnO and bulk-sized ZnO particles over time as determined by ultrafiltration and filtrate analysis using AAS. Figures show dissolution in DI water (A) and in Hoagland solution (B). Linear trendlines displayed with line equation from which rate of dissolution was calculated.

As particles were sonicated for 1 h prior to the first measurement, readings were not taken in the first hour. During this time, initial solubilisation was rapid, likely due to sonication agitating particles and facilitating dissolution by promoting high dispersion and surface cavitation, as has been demonstrated previously for copper nanoparticles by Cronholm *et. al.* (2011).

Table 2.3: Summary of results from Zn dissolution assay of nZnO and bulk ZnO particles in DI water and Hoagland solution over time.

Particle type	**Media type**	**Dissolution rate ($\mu g\ L^{-1}\ h^{-1}$)**	**Y-intercept (mg/L)**	**% dissolved after 1 day**	**% dissolved after 7 days**
50 nm nZnO	DI water	13.0	2.63	3.47	5.61
" "	Hoagland solution	37.0	2.23	3.23	9.91
Bulk ZnO	DI water	5.60	0.996	1.07	2.00
" "	Hoagland solution	49.0	1.18	2.22	10.1

Results identified that nZnO released Zn^{2+} ions at a significantly greater rate than bulk ZnO particles in DI water. However, in Hoagland solution both particles released Zn^{2+} at a greater rate than in DI water, and converse to dissolution in DI water, the bulk particles released Zn^{2+} significantly faster than the nZnO particles ($p < 0.05$) (**Table 2.3**). The percentage of the particles that had dissolved after 1 day and 7 days in suspension ranged from between 2.00 % for bulk ZnO in DI water to 10.1 % for bulk ZnO in Hoagland solution. During the 288 hours of this experiment, the dissolution of Zn^{2+} ions never reached equilibrium and hence the relationship was linear.

2.3.7 UV Visible Absorbance

The absorbance of the nano-scale and bulk-scale ZnO particles was compared at 630 nm and 405 nm wavelengths at a range of particle concentrations (**Figure 2.8 A** & **B**).

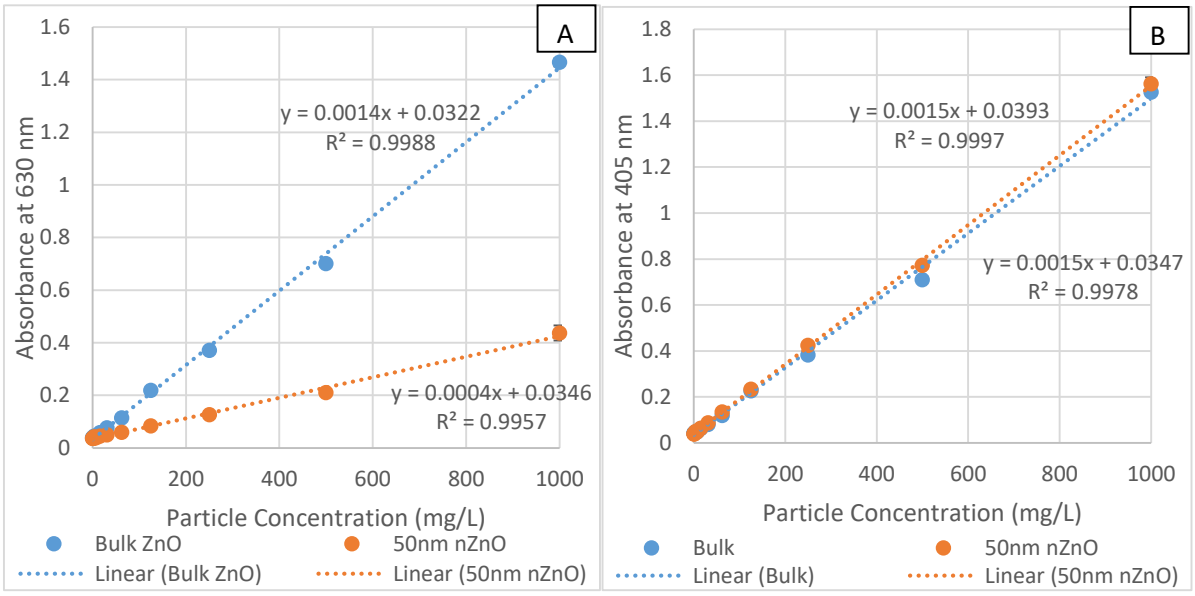


Figure 2.8 A & B: UV-visible absorbance at 630 nm (A) and at 405 nm (B) of bulk-sized and 50 nm ZnO particles dispersed in DI water over a concentration range from ~0.5 mg/L to 1000 mg/L. Absorbance values plotted against concentration with error bars showing one standard deviation above and below the mean. Linear trendlines plotted to fit data, with linear equations and R^2 values displayed on graphs.

For both particle types at both wavelengths the relationship between particle concentration and absorbance was linear up to the highest concentration tested of 1000 mg/L. This enabled linear trendlines of $R^2 > 0.99$ to be plotted in order to calculate and compare slopes, with slopes at 630 nm of 0.0014 and 0.0004 for bulk and 50 nm ZnO, respectively. The steeper gradient for bulk ZnO described the greater increase in absorbance per increment of concentration when compared to 50 nm ZnO. At 630 nm, the absorbance of bulk ZnO particles was considerably greater than for 50 nm nZnO, which was consistent with the literature in terms of smaller particles having lower absorption values at 630 nm

than larger particles (Goh *et. al.*, 2014). The energy gap for ZnO is 3.23 eV which can be used to calculate the UV wavelength below which all radiation will be absorbed using the quantum theory to produce a critical wavelength for maximum absorption of 385 nm (Fairhurst *et. al.*, 1997; More, 2007).

Incident UV energy is used for mobilisation of electrons within the atomic structure of ZnO. The proximity of 405 nm to this critical wavelength is able to explain the increased absorption relative to 630 nm. It is for this reason that nZnO offers excellent UVA and UVB absorption as their wavelengths fall between 320 and 400 nm.

These results confirmed that 50 nm nZnO had a much lower absorbance in the middle of the visible range (630 nm) than in the near UV range (405 nm), a property that allows particles to be much more transparent in sun cream formulations and yet offer the same absorbance as the bulk material near the UVA and UVB spectra. Results from this experiment were used in determining UV absorption from particles as distinct from bacterial cells at 630 nm for bacterial cultures in Chapters 3 and 6 of this report.

2.4. Discussion

Materials characterisation is an important part of evaluating particle toxicity in biological systems, with information on particle size and behaviour critical to understanding of how particles act in toxicity evaluations (Warheit, 2008). Hence, particle size, stability, ROS release, solubility and UV visible absorption for 50 nm nZnO and bulk-sized ZnO particles were examined in order to understand differences in particle behaviour when used in toxicity studies later in this project.

2.4.1. Zeta Potential Results Demonstrated Different Stabilities of Bulk and 50 nm nZnO Particles in Suspension

The pH of particle suspensions has a large role in determining the magnitude of the Zeta potential and also its charge. DVLO theory describes the stability of particles in a colloidal suspension as the sum of the attractive forces of the van der Waals and repulsive forces from the electrical double layer. Above the ZP value of ± 30 mV, the energy barrier is sufficiently large as a result of particle repulsion for the particles to remain apart and stable in suspension. Below this value the repulsive force may not be sufficient to overcome van der Waals attraction and hence if particles collide with enough energy they will be attracted to one another and flocculation will occur.

2.4.2. Particle Size for Both Particles was Defined using Complementary Methods

The particle size distributions for nZnO and bulk ZnO were measured using two different types of method; a centrifugation method based on particle movement through an increasingly viscous optically clear gradient, and a hydrodynamic method employing dynamic light scattering of a laser to determine hydrodynamic diameter of particles. It was expected that the bulk particles would be larger and more non-uniform than the engineered 50 nm nZnO particles due to their production being non selective for size or uniformity. This was confirmed by both methods and also visually by SEM imaging.

The results of the disc centrifugation method showed a bimodal size distribution for bulk particles that was not detected when DLS was used to establish hydrodynamic diameter. This is likely a result of larger particles producing a disproportionately large signal relative to the smaller particles and is a common limitation of measuring hydrodynamic diameter in non-uniform samples (Murdoch et. al., 2007). Hence, the centrifugation method was more

sensitive to smaller particles within the sample. For the 50 nm particles, the sample was more uniform and produced a broad single peak in both size determination methods. As expected, the hydrodynamic diameter was significantly larger than the diameter as measured by centrifugation and SEM visualization for both particles. Size determination revealed that bulk particles are significantly larger (around 700 nm) than 50 nm nZnO particles (around 85nm) and therefore provide a useful comparison for toxicity studies between nano and non-nano ZnO particles.

2.4.3. nZnO Dissolved Significantly Faster than Bulk ZnO in DI Water

The dissolution rates for bulk and nZnO particles were calculated from measurements of free Zn^{2+} separated by filtration from particle suspensions over time. The suspensions were initially sonicated for 1 h, during which rapid dissolution occurred. Up to 288 hours that this experiment spanned, the relationship between time and dissolution was linear and allowed calculation of dissolution rates. The rate of dissolution of nano-scale ZnO in DI water was higher than that of the bulk particles, as had been anticipated due to smaller particle size leading to an increased surface area to volume ratio.

The results obtained for particles in water were comparable to those in a study by Reed *et. al*. (2012), which used 70 nm ZnO particles and bulk ZnO purchased from Alfa Aesar, for which the calculated dissolution rates were 7.43 µg L^{-1} h^{-1} and 5.56 µg L^{-1} h^{-1}, respectively. The 50 nm and bulk ZnO particles in this study were found to have dissolution rates of 13.0 µg L^{-1} h^{-1} and 5.6 µg L^{-1} h^{-1} respectively, with a higher rate for the 50 nm particles than the somewhat larger particles in the study of Reed *et. al.* (2012). As solubility is linked to the surface area in contact with the dispersion liquid, this higher value of dissolution was not unexpected.

2.4.4. Bulk ZnO Dissolved at a Greater Rate than nZnO in Hoagland Solution

Significantly higher dissolution rates were measured for both particles in Hoagland solution than in DI water. Hoagland solution is a complex formula optimized to provide water and nutrients for plant growth in hydroponics. It contained nitrates, phosphates and sulphates in addition to a chelated form of iron, (ferric ethylenediamine-di-2-hydroxyphenylacetate). Although the iron chelate is highly stable, excess chelator could be present and facilitate Zn^{2+} dissolution from particles by binding free Zn^{2+} and shifting the dissolution dynamic in favour of higher Zn^{2+} release.

2.4.5. Mathematical Calculation of Particle Number Relative to Bacterial Cell Number

To understand the approximate numbers of particles involved in different concentrations used throughout this work, calculations were made based on diameters obtained in the disc centrifuge method (section **2.3.3**) with particle sphericity assumed for simplicity. The volume of a sphere can be calculated using the equation $\frac{4}{3}\pi r^3$ where r denotes particle radius. For the 50 nm nZnO particles, the radius was found to be approximately 42 nm, and for the bulk particles this value was around 351 nm, both values rounded to the nearest whole number.

Using this equation, the approximate volume of a single nZnO particle was calculated to be 3.10×10^{-16} cm^3 and the volume of a bulk particle was calculated to be 1.81×10^{-13} cm^3. The theoretical density of ZnO is 5.606 g/cm^3 (Morkoc & Ozgur, 2009) which was multiplied by each volume to provide the estimated mass of each particle, which for nZnO was 1.74×10^{-15} g and for bulk ZnO was 1.02×10^{-12} g. Using this value of mass per particle, the number of particles in a litre of 100 mg/L suspension was calculated to be 5.75×10^{13} for nZnO particles and 9.80×10^{10} for bulk particles. This demonstrated that the number

of nano-scale particles in a suspension of the same concentration outnumbered the bulk particles by 3 orders of magnitude.

When this is compared to the number of bacteria in a sample, approximate cell numbers can be calculated using McFarland turbidity. Later in this project (section **3.3.2**), the maximum optical density of bacterial cells reached around 0.7 measured at 630 nm wavelength after 24 hours growth. This is approximate to McFarland standard number 4, which equates to around 12 x 10^8 colony forming units (CFU) per ml (Sutton, 2011; Koch *et. al.*, 1970). Hence in one litre there would be around 1.2 x 10^{12} colony forming bacterial cells. When compared to the number of particles in one litre at 100 mg/L concentration, nZnO particles would outnumber the cells 50-fold whereas the cells would outnumber the bulk particles approximately 12-fold. This calculation was made using final bacterial optical density figures, and as such the particles will outnumber the cells by orders of magnitude more at low cell numbers at the beginning of the cell growth experiments.

This highlights the importance of dispersion and stability of particle suspensions. If the particles have sufficient charge as measured by zeta potential, they will be well dispersed and as such have maximum potential of interaction. If the zeta potential is low, the electrostatic repulsion is easily overcome and the particles will be attracted to one another due to van der Waals forces in order to diminish their high surface energy according to entropy. Hence, particles will crash out of suspension and no longer have the same potential for interaction, for example with bacterial cells or plant roots. Results from this chapter can be used in establishing key parameters involved in toxicity in subsequent chapters. There were significant differences in ZP, solubility and size between the bulk and 50 nm nZnO particles. Knowledge of these variables will allow comparison between toxic effects of nano-scale ZnO as compared with the bulk ZnO and ionic $ZnSO_4$.

3. EXAMINING THE TOXICITY OF NANO-SCALE ZINC OXIDE IN COMPARISON TO THE BULK SIZED AND IONIC FORMS TO *ESCHERICHIA COLI*

3.1. Introduction

Nanoparticle toxicity to bacteria is of interest for several reasons. Firstly, environmental release of nZnO will inevitably lead to contact with soil, which contains in the range of $1x10^6$ to $2x10^9$ colony forming units (CFU) of bacteria per gram of dry soil (Whitman *et. al.,* 1998). Hence understanding the influence these nanoparticles have on bacterial activity will indicate potential impact of environmental release (Vieira & Nahas, 2005). Secondly, antibiotic resistance is of growing importance as increasingly antibiotics are becoming ineffective against human pathogenic strains of bacteria (Aiken *et. al.,* 2014). Antimicrobial resistance occurs when a microbe develops a genetic mutation that enables it to survive the action of an antibiotic, for example ampicillin or methicillin. The World Health Organisation (WHO) global report on antimicrobial resistance recently stressed that global action is required to address the increasing level of resistance, and called for development of new antimicrobials (WHO, 2014). By analysing the antibacterial effects of nano-scale ZnO it can be determined whether it offers antibacterial properties which may be of environmental or medical relevance. In particular, by investigating toxicity using several complementary approaches it is possible to further understand the mode of action of nZnO on bacteria.

3.1.1. *E. coli* as a Model Organism

The definition of a model organism is one that is studied extensively in order to provide information and insight into the mechanisms of other organisms (Stewart *et. al.,* 2005). By conducting wide ranging experiments on one representative organism, large

quantities of data and understanding can be gathered and applied for similar or ancestrally related organisms. *Escherichia coli (E. coli)* was one of the first organisms to be studied as a model system for molecular microbiology, and has been used for over 60 years due to its ease of cultivation and rapid rate of growth. By investigating the growth inhibition and acute toxicity of nZnO on *E. coli*, information on toxicity of nZnO pertaining to Gram negative organisms can be gathered (refer to section **1.3.1** for Gram staining). In this study, two strains of *E. coli* were used to determine toxicity. Firstly, *E. coli* NCIMB #8879 was used for the growth inhibition assay to determine whether nZnO was bacteriostatic and hence inhibited growth. This strain was also used for the live-dead flow cytometry assay to determine whether nZnO was bacteriotoxic and led to absolute death of cells. The second type of *E. coli* used was modified with luminescence genes (*E. coli* HB101 pUCD607_lux) to act as a biosensor for acute toxicity from short term exposure with nZnO. Finally, an additional modified Gram negative bacterium, *Acinetobactor baylyi* was challenged with the zinc containing treatments to determine whether they demonstrated a genotoxic mode of action. In combination these methods will reveal how nZnO affects bacteria by using complimentary methods to elucidate the mechanisms of toxicity.

Previous studies have investigated the growth inhibition of nZnO on *E. coli* combined with TEM visualisation however this method is limited as it does not provide information on the viability of cells, only whether growth was inhibited and whether there were visual disruption effects (Connolly *et. al.*, 2013; Wang *et. al.*, 2012; Liu *et. al.*, 2009; Brayner *et. al.*, 2006; Thill *et. al.*, 2006). In addition, the toxic effects of nZnO are often either investigated alone or compared with either the bulk-sized or an ionic form and not both (Wang *et. al.*, 2012; He *et. al.*, 2011; Jiang *et. al.*, 2009). The work contained in this Chapter aims to determine cell viability, i.e. whether these growth-inhibited cells were dead, dying or alive, whether their metabolic activity was affected, and whether nZnO caused

damage to genes within the cell. Furthermore, it aims to compare the nano form of ZnO with both bulk-sized ZnO particles and Zn^{2+} from fully soluble $ZnSO_4$ in order to determine the main parameters involved in toxicity, such as Zn^{2+} and ROS release, zeta potential, and size as previously characterised in Chapter 2.

3.1.2. Biosensors

A biosensor may be defined as any biological material that interacts with an analyte via a transducer in order to provide information that can be measured and quantified (Zhang *et. al.,* 2011). This biological material can encompass a large range of options such as whole multicellular organisms, microbes and individual components such as antibodies and nucleic acid probes (Turner *et. al.*, 1987). A biosensor can also be likened to a 'canary in a cage', which was used to warn coal miners of dangerous gases such as methane or carbon monoxide, as the bird would be killed by the gases first and provide a warning to the miners. Similarly, whole cell bacterial biosensors such as those used in this study can act as the biological element to report toxicity of compounds; in this case nanoparticulate ZnO in comparison to the bulk and ionic forms.

There are two types of whole-cell biosensors, as distinguished by their mode of operation. Catabolic biosensors contain an inducible element, where the reporter gene is linked to a promoter which is able to be regulated by the compound under scrutiny, hence expression of the quantifiable element, for example a luminescent compound, increases in the presence of the compound to be detected (Song *et. al.,* 2009). Conversely, metabolic biosensors operate constitutively i.e. they are continuously expressing a quantifiable signal when alive and well, and expression decreases in the presence of the compound of interest, for example acutely toxic compounds. Metabolic biosensors are particularly useful for assessing the general toxicity of a compound whereas catabolic biosensors are useful for

detecting changes in a specific pathway (Zhang & Keasling, 2011; Yu *et. al.*, 2006). Whole-cell biosensors offer a useful system in which to test toxicity, as they are representative of many bacteria and also can be examined temporally, providing a dynamic measure of toxicity over time. In this study both a metabolic and a catabolic biosensor was employed, both of which used bioluminescence as the quantifiable signal. Together they were used to investigate whether ZnO was able to affect metabolism or cause genetic damage in bacteria.

3.1.2.1. Cellular Metabolism Biosensor *E. coli* HB101_pUCD607_ *lux*

The luminescent biosensor *E. coli* HB101 used had previously been transformed with a multi-copy plasmid containing the luxCDABE gene cassette (coding for luciferase enzyme) from luminescent marine bacterium *Vibrio fischerii* (Bhattacharyya *et. al.*, 2005). This enabled the cells to act as a biosensor by detecting a reduction in cellular metabolism in the bacteria as a result of contact with a toxic compound. The *lux* reporter genes are expressed throughout the normal cellular cycle, which produces a quantifiable luminescent signal based on ATP generation, the unit of energy used by the cell. Bioluminescence is proportional to the ATP production, and therefore if a compound disrupts ATP production the bioluminescence decreases measurably (Bellanger *et. al.*, 2015). This enables the biosensor to detect impairment or inhibition of metabolic activity in the cell, and hence the acute toxicity of test compounds, which can be quantified by measuring the decrease in luminescent signal.

3.1.2.2. Genotoxicity Biosensor *Acinetobacter baylyi* ADP1_*recA_lux*

The luminescent biosensor *A. baylyi* ADP1_*lux_recA* is a Gram negative bacterium that has been modified with genes from *Photorhabdus luminescens* in order to detect gene damage. This is achieved by the integration of the luminescent genes luxCDABE into *recA*,

a gene required in DNA repair (Song *et. al.,* 2009). DNA damage is indicated by regions of single-stranded DNA as opposed to normal double-stranded DNA. When DNA is damaged, *recA* is expressed in order to produce RecA protein which then repairs damaged DNA. This DNA damage is caused if a substance is genotoxic, and if so, the cells bioluminesce. The magnitude of luminescence is directly proportional to the quantity of RecA protein expressed, and hence it can be determined whether a compound has a genotoxic mode of action by measuring the luminescence relative to the control.

3.1.3. Al_2O_3 Dopant

As the 50 nm nZnO particles are doped with 6 % Al_2O_3 it was important to establish whether Al_2O_3 would have a toxic effect to *E. coli*. At 6 % by weight Al_2O_3, the concentration of Al_2O_3 within the ZnO nanoparticles was low. In this project, the maximum concentration of nZnO used was 1000 mg/L, which equated to a maximum theoretical concentration of 60 mg/L of Al_2O_3 in 1000 mg/L of nZnO particles, which assumed total dissolution of particles. In section **2.3.6** it was demonstrated that less than 6 % of bulk or nZnO particles had dissolved after 7 days in water, and as the particles were doped i.e. the Al_2O_3 was distributed throughout the particle not just coated on the surface, the maximum actual concentration of released Al_2O_3 would have been less than 4 mg/L.

From the literature several studies had demonstrated that nano-scale Al_2O_3 had no significant effect on toxicity to *E. coli* when tested over 62.5 to 250 mg/L (Sawai *et. al.,* 1995) and moderate toxicity effects were observed only at very high concentrations of 1000 mg/L (Sadiq *et. al.,* 2009). In addition, preliminary tests conducted in this study indicated that 50 nm Al_2O_3 nanoparticles (Sigma Aldrich, UK) below 125 mg/L did not inhibit growth of *E. coli* significantly more than the control (data not shown). Hence it was not considered necessary to use an Al_2O_3 control for such a low possible concentration in this study.

3.1.4. Flow Cytometry

A flow cytometer is a laser-based technology which enables the analysis of multiple parameters of thousands of cells per second by analysing the scatter of light and quantifying fluorescence (Diaz *et. al.*, 2010). Cells suspended in liquid are drawn through a capillary to align the cells to pass through a laser beam. The flow cytometer can be used to excite specific fluorescent stains with which bacteria have been incubated. Stains such as propidium iodide (PI) and SYBR green can be used in combination to report cell viability in a live/dead assay (Berney *et. al.*, 2007). Propidium iodide is used as a dead stain as it can penetrate the cell membrane of dying (moribund) or dead cells, however is excluded by live cells due to its size and charge (Hewitt *et. al.*, 2004). This provided a red signal when cells were dead or moribund, which was collected by the FL3 (red) fluorescence channel. The live stain SYBR green is a membrane permeable nucleic acid stain which binds to double-stranded DNA in preference to single-stranded DNA or RNA, and hence enters all cells but only stains live cells which contain double stranded DNA (Phe *et. al.*, 2005). The green signal was acquired via the FL1 (green) channel. SYBR green has been demonstrated to be over 10 times more sensitive than the frequently used mutagenic intercalating agent, ethidium bromide, and hence was chosen for this project in the quantification of live cells (Singer *et. al.*, 1999).

3.1.5. Statistical Analysis

Data was collected in triplicate from which the means and standard deviations were calculated. Statistical analysis was performed using a Student's t-test for pairwise comparisons, or one-way ANOVA where required. For the growth inhibition, concentration was transformed by $\log_{10}$ to produce a linear trend, and interaction of particle type and concentration was determined by use of two-way ANOVA using MINITAB version 14 (student release) software, with $p \leq 0.05$ considered significant.

3.1.6. Chapter Aims

The aims of the work reported in this chapter were to use complementary techniques to establish whether particles killed, inhibited or were acutely toxic to *E. coli,* and to detect genotoxicity using the biosensor *A. baylyi*. This provided a novel approach to determine mechanisms behind nanoparticle toxicity by comparing bulk, 50 nm nZnO and soluble $ZnSO_4$ in Gram negative bacteria, and toxicity data was related to the characteristics of the particles as determined in Chapter 2.

3.2. Materials and Methods

3.2.1. Acute Toxicity ATP-Linked Biosensor *E. coli*

Stock suspensions of the *E. coli* HB101_pUCD607_ *lux* biosensor for the acute toxicity experiments were prepared in the following manner. Lysogeny broth agar was made with 5 g/L glucose and 50 μg/ml ampicillin (LBG-A agar). The addition of the antibiotic selected for cells containing the modified plasmid and inhibited growth of non-plasmid containing cells. Frozen glycerol stocks (-80 ˚C) of *E. coli* HB101_pUCD607_ *lux* were streaked out on sterile LBG-A agar plates which were then incubated at 30 °C for 16 h. One colony was selected to be inoculated into 5ml lysogeny broth-Miller (with 5 g/L glucose and 50 μg/ml ampicillin (LBG-A broth) and this seed culture was then incubated at 35 °C at 150 rpm agitation for 6 h to produce an overnight culture. Both LB broth and agar powders in addition to glucose and ampicillin were purchased from Sigma Aldrich, UK, and media were made as per the manufacturer's instruction prior to autoclaving.

To obtain results of how luminescence changes over time and hence determine an optimum growing schedule, 1 μl of this overnight culture was added to each of 12 wells of a 96 well plate containing 199 μl of LBG-A broth. The plate was immediately placed in the

microplate reader, with luminescent reads taken every 30 minutes for 24 hours, incubated at 30 ºC throughout.

For the acute toxicity assessment of the different zinc containing treatments, 5 ml of the overnight culture were added to 95 ml of sterile LBG-A broth. The culture was incubated at 30 °C with shaking at 150 RPM for 8 hours to enable the cells to enter mid-exponential growth phase. Ten ml of this culture was transferred to sterile centrifuge tubes and centrifuged at 3000 rpm for 5 minutes to pellet the cells. Supernatant was discarded and cells were re-suspended in 10 ml sterile DI water.

Particle suspensions and $ZnSO_4$ solutions were made in either sterile DI water or 20 % Hoagland solution over a range of concentrations and sonicated for one hour. Hoagland solution is a plant nutrient media for hydroponic plant growth used later on in this study (section **5.2.2**). Aliquots of 180 µL of the required treatments were transferred by pipette into each well of a black 96 well flat, clear-bottomed plate (Nunclon, UK) in triplicate. Subsequently 20 µL of prepared *E. coli* HB101 cell suspension in DI water was then pipetted into the required wells. The plate was then placed into a BioTek Synergy HT microplate reader (BioTek Corporation, UK) on a continuous medium intensity shaking setting for 30 minutes before luminescence readings were taken. Luminescence signal from just the particles at each concentration was measured prior to analysis as a control and found to be minimal (below 100 RLU) and not significantly different to values from the water control as determined by one-way ANOVA [$F(3, 92) = 0.119$, $p = 0.948$], hence it was established that there was no need to subtract the background values from the luminescence values to control for luminescence as a result of particles as opposed to ATP-linked bacterial bioluminescence.

3.2.2. Genotoxic Assay with *A. baylyi*

Overnight culture and growth of *A. baylyi* was conducted as above for *E. coli* HB101, with the addition of 50 µg/ml kanamycin antibiotic in place of ampicillin in the broth to produce LBG-K broth, and all other culturing steps remained the same. The treatments of bulk ZnO, 50 nm nZnO and $ZnSO_4$ were made at two concentrations of 100 mg/L and 500 mg/L in DI water and sonicated for one hour. Eighty µl of LBG-K broth was pipetted into each well of a black, clear bottomed 96 well plate in addition to 100 µl of each treatment and 20 µl of *A. baylyi* suspension in DI water. This produced a final concentration of 50 mg/L and 250 mg/L for each zinc-containing treatment, in a total volume of 200 µl per well. The plate was then read for luminescence (light output) and absorbance at 630 nm (optical density for cell numbers) in a BioTek Synergy HT plate reader every 30 minutes for 6 hours. A negative control was included as the *A. baylyi* ADP1 cells had a baseline level of luminescence due to normal *recA* expression in cell maintenance. Hence all results were expressed as a percentage of the control. This was calculated after dividing the means of collected luminescent values by the means of the triplicate optical density values. This was performed in order to standardise the luminescence output to the number of cells in the sample and facilitate comparison. This was required as a strong luminescent signal could be a result of a few cells luminescing strongly, or many cells luminescing weakly, hence by controlling luminescence to optical density (which was directly proportional to cell number) it was possible to control for this effect (Sutton, 2011).

3.2.3. *E. coli* Growth inhibition

Overnight cultures of non-luminescent *E. coli* (national collection of industrial bacteria (NCIMB) #8879) were prepared in the same manner as *E. coli* HB101_pUCD607_ *lux* (section **3.2.1**) however with the omission of ampicillin antibiotic. Five ml of this overnight bacterial culture was transferred to 95 ml of sterile nutrient broth solution and

incubated at 30 °C for 8 hours to reach mid-exponential phase. This was then used to inoculate wells in a clear Nunclon 96-well flat-bottomed microplates to determine bacterial growth in the presence of different concentrations zinc-containing treatments. Growth was measured using optical density at a wavelength of 630 nm to detect cell density over 24 hours, and each combination of the ZnO particle types with bacteria was repeated in technical triplicate. Recorded values were then corrected for particle absorption using absorbance data at 630 nm acquired in section **2.3.7**, in order to produce an absorbance value as a result of bacterial growth alone.

3.2.4. Live-Dead Flow Cytometry Assay

In order to establish the proportions of live to dead *E. coli* bacteria after treatment with the zinc containing treatments, differential staining of cells with Propidium Iodide (PI) and SYBR green (both Invitrogen, UK) enabled the determination of whether the treatments were able to kill the cells i.e. bactericidal, or inhibited their growth, i.e. bacteriostatic.

Sufficient *E. coli* culture in LB broth at mid-exponential phase was transferred into a 250 ml borosilicate flask and diluted with additional LB broth until the concentration reached approximately 3 x 10^8 Colony Forming Units (CFU) as established by visual comparison to 1.0 McFarland turbidity standard (Fisher, UK). Nine ml of this diluted bacterial culture was then transferred under aseptic technique into each 50 ml polypropylene centrifuge tube (Fisher Scientific, UK) in addition to 1 ml of either 50 nm, bulk or $ZnSO_4$ suspensions at a concentration of 5000 mg/L in triplicate. Mixtures were vortexed for 30 seconds before being incubated at 30 °C with 200 RPM shaking for 4 hours. A live control was included which contained 1 ml DI water added in place of the particle suspensions and was incubated together with the other samples.

After 4 hours incubation, the samples were further diluted 100-fold with sterile DI water so that the concentration of cells was below 3 x 10^6 CFU, and the particle concentration was below 5 mg/L. One ml samples were taken from each combination and pipetted into a 1.5 ml Eppendorf vial (Fisher Scientific, UK) along with the two stains, one to stain live cells (SYBR Green (1:10^4 dilution)) and one to stain dead cells (PI (10 µg/ml)) and incubated at 25 °C for 15 m. In addition, three Eppendorf vials containing 1 ml of control live cells were heated at 70 ºC in a heat block for 15 minutes to kill cells and provide a dead control, to which the live and dead stains were added as above. All samples were then analysed using an Accuri C6 Flow Cytometer (BD Biosciences Europe, Oxford, UK) with laser excitation wavelengths of 488 nm and 640 nm. Samples passed through a 4 µm capillary and for each recorded sample a volume of 30 µl was analysed. The FL1 fluorescence channel at 530 nm was used to collect the data from the SYBR Green stain and the FL3 channel at 585 nm was used to collect data from the red PI stain. Cells which were in the process of dying were classed as moribund as they had compromised cell membranes and hence were able to uptake both stains (Davey & Kell, 1996; Kaprelyants & Kell, 1992). They occupied a separate grouping between live (green) signal and dead (red) signal when the FL1 and FL3 scatter was examined, which was gated and quantified in addition to the live and dead groups.

3.3. Results and Discussion

3.3.1. *Escherichia coli* Growth Inhibition

Growth inhibition of *E. coli* after 24 hours exposure to a range of concentrations of zinc-containing treatment was measured using optical density at a wavelength of 630 nm in order to determine whether the treatments caused reduced bacterial growth (**Figure 3.1**). The concentration values (mg/L) were transformed by $\log_{10}$ to produce a linear graph from which a line equation could be calculated. A two-way ANOVA was performed to determine

whether concentration and treatment type significantly affected growth inhibition. Treatment concentration was demonstrated to be highly significant [F (10, 98) = 52.19, $p < 0.0001$] in predicting growth inhibition of *E. coli*.

Particle type alone did not significantly affect OD_{630} ($p = 0.36$) however the interaction between treatment type and concentration was demonstrated to be significant [F (20, 98) = 2.16, $p = 0.010$]. This revealed that the combination of particle type and concentration predicted the growth inhibition. However, the treatment concentration alone was a stronger predictor. Nano-scale ZnO was not significantly more inhibitory than the bulk-sized ZnO or ionic $ZnSO_4$. From the linear equations, the concentration at which 50 % of *E. coli* growth was inhibited (IC_{50}) was calculated to be approximately 251, 282 and 398 mg/L for bulk ZnO, 50 nm nZnO and $ZnSO_4$ respectively.

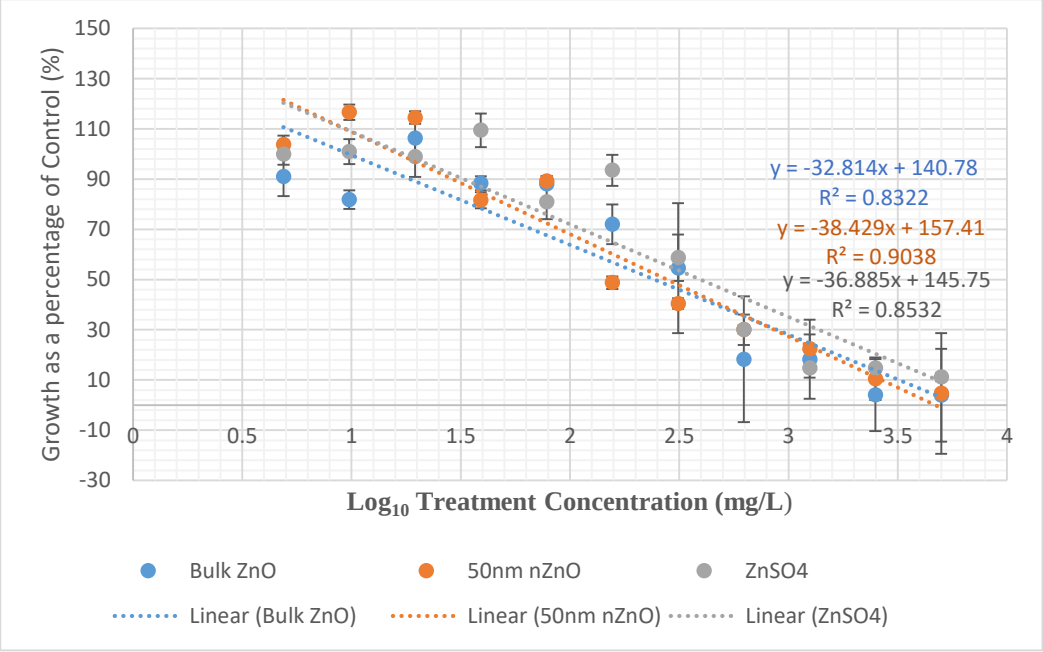


Figure 3.1: **Optical density of *E. coli* bacteria demonstrating 24-hour total growth in the presence of three zinc-containing treatments over a range of concentrations, transformed by log_{10}. Error bars denote one standard deviation above and below the mean ($n = 3$).**

3.3.2. Acute Toxicity to *E. coli* HB101

The acute toxicity biosensor *E. coli* HB101 was employed to determine the short term toxicity of the nanoscale and bulk ZnO particles and $ZnSO_4$. The bioluminescent output of *E. coli* HB101 inoculated into LBG-A broth was measured over 24 hours and results were displayed in **Figure 3. 2**. This demonstrated the period of optimum increasing luminescent output to be between 8 hours and 13 hours, and hence all subsequent acute toxicity experiments were conducted using bacteria grown to within this time frame of exponential increase of luminescent signal. High and increasing values were required in order to detect toxicity, because if the control values were decreasing, there would be difficulty in distinguishing whether the decrease in luminescence was due to bacterial senescence or due to the effects of treatment (Kjelleberg, 1993).

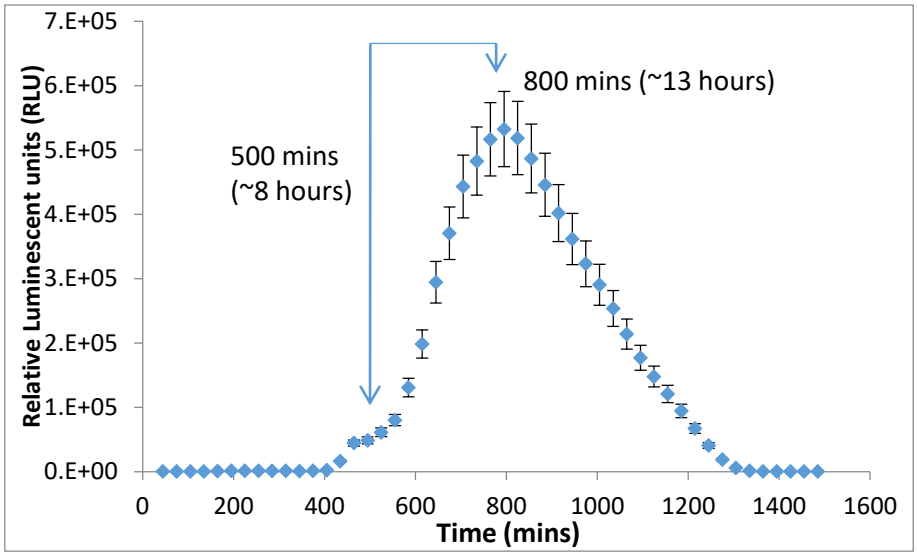


Figure 3. 2: **Relative luminescent output of *E. coli* HB101 inoculated into LBG-A broth and incubated over 24 hours. Error bars denote one standard deviation of triplicates.**

Acute toxicity experiments were conducted using the three different zinc-containing treatments in order to determine the consequences of short term (30 minute) exposure on ATP production in *E. coli* HB101. This was performed because bacterial toxicity may be an indicator of general biological toxicity (Lei *et. al.*, 2006). The percentage of ATP-linked

luminescence after 30 minutes exposure was calculated relative to the control and displayed in **Figure 3.3** for treatments dispersed in water (**A**) and Hoagland solution (**B**).

For the particles dispersed in DI water (**Figure 3.3 A**), acute toxicity to all treatments increased as the concentration increased.

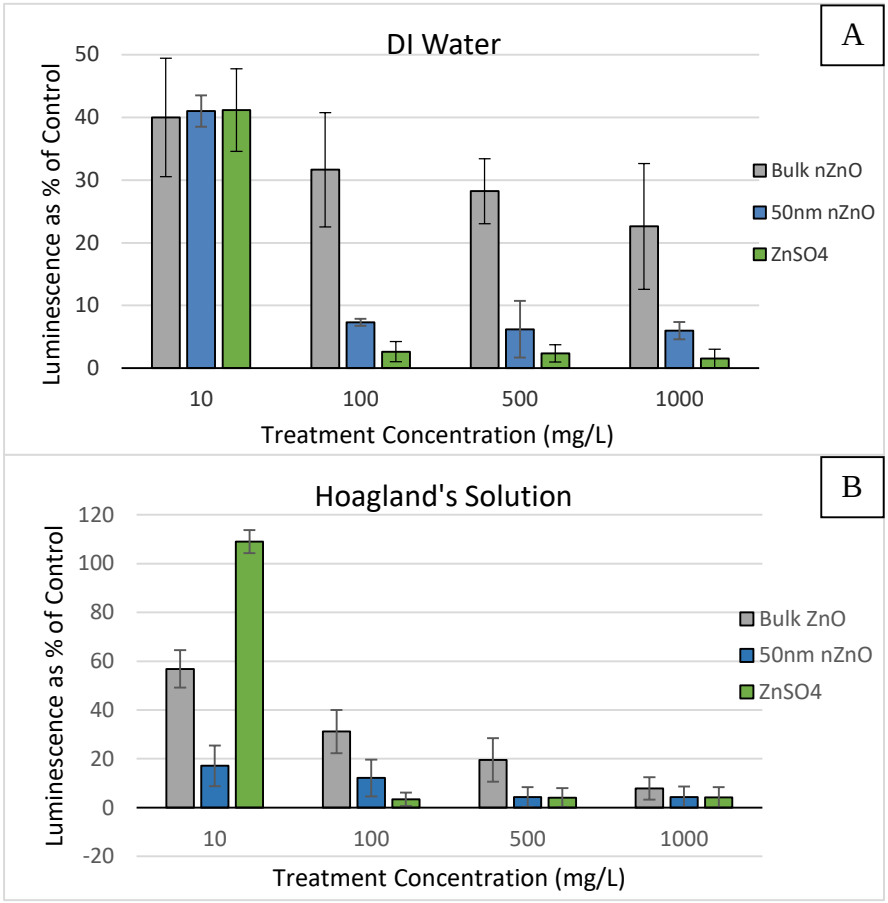


Figure 3. 3 A & B: Bioluminescent output depicting acute toxicity after exposure to three treatments; nanoscale and bulk ZnO particles and $ZnSO_4$, at 4 concentrations to luminescent *E. coli* HB101 for 30 minutes, expressed as a percentage of the control. Treatments dispersed in DI water (A) or 20 % Hoagland solution (B). Error bars represent one standard deviation of triplicates.

At the lowest concentration of 10 mg/L, treatments had reduced the luminescence by around 60 % relative to the control, however there was no significant difference between treatment types ($p < 0.01$). This demonstrated that all three treatments were similarly acutely toxic at a concentration of 10 mg/L. At the higher concentrations of 100, 500 and 1000

mg/L, the luminescence after treatment with nano-scale ZnO and $ZnSO_4$ had decreased significantly ($p < 0.001$) to around 6 % and 3 % of the control respectively.These values were consistent at all three of the concentrations of nZnO and $ZnSO_4$, which demonstrated that at 500 or 1000 mg/L, the toxicity was not significantly different to that from a concentration 100 mg/L when dispersed in water. With the bulk, however, the decrease in luminescence was not as pronounced, with the lowest luminescent output reaching 22 % of the control. The luminescence after bulk treatment revealed a downward trend with increasing concentration, however differences after treatment with 100-1000 mg/L were not significant ($p > 0.05$).

When the treatments were dispersed in the plant-growth media Hoagland solution, the acute toxicity response was different to that in water (**Figure 3.3 B**). At the lowest concentration of 10 mg/L, all treatments were significantly different from one another ($p < 0.05$), with 50 nm nZnO demonstrating the highest level of acute toxicity with values of around 20% that of the control. This demonstrated that in Hoagland solution, 50 nm nZnO was significantly more acutely toxic than in DI water ($p < 0.01$). The $ZnSO_4$ at this concentration demonstrated no significant toxicity in Hoagland as compared to the control ($p = 0.34$) which was significantly less toxic as compared to when it was dissolved in DI water (around 40 % and 110 % respectively). At the higher concentrations of 100 mg/L to 1000 mg/L, $ZnSO_4$ caused more than 95% reduction in luminescence which demonstrated that it was highly acutely toxic, followed by 50 nm nZnO at 90% decrease or greater, and finally bulk ZnO. In summary, Hoagland solution increased the toxicity of particles, and reduced the toxicity of the lowest concentration of $ZnSO_4$.

These results demonstrated that the acute toxic response of bioluminescent *E. coli* depended on the media in which the treatments were dispersed. In DI water at 10 mg/L, all treatments were similarly toxic however this was not the case when dispersed in Hoagland

solution, where the nano-scale ZnO was the most toxic. The increased toxicity of the particulate treatments when in Hoagland solution was unexpected, as the increased solute potential of Hoagland solution when compared to DI water was anticipated to reduce osmotic shock of bacterial cells. Osmotic pressure is a colligative property i.e. dependent on quantity of solutes within a solution rather than the types of ion present hence it was known that Hoagland solution was of higher osmotic pressure than DI water (Landowne, 2006). It was possible that compounds within the Hoagland solution increased the toxicity of the treatments, perhaps producing a synergistic increase in toxicity when in combination. However, when the dissolution of particles in DI water and Hoagland solution was investigated in section **2.3.6** it was demonstrated that the solubility of both bulk and nano-scale ZnO was higher in Hoagland solution than DI water. This could explain the increased toxicity of particulate treatments in Hoagland solution as compared to DI water.

The Hoagland solution also contained the divalent ion chelator EDDHA, purchased pre-bound to iron. If it was produced by the manufacturer with an excess of the unbound chelator molecule (which is likely as it would ensure all of the iron was chelated), this could explain the significant reduction in toxicity of the ionic treatment, $ZnSO_4$, as Zn^{2+} can also bind to EDDHA, and hence would effectively have been removed from solution. This may have contributed to the reduced toxicity of $ZnSO_4$ in Hoagland solution as opposed to in DI water. However, the greater toxicity of particles suggested that this may not have been the case, as the measured solubility of Zn^{2+} was higher in Hoagland solution and by this theory would have become bound by EDDHA. However, if Zn^{2+} was bound to a chelator the solubility testing method was unable to distinguish between EDDHA-Zn and free Zn^{2+}. The balance between solubility and Zn^{2+} chelation therefore could be important in determining acute toxicity of the zinc-containing treatments.

In addition, the zeta potential (surface charge) of the nano and bulk-scale ZnO particles was investigated in both DI water and Hoagland solution in section **5.3.8.** Surface charge indicated particle stability, and it was demonstrated that nZnO was more stable than bulk ZnO in DI water and hence was significantly more disperse. In Hoagland however the difference was smaller, with bulk particles detected to be slightly less stable than nZnO particles but not to the same degree as in DI water. This trend was reflected in the acute toxicity data, as bulk and nano ZnO treatments caused a greater difference in toxicity when in DI water than in Hoagland solution, with the more stable treatment, nZnO, being more toxic in both instances. This demonstrated that particle stability, as measured by zeta potential, is likely a strong indicator of bioavailability – a major factor in toxicity, as the better dispersed the particles were, the greater the chance for interaction and hence greater propensity towards toxicity.

3.3.3. Genotoxicity to *A. baylyi*

The ability of the three zinc-containing treatments to induce bacterial gene damage was investigated using luminescent genotoxicity biosensor *A. baylyi* (**Figure 3.4**). An increase in luminescence represented upregulation of *recA* to produce RecA protein involved in DNA repair, and hence indicated gene damage. It was demonstrated that 50 mg/L of each treatment (**Figure 3.4 A**) caused an increase in genotoxicity relative to the control after 3 hours exposure. At each time point the toxicity of 50 nm nZnO was significantly lower than with bulk ZnO or $ZnSO_4$ ($p < 0.05$). This indicated that 50 nm nZnO induced a lower level of DNA damage when compared with the same concentrations of the bulk-sized ZnO or $ZnSO_4$. This was contrary to the acute toxicity results which previously demonstrated that 50 nm nZnO caused greater acute toxicity than bulk ZnO to *E. coli* HB101. However, the inhibition assay corroborated the genotoxicity data, as it also demonstrated that bulk ZnO was more inhibitory to *E. coli* as it had a lower IC_{50} value than 50 nm nZnO, followed by

$ZnSO_4$ (251, 282 and 398 mg/L respectively). For $ZnSO_4$, the genotoxic response was similar to that induced by bulk ZnO, as the luminescence values were not significantly different at 10 out of 13 time points ($p < 0.05$).

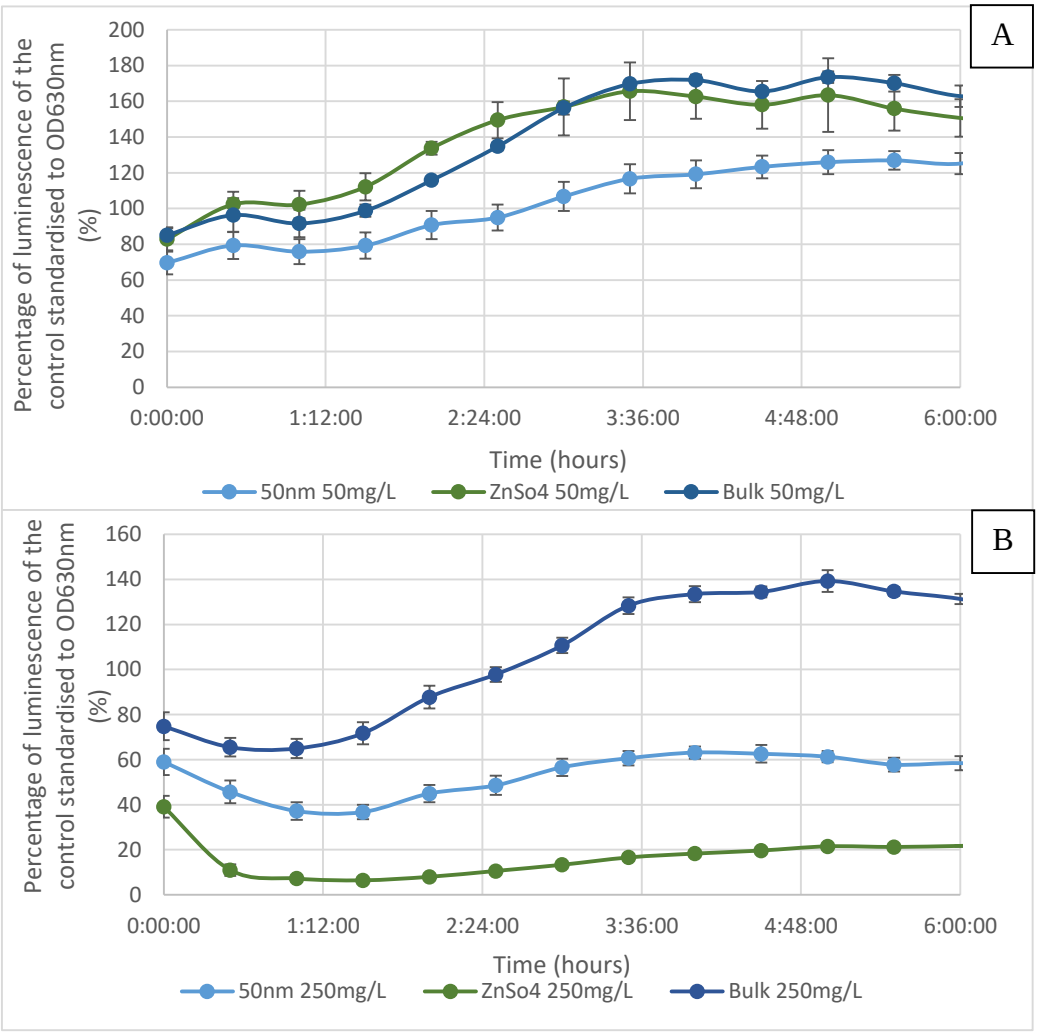


Figure 3.4 A & B: Bioluminescence of genotoxicity biosensor *A. baylyi* after exposure to three treatments, nanoscale and bulk ZnO particles and $ZnSO_4$ over time, at 50 mg/L (A) and 250 mg/L (B). Values expressed as a percentage of the negative control and standardised to optical density as measured at 630nm to control for bacterial growth. Error bars represent standard deviation of triplicates.

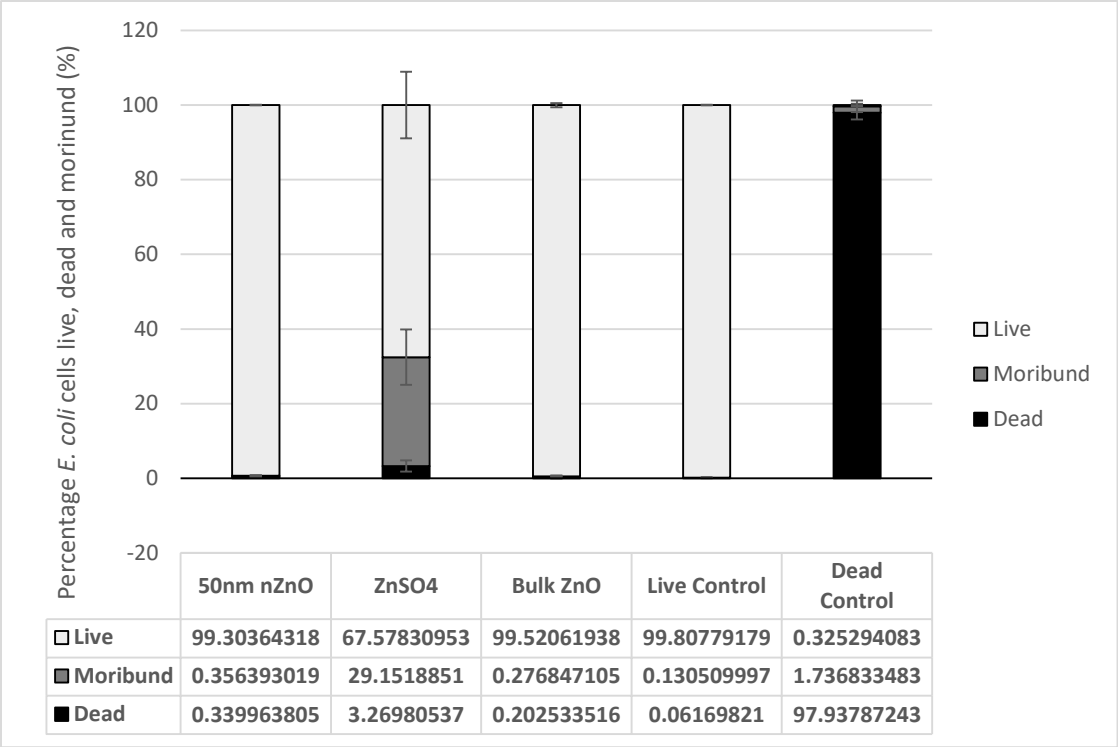
In addition, the luminescence of *A. baylyi* after a higher treatment concentration of 250 mg/L was also measured and the results were displayed in **Figure 3.4 B**. At all of the time points the treatments had significantly different luminescence values ($p < 0.01$), with a significant increase in genotoxicity relative to the control detected after bulk ZnO treatment.

The response from $ZnSO_4$ treatment was very low, with values of around 20 % or below that of the negative control. This indicated that serious cell damage had occurred which interfered with or prevented the luminescent output from being detected (Chan *et. al.,* 2013). These results indicated that the lower treatment concentration of 50 mg/L, as displayed in **Figure 3.4 A,** was a more appropriate concentration for comparison of genotoxicity of the test compounds.

3.3.4. Flow Cytometry

After having determined the acute, inhibitory and gene toxicities of the three treatments, cell death was quantified using flow cytometry. This method furthered the understanding of the mechanisms of toxicity for all three treatments. Flow cytometry of *E. coli* cells treated with a high concentration of 500 mg/L of each 50 nm nZnO, bulk ZnO and $ZnSO_4$ was conducted in conjunction with live and dead stains in order to determine whether the treatments resulted in cell death or morbidity (**Figure 3.5**).

Data was analysed by plotting log FL3 Red (dead) versus log FL1 Green (live) scatter and using four gates to distinguish background scatter, live, dead and moribund *E. coli* cells. Data was displayed as percentage of total counts (with background scatter excluded) for each treatment all at 500 mg/L concentration. The results indicated that the proportion of dead cells was less than 0.5 % after treatment with bulk or nano-sized ZnO particles, with no significant differences in dead, moribund or live cell number between the two treatments (p = 0.255, p = 0.330 and p = 0.274 respectively). This revealed that both the nano form and bulk forms of ZnO resulted in the same numbers of live, moribund and dead cells within error, and indicated that their potential effect of absolute death in *E. coli* was similarly minimal. With $ZnSO_4$ however, significantly more cells were dead and moribund, and fewer were live (in all comparisons $p<0.05$).



	50nm nZnO	ZnSO4	Bulk ZnO	Live Control	Dead Control
Live	99.30364318	67.57830953	99.52061938	99.80779179	0.325294083
Moribund	0.356393019	29.1518851	0.276847105	0.130509997	1.736833483
Dead	0.339963805	3.26980537	0.202533516	0.06169821	97.93787243

Figure 3.5: Proportion of dead, moribund and live *E. coli* cells using flow cytometry in conjunction with live stain (SYBR Green) and dead stain (Propidium Iodide) after treatment for 4 hours with 500 mg/L ZnO. Error bars represent one standard deviation of triplicates. Table includes percentages of live, dead and moribund cells for comparison.

This demonstrated that the ionic form of Zn^{2+} had a greater bacteriocidal effect on *E. coli* than either of the two particulate treatments. This revealed that Zn^{2+} ions had a large role in absolute death in cells, whereas 4 hours exposure of the high concentration of 500 mg/L of nanoparticulate ZnO did not cause cell death. In addition, cells that were able to uptake both stains were classed as moribund. This property indicated that there was structural damage to the bacterial membrane, which had increased their porosity and reduced their selectivity. Minimal quantities of cells were classed as moribund after treatment with both particle types, however, with $ZnSO_4$, nearly 30% of cells fell into this category. This demonstrated that the quantity of Zn^{2+} ions contained in 500 mg/L $ZnSO_4$ (~114 mg/L as determined by calculation from molecular weight) was sufficient to damage the membrane enough to allow entry of the nucleic acid stain PI which is normally excluded by healthy cell

membranes. This identified a mechanism of toxicity induced by high levels of Zn^{2+} ions as being cell membrane disruption, which was not detected after treatment with the nano-scale or bulk-sized ZnO particles. This is likely due to their significantly lower solubility of 13.0 and 5.6 µg L^{-1} h^{-1}, respectively, and provided evidence that high Zn^{2+} release strongly correlated to cell morbidity and death.

The results indicated cell membrane disruption which was concordant with the findings of Brayner *et. al.* (2006) which demonstrated that smaller 20nm nZnO particles caused triple membrane disorganisation and lead to internalisation of nZnO particle in *E. coli*, however this was determined by TEM analysis and hence was a non-numerical observation. The results from this live/dead assay clarified the biocidal effect by quantifying cells which were dying or dead after treatment, which demonstrated that the numbers of dying or dead cells after particulate treatment were minimal in comparison to treatment with $ZnSO_4$. It also demonstrated that at the same concentration, nano ZnO was no differently bacteriocidal to the bulk-sized ZnO, which was also reflected in the growth inhibition results.

3.4. Discussion

The research detailed in this chapter determined the toxicity of the three treatment types; 50 nm nZnO, bulk ZnO and $ZnSO_4$ on the model bacteria *Escherichia coli* to obtain a better understanding of the potential toxicity in other bacterial species (Cooper, 2000). A multiple technology approach was used to distinguish different types of toxicity displayed by the nano-form compared to the bulk and ionic treatments. The results revealed that both the nano and bulk forms of ZnO were a bacteriostatic, whereas $ZnSO_4$ acted as a bacteriocidal agent, as determined by live/dead staining of *E. coli* cells post exposure. The term

bacteriostatic is used to define toxic compounds which causes inhibition of bacterial growth, as opposed to bacteriocidal agents which cause bacterial cell death.

3.4.1. The Nano-Form of ZnO Did Not Cause Greater Inhibition or Cell Death than the Bulk Form.

The growth inhibition and flow cytometry results demonstrated that nano-scale ZnO did not inhibit growth or kill cells significantly more than the bulk form. Bacterial growth and absolute cell death are important indicators in evaluating the efficacy of an antimicrobial agent, and the fact that the nano-form of ZnO was no more toxic than the bulk form was in interest as it indicated that the impact of accidental nZnO release may be of similar consequence to that of the bulk material to bacteria.

However, when the two whole cell bioreporters were employed to detect acute and gene toxicity, there were differences between the three zinc-containing treatments. There was a greater initial acute toxicity response from *E. coli* HB101 treated with the nano form than the bulk form. Further investigation with *A. baylyi* ADP1 revealed that the nano-scale ZnO did not induce as strong a genotoxic response as the bulk form or ionic form after treatment at a concentration of 50 mg/L. These differences demonstrated that although the nano-scale ZnO particles were more acutely toxic than the bulk in a short-term exposure of 30 minutes, they caused significantly less genetic damage than the bulk particles. This acute toxicity could be a result of the smaller particle size and greater solubility of the nano-scale ZnO as detailed in Chapter 2 which would allow greater interaction of nanoparticles with the bacterial cells than with the bulk particles. This would in turn cause greater initial toxicity due to greater contact and release of Zn^{2+}. The $ZnSO_4$ treatment caused significantly greater acute and genotoxicity, hence Zn^{2+} had a strong role in toxicity, and the solubility of nano and bulk ZnO particles was demonstrated to be much lower than that liberated from $ZnSO_4$.

However, the bulk particles were demonstrated to release significantly more ROS than the nano-scale ZnO particles in Chapter 2, which have previously been demonstrated to cause gene damage (Kang *et. al.,* 2012). These results suggested a balance between Zn^{2+} liberation, size and ROS release when explaining toxicity, and also identified the importance of separating modes of toxicity in order to better understand overall impact.

3.4.2. Evidence for a Large Role of Zn^{2+} Liberation in Acute Toxicity

The solubility of both particle treatments was characterised in Chapter 2, which demonstrated that the nano-form was significantly more soluble than the bulk form in DI water, however both particles were more soluble and had a similar quantity of Zn^{2+} released when dispersed in Hoagland solution. This correlated positively with the increased acute toxicity of particles in Hoagland solution as compared to DI water. Furthermore, cell death and morbidity was shown to be minimal as a result of particle treatment, however ionic treatment caused nearly 30 % morbidity and over 3 % cell death, which was around 10 times that measured after particulate treatment. These findings were in agreement with the conclusions of several recent studies that Zn^{2+} has a large role in nZnO toxicity (Li *et. al.*, 2013).

3.4.3. ROS as a Proposed Mechanism for Genotoxicity

In Chapter 2 it was demonstrated that the bulk ZnO particles released significantly greater quantities of ROS than the nanoparticulate form. Release of ROS from ZnO was previously indicated by Sawai *et. al.,* 1996 and Yamamoto *et. al.,* 2004, who demonstrated that ROS such as H_2O_2 were generated by nano-scale ZnO as measured with the alternative methods of chemiluminescence and spectrophotofluorometry. In the genotoxicity experiment using biosensor *A. baylyi* ADP1, lower genotoxicity was detected as a result of nano ZnO treatment than bulk sized ZnO or $ZnSO_4$ treatment. Release of ROS is known to cause gene

damage and has been well documented (Kang *et. al.*, 2012; Cooke *et. al*., 2003; Wiseman & Haliwell, 1996). The solubility of nZnO was greater than bulk-sized ZnO, however, the genotoxicity was greater as a result of bulk ZnO treatment, it is likely that the bulk ZnO was more genotoxic as a result of greater ROS release. Although high concentrations of Zn^{2+} were demonstrated to cause high genotoxicity from $ZnSO_4$ treatment, magnitude of ROS release potentially explained the difference in genotoxicity between 50 nm and bulk-sized ZnO.

3.4.4. Importance of Understanding the Mode of Action of Antimicrobial Agents

Increased understanding of the modes of action novel materials such as nZnO particles have on bacteria is of great importance in determining the potential for use as an antimicrobial agent in numerous applications, such as medicine and agriculture. It is also essential to know their potential and relative toxicity in other applications, in particular with the forthcoming increased emphasis on the REACH regulations (http://www.hse.gov.uk/reach/). It was demonstrated that nZnO was useful as an inhibitory agent against bacterial growth, however it did not lead to cell death at the concentrations tested. Its greater initial acute toxicity than bulk ZnO may enable it to be slightly more effective than the bulk form soon after exposure, however, absolute cell death remained minimal.

Toxicity was measured in various forms, including inhibition, acute and geno-toxicity, as well as cell death. Results suggested that inhibition did not differ significantly between treatments, whereas acute toxicity and cell death was greater from $ZnSO_4$ and nano-scale ZnO, and hence likely a result of Zn^{2+} release as well as dispersal as measured by zeta potential. Genotoxicity was likely a result of ROS release and Zn^{2+} at high concentrations.

Several studies have suggested that nZnO toxicity in *E. coli* was a result of Zn^{2+} release from the nanoparticles (Li *et. al.,* 2013; Liu *et. al.,* 2009, Brayner *et. al.,* 2006), however, they did not include a bulk-sized control, hence all comparisons were made solely against the ionic form. This study demonstrated that the growth inhibition was not significantly different between bulk and nano-scale ZnO despite the higher solubility of the nano form. It was however demonstrated that Zn^{2+} release may have had a role in acute toxicity, reaffirming the need to distinguish modes of toxicity. In conclusion, it is likely that different particle characteristics such as solubility, zeta potential and ROS release are responsible for different aspects of toxicity.

With recent reports highlighting the need for critical evaluation of nanomaterial toxicity (OECD, 2011; European Commission, 2009; RCEP, 2008), methods such as the biosensor and growth studies employed in this study are useful in distinguishing between acute toxicity and inhibition to growth. Comparison of the nano form with the bulk-sized material is of great importance as the bulk-sized material has been commercially available for much longer than the nano-form, and hence has had more thorough toxicological analysis, and in the case of ZnO has been granted Generally Regarded as Safe (GRAS) status by the FDA (FDA, 2006). Through comparison with the nano, bulk and ionic forms the relative toxicities were established, and the information used for determining antibacterial action of the nanoparticles. From this study it was demonstrated that the 50 nm nZnO particles were no more toxic than bulk-sized ZnO in terms of bacteriostatic, genotoxic and bactericidal behaviour to *E. coli*; an important result in assessing potential impact of nanoparticulate ZnO toxicity relative to its bulk counterpart.

4. EXAMINING THE TOXICITY OF NANO-SCALE ZINC OXIDE IN COMPARISON TO THE BULK SIZED AND IONIC FORMS IN SEVERAL IMPORTANT FOOD PLANTS

4.1. Introduction

In this chapter, the relative toxicity of 50 nm nanoparticulate ZnO, bulk sized ZnO and ionic Zn^{2+} in the form of $ZnSO_4$ was examined in four fast growing plant species in order to determine whether the nanoparticle form was differently toxic to the bulk or ionic form. Two dicotyledons: *Brassica oleracea* (cabbage v. April) and *Lepidiumus sativum* (common cress), and two monocotyledons: *Festuca pratensis* (meadow fescue) and *Lolium perenne* (perennial ryegrass), were investigated. By examining the toxicity in several different plant types it was possible to determine whether the treatments affected root and stem elongation, a measure frequently used to determine phytotoxicity (Lin & Xing, 2008).

Prior to this study, particles were characterised in terms of size, solubility, relative ROS release, and zeta potential (Chapter 2). This understanding of particle characteristics was then applied to observations in toxicity in order to identify key determinants. Understanding how particle-type affected organisms across different species is vital in terms of assessing potential environmental effect. By comparing the toxicity and relating this to material differences in the particles, as measured in Chapter 2, it was possible to gain a better understanding of the potential mechanisms of nano-scale ZnO, bulk and $ZnSO_4$ toxicity.

4.1.1. Early Developmental Phytotoxicity

The process of seed germination includes three main phases; imbibition, where moisture is drawn in through the seed coat; the activation process, where biochemical processes begin to occur within the moistened endosperm; and intra seminal growth, leading to protrusion of the radicle from the embryonic plant. (Labouriau, 1970). In order to compare the effect of zinc containing treatments applied at different stages of the plant life cycle, early phytotoxicity studies were performed in addition to the hydroponic studies discussed later in Chapter 5. This enabled the effect on resultant root and stem length of the treatment soaking into the external seed coat to be measured. Root and stem elongation is an established method for determining toxicity in plants (Visiola *et. al.,* 2014; Durieux *et. al.,* 1995). The results from this assay provided information on whether particles had an effect on the root length and stem length of two monocotyledon and two dicotyledon plants after one week of growth with exposure to three Zn-containing treatments, with reduced growth an indicator of toxicity.

The comparison of monocotyledons and dicotyledons is useful as they encompass a large number of angiosperms (flowering land plants) (Paterson *et. al.,* 2004). By identifying trends in toxicity between bulk ZnO, nano-scale ZnO and $ZnSO_4$, the thinking was that it might be possible to predict toxicities based on the type of plant. Both types have the root vascular tissues xylem and phloem in the centre of the root (see page 26), but monocotyledons have their root xylem and phloem contained in a ring, whereas dicotyledons have a cross shaped xylem with the phloem in between (Nelson *et. al.,* 1997). The stem vascular structure differs in that monocotyledons have narrow and scattered bundles of vasculature, whereas dicotyledons have an outer ring of vascular bundles. The differences in these water and solute containing vascular tissues within the plant may affect their ability to

uptake particles; hence it is important to establish whether there were patterns in terms of classes of particles in order to predict toxicity in the event of Zn exposure.

4.1.2. Need for a More Reliable Medium than Damp Filter Paper

Many previous studies involving early developmental toxicity assays have employed the use of filter paper saturated with test solution (Ma *et. al.*, 2010; Lee *et. al.*, 2008; Lin & Xing 2007 & 2008). However, in preliminary studies in this research project it was found that a filter paper based system provided too heterogeneous an environment for growth, with plant roots following the contours of the paper and dish. This led to a large variance in root and stem length, and hence unacceptably high standard deviations. Preliminary results yielded standard deviations of around 40 % even with a large sample size of $n > 35$ plants (data not shown). This was largely due to the fact that the particles stayed on top of the filter paper, and hence roots grew away from the tops of the filter papers and into the moist environment below the paper. As this was such a heterogeneous environment and did not yield highly replicable results it was decided that a new approach was needed to reduce the error of such studies. A homogenous testing system using water-based agar to suspend particles was consequently developed for assessing the impact of particle exposure to germinating seeds and seedlings under sterile conditions.

Technical agar dispersed with different zinc-containing particles was used to ascertain the effect on germination, root and shoot length of the four different fast-growing plant species cabbage, cress, fescue and rye. Meadow fescue and perennial ryegrass are widespread throughout the UK and are frequently used in grazing seed mixtures due to their ability to thrive throughout winter and good leaf yield. Cabbage and cress are important food plants of which the entire aerial portion is consumed. The use of these four species allowed

comparisons between monocotylendon and dicotyledons in order to identify patterns of toxicity and to determine if this response was correlated to the physiology of the plant.

4.1.3. Al_2O_3 as a Dopant

In corn, cabbage and carrot it was determined that 200 mg/L Al_2O_3 had no significant effect on root elongation relative to the control (Yang & Watts, 2005). A study on wheat identified that 40 nm Al_2O_3 nanoparticle treatment resulted in no difference between seed germination, shoot length and biomass as compared to the control when treated with up to 1000 mg/L Al_2O_3, and there was no negative impact on root length (Riahi-Madvar *et. al.*, 2012). Hence an Al_2O_3 control was not deemed necessary for such a low possible concentration.

4.1.4. Plant Rhizosphere

The plant root-media interface and proximal media is known as the rhizosphere, and is a complex and dynamic environment (Kuzyakov & Domanski, 2000). The secretion of plant root exudates directly influences this local area for both the attraction of mutualistic microbes such as rhizobia and mycorrhizae, and to deter pathogenic microbes (Taylor *et. al.*, 2009). Release of organic acids and chelators facilitates mobilisation of essential metals such as zinc to increase bioavailability. In this chapter, this immediate area surrounding the plant roots was investigated with a novel agar visualisation system. By using technical agar to suspend particles in a 3D homogeneously dispersed state it was possible to observe visible effects to the nanoparticles. In addition, two pH indicators were employed to determine the pH of the root surfaces and local area.

4.1.5. Chapter Aims

The work presented in this chapter aimed to: a) identify trends in inhibition of root and stem elongation by bulk ZnO, 50 nm nZnO and $ZnSO_4$ treatment in four plant species by

using an improved growth media method, b) draw comparisons in ZnO toxicity between two monocotyledonous and dicotyledonous species, c) hypothesise mechanisms of toxicity, and d) visualise root exudate effects on nanoparticles and pH using a novel visualisation system.

4.2. Materials and Methods

4.2.1. Particles

4.2.1.1. Particle Suspensions

One litre of sterile water was prepared by autoclaving DI water in a 1000 ml borosilicate vented cap bottle (Fisher, UK). Zinc containing treatments were prepared in 50ml polypropylene centrifuge tubes. Each of 50 nm nZnO, Bulk ZnO and $ZnSO_4$ was prepared to three concentrations in 10 ml of sterile DI water. Stock solutions were made for the effective final concentrations to be 10, 50 and 100 mg/L in one litre of agar. A control of sterile water was also prepared. Each suspension was then sonicated for 1 hour prior to mixture with cooled liquid technical agar.

4.2.1.2. Particle Dispersed Agar

Preliminary testing identified 0.6 % w/v strength technical agar (Oxoid LP0013, UK) as optimum for dispersal and plant growth. This was half strength according to the manufacturer's suggestion of 1.2 % w/v working strength. The gel was too firm for plant roots to penetrate at 1.2 % w/v and too sloppy to maintain even dispersion of particles at 0.3% w/v. Hence, 6 grams of technical agar was mixed with 990 ml DI water (0.6% w/v) and a 25 mm magnetic stirrer bar in each of 10 vented flasks before being autoclaved. Agar was cooled to 40 ºC before the addition of freshly sonicated particle suspensions (three zinc treatments at three concentrations plus control). Media was stirred magnetically throughout

the addition of particle suspensions to homogenise the mixture. Ten ml of sterile DI water was added to the control agar. Twenty ml of each type of particle-modified agar was pipetted onto sterile 90 mm Petri dishes chilled at 4 ºC for 1 hour in a fridge before use.

4.2.2. Seeds

For the root and stem elongation experiments, seeds of *B. oleracea* and *L. sativum* were obtained from Seedparade, UK (www.seedparade.co.uk) and *F. pratensis* and *L. perenne* were purchased from Emorsgate Seeds, UK (www.wildseed.co.uk). Suppliers confirmed that seeds were untreated and free from pesticides or additives. Seeds were stored in paper bags wrapped in plastic at temperatures below 20ºC. For the agar visualisation assays, *Hordeum vulgare* (barley) (LS Plant Breeding, Cambridge, UK) was chosen as its larger size afforded a better visual representation of local root effects, and it provided additional information for the hydroponic growth assays of barley in Chapter 5.

4.2.3. Seed Surface Sterilisation

All seed types were individually surface sterilised in 50 ml polypropylene centrifuge tubes. A solution of 10 % sodium hypochlorite and 70 % ethanol was prepared in sterile DI water and 10 ml was added to each tube. Tubes were vortexed for 5 seconds before seeds were allowed to soak for 5 minutes after which the supernatant was discarded. Ten ml of sterile DI was added to the seeds, tubes were vortexed for 5 seconds, and supernatant discarded. The sterile DI water wash was repeated 5 times before seeds were placed on the appropriate agar using sterile stainless steel tweezers.

4.2.4. Early Developmental Phytotoxicity Assay

Twenty-four surface sterilised seeds each of rye, fescue, cabbage and cress were placed on three agar plates of each treatment type and concentration, amounting to each treatment and concentration being tested with 8 seeds of each species in triplicate dishes.

Three control dishes were included for each species. Dishes were covered with foil for 2 days to synchronise germination before it was removed and plants were allowed to grow for 5 further days. During this time, roots grew and entered the agar and hence were in contact with evenly dispersed test compounds. After 7 days total, seedlings were removed and their roots and shoots measured using Vernier callipers to the nearest 1 mm. Results were recorded from which mean values for each treatment at different concentrations were calculated along with standard deviations.

4.2.5. Visualisation Agars

Three visualisation agars were developed; a 50 nm nZnO dispersed agar and two pH indicator agars: patent blue (pKa ~ 2.78) and bromocresol purple (pKa ~ 6.21). Eight sterilised barley seeds were then placed on each Petri dish under aseptic conditions and allowed to germinate and grow for 7 days before being photographed to visualise the pH change and nanoparticle clearing around the root-media boundary. Colour change of agar was tested using a control of pH 4 HCl solution for the bromocresol purple and pH 2 for the Patent blue which ensured colour change would occur below the threshold of 5.21 and 3.0 respectively.

4.2.5.1. Nano-scale 50 nm ZnO visualisation agar

Technical agar No. 3 (Oxoid LP0013, UK) was made to 0.6 % w/v strength with DI water before being autoclaved. Agar was allowed to cool to 40 °C before freshly sonicated 50 nm nZnO particle solution was added to a final concentration of 100 mg/L. Nanoparticle containing agar was stirred thoroughly with a 20 mm magnetic stir bar before being transferred to chilled 90 mm polystyrene vented Petri dishes (Fisher Scientific, UK) under aseptic technique.

4.2.5.2. Bromocresol purple indicator agar

The bromocresol purple indicator agar was adapted from a technique used to distinguish acid-producing bacteria such as *Lactobacillus casei*, and also in plant root acidification by Li *et. al.,* (2007) who used a similar agar-bromocresol gel to visualise acidification of the rhizosphere in fava bean and maize. However, the concentrations used in their study were 6 g/L (0.6 % w/v) of agar and 0.1 g/L of bromocresol purple. In preliminary tests conducted prior to this experiment, it was found that a softer gel made at 25 % of the manufacturer suggested working strength, combined with a stronger concentration 0.16 g/L bromocresol purple, as often used in microbiological experiments (Lena *et. al.*, 2015; Kimoto-Nira *et. al.*, 2012), allowed for better visualisation.

Technical agar was made at 0.3 % w/v with 80 % DI water and 20 % tap water and autoclaved before being cooled to 40 °C. The addition of 20 % tap water was found to be essential to enable a colour change to occur. This was due to the low electrolytic conductivity of pure water. Stock solution of 16 g/L bromocresol purple was made by dissolving 0.16 g bromocresol purple indicator reagent (Sigma Aldrich, UK) in 10 ml 95 % ethanol solution. Stock solution was then filter sterilized using a 0.2 µm syringe filter (Fisher Scientific, UK) into a 50 ml sterile polypropylene centrifuge tube. One ml of this stock solution was used per litre of technical agar to give a final bromocresol purple concentration of 0.16 g/L, added under sterile conditions to cooled agar before pouring into chilled sterile 90 mm Petri dishes as above. Quantities of reagents used were chosen after having previously been optimised in preliminary experiments.

4.2.5.3. Patent Blue V Indicator Agar

Technical agar was made as above at 0.6 % w/v with 20 % tap water and 80 % DI water and autoclaved. Stock Patent blue V indicator solution was made by dissolving 0.25 g

of patent blue indicator (Sigma, Dorset, UK) in 10 ml sterile water. Two ml of this stock was then pipetted into 500 ml cooled technical agar and poured into chilled Petri dishes and allowed to set.

4.2.6. Light Microscopy

For growth of plants used in light microscopy, agar plates with 50 mg/L bulk and nZnO containing treatments were made as above. Surface sterilised seeds were placed on 0.3 % w/v technical agar dispersed with zinc containing treatments and grown for 7 days total. Seedlings were carefully removed from the agar and the lower 1 cm of the root was excised using a razor blade. Root tissue was placed on a microscope slide with a drop of DI water and 20 mm glass coverslip. Slides were examined using a Motic AE31 microscope at 40x magnification. Images were captured using Motic Images Plus software (version 2.0) and scale bars constructed using Gimp 2.8 software.

4.2.7. Solubilisation of ZnO Particles with EDTA

The solubility as measured by UV absorbance of ZnO particles in the presence of the chelator ethylenediaminetetraacetic acid (EDTA) was investigated for two reasons. Firstly, in the hydroponic barley growth experiments described in Chapter 5, the roots were washed for 5 minutes with 0.1 M EDTA. This was an established technique to remove surface bound zinc, however, it was deemed important to determine whether particles would actually be dissolved by this process. Secondly, the ability of chelators to dissolve ZnO was important when considering natural release of plant chelators in root exudates, and in understanding the results of the nanoparticle visualisation assay, hence the ability of ZnO particles to dissolve in the model chelator EDTA was of considerable interest.

A serial dilution of 50 nm nZnO and bulk ZnO particles was made from 1000 mg/L to 0.488 mg/L in a Nunclon clear-bottomed 96 well plate. A multichannel pipette was used to halve the concentration of particles each time by the addition of 100 µl DI water. Solutions of 10 ml of 1.0 M and 0.01 M $Na_2EDTA•2H_2O$ (Fisher, UK) were made in DI water in a 30 ml amber glass vial. Twenty µl was removed from each of the wells from the 96 well plate and replaced with 20 µl of either 1.0 M or 0.1 M EDTA solution to provide an effective concentration of 0.1 M or 0.01 M in each well. The absorbance of each well was then measured at 405 nm using a BioTek Synergy HT microplate reader (BioTek Corporation, UK) every 5 minutes for 30 minutes. The 405 nm wavelength was chosen due to its proximity to the critical wavelength for maximum absorbance of light and hence even a small concentration of particles led to a high absorbance value, providing a high sensitivity to the technique.

4.2.8. Statistical Analysis

Graphs were constructed using means of all root and stem elongation data, and error bars depicted one standard deviation above and below the mean. Statistical significance was determined by comparison to the control using a Student's t-test, with a p value of below 0.05 determining significance at a 95 % confidence level. For each species, treatment and concentration, early developmental phytotoxicity assay had a sample size of $n = 24$.

4.3. Results and discussion

4.3.1. Early Developmental Phytotoxicity Assays

Two monocotyledonous plants (fescue and rye) were compared to two dicotyledonous plants (cabbage and cress) in terms of stem and root length when grown in technical agar impregnated with bulk-sized ZnO, 50 nm nZnO or $ZnSO_4$ over a concentration range. Graphs were constructed for each treatment type and each plant subsection (root or stem), with all four species expressed as a percentage of the control and plotted together to allow comparison. The approximate concentration at which 50 % of the root elongation was inhibited (IC_{50}) was found by interpolation from graphs in **Figure 4.1** and displayed in **Table 4.1**. The IC_{50} values demonstrated that bulk ZnO and nZnO were similar and very toxic to the two dicotyledonous species (5 to 7 mg/L) however in the monocotyledonous species the value for the nano form was significantly greater than for the bulk ZnO, which indicated that nZnO was less toxic to monocotyledons than the bulk ZnO material.

Table 4.1: Approximate IC_{50} values (mg/L) interpolated from root elongation graphs in Figure 4.1 of two dicotyledons (in bold); cress and cabbage, and two monocotyledons; rye and fescue. Values represent concentration at which 50 % of root elongation was inhibited.

	Bulk ZnO (mg/L)	$ZnSO_4$ (mg/L)	50 nm nZnO (mg/L)
Cress	**5**	**10**	**6**
Cabbage	**6**	**26**	**7**
Rye	10	34	66
Fescue	12	20	72

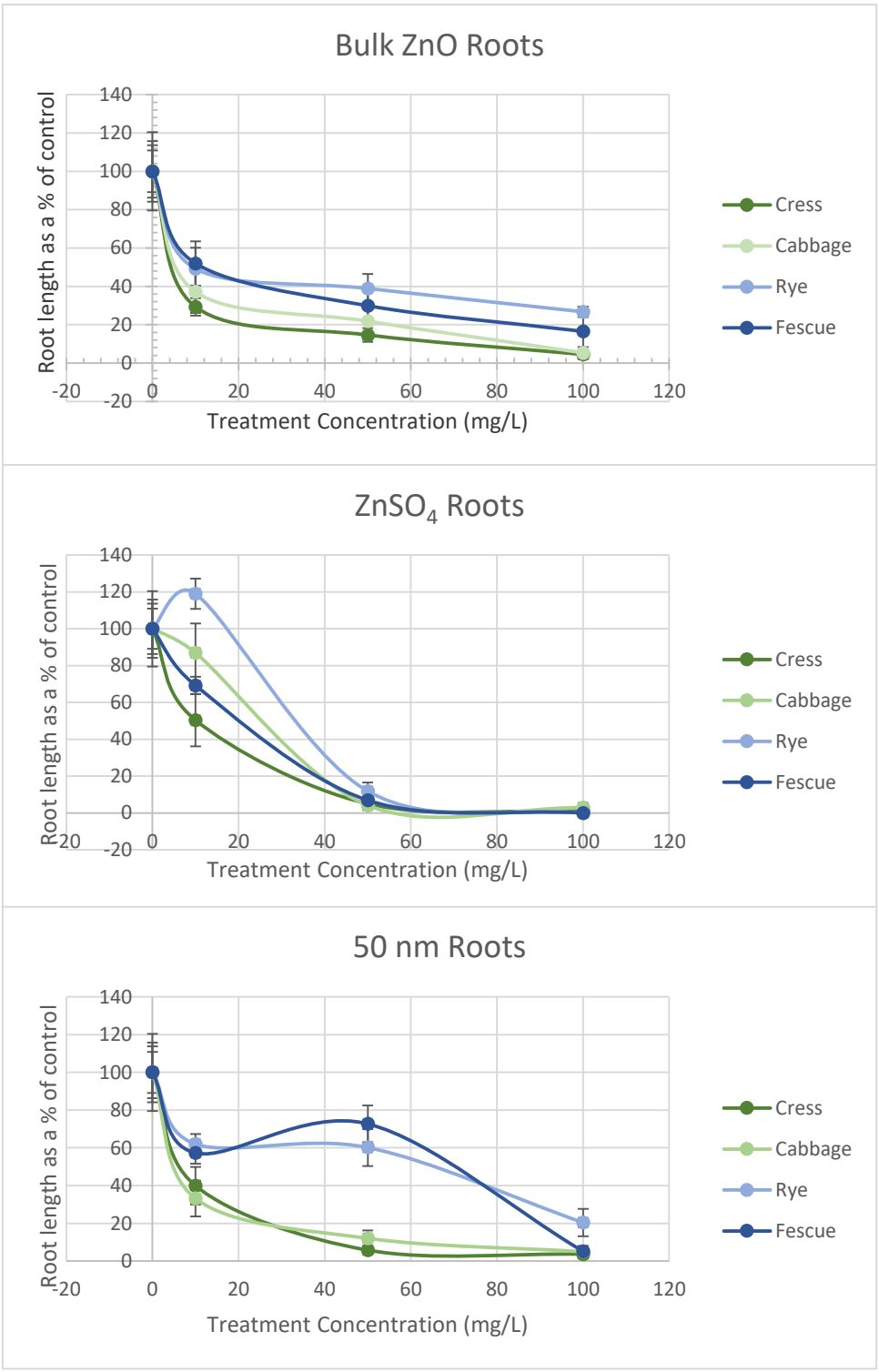


Figure 4.1: Three graphs detailing the change in root length of four species of plant with increasing concentrations of bulk ZnO, 50 nm $ZnSO_4$ and nZnO relative to the control for each species. Monocotyledons were shown in blue (rye and fescue) and dicotyledonous were shown in green (cabbage and cress). For each treatment *n* = 24 and error bars denoted one standard deviation.

For easy comparison the dicotyledonous species were plotted in green and the monocotyledonous species in blue (**Figure 4.1**). For the root lengths, a concentration dependent decrease in root length was measured for all species. At the lowest concentration of the two particle treatments, 10 mg/L, there was a decrease in root length for all four species, however with the ionic treatment of $ZnSO_4$ there was root length stimulation in rye, and cabbage roots were not significantly different to the control ($p < 0.05$). The other two species fescue and cabbage showed a decrease in root length as a result of 10 mg/L $ZnSO_4$ treatment.

With $ZnSO_4$ treatment, there was no noticeable trend in root length between the two classes of plant, monocotyledon and dicotyledon. With bulk ZnO treatment, root attenuation was significantly greater in dicotyledons than monocotyledons at 10 mg/L and 50 mg/L concentration. With 50 nm nZnO treatment the reduction in root growth showed two distinct trends according to whether the plants were monocotyledons or dicotyledons. At the middle concentration of 50 mg/L there was a highly significant difference between the two classes (all four comparisons had $p < 0.001$), with monocotyledons demonstrating reduced impact on root attenuation as a result of 50 nm treatment (around 60-70 % of control length) as compared to dicotyledons (below 20 % of the control length). These results indicated that there was a higher level of treatment tolerance by monocotyledons when treated with particulate treatments, however by 100 mg/L concentration of all treatments all roots were below 30% the length of the control.

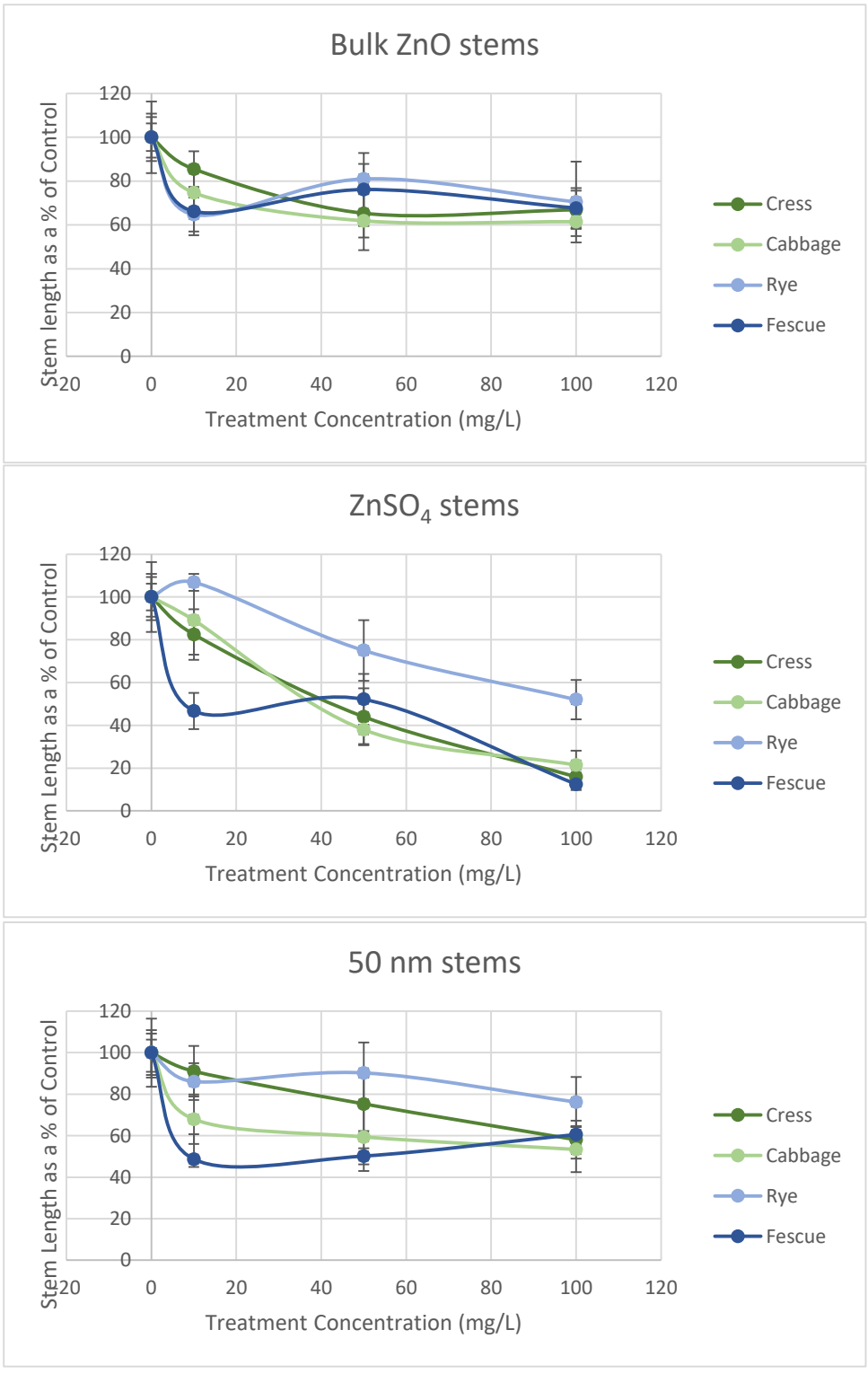


Figure 4.2: Three graphs detailing the change in stem length of four species of plant with increasing concentrations of bulk ZnO, 50 nm $ZnSO_4$ and nZnO relative to the control for each species. Monocotyledons were shown in blue (rye and fescue) and dicotyledonous were shown in green (cabbage and cress). For each treatment *n* = 24 and error bars denoted one standard deviation.

The stem elongation values for all four plants treated with bulk, nZnO and $ZnSO_4$ were displayed in **Figure 4.2**. For the stem lengths, there was a slight decrease as the concentration of treatments increased. After treatment with the particulate forms of ZnO, stem length decreased by between 20 % and 45 % after treatment with the highest concentration, 100 mg/L. This was contrasting to the root results, where more than 75 % root attenuation was detected. This demonstrated a reduced impact of treatment to stems as compared to roots. The roots were in direct contact with the nanoparticles suspended in the agar matrix whereas the stems grew away from the media, which suggested physical contact of the treatments had an important role in toxicity.

With the bulk particles, the stem lengths followed a trend according to whether the plants were monocotyledons or dicotyledons. The monocotyledon (blue) stem lengths decreased slightly in a downward sigmoidal curve, with a peak at 50 mg/L, however values were non-significant between stem lengths from 10 to 100 mg/L concentrations. Both rye and fescue followed this trend which demonstrated up to 35 % stem attenuation. For the dicotyledons, the trend was a negative slope according to increasing concentration, with a maximum of 40 % reduction in stem length. The differences between stem lengths after 50 mg/L and 100 mg/L of bulk treatment were non-significant for both cabbage and cress. The same downward sigmoidal curve trend was detected with the ionic $ZnSO_4$ treatment, however stem attenuation was much greater than in either of the two particulate treatments, with the two dicotyledons and fescue demonstrating around 80 % decrease in stem length. This was not the case for rye, which showed slight stimulation at the lowest concentration of 10 mg/L as opposed to the other monocotyledon, fescue which showed a dramatic decrease in stem length by 50 % from the control. With the 50 nm nZnO treatment, all stem lengths decreased as concentration increased, whereas fescue was more sensitive than rye. After

treatment with the lowest concentration of 10 mg/L, all stem lengths remained the same length within error and within species as the concentration increased.

The results from this study demonstrated that root length was more sensitive to treatment than stem length (**Figure 4.3**).



Figure 4.3: Photograph of cress seedlings germinated on (from left to right) 100 mg/L, 50 mg/L, 10 mg/L of nZnO containing agar, and control technical agar, showing pronounced effect on root elongation and a lesser effect on stem elongation.

There was also a trend between the two monocotyledons and dicotyledons chosen and different treatment types. The particulate treatments, bulk and nZnO, did not cause root or stem length stimulation from the control at any concentration whereas $ZnSO_4$ stimulated rye root and stem length. The unanticipated result of 50 nm causing the ‘s’ shaped curve in monocotyledon root length (**Figure 4.1**) demonstrated a strong difference in 50 nm nZnO behaviour as distinct from $ZnSO_4$ or bulk ZnO. The graph shapes of root elongation for the

three treatments were distinct from one another which demonstrated the usefulness of using root elongation as a primary measure of toxicity over stem elongation (Stampoulis *et. al.*, 2009).

In the agar Petri dishes containing 50 and 100 mg/L nano-scale ZnO particles, it was noticed that the roots of the two monocotyledons, rye and fescue, had caused a 'clearing' effect of the nanoparticles. This phenomenon was not observed with the bulk ZnO dispersed plates. The beginnings of nZnO clearing was also observed for the two dicotyledonous species however their roots were very short (below 20 % of the control) and hence had not penetrated far into the agar so the effect was not as pronounced. The dispersed nanoparticles appeared a hazy bluish colour, but 2-3 mm around the root this had become clear (**Figure 4.4**). It was possible to observe that the very tip of the root had not yet caused clearing.



Figure 4. 4: Photographs of the 'clearing' of nano ZnO from around the roots of the monocotyledon rye on 100 mg/L nZnO dispersed technical agar after 5 to 7 days growth in sterile conditions. For size reference, each seed is approximately 6 mm long.

4.3.2. Microscopy of Roots

The end portion of roots after treatment with bulk and nZnO particles was investigated by light microscopy (**Figure 4. 5 A-C**).



Figure 4.5 A-C: Light micrographs of representative roots after 7 days growth of cabbage in A) technical control agar, B) 50 mg/L Bulk ZnO agar, and C) 50 mg/L 50 nm nZnO dispersed agar. Images in B and C suggested root cap damage, possibly with increased damage as a result of Bulk ZnO contact. Scale bars denote 100 µm.

Cabbage was found to be representative of all the four species of plant root investigated. The very end of the root tip contained the apical meristem which is covered by the root cap, which protected the growing root. In the control images, (**Figure 4.5 A**) it was possible to observe intact, smooth root caps which covered the apical meristem. After treatment with 50 mg/L of the bulk ZnO particles, the root caps had begun to slough away from the root to form a population of detached root border cells (**Figure 4.5 B**). A large mass of cells at the root tip was detected after bulk ZnO treatment, whereas after 50 nm nZnO treatment (**Figure 4.5 C**) there was noticeable root cap damage as compared to the control, however the sloughed away cell populations were smaller than in those treated with bulk ZnO particles. This indicated that both particulate treatments had caused mechanical detachment of border cells from the root cap, with bulk treatment having caused greater damage, perhaps as a result of the root making contact with physically larger particles. When considering the observations from **Figure 4.4** it was possible to see that the very tip of the root had not caused any clearing of nanoparticles. Root tips push through a substrate, producing lubrication and sloughing off border cells to facilitate movement through the substrate and also to provide carbon to local microbes. This mechanical pushing against the particles suspended in the substrate likely caused the root cells to slough off as observed in the light micrographs. If the apical meristem and zone of elongation was damaged by the particles, this would reduce root growth. In the light micrographs it was not possible to see any obvious damage to the area behind the root cap however even minor damage has been demonstrated to cause a reduction in root growth (Hawes et. al., 2000).

4.3.3. Agar Visualisation

After observing the clearing of nanoparticles around the roots in the early developmental phytotoxicity assays, further investigation was conducted in order to ascertain the likely causes of the clearing. Barley was chosen to provide information on pH and effects of barley root exudates used in the zeta potential experiments and hydroponics experiments in Chapter 5. In addition, the larger physical size of barley seedlings enabled better visualisation of the root-media interaction. By growing barley from seed on sterile Petri dishes in different visualisation media, root exudate effects on nZnO and pH were observed. Bromocresol purple is an indicator salt which turns yellow at pH $\leq$ 5.21 and remains purple above this threshold. Patent blue is an indicator salt that turns yellow at pH of 3.0 or below, and remains blue above this level. The agar concentration was optimised for appropriate diffusion of colour from roots to allow good visualisation and distinction between boundaries. With the indicator dissolved in dilute technical agar, we were afforded a 3D visualization of acidification.

A clearing phenomenon was again observed with the nanoparticle dispersed technical agar with barley, where the milky translucent media containing nanoparticles became clear and transparent around the roots (**Figure 4. 6**)

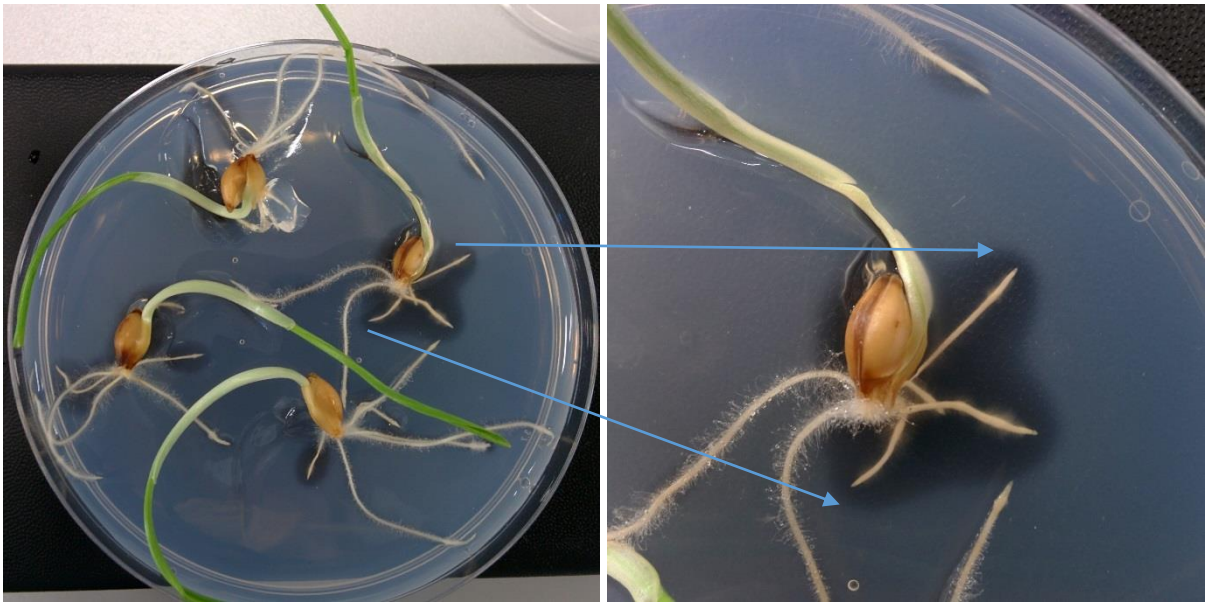


Figure 4.6: Technical agar with 100 mg/L dispersed 50 nm nZnO particles. Particles dispersed in agar give a bluish milky appearance which disappears directly around the root leaving a 'cleared' area suggesting dissolution of nZnO facilitated by acidic exudates.

The clearing phenomenon was observed within 3-6 mm around roots with the widest clearing around the basal root and root hairs that entered the agar, and the narrowest clearing around the root tip. It was possible to observe that clearing of nanoparticles only occurred when the roots entered the agar. Several roots grew on top of the agar however it was only when the root made physical contact that the clearing occurred.

The root cap at the tip of the root protects the root and the meristem, the location of cell division. The cells produced by the meristematic region form the elongation zone and hence the newest cells are near the end of the root, and the oldest cells are nearer the base of the plant (Russell, 1977). This correlated with the distribution of clearing, where older cells had had longer to release exudates and hence the exclusion zone was larger than at the root rip. This suggested that the root exudates were causing the clearing of the nanoparticles.

To determine the pH of the area around the roots, bromocresol purple indicator agar was used (**Figure 4.7**).

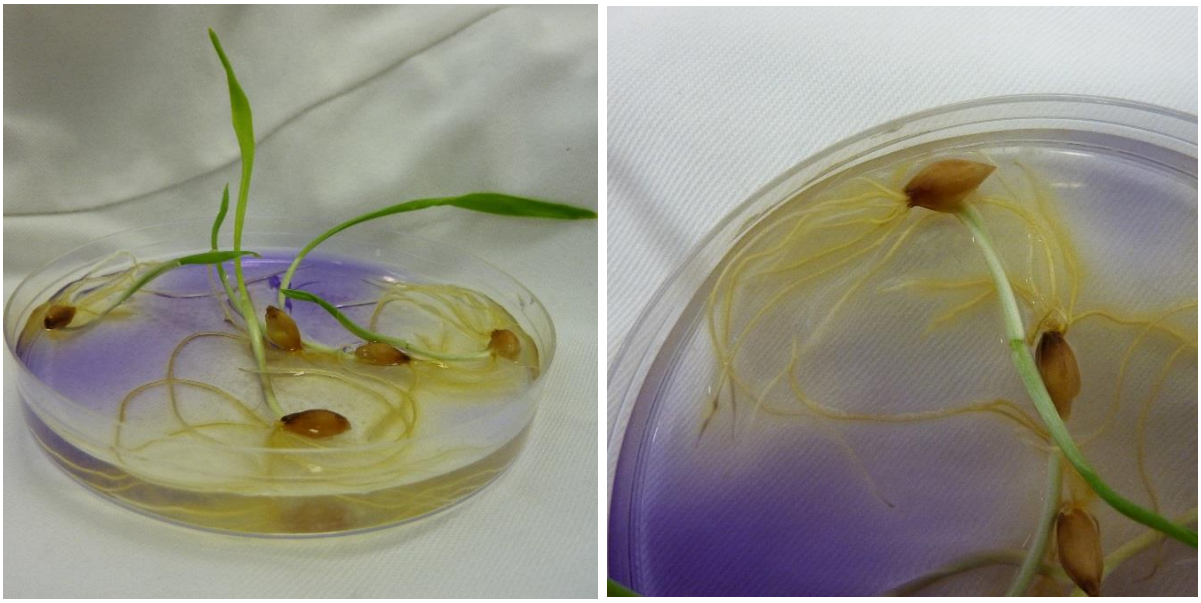


Figure 4. 7: Technical agar (0.3 % w/v) with bromocresol Purple indicator to visualise pH change from root exudates (yellow < pH 5.21 < purple). Yellow zones surrounding root growth indicated release of acidifying exudates after 7 days growth of barley.

Colour change from purple to yellow occurred within 1-5 mm around the basal and lateral roots which showed acidification of the proximal media by the roots. This indicated that the pH of the local area around the roots was below pH 5.21. The colour change was detected as early as 3 days after sowing. The strongest colour change was observed on the root surfaces themselves, which were stained a strong yellow.

The clearing of the nanoparticles in **Figure 4. 6** coincided with the areas of pH ≤ 5.21 observed with the bromocresol purple indicator. Root exudates are known to be slightly acidic as a result of organic acid release (Dakora *et. al.,* 2002) and the indicator agar confirmed this. To determine whether they reached pH 3 or below, barley was also grown on indicator agar containing Patent blue (**Figure 4. 8**).

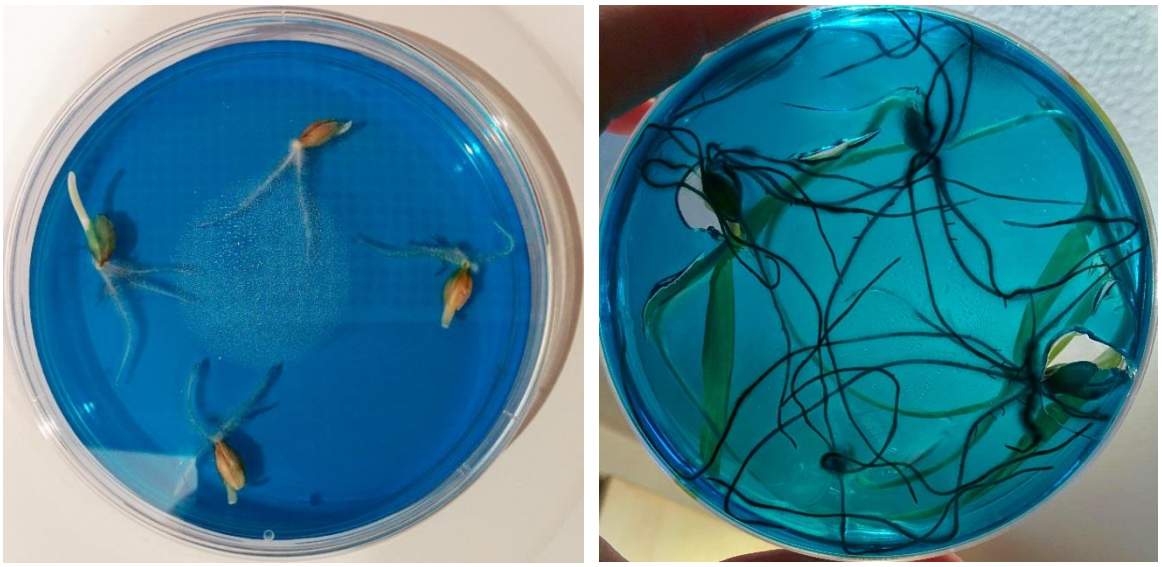


Figure 4. 8: Technical agar with Patent Blue indicator to visualise pH change from root exudates (yellow < pH 3.0 < blue). No yellow zones indicated that pH of root exudates did not reach as low as pH 3.0 after 3 days (left) or 7 days (right).

The results of the patent blue visualisation demonstrated that the exudates did not reach a pH of 3.0 or below within 7 days of barley growth. When this was compared with the bromocresol purple results it identified that the area immediately around the roots was acidified between a pH of 3.0 and 5.2. This had implications on nanoparticle stability as ascertained by zeta potential over a range of pHs in Chapter 2, where it was demonstrated that particle stability decreased slightly from pH 7 to pH 5.5. The stability of nZnO and ZnO in the presence of root exudates was further investigated in Chapter 5, where the liquid based growth systems of hydroponics meant that nanoparticle dispersion state was of increased importance, as opposed to the artificially maintained well dispersed particles in this agar assay.

The nanoparticle clearing effect was further examined by pipetting decreasing pHs of HCl on the same nanoparticle agar plates, however this did not lead to a visible clearing of nanoparticles, even down to pH 3.2. However, when 0.01 M EDTA solution was pipetted onto the nanoparticle agar plates, clearing was observed within 5 minutes (**Figure 4. 9**). This demonstrated that the chelator EDTA alone at 0.01 M was sufficient to dissolve the nanoparticles, whereas the pH 3.2 HCl acid was not. This revealed that chelators released in plant root exudates may have a large role in solubilising Zn^{2+} from nZnO, and not the acidic conditions as previously considered. This demonstrated that although the pH decrease correlated with the clearing zones, it was more likely that organic chelators such as citrate, malate etc. within the acidified exudate were responsible for the clearing.

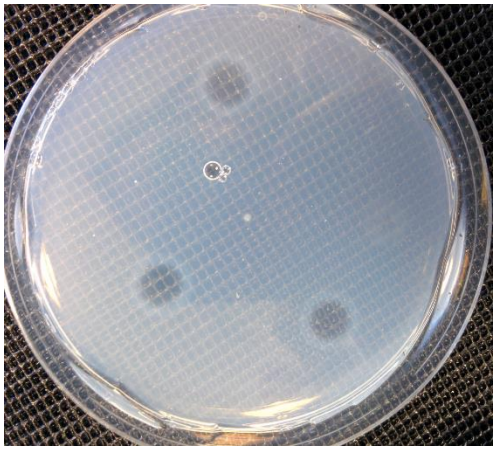


Figure 4.9: Technical agar dispersed with 100 mg/L 50 nm nZnO five minutes after three 100 µl aliquots of 0.01 M EDTA were pipetted onto the surface. Clearing of nanoparticles was observed similar to that previously demonstrated by barley roots.

4.3.4. UV-Visible Absorbance with the Chelator EDTA

The ability of the chelator EDTA to clear the nanoparticle was further investigated by UV visible absorbance at a wavelength of 405 nm. For particles in 0.1 M EDTA, absorbance values were not significantly different to the control values of water ($p < 0.01$) which demonstrated total dissolution of particles within 5 minutes even at the highest concentration of 1000 mg/L. This result validated the use of 0.1 M EDTA solution as a rinse to remove surface bound ZnO particles from plant roots in Chapter 5.

For absorbance values of particle suspensions containing the lower concentration of 0.01 M EDTA, differences were detected between bulk and 50 nm nZnO particles, therefore 3D bar graphs of mean values were constructed to demonstrate the dissolving of particles over time (**Figure 4.10 A & B**). The results revealed that 50 nm nZnO was fully dissolved by 0.01 M EDTA within 10 minutes, even at the highest particle concentration of 1000 mg/L (**Figure 4.10 B**). For the bulk ZnO particles, dissolution was much slower, with dissolution not occurring within 30 minutes (**Figure 4.10 A**).

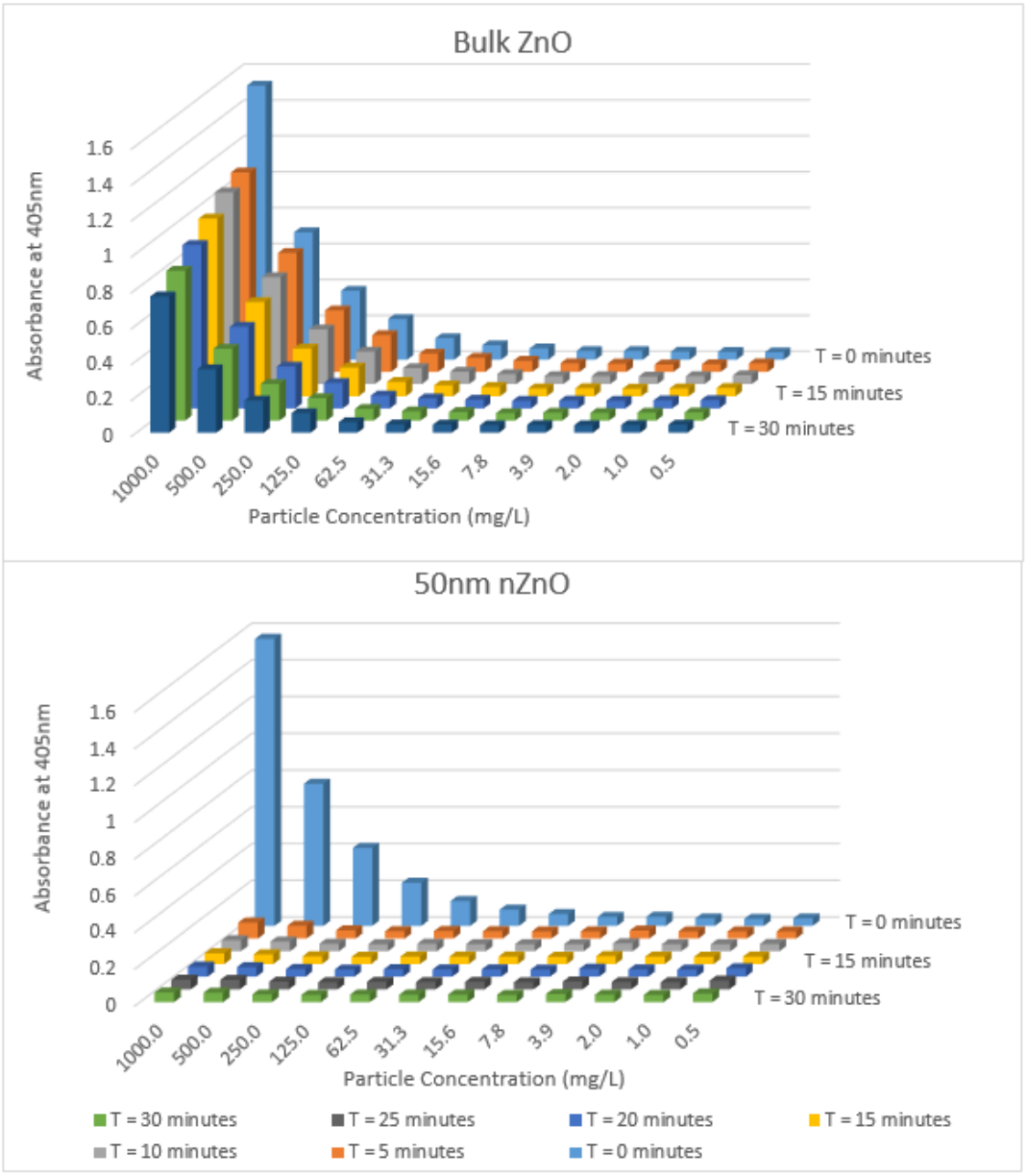


Figure 4.10 A & B: Absorbance of bulk and 50 nm nZnO particles over time and particle concentration, as measured at 405 nm after addition of EDTA solution to a final concentration of 0.01 M for A) bulk ZnO and B) 50 nm nZnO particles (*n* = 3).

This demonstrated a size specific effect on dissolution of particles over time when in the presence of a chelator, EDTA. The larger surface area to volume ratio of the nano-scale particles likely facilitated dissolution by providing a larger surface for reaction to occur. EDTA was able to dissolve particles by binding to Zn^{2+} ions. This would have removed the free Zn^{2+} from the area around the particle, providing a steeper concentration gradient from

particle surface to media and hence facilitating dissolution. With the bulk particles, the interaction between EDTA and the particles was limited as there was less surface area for interaction, hence the dissolution rate was slower. This result corresponded to the observation that 0.01 M EDTA caused a clearing in the nZnO agar, and that bulk ZnO particles in agar did not clear around the root whereas the 50 nm nZnO particles did.

The test concentrations used in the root and stem elongation study seemed low except when the number of particles was considered; even just 10 mg/L of particles entailed 5.75 x 10^{12} individual particles for nZnO particles and 9.80 x 10^{9} for bulk particles (as determined in section **2.2.5**). As they were highly dispersed in the agar matrix there was a high potential for interaction between individual particles and plant roots.

4.4. Discussion

4.4.1. Significant Reduction in Root Elongation Detected in Four Species as a Result of Zinc-Containing Treatments

Four plant species were grown on technical agar containing three concentrations of bulk ZnO, nanoparticulate 50 nm nZnO, and fully dissolved $ZnSO_4$. All three treatment types caused significant attenuation of root growth relative to the control at concentrations of 50 mg/L and above. The IC_{50} values were calculated in order to compare the approximate concentrations that cause 50 % decrease in root length relative to the control. It was found that bulk and nZnO treatments both had similarly low IC_{50} values in the two dicotyledonous species cress and cabbage. With the monocotyledons however, the bulk ZnO was demonstrated to be more toxic than the nZnO, with IC_{50} values of 10 to 12 mg/L for treatment with bulk, and 66 to 72 mg/L for 50 nm nZnO treated plants. However, when the shape of the graph of concentration versus root length was considered for 50 nm nZnO it was

noted that there were unexpectedly high readings at 50 mg/L for both rye and fescue that caused a downward ‘s’ shaped slope. This suggested that a lower concentration of 10 mg/L was more toxic than 50 mg/L to monocotyledons. This could be explained by different internal regulation mechanisms within monocotyledonous plants. Zinc toxicity is characterised by necrotic lesions on older leaves and reduced growth (Wallnoffer and Engelardt, 1994). The plants in this assay were very young, and as such there were no older leaves and this form of visual toxic response was not observed. However, a reduction in growth was detected which suggested zinc toxicity. Another potential reason for the reduced growth was identified in the light micrographs as root cap damage as a result of particulate treatment. Physical abrasion and damage of the vital apical meristem would lead to attenuated root growth as detected in the growth assays. As the IC_{50} values for the highly ionic $ZnSO_4$ were greater than for the particles, and the larger bulk particles caused greater root attenuation and root cap damage, it is possible to determine that particle abrasion likely had a leading role in the toxicity demonstrated in this experiment.

Zinc at high concentrations is intrinsically toxic and the results demonstrated that toxicity likely occurred from the combination of dissolved zinc and physical particle contact. It suggested that it was this and not the fact the test material was in nano form that was responsible for toxicity. The lower IC_{50} values for nano-scale ZnO was likely due to the increased solubility of the nanoparticulate form of ZnO, which decreased the toxicity as it reduced the physical particle contact and subsequent root damage**.**

The strong effect that all three of the zinc containing treatments had on root elongation would have a highly detrimental effect to plants in the field. Roots are required to absorb water and inorganic nutrients, to support and anchor the plant and often to act as a storage organ for starches (Prasad, 2004). A pronounced decrease in root length would therefore limit these essential plant functions.

4.4.2. Trends in Toxicity Between Monocotyledons and Dicotyledons

Lin and Xing (2007) used both monocotyledons and dicotyledons in their study of nano-scale ZnO toxicity, however no bulk-sized comparison was used, and results were not discussed in terms of monocotyledon and dicotyledon classification. The approach of agar-dispersed treatments was employed and included a bulk and ionic control to compare two monocotyledons and two dicotyledons. The results of this study indicated that it might be possible to predict toxicity based on whether the plant is monocotyledonous or dicotyledonous. Both dicotyledons were highly sensitive to all treatments whereas monocotyledons were significantly more tolerant to 50 nm nZnO than to the bulk ZnO in terms of root elongation. When the material characteristic results from Chapter 2 were considered, 50 nm nZnO had a higher solubility of approximately 5 mg/L after 7 days in water as opposed to bulk which was around 2 mg/L. It was also previously demonstrated that bulk ZnO released significantly more ROS than 50 nm nZnO particles. Despite the fact there were 3 orders of magnitude more nZnO particles than bulk particles in a well dispersed system (as calculated in section **2.4.5**), the bulk had a lower IC_{50} value than the 50 nm nZnO in monocotyledons, which demonstrated increased toxicity. This could be a result of the conflict between essential quantities of zinc and toxic levels, with monocotyledons and dicotyledons having different threshold values. Dicotyledons demonstrated higher toxicity from both particulate forms of ZnO than the ionic Zn. Monocotyledons demonstrated higher toxicity from bulk than from ionic or 50 nm nZnO. These observations could have been a result of larger bulk particles damaging the plant root cells of all the four species tested by mechanical abrasion as the roots grow past them. The smaller 50 nm particles had less mass and hence may have been physically displaced more easily than the bulk particles. They were also more likely to have been dissolved as a result of the root exudates and hence not offer resistance. This mechanical damage was identified in the light micrographs of root tips

post-exposure, with much greater disruption to the root caps in the particulate treatments than the control. In addition, no clearing around the roots was observed with the bulk treatments with any of the four species. This indicated that the particles were too large to dissolve, and hence the mechanical abrasion would be much greater than with the 50 nm nZnO particles which may have completely dissolved as a result of root exudate release. This reduced solubility of bulk was previously demonstrated a) in the dissolution assay in water in section **2.2.7** and b) in the optical density dissolution experiment of particles in EDTA solution in this chapter. This observation helped to form the hypothesis that plant toxicity as measured by root elongation was a product of the dispersion and mechanical action of particles, with high levels of Zn^{2+} liberated by the $ZnSO_4$ not causing as much toxicity as the bulk particles, indicating that the Zn^{2+} solubility was less important than the physical particle contact and potentially ROS release by the large particles.

4.4.3. Nanoparticle Agar Matrix Maintained Particle Dispersion Throughout Toxicity Assay

Nanoparticle agar had previously been developed for Al_2O_3, Ag, ZnO and Cu (Riahi-Madvar *et. al.,* 2012; Lee *et. al.,* 2012; Mahajan *et. al.,* 2011) however these studies used plant media agar which contained essential nutrients to support plant growth. Over a short exposure period of 7 days as used in this study sufficient nutrients are provided by the seed and energy by the newly photosynthesising seedling and hence the supplementary nutrients are not necessary (Fenner *et. al.,* 2005). The salts used in plant nutrient media such as $Ca(NO_3)_2$, $MgSO_4$ and KH_2PO_4 increase the ionic strength of the solution which is known to interfere with nanoparticle stability (Sperling *et. al.,* 2010). Hence it was proposed that a water-based agar system provided a superior system for testing nanoparticle toxicity in early developmental phytotoxicity studies.

The agar matrix in which the nanoparticles were suspended could have provided an artificially high particle dispersion stability, as particles were well dispersed throughout the 7 day experiment. This could be compared to a suspension with zeta potential greater than ± 30 mV if the particles were in normal liquid suspension. Hence it is proposed that this method of toxicity testing for plant species is optimum for determining the maximum toxicity as a result of the treatment. In environmental conditions, particulate adsorption and ligand binding will reduce bioavailability significantly, and as a result actual toxicity will be lower (Darlington *et. al.,* 2009).

4.4.4. Agar Visualisation Methods Indicated that Root Exudate influenced Particle Dissolution

Together the agar visualisation assays provided a view of the pH change that occurred in the rhizosphere, and the visible effect this had on nanoparticle suspensions as a result of root exudation. This sequence of pH and nanoparticle visualisation techniques demonstrated that roots acidify the local 3 to 4 mm to a pH between 3 and 5.2. As the nanoparticles were undetectable in the same area as the pH was demonstrated to decrease, it was initially considered likely that the lowered pH was facilitating dissolution of particles. However, subsequent addition of acid within the pH 3 to 5.2 range demonstrated no clearing, and 0.01 M EDTA did, which conjectured that chelators play a large role in solubility of ZnO particles through increasing the rate of solvation by binding with free Zn^{2+}.

The balance between ionic dissolution of metal ions and solid phase materials is inexorably linked to the pH of the solution (Sauve *et. al.*, 1997). However, in a situation with low pH and the presence of chelating agents in the root exudates as demonstrated in this chapter, the effect of bioavailability was pronounced. This is a mechanism used by plants

which are usually in a zinc limited environment in order to increase bioavailability of zinc for uptake and nutrition (Bertin *et. al.*, 2003).

4.4.5. Particulate Versus Ionic Effect of Treatments

From the particle solubility experiments conducted in section **2.3.6**, it was demonstrated that approximately 5 mg/L and 2 mg/L of dissolved zinc was liberated from 100 mg/L of 50 nm nZnO and bulk ZnO particles respectively when suspended in water for 7 days. The concentration of zinc liberated from 100 mg/L $ZnSO_4 \bullet 7H_2O$ was calculated and found to be over 22 mg/L, which was considerably greater than from both particulate treatments. Despite this, the IC_{50} values for $ZnSO_4$ were greater than either particulate treatment for dicotyledons, which demonstrated lower toxicity. This indicated that it was not the concentration of dissolved zinc alone that was causing the toxicity at lower concentrations, and that there was a particle specific effect.

In monocotyledons, root length was attenuated slightly less than in dicotyledons and hence there was a greater surface area of root to release root exudates and dissolve the nanoparticulate form, but not the bulk form due to its size as demonstrated in the EDTA absorbance results in section **4.3.4**. This then explained the high IC_{50} values for 50 nm nZnO of 66 - 72 mg/L, as the nanoparticles had dissolved around the root, which reduced particle abrasion. The dissolved concentration of zinc had previously been demonstrated to be over 4 times lower from the nanoparticles than from the $ZnSO_4$. The 50 nm nZnO was less toxic than the $ZnSO_4$ in monocotyledons as it released less zinc when solubilised by the root exudates, and was less toxic than the bulk ZnO particles as they did not fully dissolve and hence caused more physical root damage. These observations indicated that the nanoparticles were less toxic to monocotyledons than the bulk or ionic forms as a result of their smaller size facilitating their dissolution by chelator-containing root exudates. As the majority of

global food crops are monocotyledonous (Reed, 2008), this demonstrated that environmental release of nZnO may cause less phytotoxicity than if the bulk form were released. For the dicotyledons, the nano form was not differently toxic to the bulk form in terms of IC_{50} values. This indicated that although dicotyledons are more sensitive to ZnO than monocotyledons, the nanoparticulate form does not induce greater phytotoxicity than the bulk form. These results in combination indicated that the nanoparticulate form of ZnO may be equally or less phytotoxic than the bulk form as a result of its size and the action of plant root exudates. In terms of the environmental impact of nZnO release, these results suggested that the nano form may not pose any additional concern to the bulk form of ZnO, in particular for monocotyledons, which form the majority in global crop production.

5. DETERMINING IMPACT OF PLANT TREATMENT WITH ENGINEERED NANO-SCALE ZINC OXIDE IN HYDROPONICS

5.1. Introduction

The research detailed in this chapter focused on the effects of the uptake of nano-scale ZnO on economically important plants using a hydroponic (liquid-based) growth system. For this, two food crop plants were selected, *Hordeum vulgare* (barley), and *Solanum lycopersicum* (tomato). For the barley, the biomass and uptake of zinc was quantified after treatment with nZnO, bulk ZnO and $ZnSO_4$. For dwarf tomato the variety MicroTom was chosen for a long term assay conducted with nZnO and bulk ZnO to determine whether an impact on flowering time and tomato formation could be detected as a result of treatment.

Plants are primary producers and as such we rely on them to capture solar energy and convert it to a food source, an essential link in the food chain. Equally, should nZnO not be differently toxic to zinc in bulk or ionic form, particularly in small quantities, small amounts of accidental ZnO release may in fact offer a route to biofortification as zinc is an essential and globally limited nutrient, with one third of the world's population suffering as a result of zinc deficiency (Hambidge, 2000). The high mobility of nanoparticles as a result of their size facilitates their movement through water systems in the environment, and hence they can make contact with plant roots. The product of this interaction is important for considering what happens to the material at its end-of-life, and the consequences of nanomaterial release into the environment (Horst *et. al.,* 2009; Lin *et. al.,* 2008).

The large scale production of nZnO is likely to increase over coming years, so it is increasingly important to determine whether it is toxic to important crop plants such as

barley and tomato, and whether it is differently toxic to the bulk-sized or ionic forms. Barley was chosen for the zinc uptake quantification experiments due to its high economic importance as a food crop for both humans and animals globally, and in particular its large scale production in the UK, with over 7 million tonnes produced in 2013 alone (FAOSTAT, 2015). In addition, tomato plants were chosen as over 20 million tonnes of tomatoes were produced in Europe in 2012. Examining the impact of engineered nZnO on such important food plants is of vital concern, as highlighted in the OECD report on nanosafety published in 2011 which emphasised that environmental studies on nZnO should be prioritised (OECD, 2011).

5.1.1. Determining Barley-Zn Toxicity and Uptake

Information gathered on the uptake of zinc and impact of nZnO on root and shoot biomass can help provide a better understanding of the mechanisms of nZnO toxicity and its potential impact on plants. The quantity of zinc able to enter plants treated with nZnO reflects how bioavailable zinc contained in the nano-scale ZnO was, when compared to the bulk ZnO and $ZnSO_4$. The biomass of the barley post-treatment indicates whether the treatments affected the growth, and identified any differences between root and shoot tissue development (Singer *et. al.,* 2007; Smith *et. al.,* 2000). The combination of zinc uptake and biomass were used to determine the overall effect of NPs in plant systems and suggest potential mechanisms of toxicity. Previous studies have examined the toxicity of metal oxide nanoparticles on plants, but the impact of nZnO on *Hordeum vulgare* has not yet been reported, and is most likely due to the sheer number of permutations of nanoparticles and plant species assessment combinations. The interaction of barley and ZnO ENPs was chosen as they are both of significant commercial importance in the UK, and nZnO production is increasing year on year.

5.1.2. Hydroponic Barley Growth

Hydroponic systems offer a highly controllable environment for plant growth while providing essential nutrients. For this study, modified 20% Hoagland solution was used as the growth medium to provide essential micronutrients for plant growth. This is a growth medium developed for optimal plant growth in hydroponics, and contains a mixture of trace elements in metal salts, in addition to a chelated form of iron (see section **5.2.2** for exact composition). Ideally, DI water would be used for ENP toxicity assessment as this would limit potential interactions of ENPs with metal salts and chelating molecules, however water alone would not sustain plant growth for long enough to carry out the toxicity experiment. Growth in water alone would induce malnutrition which would manifest as deficiency symptoms, and these may be confused with nanoparticle toxicity symptoms such as reduced biomass and chlorosis of the leaves (Wood & Lass, 1975). Hence, a dilute form of nutrient-containing Hoagland solution was used. Furthermore, ZnO particles were suspended in both Hoagland solution and water in the zeta potential and solubility analyses, in order to better understand nZnO behaviour in different media.

5.1.3. Zeta Potential of Particles in Different Media

By measuring the zeta potential of particles in different biologically relevant media such as root exudates and hydroponic solution, it is possible to obtain a much better idea of particle stability when in biological experiments and real world conditions, as opposed to knowing the zeta potential of particles in water alone (Jiang *et. al.*, 2009). It is hypothesised that nanoparticles interact with macromolecules contained within the biological media, such as by adsorption, ligand displacement and flocculation (Lowry *et. al.*, 2012). A summary of the potential interactions is shown in **Figure 5.**. These interactions can have a significant effect on the behaviour of the nanoparticles, and zeta potential is an important indicator of particle stability in these more complex media.

For the root exudates collected in the hydroponic experiments described in section **5.2.4**, the total organic carbon (TOC) was measured to provide an indicator of concentration of organic plant-secreted compounds within the solution. Plant exudate composition is highly dynamic and varies greatly between plants, with between 10 and 30 % of the carbon captured from the atmosphere being released in root secretions (DeJong *et. al.*, 2010; Taylor *et. al.*, 2009; Kuzyakov & Domanski, 2000). The primary constituent of root exudate is carbon-containing compounds, and as a result, the TOC value is a good indicator of the concentration of organic carbon compounds within the solution (Uren, 2000). How these exudates affect nZnO solubility and colloidal stability is important in assessing the potential impact to plants, hence the zeta potential of the bulk and nZnO particles in barley root exudate containing media was investigated in this chapter.

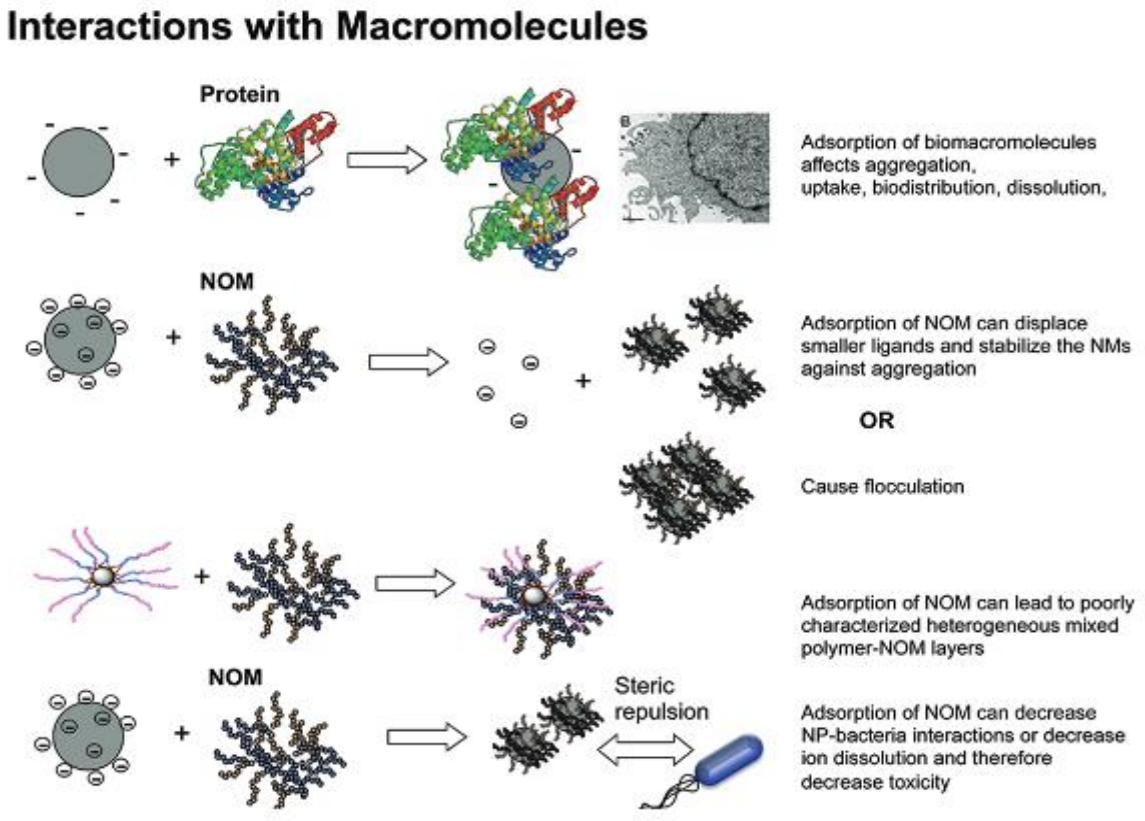


Figure 5.1: Potential transformations of nanomaterials (NMs) in the environment, adapted with permission from Lowry *et al.* (2012). Copyright 2012 American Chemical Society. Diagrams describe theoretical interactions between carbon nanotubes (CNTs), silver nanoparticles and natural organic matter (NOM).

5.1.4. Investigation into the Long-Term Effects of Zinc-Containing Treatments in Hydroponically Grown Tomato Plants

A long-term study was undertaken on a dwarf tomato species in hydroponics, *Solanum lycopersicum* v. MicroTom. This study involved long term growth in the presence of 100 mg/L nZnO or bulk ZnO particles carried out over 18 weeks in order to determine whether particle treatment influenced flowering and tomato formation. It was noted when the first flowers formed for each treatment, and the number of tomatoes that were produced, how many ripened within the three month period and the individual masses of each tomato. The aim of this experiment was to determine whether further work is required to investigate the long-term growth effects of nanoparticle treatment, with potential impact to agriculture in terms of influencing time to flower and fruit formation.

5.1.5. Chapter Aims

This work assessed the uptake of zinc in barley from different zinc-containing treatments including 50 nm ZnO, bulk size ZnO and $ZnSO_4$, along with dry biomass, particle solubility and zeta potential of particles in different biologically relevant media. It aimed to determine not only zinc uptake and barley biomass, but how barley root exudates affected stability of nZnO and in turn whether this was linked to toxicity and uptake. In addition, an investigation into long term treatment of MicroTom tomatoes was aimed to determine whether ZnO induced a physiological response, and the extent to which this varied between nZnO and bulk-sized ZnO treatments.

5.2. Materials and Methods

5.2.1. Zinc-Containing Treatments

Zinc oxide at both nano (50 nm) and bulk scale (~700 nm), and zinc sulphate as an ionic control were purchased from Sigma Aldrich, UK and characterised as detailed in Chapter 2. Fifty nm nZnO had a purity of > 97% with a particle size of < 50 nm (BET) and a surface area of > 10.8 m^2/g and 6% Al_2O_3 as a dopant. Bulk ZnO was reagent grade and had a purity of > 99.0 %. Zinc sulphate was in heptahydrate form ($ZnSO_4 \cdot 7H_2O$). All particle suspensions were sonicated in a Branson 3510 ultrasound bath (Sigma Aldrich, UK) at 40 kHz for one hour immediately prior to use to facilitate dispersion and reduce agglomeration.

5.2.2. Hydroponic Solution

A modified version of Hoagland hydroponic media (Hoagland & Arnon, revised 1950) solution was used at 20% working strength. The media solution was modified to provide a low zinc concentration of 0.4 µM $ZnSO_4 \cdot 7H_2O$, in order to provide some essential zinc for nutritional purposes while maintaining a low background level. Stock solutions for the modified Hoagland media were prepared in 500 ml volumetric flasks using MilliQ water, before being transferred to storage bottles and refrigerated. The final solution contained 1.0 mM KNO_3, 0.8 mM $Ca(NO_3)_2$, 0.4 mM $MgSO_4$, 0.2 mM KH_2PO_4, 20 µM ferric ethylenediamine-di-(2-hydroxyphenylacetate) (Duchefa Biochemie, Haarlem, The Netherlands), 20 µM H_3BO_3, 4 µM $MnCl_2$, 0.4 µM $CuSO_4$, 0.4 µM $ZnSO_4 \cdot 7H_2O$, and 0.2 µM Na_2MoO_4. All chemicals used were of analytical grade (98% pure and above) and purchased from Sigma Aldrich, UK.

5.2.3. Barley for Hydroponics

Untreated seeds of barley (*Hordeum vulgare*) variety Westminster (L.S. Plant Breeding, Cambridge, UK) were germinated on damp vermiculite for 7 days in total, with an

initial period of 3 days under foil to exclude light in order to synchronise germination. Eight plants were then transplanted into each of 10 containers with 1.2 L of 20% strength Hoagland solution.

Containers were opaque to prevent light reaching the solution thus limiting algal growth. Each lid had 8 holes into which each plant was placed and supported using sponge plugs so that roots were in contact with the nutrient solution. Barley plants were then grown and acclimatised in hydroponics for 13 days prior to treatment. Plants were kept in a glasshouse with natural light supplemented by sodium-vapour lamps to provide a 12 hour photo-period; temperatures were between 25 °C and 35 °C during the light period and averaged 15 °C in the dark period. In order to investigate the effects of treatment on biomass and zinc content of *H. vulgare*, 50 nm nZnO was compared with that of bulk-sized ZnO, an ionic control of $ZnSO_4$ and a control of low zinc modified Hoagland solution. A concentration range of the different treatments was given to simulate an exposure event, resulting in three different initial concentrations per treatment type.

The 10 boxes were randomly assigned a treatment using a random number generator (RAND function) in Microsoft Excel 2003, and the 20 day old plants were then treated once with their allocated zinc-containing compounds. Particles were dispersed in 50ml Hoagland media before being sonicated for 1 h and then added to the containers and stirred for 1 m. Container volume was maintained at 1.2 L throughout the experiment by topping up the container with Hoagland solution daily to replenish used media. Containers were stirred daily using a clean stainless steel spatula. Plants were then harvested and analysed 7 days after initial treatment.

5.2.4. Collection of Barley Root Exudates

Four week old control barley root exudate was collected after the hydroponic experiments above. Fifty ml samples of used 20 % Hoagland media containing root exudates after barley plant treatment at the highest treatment concentration of 500 mg/L from each treatment together with the control (no zinc-containing treatment) were filtered through grade 1 Whatman filter paper into 50 ml polypropylene tubes. In addition, the roots of barley seedlings grown at the same time as those transplanted into hydroponics that had been maintained on watered vermiculite for a week were washed with DI water and the washings collected in 50 ml centrifuge tubes after filtration. All tubes were then centrifuged at 5,000 RPM for 15 minutes to pellet particulates and the supernatant was passed through a 0.22 µm syringe filter into sterile 50 ml centrifuge tubes under aseptic technique. This produced barley root exudates in both water and Hoagland solution; a soup of organics; for comparison.

Total organic carbon (TOC) using a Shimadzu TOC-VCPH analyser (Shimadzu, UK) values were obtained for both seedling washings and Hoagland solution plus exudates from the control barley, and found to be 50.18 ± 0.33 and 52.4 ± 0.45 ppm respectively. These solutions were then frozen at –80 °C and used subsequently for zeta potential and bacterial toxicity analyses (see sections **5.2.7**, **6.2.2.3**, and **7.2.1.3**).

5.2.5. Dry Biomass Assessment of Barley

After 7 days of treatment both the aerial portion of each plant and the root network for each box was harvested using a stainless steel razor blade. Roots were washed in deionised water three times before and after being washed with 0.1 M EDTA solution to remove surface bound zinc, after which all plant material was dried for 48 hours in an oven at 60 °C. The aerial portion of each plant from each box was then weighed to 3 decimal

places, and the roots were weighed collectively and the total divided by the number of plants as they were unable to be separated after growing entangled.

5.2.6. Zinc Quantification of Barley Tissues

After drying the plant material, the aerial portion of each plant was ground to a powder using an agate pestle and mortar and a clean stainless steel spatula was used to collect an aliquot weighing about 0.2 g from each plant sample. For the roots, all the roots from each treatment were ground in the same manner and three samples of about 0.2 g were taken. Each sample was then weighed to 3 decimal places and digested with 3 ml of 70 % nitric acid (Sigma, UK) in 50 ml polypropylene centrifuge tubes. Samples were left to digest for 48 hours before being made up to 10 ml volume with MilliQ water and filtered through Whatman grade 1 filter paper. Filtrate was then topped up to 50 ml by the addition of more MilliQ water before samples were analysed using an Agilent Atomic Absorption Spectrometer (AAS) (Agilent, UK). The instrument was calibrated using zinc chloride standards prior to use and MilliQ water was used as a zero control. Samples were diluted further if required in order for measurements to fit within the calibration range. Zinc content was recorded as a concentration in ppm from which the zinc content per gram of plant material was then calculated. Averages and standard deviations of zinc content per treatment in both roots and shoots were then calculated.

5.2.7. Zeta Potential of Particles in Different Media

Six different media were chosen to determine the stability and charge of particles in the media used for the hydroponic experiments with and without root exudate influence. Particle suspensions were made at 100 mg/L concentration in six different media; DI water, pH 5.8 HCl solution, 20 % Hoagland solution, 1 week old barley root washings in DI water, 4-week-old control barley root exudate in Hoagland solution and nutrient broth.

Hydrochloric acid solution was made at a concentration of 1.6 µM HCl (pH 5.8) using DI water. This pH was chosen as this was the measured pH of the root exudate solutions and hence acted as a pH control for the exudate solutions. In addition, for zeta potential values of particles in bacterial experiments described in Chapter 3 and 7, bacterial nutrient broth was made by adding 25 g of lysogeny broth-Miller powder with 5 g/L glucose (both from Sigma Aldrich, UK) to 1 litre of DI water prior to autoclaving at 121 ºC for 15 minutes. Zeta potential values were obtained in triplicate using a Malvern ZetaSizer Nano ZS (Malvern instruments, Worcestershire, UK).

5.2.8. Barley Seed Surface Sterilization

Seeds are non-sterile and as such can contain bacteria and fungal spores which would contaminate the agar used in the barley seed soak assay below. Barley seeds were surface sterilised by soaking in 10 % hypochlorite and 70 % ethanol solution for 15 minutes before being washed five times with sterile DI water under sterile conditions as described in section **4.2.3**. They were then placed onto the relevant agar plates using sterile stainless steel tweezers using aseptic technique.

5.2.9. Barley Seed Soak Assay

In order to determine the effect of an exposure event to barley seeds pre-germination, a seed soaking assay was developed, in which seeds were soaked in different treatment concentrations and allowed to germinate and grow for 7 days to produce seedlings. This allowed determination of the effects on root and shoot elongation after ZnO exposure to seeds as opposed to roots. After surface sterilization of barley as described above, 20 seeds were soaked in sonicated 50 nm nZnO, bulk and $ZnSO_4$ suspensions at 10, 50 and 100 mg/L concentrations for 90 minutes. Concentration range was chosen after this range produced significant root attenuation in agar-based early developmental phytotoxicity experiments in

section **4.3.1**. They were then placed onto sterile technical agar made at 0.6 % w/v as previously described in section **4.2.5.1**, with the omission of nanoparticles, and were allowed to germinate under foil for 2 days, after which point the foil was removed. They were then grown for 5 days further until the plants were carefully removed and the root and shoot elongation measured using Vernier callipers.

5.2.10. Hydroponic Growth of MicroTom Tomato Plants

Tomato seeds were germinated on damp vermiculite under foil for 2 days. Seedlings were watered as required to maintain a damp root environment for 2 weeks at which point 8 individual plants were carefully removed and placed into each of three hydroponic containers containing 1.2 L of 20 % Hoagland solution and supported by foam plugs as described earlier in section **5.2.3**. Plants were kept in a BudBox V2 XL grow tent (BudBox, UK) supplemented by red and blue lamps producing around 5.0 klux of light as determined by a CEM DT-1308 Light Meter (CEM, UK) for 8 hours per day. Temperature, CO_2 and humidity were measured continuously using an Extech CO100 CO_2 monitor (Extech instruments, UK) and found to be between 20 to 25 ºC throughout, with 450 to 550 ppm CO_2 and approximately 40 % humidity. Plants were allowed to acclimatise to the hydroponic systems for 4 weeks during which time any used media was replenished. After this 4 week period, containers were randomly assigned a treatment of either no particles (control), bulk ZnO, or 50 nm nZnO particles, at which point particle containing suspensions which had been sonicated for 1 hour in Hoagland solution were added to the appropriate container and stirred for one minute to produce a final treatment concentration of 100 mg/L. Plants were then continually replenished with fresh 20 % Hoagland media as required and the hydroponic solution was stirred for one minute 5 times per week. Each container was checked five times per week and any physiological differences such as bolting, flower and tomato formation were noted.

After 18 weeks of growth (12 weeks post initial treatment) the number of red, orange and green tomatoes was counted for each treatment. This time point was chosen as no new flowers had been produced by the plants for 1 week and all existing flowers had either attenuated or progressed to fruit formation. Tomatoes were checked daily for ripeness and were deemed ripe when entirely red in colour and the stem holding the tomato yielded to very little pressure. Subsequently, ripe tomatoes were harvested and dried at 60 ºC for 48 hours, after which point their dry mass was measured to three decimal places.

5.2.11. Statistical Analysis

Each hydroponic box contained 7 - 8 plants and all subsequent shoot measurements were averaged and the standard deviation calculated and displayed graphically. For root and stem elongation in the barley seed soak assay, averages and standard deviations of 20 plants for each treatment type were calculated. Zeta potential data was taken in triplicate from which the average and standard deviation were calculated. Data was analysed using a Student's t-test and 1-way ANOVA with further post hoc Tukey analysis for comparison of means of groups using 0.05 as the alpha value.

5.3. Results and Discussion

The response of the barley seed exposure was assessed by measuring the individual root and stem lengths of seedlings to determine how individual parts of the seedlings reacted to treatment exposure.

5.3.1. Barley Seed Soak Assay

For the seed soak assay, root and stem lengths of barley seedlings were measured and displayed in **Figure 5.2 A** & **B.**

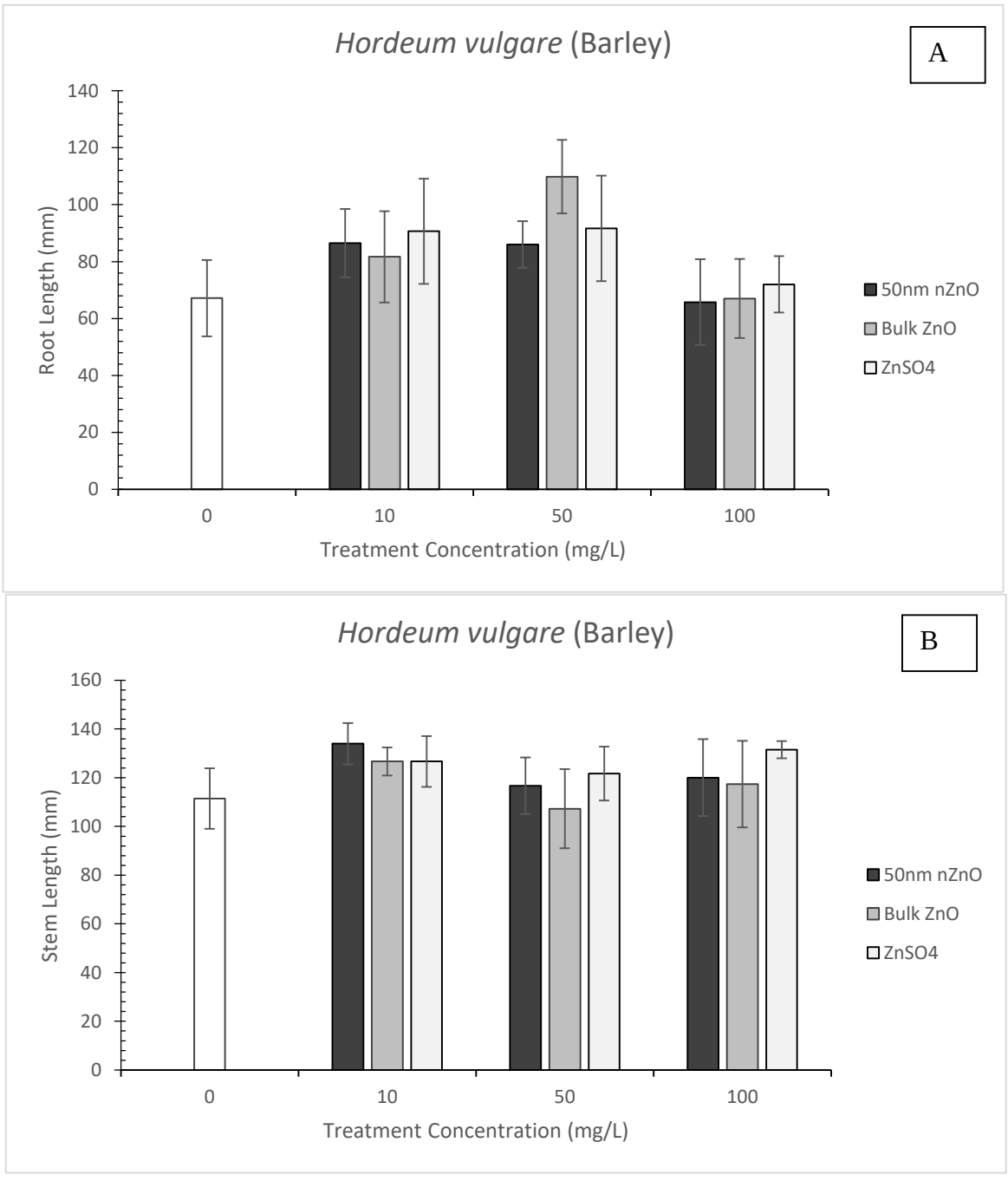


Figure 5.2 A & B: Root lengths (A) and stem lengths (B) of 7 day old *Hordeum vulgare* seedlings after the seeds were soaked in zinc-containing treatments for 90 minutes before germinating and being grown on sloppy technical agar. Error bars denote one standard deviation above and below the mean (*n* = 20).

Results were analysed using 1-way ANOVA. For stem length, differences between groups were non-significant ($p = 0.277$). No further interaction between groups was found as determined by Tukey-Kramer minimum significant differences (MSD) analysis. This demonstrated that treatment type or concentration had no effect on stem length up to 100 mg/L.

However for root length, 1-way ANOVA identified a significant difference between treatments ($p < 0.002$) with post-hoc Tukey-Kramer MSD analysis identifying interactions between bulk 50 mg/L with $ZnSO_4$ 100 mg/L, control, and bulk 100 mg/L. This demonstrated that the bulk particles significantly stimulated root growth at 50 mg/L as compared to the control, and at the highest concentration of 100 mg/L there was no difference between the three treatment types. This identified that there was no reduction in root length for any treatment at any concentration up to 100 mg/L, and slight stimulation was detected as a result of bulk ZnO treatment at 50 mg/L.

The data demonstrated that the soaking of barley seeds in solutions containing nanoparticulate ZnO caused no detectable attenuation of root or stem length relative to the control up to 100 mg/L. In addition, no impact on germination was observed, with all seeds germinating within the 2 days under foil. This suggested that the treatments were either unable to permeate the seed coat and enter the starch-rich endosperm that provides nutrition to the embryo, or treatment concentration was insufficient to cause a decrease in subsequent development. The germination and development of corn has previously been shown to be affected by seed soaking treatment, but only at the very high concentration of 2000 mg/L of exposure (Lin & Xing, 2007). The same concentration range of 10 - 100 mg/L was demonstrated to cause significant attenuation of root lengths of the four species tested in section **4.3.1**, when the particles were homogeneously dispersed in the agar support media and roots made direct contact with the particle media. In this seed soak assay, the application

of nanoparticles was to the seed coat, as opposed to in direct contact with the roots. In the particle agar the exposure to particles was also constant throughout the assay of 7 days, whereas in the seed soak assay there was a one-time application of treatment. This indicated that the mode of treatment was important in determining how the stem and root lengths were affected. In terms of implications for environmental release of nano ZnO particles this revealed that contact with seeds was potentially less of a concern than contact with root systems. This was not unexpected as seed coats have evolved to be durable and protective of the embryo within, whereas roots have evolved to be partially permeable and sequester nutrients. This highlighted the differences between alternative nanoparticle toxicity testing methods in plants and the fact that different parts of the plant can respond differently.

5.3.2. Toxicity of nZnO, Bulk ZnO and Zn^{2+} to Barley in Hydroponics

Plants were deliberately only treated for 7 days in hydroponics in order to maintain plants in relatively good health. After 7 days of treatment, some chlorosis was detected, particularly in the older leaves and in plants treated with 500 mg/L $ZnSO_4$, which correlated with the lowest root biomass of all plants treated in the study (Supplementary S1). This demonstrated that high Zn^{2+} concentration had a role in reducing biomass and chlorophyll discolouration. Dry biomass of root and aerial plant portions was measured from oven dried plant tissues and displayed in **Figure 5.3**. For the dry biomass of the root tissues increased mass was observed at the lowest concentration of 10 mg/L for bulk and $ZnSO_4$ treatment, but not for 50 nm nZnO which remained similar to the control. The higher concentration of 100 mg/L resulted in a decrease in mass relative to the control for 50 nm nZnO and at 500 mg/L all treatments appeared to reduce biomass relative to the control with the greatest reduction observed with $ZnSO_4$.

For the total dry biomass of the barley plants, all treatments at all concentrations had a significantly reduced biomass compared to the control as determined using a Student's t-test ($p < 0.05$). This demonstrated that even low concentrations of 10 mg/L of all treatments were able to reduce overall biomass. The reduction in biomass at the lowest treatment concentration of 10 mg/L demonstrated that 50 nm nZnO was significantly more toxic than bulk or $ZnSO_4$ treatments.

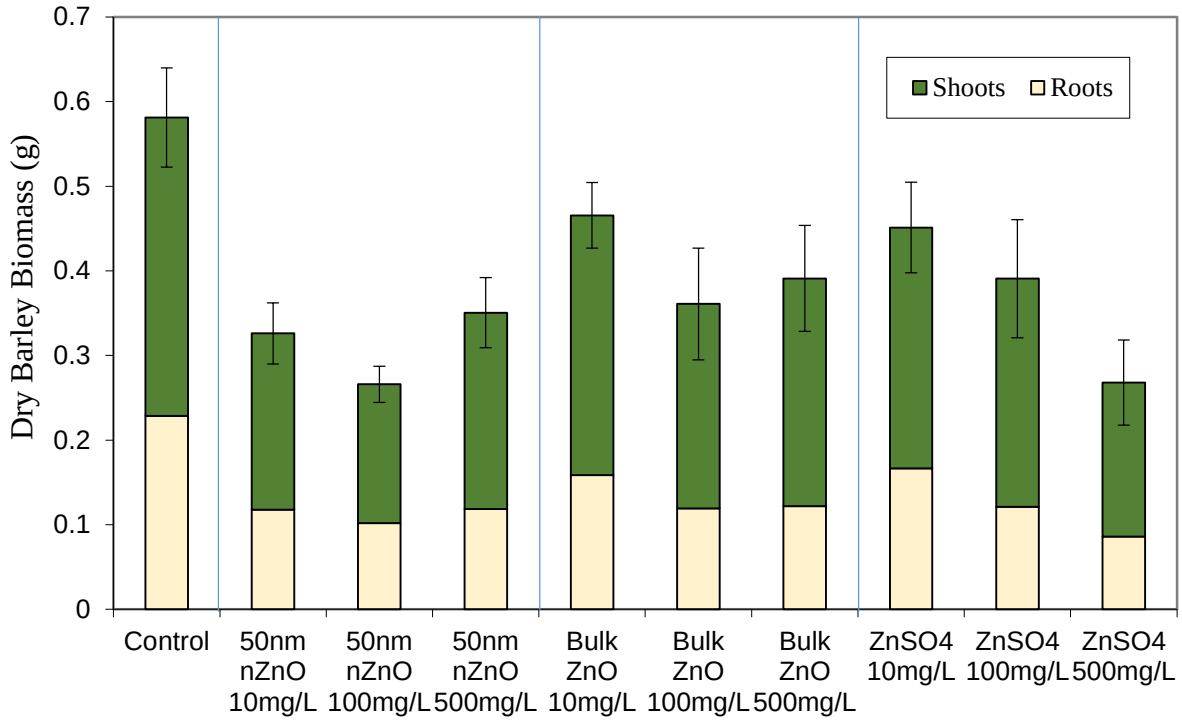


Figure 5.3: Dry shoot and root biomasses of *H. vulgare* per plant after treatment with 3 different concentrations of 50 nm nZnO, bulk ZnO and $ZnSO_4$. Error bars represent one standard deviation above and below the mean (n = 8).

At the highest concentration of 500 mg/L nZnO, both root and shoot biomasses increased from the 100 mg/L treatment biomasses despite the fact there were 5 times more particles present in the media. This suggested that either the plants may have been able to tolerate higher concentrations of 500 mg/L better than 100 mg/L or 10 mg/L, or that the increased number of particles in the highest concentration meant particles were more likely

to collide and overcome their electrostatic repulsion, and hence they crashed out of suspension, reducing their bioavailability. The latter proposed mechanism for reduced toxicity was supported by the zeta potential data. This demonstrated that both bulk and nZnO were below the threshold of stability of 30 mV and hence were likely to crash out over time. This hypothesis was supported when examining the biomass after treatment with the non-particulate $ZnSO_4$ treatment. This revealed a much more concentration dependent decline in biomass according to treatment. With both particle treatments the same reduced toxicity at the highest concentration was demonstrated, which suggested particle dispersion state had an important role in plant toxicity as measured by biomass.

It is also possible that tolerance mechanisms within the plant controlled liberation of Zn^{2+} ions from the particles, or uptake of these ions, ion chelator complexes or both. This could be achieved by influencing the concentration of chelating phyto-metallophore release to ameliorate toxic effects, as has been previously demonstrated with aluminium (Heim *et. al.*, 2001). This could also explain the particle specific effect as opposed to the concentration dependent response to ionic treatment.

5.3.3. Uptake of Zinc by Barley

The zinc content of the root tissue was dose dependent at all test concentrations, with 50 nm nZnO treatment resulting in the greatest uptake from all treatments within each concentration (**Figure 5.4**). The control containing low zinc modified Hoagland solution resulted in very little zinc having been detected in root (0.019 mg/g) or aerial tissues (0.026 mg/g). Very high levels of zinc were detected in the root tissues, with the highest measured concentration of 47 mg/g Zinc determined for plant roots treated with the highest concentration of 500 mg/L 50 nm nZnO.

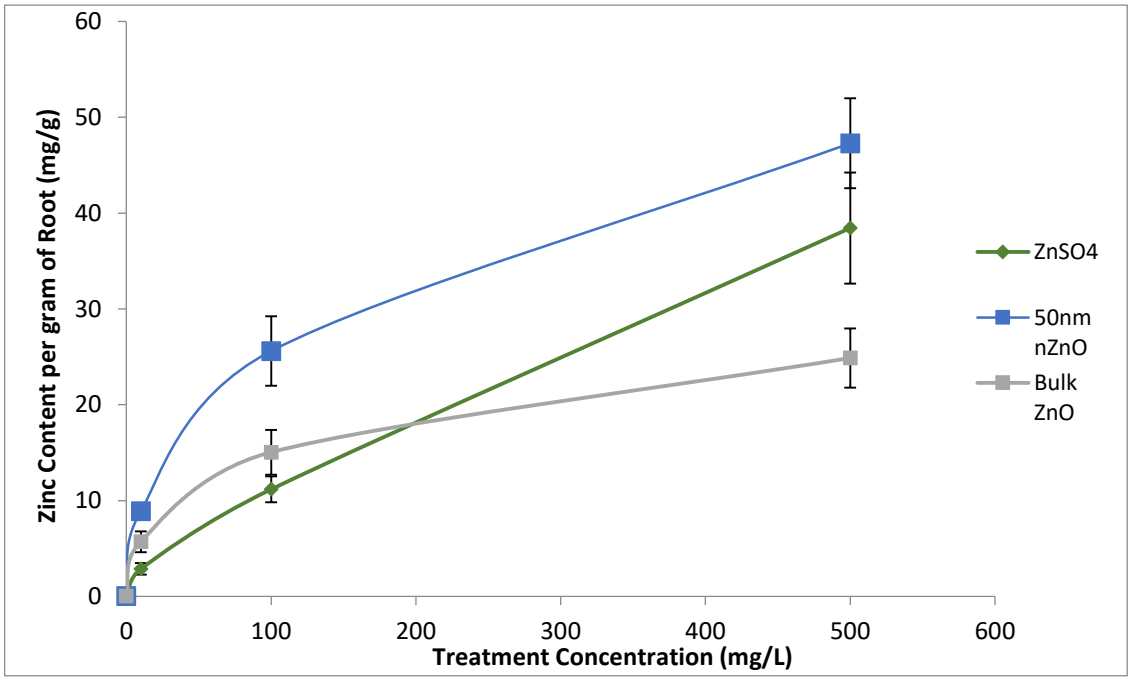


Figure 5.4: Zinc content of root tissues of *H. vulgare* after treatment with 3 different concentrations of 50 nm nZnO, bulk ZnO and $ZnSO_4$ (mg/g). Error bars represent one standard deviation above and below the mean (*n* = 3).

The zinc content of the aerial plant portions of the plant was an order of magnitude smaller than in root tissues. Zinc content varied according to treatment type, with significant differences between all 3 treatments at the lowest concentration of 10 mg/L (**Figure 5.5**). At this concentration, 50 nm nZnO treatment caused the greatest accumulation of zinc within tissues, with 103.5 % more zinc entering the aerial part of the plant than from the bulk treatment and 315.4 % more than from $ZnSO_4$. At a concentration of 100 mg/L 50 nm nZnO, plant zinc content increased, and 50 nm nZnO still caused a significantly greater quantity of zinc in tissues than the other treatments ($p \leq 0.001$). The quantity of zinc within aerial plant tissues after just 100 mg/L of 50 nm nZnO treatment did not differ significantly to that observed from 500 mg/L of the fully soluble $ZnSO_4$ despite a five-fold increase in concentration (3.00 mg/g and 2.92 mg/g respectively, $p = 0.42$).

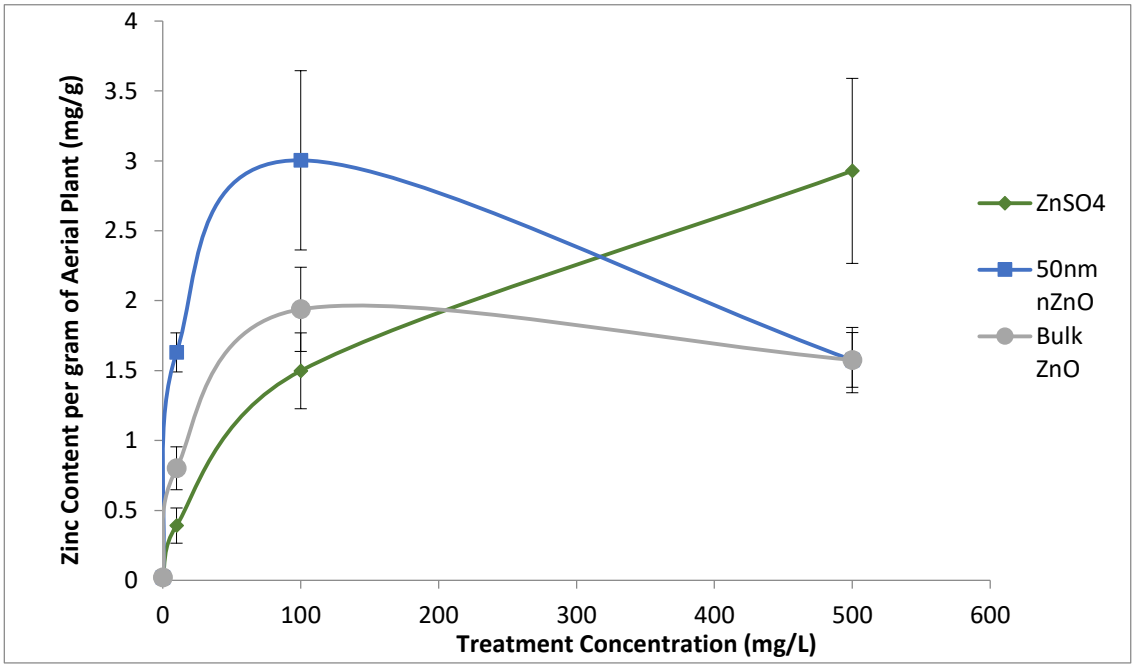


Figure 5.5: Zinc content of stems and leaf tissues of *H. vulgare* after treatment with 3 different concentrations of 50 nm nZnO, bulk ZnO and $ZnSO_4$ (mg/g) Error bars represent one standard deviation above and below the mean ($n = 8$)

5.3.4. Translocation of Zinc from Root to Shoot

The upwards translocation of zinc from the root to the shoot was calculated by dividing aerial zinc by total plant zinc content, and converted into a percentage of total plant zinc (**Table 5.1**). The higher the percentage, the greater the translocation effect of zinc from root to shoot. The translocation effect varied from 50.16 % (from the control) to 6.87 % (from nZnO at 500 mg/L) depending on different treatments and concentrations. At the lowest concentration of treatments, 10 mg/L, there was no significant difference between nano-sized and bulk ZnO ($p = 0.24$), and at the higher concentrations, 100 mg/L and 500 mg/L, there was significantly more translocation of zinc from the bulk sized particles than the nano-sized ($p = 0.001$ and $p < 0.0003$ respectively). This was also true for nano-sized zinc oxide and $ZnSO_4$, where there was significantly more translocation from the ionic zinc treatment ($p < 0.003$ for all three concentrations). When this was related to the Zn^{2+} dissolution data collected in Chapter 2, it was found that the order of most translocation correlated with the order of solubility in Hoagland solution. The $ZnSO_4$ was fully soluble, and lead to the highest translocation values at 100 mg/L and 500 mg/L treatment concentrations. Next in terms of solubility in Hoagland solution were the bulk particles, and finally the nZnO particles. This order was reflected in the data, as the least translocation was detected as a result of nZnO treatment.

Table 5.1: Percentage (%) of total plant zinc found in aerial plant. Tabulated to show the translocation effect ± one standard deviation (%) (*n* = 8). High values represent translocation of zinc from root to the shoot, low values represent zinc remaining in root tissues.

Treatment Concentration	0 mg/L (%)	10 mg/L (%)	100 mg/L (%)	500 mg/L (%)
Control	50.16 (± 3.32)			
New 50 nm nZnO		19.80 (± 1.19)	15.26 (± 1.53)	6.09 (± 2.40)
Bulk ZnO		18.92 (± 2.97)	17.94 (± 0.72)	11.34 (± 1.77)
$ZnSO_4$		17.87 (± 0.56)	20.75 (± 0.82)	13.55 (± 2.88)

5.3.5. Physiological Response to Treatment in MicroTom Tomato Plants

The flowering time for each tomato plant in each treatment was noted by daily observation throughout the experiment. All the plants treated with nZnO showed a bolt response after only 1 week of treatment. This was characterised by an elongation in the stem and a reduction in leaf size and number relative to the control. In addition, early flowering was observed in the nZnO treated plants, with the first flower produced when the plants were just 5 weeks old, 10 days prior to the first flower in the control. Five flowers had been produced by the 50 nm nZnO treated tomato plants by the time the first flower had been produced by the control plants at 6 weeks and 3 days old and then the bulk plants produced the first flower 2 days after the control. Plants from all treatments produced multiple flowers by the time the plants had reached 8 weeks old. As a result of early flowering, the 50 nm treated plants were the first to start producing fruit. By week 18 however, the control had produced nearly double the number of fruits. For photographs of development progression see Supplementary S2.

5.3.6. Ripening and Quantities of Tomatoes Produced

After 18 weeks, no new flowers had been produced for a week, and all existing flowers had either attenuated or developed into tomatoes. Each pot contained 8 plants and the total number of red, orange or green tomatoes was counted and expressed in **Figure 5.6.** The results showed that the control plants had produced nearly twice the number of tomatoes as the 50 nm treated plants, and nearly three times the quantity as the bulk ZnO treated plants. The number of tomatoes that had ripened by this point was 13, 5 and 2 for control, 50 nm nZnO and bulk ZnO respectively. The preliminary results from this experiment indicated that 50 nm nZnO induced early flowering and fruiting when compared to the control and bulk treatments. However, when the number of fruit produced was compared, it appeared that 50 nm nZnO had a lower impact on tomato formation than its bulk counterpart. It was not possible to analyse whether the bulk and nZnO were significantly different from one another in terms of time to flower and tomato production.

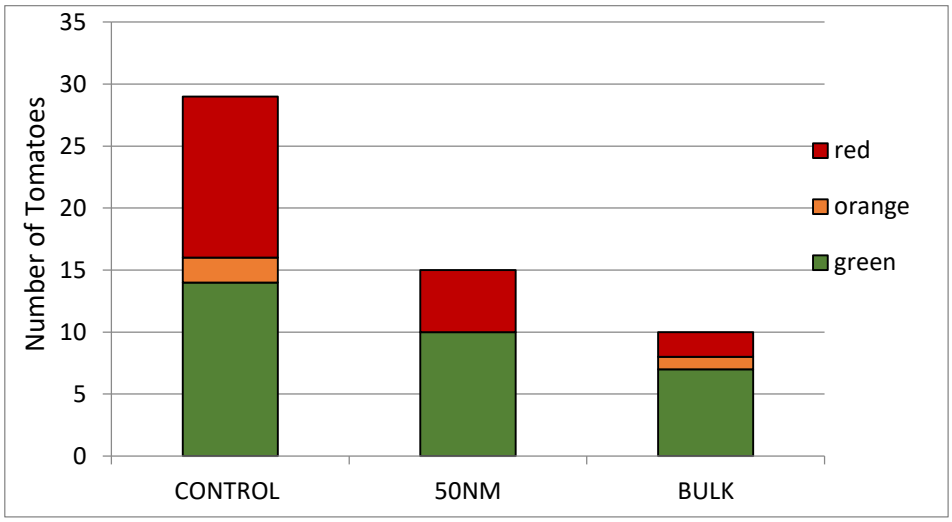


Figure 5.6: Number of red, orange and green tomatoes produced by MicroTom plants for each treatment after 18 weeks growth, 12 of which were in the presence of the 100 mg/L zinc-containing treatment (*n* = 8 plants per treatment).

5.3.7. Dry Mass Assessment of Ripe Tomato Fruit

The ripe fruits from the hydroponic study of MicroTom plants were harvested and dried and their average masses plotted in **Figure 5.7.** There was no significant difference between any of the treatments in terms of fruit biomass; however it should be noted that only 2 ripe fruit were produced in the case of bulk ZnO. The non-significant difference in fruit biomass between the 50 nm nZnO particle treatment and the control indicated that nZnO treatment may influence the number of tomatoes produced but not their average mass.

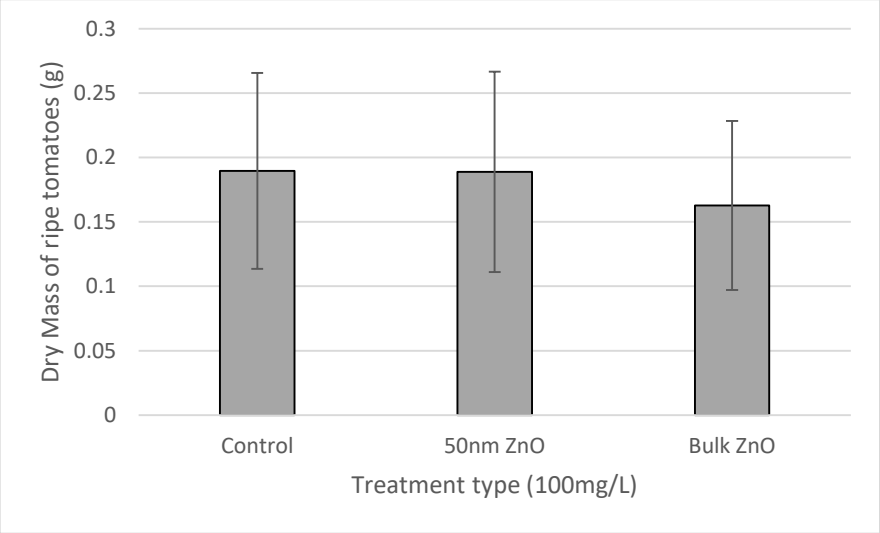


Figure 5.7: Dry mass of individual ripe tomatoes as harvested from 18 week old MicroTom plants grown in the presence of 100 mg/L bulk ZnO or nZnO particles. (For control, *n* = 13; 50 nm, *n* = 5; bulk, *n* = 2). Error bar denotes one standard deviation above and below the mean.

5.3.8. Zeta Potential of Particles in Different Media

Zeta potential varied between different particles and different media (**Figure 5.8)**.

In water, the zeta potential value was significantly greater for nZnO than for bulk ZnO ($p < 0.003$), showing greater colloidal stability. The presence of root exudates improved stability of both nZnO and bulk ZnO particles in Hoagland solution ($p < 0.003$ and $p < 0.005$ respectively).

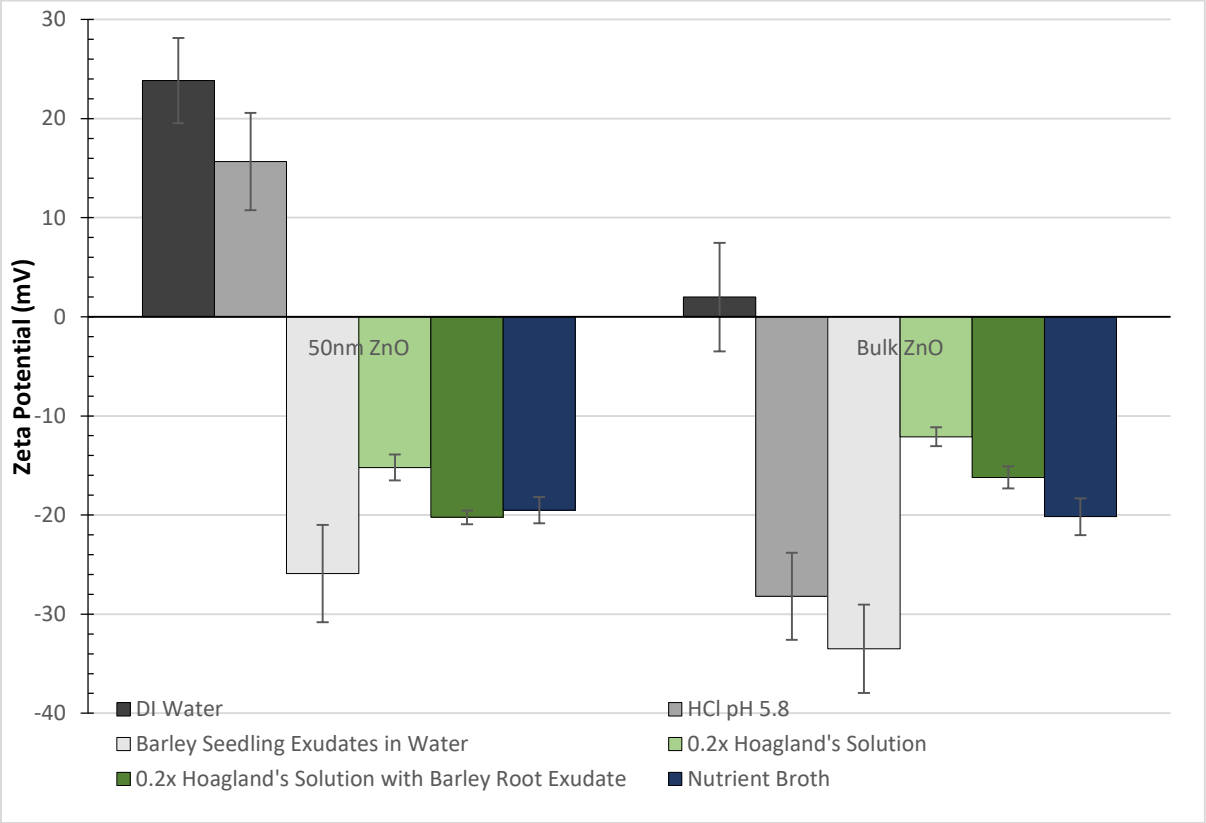


Figure 5.8: Zeta potential (mV) of 100 mg/L dispersions of 50 nm and bulk-sized ZnO particles in 6 different biologically relevant media. Error bars represent one standard deviation (*n* = 3)

Furthermore, seedling exudates changed the charge of 50 nm nZnO particles; the zeta potential changed from positive in water to negative in exudate solution. They had the same effect on bulk ZnO particles, significantly increasing the magnitude of the zeta potential value from around +2.0 mV to -33.5 mV, which dramatically increased stability. Zeta

potential values of nZnO and bulk ZnO were not significantly different from one another when in seedling washings (p = 0.059) suggesting stability of particles was similar when in contact with exudates. Bulk ZnO colloidal stability was near zero in water however became much more negative with seedling exudate influence. This was the only mixture that reached a zeta potential of greater than ± 30 mV, which is the benchmark often used as an indicator for stability, i.e. the particles are unlikely to agglomerate over time. All other mixtures showed a lesser zeta potential value, indicating their likelihood to agglomerate over time and become less bioavailable. This was demonstrated after leaving two cuvettes containing 100 mg/L nZnO in Hoagland solution and DI water for 24 hours (**Figure 5.9**).

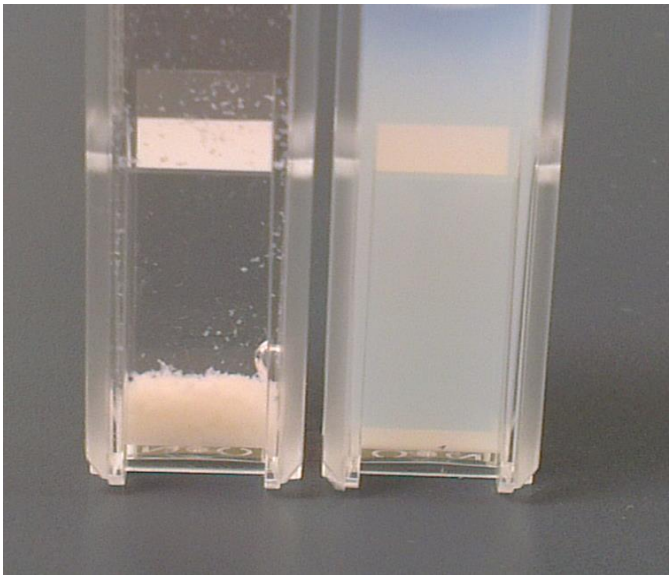


Figure 5.9: Photograph of 1 cm cuvettes containing 100 mg/ L of 50 nm nZnO in Hoagland solution (left) and in DI water (right) after standing for 24 hours. Zeta potential values were -15.2 mV and +23.8 mV respectively, hence in Hoagland the particles had flocculated due to low stability, whereas in water they were still well dispersed.

In Hoagland solution, the particles flocculated and crashed out of suspension. This showed that during the hydroponic treatments that lasted 7 days the particles were unlikely to be well dispersed, and although suspensions were stirred daily the particles were likely to have settled out of colloidal suspension. This demonstrated a limitation to the method of

nanoparticle toxicity studies in hydroponic solution, however soil studies have been found to have similar limitations due to particle adsorption to soil particles. For both particles, seedling exudate influence in water led to a greater zeta potential value than root exudate influence in Hoagland solution, suggesting that the plants in this study were able to positively influence particle stability.

In the particle-dispersed agar assays described in Chapter 3, particles were maintained at an optimally dispersed state for the duration of the experiment by being trapped in a solid agar matrix immediately post sonication. As a result, up to 100 % attenuation of root length of both monocotyledonous and dicotyledonous species was observed at concentrations of 100 mg/L, which is significantly lower than the highest concentration used in the hydroponic experiment of 500 mg/L.

5.4. Discussion

The zinc content of *Hordeum vulgare* (Barley) v. Westminster grown hydroponically was investigated after treatment with ZnO particles (50 nm and bulk (~700 nm) sized) and Zn^{2+} ions from zinc sulphate, after which plant biomass was measured along with zinc content with an Atomic Absorption Spectrometer (AAS) to quantify zinc uptake within root and shoot tissues. Zinc content of both roots and aerial plant tissues was significantly greater as a result of 50 nm nZnO treatment than with bulk-sized ZnO or $ZnSO_4$, except at the highest concentration used in this study, 500 mg/L, where zinc uptake from 50 nm nZnO was around 40 % lower than that observed from 100 mg/L 50 nm nZnO, suggesting plant regulation of uptake at high concentrations, or reduced bioavailability of nZnO at higher concentrations.

5.4.1. Plant Toxicity Response was Different for Nanoscale ZnO

The plant response to metal toxicity has previously been categorized into two types of response; the limitation of metal uptake and translocation, and induced mechanisms within the plant to increase tolerance. Different plant species might use either or both strategies in coping with increased metal bioavailability, as an excess of essential metals like zinc can lead to reduced growth and toxicity at a cellular and metabolic level (Marschner *et. al.*, 1995). Essential micronutrients such as zinc can cause stimulation at low concentrations, tolerance at average concentrations and toxicity at high concentrations. In this study, zinc was able to enter barley plant root and shoot tissue from hydroponics containing 50 nm nZnO particles. The amount of zinc detected in plant tissues was an order of magnitude higher in root tissues than shoot tissues, which suggested either that treatment was staying in the roots or that plant uptake into the aerial plant was restricted. Nano-scale zinc oxide behaved differently to the bulk and ionic material. Zinc content within aerial plant tissues after treatment with 100 mg/L of 50 nm nZnO was similar to the tissue content after treatment with 500 mg/L of the fully soluble $ZnSO_4$, suggesting that zinc was able to enter the plant from nZnO treatment more efficiently than from the ionic form at this concentration. This may be due to exudates facilitating the solubility and stability of the nZnO, as zeta potential data showed that plant root exudate influence increased the negativity of both nZnO and bulk ZnO particles in Hoagland solution, increasing stability and reducing tendency to agglomerate.

5.4.2. Translocation of Zinc from Root to Shoot was Lower for Nanoparticulate than Bulk or Ionic Treatments

The ability to quantify zinc uptake and translocation from engineered nano-scale zinc oxide (nZnO) is an important consideration in determining the effect of nZnO on mainstay edible crop plants, as well as quantifying the potential removal of zinc from nZnO

contaminated environments. When the proportion of total zinc that was able to be translocated from root to shoot in barley was examined, it was found that plants treated with nZnO had lower translocation than those treated with both ionic and bulk forms of zinc-containing treatment controlled for zinc content.

The low translocation within plant tissues of zinc from particulate treatment meant that most of the zinc remained in the roots, which could be as a result of particle adsorption to root surfaces or internalisation. Although roots were washed thoroughly with both water and 0.1M EDTA solution which should have dissolved and remove any adsorbed ZnO, it was possible that some remained, and/or that zinc is physically within the root tissues. Either of these eventualities would explain low translocation. In Chapter 4, clearing of nZnO was observed in the nanoparticulate dispersed technical agar plates which suggested local dissolution of particles around root surfaces. This indicated that the higher root presence of zinc in the hydroponic experiments came from within the tissues rather than from external adsorption.

The majority of studies have examined young plants between 0 and 15 days old, particularly in the case of ZnO studies (Lopez Moreno *et. al.*, 2010, Lin and Xing 2007, 2008), whereas this study sought to investigate the effects on older plants treated for 7 days from 20 days and 27 days onwards. The advantage of this was that their vascular systems were better developed and provided a better insight into the effect of ENPs on more established plants, and any differences between biomasses were more easily distinguishable and able to be analysed.

5.4.3. Plant Root Exudates Modified ZnO

Plant uptake of zinc has evolved to be efficient as plants are usually zinc limited in most soils. The bioavailability of metals can limit the plants ability to sequester these ions,

and as such they have developed different methods to maximise uptake (Dakora *et. al.*, 2002). Particularly in areas of low free metal ion concentration the plant must employ measures to liberate free ions from chelated or bound forms, such as by lowering pH and releasing organic chelators and reducing agents.

Barley releases phytometallophores; metal complexing ligands which can bind to metal ions in order to scavenge them from solution (Kochian, 1993). There is some evidence that gramminaceous monocotolydons such as barley can absorb phytometallophore complexes directly (Romheld & Marchner, 1986, Erenoglu *et. al.*, 2000, Tolay *et. al.*, 2001), and this combined with controlled reduction to metal ions provides an easy supply of essential metals. Zinc movement within root tissues can be facilitated by phytometallophores, in addition to metallothioneins in order to keep free Zn^{2+} ion concentration low to reduce potentially harmful redox reactions (Palmgren *et. al.*, 2008). In this experiment root zinc content was found to be concentration dependent, whereas this was not the case for shoots. As the AAS measures total zinc in any form, it is possible that the plants had internally bound the zinc to chelators in order to keep the free Zn^{2+} ion concentration low and in order to control uptake into the aerial portions of the plant. This could explain the low impact of increased concentration on biomass and chlorosis across all treatments.

In summary, it was demonstrated that 50 nm nZnO affected barley differently to bulk ZnO and ionic zinc from zinc sulphate in terms of tissue zinc content and biomass. Zeta potential analysis showed that particles had different charges in different media. The results showed that the presence of root exudate in Hoagland media elicited a significantly larger negative value than with Hoagland alone for both particle types, demonstrating that root exudates increased stability of both bulk sized and nano-scale zinc oxide. In the plant-

modified Hoagland media the bulk ZnO particles had a more negative value than the nZnO particles which implied greater stability.

The root zinc content was far greater from nZnO than both other treatments at all concentrations. The same was true for the shoot zinc content except at the highest concentration, where nZnO and bulk ZnO resulted in a very similar tissue concentration of zinc. This was significantly less than that from $ZnSO_4$ at that concentration. The aerial portion of the plant never made direct contact with the zinc-containing treatments, and so any zinc contained within aerial tissues was the result of uptake from the roots.

From the agar visualization studies of barley in Chapter 4 it was noted that the nanoparticles appeared to clear around the root, which corresponded with the areas of low pH, suggesting biomodification of the particles by exudates, and dissolution likely mediated by the chelating fraction of the exudates, as demonstrated by the same clearing on the nanoparticle dispersed agar plates observed on addition of 0.1M EDTA solution but not pH 5 HCl.

5.4.4. Zeta Potential of Particles Changed as a Result of Root Exudate Influence

The zeta potential results revealed that nanoparticle stability was greatest with barley seedling exudates in water, followed by nZnO in DI water alone. With root exudates in Hoagland solution, particles had greater stability than when in Hoagland solution alone. This change demonstrated that Hoagland solution had a negative impact on particle stability. This was probably the result of the increased ionic strength imparted by the components of Hoagland solution. Electrolytes such as the $MgSO_4$ and $Ca(NO_3)_2$ salts contained in Hoagland solution were able to reduce the energy barrier required to overcome repulsive

forces from particle surface charge, and if this energy barrier was sufficiently decreased, NPs crashed out of suspension.

5.4.5. Tomato Plants Flowered Early as a Result of nZnO Treatment

With the addition of 100 mg/L of nZnO particles, bolting of the stems was observed and this corresponded with early flowering with respect to the control and the bulk ZnO treated plants. This lead to early tomato formation, however after 18 weeks the control had produced nearly double the number of tomatoes as the 50 nm ZnO treated plants.

The results from this experiment suggested that a full scale assay would be worth pursuing in the future in order to further investigate the potential use of nZnO to promote early flowering in agriculture. This information may be of interest to tomato growers who theoretically may be able to use this knowledge to apply a small dose of nZnO particles to tomato plants in order to induce early flowering and tomato formation according to requirement. An example of this might be if the weather forecast suggested that unfavourable conditions are imminent then flowering time could be artificially induced a week early. If the particles were then able to be removed from the system after the stimulation had occurred it is possible that the tomato yield might not be affected.

Of all the physical barriers used in sunscreens, zinc oxide exhibits the broadest protection from UV rays (Pinnell *et. al.*, 2000). Particles that enter the environment through waste streams are unlikely to be in pristine, uncoated condition, particularly due to the oils that coat them in sun protective products, and as such any toxicity results from pristine nZnO are likely to over-estimate environmental toxicity. The nZnO examined in this study had no oil-based coatings and hence is likely to exhibit greater toxicity than particles released into the environment from sunscreens and coatings (Johnson *et. al.*, 2011), however, the reduced zeta potential of particles as a result of dispersion in Hoagland solution meant that particles

were less than optimally (heterogeneously) dispersed and hence were less bioavailable. This study identified that the translocation of zinc from root to shoot correlated with the solubility of the particles in Hoagland solution, with greater translocation as solubility increased (in order of most to least: $ZnSO_4$ > Bulk ZnO > nZnO). However, the overall uptake was higher as a result of nZnO treatment, which suggested that small size and increased zeta potential may increase the quantities of zinc able to enter the plant. This may enable the future prediction of toxicity of zinc oxide and potentially other metal oxide nanomaterials based on size and zeta potential measurements.

This study also identified that nZnO might be useful in promoting early flowering of tomato plants, with scope for future experiments to investigate an optimum dose of nZnO that could be introduced to hydroponically grown tomato plants in order to influence flowering and fruiting, though at the risk of reducing yield.

6. MATERIAL PROPERTIES OF AN AGED FORM OF NANO-SCALE ZINC OXIDE AS COMPARED WITH A NON-AGED FORM

6.1. Introduction

6.1.1. Nanoparticle Ageing

Ageing in nanoparticles is a particularly understudied area in terms of particle behaviour and toxicity analysis, with significant implications for manufacturers and also for impact on end of life disposal (Cao *et. al.*, 2013, Liu & Hu., 2005). Recently an increase in the number of studies on physical changes of nanomaterials over time indicate that ageing processes include oxidation, sintering (aggregation), switching of oxidation states, change in catalytic activity, displacement of surface ligands, and changes in size and surface chemistry including carbonate formation (Cao *et. al.*, 2013; Mudunkotuwa *et. al.*, 2012; Kuchibhatla *et. al.*, 2012; Woo *et. al.*, 2008). Increased knowledge on particle changes and evolution over time will be of great importance for manufacturers who can test the materials for efficacy for the designed purpose e.g. photocatalysis, conductivity or UV-absorption after ageing to better inform their knowledge on shelf-life (Davis *et. al.*, 2006). By assessing the differences in material characteristics of the 'Old' 50 nm nZnO particles compared to the non-aged 'New' form, the physical changes as particles evolve over time can be identified. Both particles are ZnO doped with 6% Al_2O_3 with their only difference being age. Hence examining their size, release of ROS, solubility and surface charge will provide vital information on temporal changes in the ZnO nanoparticles after exposure. These two particles will then be examined for toxicity in biological systems in Chapter 6, with any differences then able to be related to their material properties as examined in this chapter.

6.1.2. Nanoparticles Used in Study

This work sought to examine the difference in toxicity between 4-year aged and un-aged 50 nm nZnO powder purchased new from Sigma Aldrich designated 'Old' and 'New' respectively. The Old form had been opened and stored in the original container for 4 years in ambient conditions, whereas the New form was ≤ 6months old during the analyses and was maintained in the original container. As ageing is a difficult phenomenon to quantify, particles were treated as would be expected within a lab setting; kept on a lab shelf in standard laboratory conditions of 18 ºC – 25 ºC out of direct sunlight in the original amber glass packaging, and opened infrequently for fewer than 5 minutes at a time. The new 50 nm particles were kept sealed in a zip-lock bag in their original amber glass container, fewer than 6 months since having been opened and stored otherwise in the same conditions as the old particles in terms of positioning, frequency of opening and temperature.

To determine whether there was a chemical and physical difference between particles; size, ROS release, and surface charge and chemistry were examined along with UV-visible absorption, and then related to any differences observed between the two particles in terms of plant and bacterial toxicity in Chapter 7.

6.1.3. Zeta Potential

The surface charge of particles can be deduced by the zeta potential; it is the difference in charge in millivolts (mV) between the electrical double layer on the particle surface, and the bulk solution (Honary *et. al.*, 2013; Shaw, 2009). Zeta potential offers information on particle stability, with readings greater than ±30mV indicating stability over time due to sufficient electrostatic repulsion between particles (Rao *et. al.*, 2013). Below these values, van der Waals attraction is sufficient to overcome electrostatic repulsion over time and particles may agglomerate and crash out of suspension (Prach *et. al.*, 2013). In this

study, the differences in zeta potential of Old and New 50 nm nZnO particles in six different media was measured to provide information on bioavailability of particles in the different media used for each biological assay.

6.1.4. Zinc Solubility of Particles

Solubility of nanoparticles is an important factor in nanoparticle toxicity (Cronholm *et. al*., 2011, Yamamoto *et. al*., 2001). In this chapter, rates of dissolution were calculated for Old versus New nZnO particles in both DI water and Hoagland solution.

6.1.5. Hydrodynamic Diameter

For hydrodynamic diameter measurement of particles to determine approximate size in liquid suspension, dynamic light scatter (DLS) analysis was used. From the direct measurements of scattered light, the Malvern software calculated hydrodynamic size based on the Stokes-Einstein relationship due to particle movement under Brownian motion through a known viscosity liquid (James & Driskell, 2013) (section **2.1.1.1**).

The phenomenon of an increase in particle size over time has been previously documented (Whitley *et. al.*, 2013; Yu *et. al.*, 2012). This can occur as a result of Ostwald ripening, where the size of particles increases over time in a thermodynamically-driven process due to the fact that larger particles are more energetically favourable (Ostwald, 1891). Nanoparticles, with their large surface area to volume ratio, are less energetically favourable than larger particles, as there are more surface atoms exposed relative to the number of more stable, fully bound atoms within the crystal (Gupta *et. al.*, 2006). As entropy, i.e. disorder within a thermodynamic system, can never decrease, the system moves towards increased entropy and eventually thermodynamic equilibrium, hence, the less entropically favoured smaller nanoparticles evolve into becoming larger, more stable particles (Yarmand *et. al.*, 2014). From ambient moisture to which the aged nZnO particles

in this study are exposed, combined with the slight solubility of ZnO, it is likely that a small number of very small crystals on the particle surface dissolve and redeposit on the surfaces of larger crystals, causing an increase in size as described by Otswald ripening. This, combined with agglomeration by van der Waals attractive forces and electrostatic repulsive forces, dictates the observed size of particles and is often attributed to size increase from ageing (Davis *et. al.*, 2006). By using DLS, a size distribution can be recorded, providing information on particle size differences between Old and New nZnO particles. A size distribution provides more information than a mean diameter measurement alone, as the proportion of smaller to larger particles is revealed.

6.1.6. Fourier Transform Infrared Spectroscopy (FTIR)

FTIR is a spectroscopic method to determine the molecular 'fingerprint' of a substance. It is used to determine the identities of components in a mixture by irradiating it with infrared (IR) and analysing the absorption and transmission through the sample (Griffiths & Hasseth, 2007). Each absorption peak relates to the vibration frequency between bonds of the atoms within the sample, hence the spectrum produced is unique to each material. It is frequently used due to its high sensitivity, rapid measurements and reliable internal calibration using a HeNe laser standard (Prati *et. al.*, 2010). Hence results are highly accurate and reproducible in qualitatively identifying unique compounds. (Liu and Yan, 2011).

As it was hypothesised that there would be differences in surface chemistry between the two particles because of age, FTIR was used to analyse surface chemistry and detect surface bound molecules. This was used along with other methods including zeta potential, ROS quantification, UV visible absorption and size analysis to characterise the 2 particles and then relate differences observed to their behaviour in biological systems.

6.1.7. UV Visible Spectroscopy

The UV-visible absorbance of a material is an important factor in material optical properties, and is closely linked with particle size as previously discussed in section **2.1.6**. Hence, the measurement of UV-visible absorbance of the Old vs New 50 nm nZnO particles is of interest, both in ascertaining whether there was a change in optical properties as a result of ageing as well as the ability to link any observations with size data.

6.2. Materials and Methods

6.2.1. Nanoparticles

This work aimed to determine whether 50 nm nZnO particles subject to 4 years of ageing in ambient conditions were differently toxic than 50 nm nZnO opened for ≤ 6 months and kept in a plastic Ziploc bag to minimise contact with air. The aged nanoparticles were stored in the original opened bottle on a workbench shelf. Both particles were originally purchased new from Sigma Aldrich and were stated as zinc oxide > 97 % < 50 nm particle size (confirmed by BET) containing 6 % Al_2O_3. Although particles were from different batches provided by the same supplier, both powders had a formula weight of 81.39 g/mol and conformed under X-ray fluorescence (XRF) and X-ray diffraction (XRD) analyses in terms of crystal structure, size and composition.

6.2.2. Material Characterisation

Material characterisation of size, zeta potential and ROS quantification for both particles was performed using previously described methods (sections **2.2.3, 2.2.6** and **5.2.7**). Zeta potential of particles was measured for both particles to determine differences in colloidal stability between the two particle types in different biologically relevant media. In addition, FTIR analysis on both particle types was conducted to determine surface chemistry differences between both particle types. Absorbance values for both particle types were also

compared using UV Visible Spectroscopy over a concentration range to examine differences in optical characteristics between particles.

6.2.2.1. FTIR Analysis

New and Old nZnO particles were suspended in 70 % isopropanol alcohol at a concentration of 100 mg/L and sonicated at 40 KHz for one hour. An aliquot of 100 µl was pipetted onto a 10 mm x 10 mm clean silicone wafer and air dried to allow isopropanol evaporation for 24 h at 25 ºC in a drying cabinet. Each wafer was then analysed with a Varian Excalibur FTS 3500 FTIR (Agilent; Cheshire, UK) spectrometer with wavenumber range from 4,000 to 500 cm^{-1}. Measurements of absorbance were taken for each wavenumber by Assia Taferka; D.Phil candidate in Materials Science, University of Oxford, and recorded by the software. Subsequently, results were displayed graphically and the two particle types layered for comparison. Peaks were identified using data on compound type and frequency range compiled by Silverstein *et. al.*, (1998) and Solomons *et. al.*, (2001). Peak analysis qualitatively identified chemical modifications to the particles surface (Fang *et. al.*, 2008).

6.2.2.2. DLS Size Measurement

In order to establish the hydrodynamic diameter of the two different particles in water based suspensions, dynamic light scattering (DLS) was employed. Cuvettes containing sonicated 100 mg/L nZnO particles dispersed in DI water were placed in a Malvern ZetaSizer Nano-S (Malvern Instruments, UK) and analysed at a maintained temperature of 20 ºC with a count rate of 260 per second and a measurement duration of 90 seconds according to manufacturer's instruction (as described in section **2.2.3**). Measurements were taken in triplicate and all data was checked to conform by the software quality control analysis.

6.2.2.3. Zeta Potential

Zeta potential of particles was performed as per section **5.2.7**, with both Old and New 50 nm nZnO particles dispersed in the 6 chosen biologically relevant media at a concentration of 100 mg/L and sonicated for 1 hour at 40 kHz. As previously described, these media included DI water, HCl dissolved in DI water adjusted to pH 5.8 as a pH control for the root exudate solutions, Hoagland media (pH 6.2 ± 0.08), barley seedling exudates in water (pH 5.81 ± 0.10), and Hoagland solution with control barley root exudate (pH 6.04 ± 0.12). The barley seedling exudates in water and control barley exudates in Hoagland solution were further characterised using total organic carbon (TOC) analysis, for which the values were comparable at 50.18 mg/L ± 0.33 and 52.4 mg/L ± 0.45 respectively (see section **5.2.4**). In addition, lysogeny broth-Miller (Sigma Aldrich; Dorset, UK), as used in all microbiological experiments in this report, was used as a sixth test media to determine particle charge in the microbiological experiments as well as for the plant related experiments. All measurements were made in triplicate from which the mean and standard deviation was calculated.

6.2.2.4. Reactive Oxygen Species Quantification

The relative release of ROS from the surface of the nanoparticles was examined using the fluorescent dye coumarin as described in section **2.2.6** to detect the relative levels of OH radicals released at the particle surface (Louis *et. al.*, 2004).

6.2.2.5. UV Visible Spectroscopy

Both particle types were examined optically using the BioTek microplate reader at wavelengths of 630 nm and 405 nm, method as described in section **2.2.8.** Values of particle absorbance at 630 nm were used to distinguish optical density from particles and optical

density as a result of bacterial growth by the subtraction of the particle absorbance value from the total.

6.2.2.6. Zinc Dissolution Assay from Old and New 50 nm nZnO

Dissolution experiments were carried out as described in section **2.2.7** with 100 mg/L suspensions of New and Old nZnO particles in DI water and Hoagland solution over 288 h.

6.3. Results and Conclusions

6.3.1. Zeta Potential

The zeta potential of the two particles in 6 different media was measured and the recorded data displayed in **Figure 6.1**. Results showed no significant difference between particle types in five out of six media however the difference was highly significant in DI water (p = 0.0019). This demonstrated that the New 50 nm nZnO particles had a significantly greater surface charge than the Old nZnO particles when dispersed in DI water, which indicated greater stability. The zeta potential of the Old nZnO particles in water was around zero, which showed that they were around the isoelectric point and were not stable in suspension. However, with the addition of different media, all containing solutes which affected the charge of the particles, there was no significant difference between the two particles. This showed that the addition of biological media eliminated the differences in zeta potential between the Old and New nZnO particle types, and made their surface charge highly similar within error. This is a very important observation as many studies make assumptions of stability based solely on particle behaviour in DI water, as opposed to within biological media, and hence any inferences made to particle stability in media from data obtained in DI water might be erroneous.

The greatest particle stability was found with the addition of barley seedling exudates in water, which gave the ENPs a significantly greater zeta potential than the barley root

exudates in Hoagland solution. The values for New and Old particles in seedling exudates in water were -25.9 ± 4.90 mV and -26.9 ± 4.77 mV respectively, which were the greatest values observed in all media. The greater stability of particles in seedling exudates in water as opposed to barley exudates in Hoagland solution may be explained by the lower zeta potential in Hoagland solution alone, which was -15.2 mV, when compared to the New nZnO particles in water alone, which was +23.8 mV. This demonstrated that the Hoagland solution alone reduced stability, and the presence of root exudates increased stability, both when in water and in Hoagland solution. This showed that barley root exudates facilitated nZnO particle stability by increasing the magnitude of the zeta potential, which made the surface charge significantly greater and reduced the tendency of particles to crash out of solution. The exudates had this effect on 50 nm nZnO in both water and Hoagland solution, which showed an important role of plant root exudates in particle behaviour and stability.

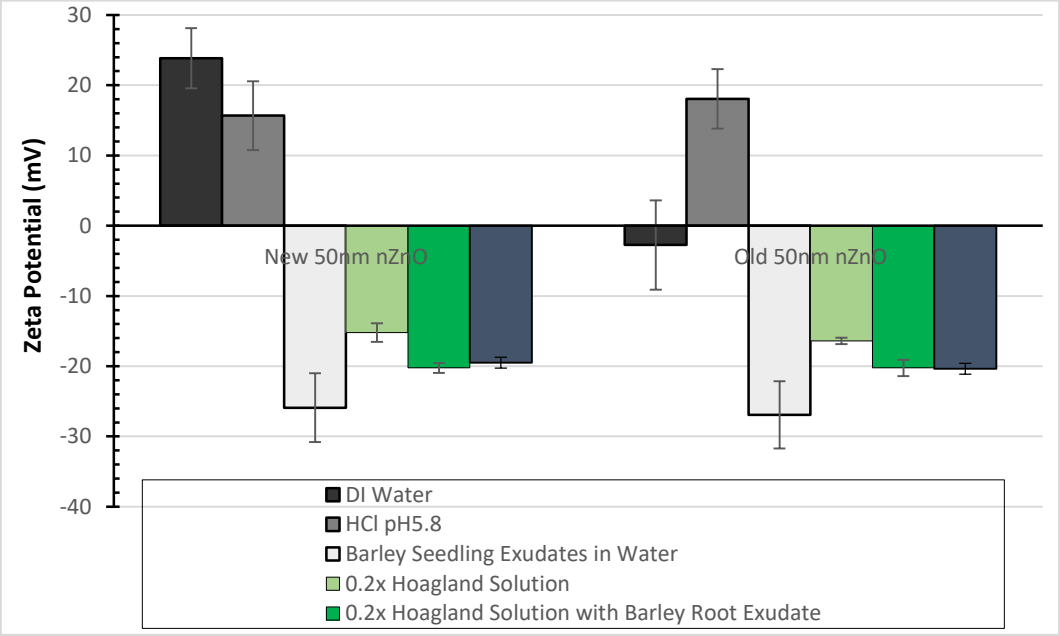
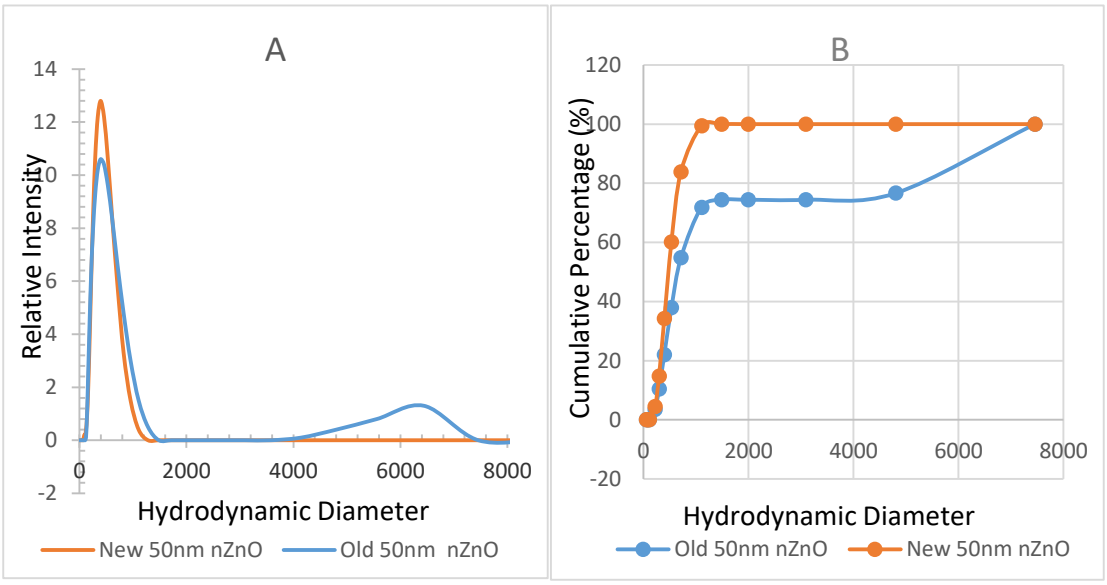


Figure 6.1: Zeta potential of two differently aged 50 nm nZnO particles 'New' and 'Old' in 6 biologically relevant media. Zeta potential was measured at 100 mg/L particle concentration in DI water, HCl at pH 5.8 to match root exudate solution, Hoagland solution (pH 6.2 ± 0.08), barley seedling exudates in water (pH 5.80 ± 0.10, total organic carbon (TOC) value 50.18 ± 0.33 mg/L), Hoagland solution with barley root exudate (pH 6.04 ± 0.12, TOC value 52.4 ± 0.45 mg/L)

6.3.2. Hydrodynamic Diameter of Particles

During all experiments, particles were used in water based suspensions and hence hydrodynamic diameter was an important factor in particle behaviour, as a result of the effect on movement caused by the electric dipole layer surrounding the particle. To determine whether there was a difference in hydrodynamic diameter distribution DLS was used to compare size distribution by relative intensity of both 'New' and 'Old' 50 nm nZnO (**Figure 6.2 A**) and also cumulative percentage to determine relative proportion of particle sizes (**Figure 6.2 B**).



Figures 6.2 A & B: Hydrodynamic Particle size of 'Old' and 'New' 50 nm nZnO as measured by dynamic light scattering (DLS), displayed as relative intensity (A) and as cumulative percentage of counts from integrated DLS measurements (B).

The relative intensity of DLS scatter for both particles related to different hydrodynamic diameters was displayed graphically in **Figure 6.2 A**. A primary peak at 396 nm was recorded for both particle types, with the peak for Old nZnO having a lower intensity than for New nZnO. Old nZnO displayed a bimodal distribution, as a smaller secondary peak was recorded for Old nZnO at around 6000 nm, which was not observed for

New nZnO. This explained the mean hydrodynamic diameter as reported by the software of 506.7 ± 126.2 nm and 400.4 ± 56.22 nm for Old nZnO and New nZnO respectively.

A cumulative percentage was calculated from raw size distribution data in order to show the distribution of sizes between the two particle types Old and New 50 nm nZnO (**Figure 6.2 B**). It showed that the hydrodynamic diameter of around 75 % of Old nZnO particles was 1100 nm or below, whereas this was the case for nearly 100 % of the New nZnO particles. Less than 3 % of Old nZnO particles were between 1100 nm and 4800 nm and the remaining 22 % were large aggregates and agglomerates in the 5000 to 7500 nm range. This showed that a large proportion of particles were bigger, however the lack of particles in the 1100 to 4800 range showed that they are unlikely to be agglomerating gradually from the smaller size, but have instead formed larger particle clusters.

6.3.3. FTIR Spectroscopy

The FTIR spectra for Old and New 50 nm nZnO particles is shown in **Figure 6. 3**.

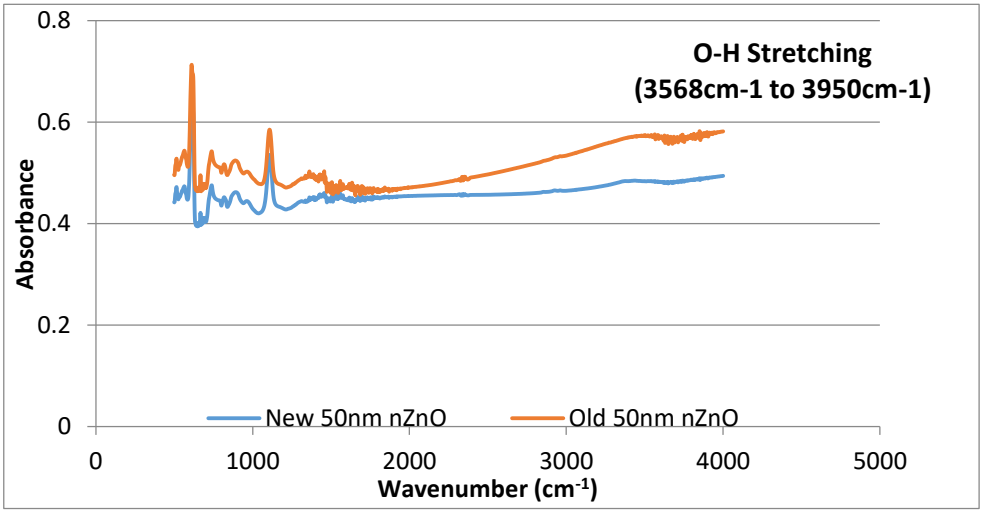
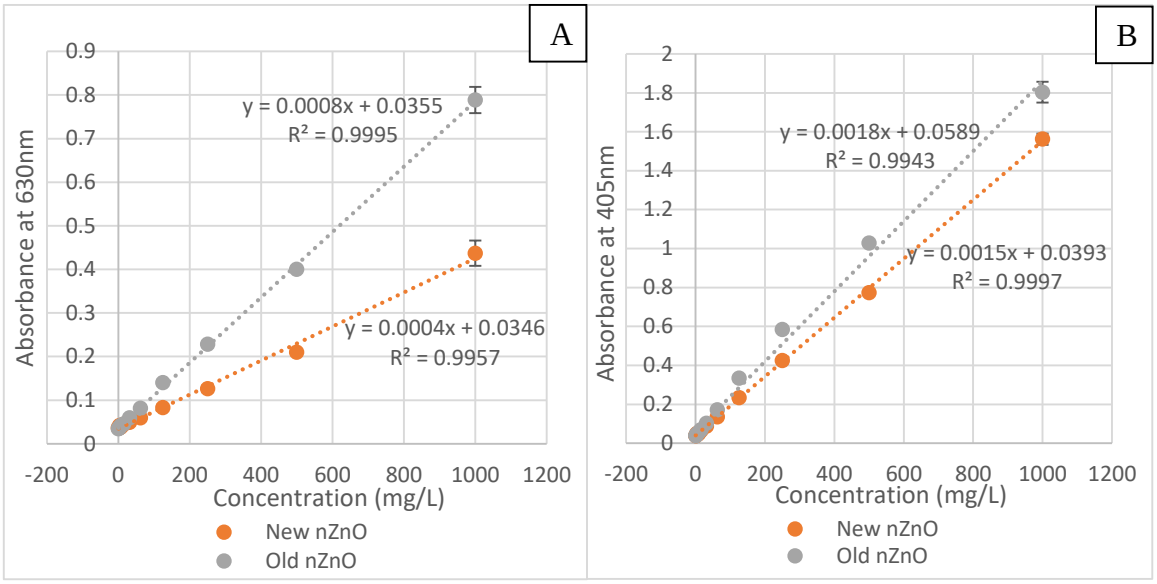


Figure 6.3: FTIR absorbance spectrum of Old 50 nm nZnO and New 50 nm nZnO particles, plotted against wavenumber (cm^{-1}).

The spectra were comparable for both particles, with primary peaks at 610 cm^{-1} and 1124 cm^{-1} identified as C-H bending and C-O stretching respectively from the isopropanol dispersant. A notable difference at a wavenumber of around 3568 cm^{-1} to 3950 cm^{-1} was detected between the two particles, which was identified as O-H stretching and showed Old 50 nm nZnO had greater O-H stretching than New nZnO. This included the range identified as hydroxyl adsorption bands (3672 cm^{-1} -3714 cm^{-1}) and not hydrogen bonds of surface water and water complexes (3260 cm^{-1} -3360 cm^{-1}) (Fang *et. al.*, 2008). Both particles showed a series of small peaks around 1645 cm^{-1} associated with O-H bending (Grassian *et. al.*, 2007). The results were consistent with current knowledge on metal oxide surfaces; they have surface O-H groups which are able to readily adsorb ambient water. In particular, the spectra showed that Old nZnO had more hydroxyl groups associated with its surface than New nZnO.

6.3.4. UV-Visible Absorbance

The absorbance of both Old and New 50 nm nZnO particles was measured over a range of 12 concentrations at 630 nm and 405 nm wavelengths and the results shown in **Figures 6.4 A** & **B.** The relationship between concentration and absorbance was linear at both wavelengths for both particle types up to 1000 mg/L, with absorbance increasing as concentration increased. The greatest absorbance was at 405 nm, where at the highest concentration of 1000 mg/L, Old nZnO particles had an absorbance of 1.80 ± 0.05 and New nZnO particles had an absorbance of 1.56 ± 0.04. At both wavelengths, both particles had significantly different absorption values at all concentrations. Absorbance values at 630 nm provided the base absorbance for particles used in bacterial growth assays, which allowed absorbance as a result of particles to be subtracted from the total absorbance in order to distinguish bacterial growth.



Figures 6.4 A & B: UV-visible Absorbance at 630 nm (A) and 405 nm (B) of Old and New 50 nm nZnO particles dispersed in DI water over a concentration range from ~0.5 mg/L to 1000 mg/L. Absorption values plotted against concentration with error bars showing one standard deviation above and below the mean. Linear trendlines plotted to fit data, with line equations and R^2 values shown on graphs.

6.3.5. Reactive Oxygen Species Release

The comparative release of ROS from both particle types was measured by detecting fluorescence at an excitation wavelength of 345 nm and emission of 450 nm from 7-hydroxycoumarin after 72 hours contact in amber vials to prevent UV photocatalysis. The percentage of fluorescence relative to the negative control was displayed in **Figure 6.5**.

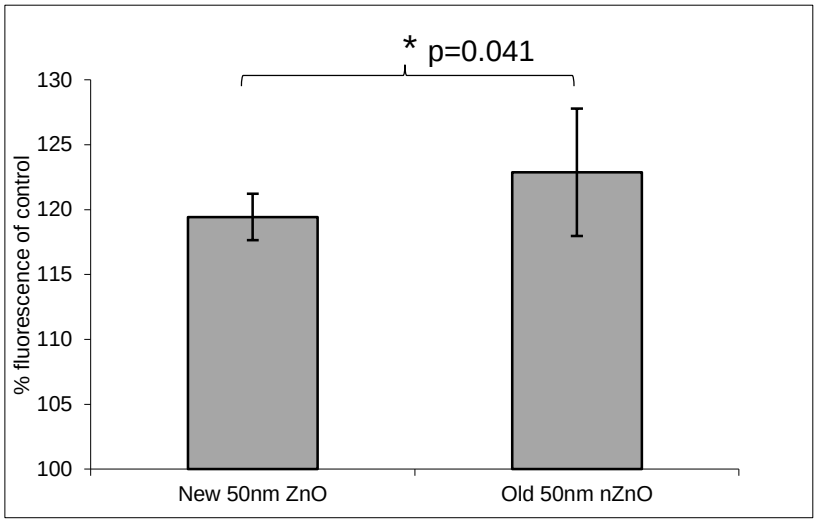
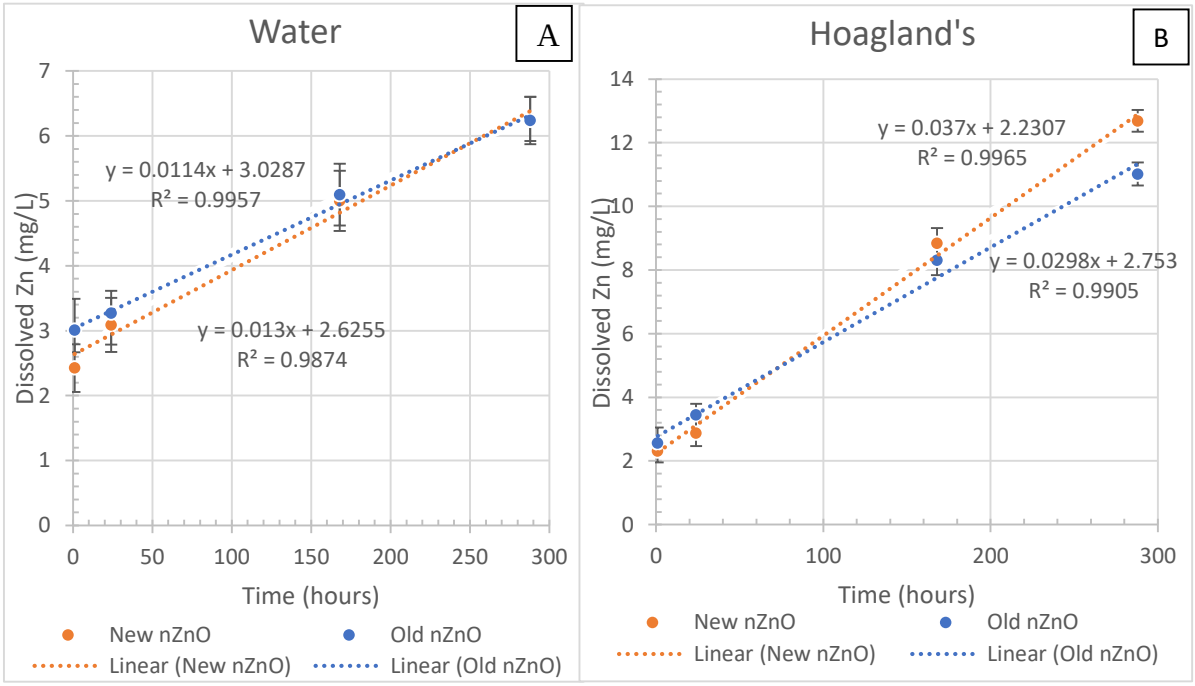


Figure 6.5: reactive oxygen species release from Old and New nZnO particles as determined by exposure to fluorescent dye coumarin for 72 h. Data expressed as a percentage of the negative control. Error bars show one standard deviation above and below the mean of triplicates.

The fluorescence signal was significantly different (p = 0.041) as determined by Student's t-test, with Old nZnO particles releasing significantly more ROS than New nZnO particles. Although the difference was significant, the Old nZnO particles only released around 3% more ROS than the New nZnO particles which showed there was only a small increase in ROS production from Old nZnO particles. There was no significant difference between the negative control and both particles detected before 72h (data not shown) despite measurements made at 1, 4, 8, 24 and 48 hours which showed that it took a minimum of 72h for ROS release from the particle surface to be within detectable limits.

6.3.6. Zinc Dissolution Assay

The soluble zinc from 100 mg/L Old and New nZnO particles was determined by ultrafiltration and quantification by AAS absorbance to obtain values of dissolved zinc over time in DI water and Hoagland solution (**Figure 6.6 A** & **B**). Linear trendlines were plotted to obtain the rate of dissolution over the 288 hours in both media, the values for which were displayed in **Table 6.1**.



Figures 6.6 A & B: Dissolution of Zn^{2+} from 50 nm nZnO and bulk-sized ZnO particles over time as determined by ultrafiltration and filtrate analysis using AAS. Figures show dissolution in DI water (A) and Hoagland solution (B). Linear trendlines displayed with line equation from which rate of dissolution was calculated. Error bars denote one standard deviation of triplicates.

Table 6.1: Summary of Zn dissolution from New and Old nZnO particles in DI water and Hoagland solution over time.

Particle type	Media type	Dissolution rate ($\mu g\ L^{-1}\ h^{-1}$)	Y intercept (mg/L)	% dissolved after 1 day	% dissolved after 7 days
New nZnO	DI water	13.0	2.626	3.47	5.61
New nZnO	Hoagland solution	37.0	2.231	3.23	9.91
Old nZnO	DI water	11.4	3.029	3.79	5.90
Old nZnO	Hoagland solution	29.8	2.753	3.47	9.70

For both particles in DI water the rates of dissolution were not significantly different at each of the sampling points ($p > 0.05$) as determined by Student's t-test. The dissolution rates were much higher in Hoagland solution than in DI water for both particles, consistent with the dissolution results in Chapter 2 which demonstrated that Hoagland solution facilitated dissolution of ZnO particles. The measured dissolved zinc was not significantly different between Old and New nZnO particles at all sample points in Hoagland solution except 288 hours where New nZnO released significantly more zinc ($p < 0.01$). This led to a higher calculated dissolution rate for New nZnO than Old nZnO particles in Hoagland solution, with rates of 37.0 and 29.8 $\mu g\ L^{-1}\ h^{-1}$ respectively. The calculations revealed that around 10% of the particles by zinc mass had dissolved after 7 days in Hoagland solution.

6.4. Discussion and Conclusions

This study was undertaken in order to establish whether there were age-related changes to the material properties of two 50 nm ZnO particles, one aged and one fresh. Changes in surface charge and chemistry along with particle size, UV-Visible absorption and ROS release were examined and compared between the two particles in order to make observations on differences. The information gathered in this chapter was then used to explain any differences observed in toxicity between the two particles in biological systems in Chapter 6. Furthermore, it aimed to provide information for manufacturers in order to advise on age-related changes of nZnO and to better establish shelf life guidelines.

6.4.1. Particle Size Differs Between Old and New nZnO Particles

The particle size in hydrated systems was found to be significantly different between Old and New particles in terms of hydrodynamic diameter. The average hydrodynamic diameter as measured in DI water showed that Old nZnO particles were around 25 % larger than New nZnO particles (approximately 506 nm and 400 nm respectively). This was post-sonication for one hour and measurements were taken immediately after sonication, which in theory suggested particles had aggregated over time, as sonication was able to break up agglomerates but not aggregated particles.

The hydrodynamic diameter cumulative size distribution revealed that the larger average diameter of the Old nZnO particles was as a result of 22 % of particles measuring between 4800 and 7500 nm in suspension. As particle suspensions were sonicated prior to analysis it is most likely that this 22 % represents the hydrodynamic diameters of aggregated particles which have sintered together over time. However, intensity data in **Figure 6.2 A** showed that the primary peak at around 500 nm had the same slope for both Old and New nZnO, just with a lower peak intensity. This showed that a significant fraction of Old and

New nZnO particles were of the same hydrodynamic diameter. It would be anticipated that the primary curve for Old nZnO would be the same as the curve for New nZnO, only shifted right as a result of all individual particles undergoing Ostwald ripening and increasing incrementally in size. However the initial slope was comparable for both particle types, which indicated that many of the Old particles had not become larger, but instead there was a discrete peak for Old nZnO at around 6000 nm, which indicated that a subsection of Old nZnO particles had aggregated or agglomerated more than New nZnO particles. This was in agreement with zeta potential data of both particles in DI water, where Old nZnO had a significantly lower value than New nZnO, which decreased the stability of particles in suspension and made agglomeration more likely. This showed that it was likely that the increased average size of Old nZnO particles was not due to gradual Ostwald ripening, but instead due to aggregation or agglomeration. It is not possible to definitively determine whether the larger particles were due to aggregation or agglomeration, as although the particles were sonicated thoroughly prior to analysis, the zeta potential of around zero mV meant the particle suspensions of Old nZnO particles were highly unstable and prone to agglomeration.

6.4.2. Zeta Potential of Old and New nZnO Particles Differs Only in Water

With regards to zeta potential, the differences were only significant when the particles were dispersed in DI water. In all 5 other biologically relevant media there was no significant difference between zeta potential values. This showed the importance of media on particle surface charge, and reinforced the need for zeta potential data to be recorded for particles in all media used (Schulze *et. al.*, 2008). Biological media contain a greater number of solutes and ligands which were able to modify the surface charge of the particles (Cho *et. al.*, 2012). Most notably, the presence of root exudates in Hoagland solution significantly increased the zeta potential from around -15 mV to -20 mV for both particles. Although this

was below the threshold for colloidal stability of ± 30 mV, it is still an increase in stability induced by plant root exudate compounds. This showed that nZnO particles have increased stability in the rhizosphere as a result of plant root influence, which, by reducing the tendency to agglomerate, would increase the bioavailability of the particles. This was still a lesser value than in DI water for New nZnO, however significantly more stable for Old nZnO. Also of note was the zeta potential change as a result of barley seedling exudates in DI water when compared to DI water alone. The surface charge changed from positive to negative, with both particles having a similar value of around -26 mV. This was greater than the zeta potential with the barley root exudates in Hoagland solution, which showed that Hoagland solution decreased particle stability and root exudates increased stability. As both the root exudate solutions were collected from the bulk solution shaken from the roots they represent a dilute form of root exudates. At the root surface, the source of exudation, there is a much higher concentration of root secreted compounds. This boundary layer is likely to have a strong effect on particle stability at the root-root environment interface and it is likely that particle stability will be even greater at this location as a result of the higher concentration of root exudates.

6.4.3. UV Visible Absorption Greater for Old than New nZnO Particles

New nZnO particles had lower absorption values, which is consistent with the literature in terms of smaller particle size leading to lower absorption values particularly at 630 nm (Goh *et. al.*, 2014). As the particle size for New nZnO was previously demonstrated to be smaller than for Old nZnO as measured by DLS in section **6.3.2**, the UV-visible absorption values were concordant with these findings.

6.4.4. FTIR Spectra Showed More Hydroxyl Groups on Old nZnO Surface than New nZnO.

The ZnO particles were prepared in 70 % isopropanol ($CH_3CHOHCH_3$) and commensurately peaks at 620 cm^{-1} and 1124 cm^{-1} were detected, attributed to C-H bending and C-O stretching respectively from isopropanol associating with the particle surface. The larger signal in the 3568 cm^{-1} to 3950 cm^{-1} range was associated with hydroxyl groups on the particle surface. This could be as a result of a greater number of OH radicals associated with the surface, OH from the isopropanol as a result of molecules trapped in a more porous particle surface, or a greater number of water molecules having reacted on the particle surface due to their increased age. The coumarin assay demonstrated that the quantity of hydroxyl (OH) radicals from either particle type was not significantly different from the negative control until 72 h had elapsed. This showed that the OH stretching from FTIR was unlikely to be as a result of OH radicals, and instead likely to be as result of greater porosity, aggregation-trapped water or surface reacted water. The lack of peaks in the 3260 cm^{-1} -3360 cm^{-1} region showed that it was unlikely that there were H-bonds of surface reacted water, hence the difference could be attributed to greater porosity or water involved in the aggregation process.

6.4.5. Dissolution of Old and New nZnO Not Significantly Different in DI Water

As Old nZnO particles were demonstrated to be slightly larger than the New nZnO particles, it was hypothesised that there would be a difference in solubility as a result of a larger surface area to volume ratio in New nZnO particles. However, in DI water there was no significant difference between the dissolution of both particles.

In Hoagland solution after 12 days the measured soluble zinc was significantly higher for New nZnO than Old nZnO particles, whereas there was no significant difference after 7 days. This demonstrated that within 7 days the particles had comparable solubility. As all bacterial and hydroponic experiments involving a comparison between New and Old nZnO particles lasted 7 days or less, it was demonstrated that there was no significant difference of solubility between the two particles and hence any differences detected in toxicity were not likely to be a result of different release of Zn^{2+} ions.

6.4.6. Limitations of Research

The ageing of nanoparticles over time is a poorly defined concept and varies according to particle type, ambient storage conditions, humidity and time. However, it is important to get some assessment on how the material changes when entering into the environment, not least it will alter the toxicity profile and hence baseline studies. In addition, in terms of engineered applications it is important to know the properties of the materials. This study demonstrated the fact that temporal changes in the material properties need to be considered.

Changes in material properties due to ageing are likely to vary between storage places and manufacturers. This study focusses on the ambient ageing over around 4 years of purchased nano-scale ZnO, and hence is a study that is not easy to repeat. Nonetheless, it is particularly interesting information for material, environmental and engineering sciences, and with enough information on particle change over time it may be possible for predictions to be made on the impact ageing and particle evolution has on toxicity to multiple species. Certificates of analysis provided by Sigma Aldrich showed particles conformed to the same properties including size and chemical formula when synthesised. Ideally the samples would have been from the same batch, however within the time constraints of a D. Phil it was not

possible to age particles for nearly 4 years and then perform comparisons, which was considered necessary in order for particles to have changed significantly enough over time to have different toxicity in biological systems, hence the two batches underwent a number of analyses to compare and relate any differences to these properties.

It would be impossible to age and non-age the same batch of ENPs because as they are bought simultaneously they will both be of the same age, and hence the only differences then would be as a result of different storage conditions as opposed to ageing. This study at least provides a comparison of two particles which are chemically similar and have slightly different physical properties.

6.4.7. Importance of Study

This body of work is of particular importance for researchers investigating particle properties in the lab, as often it may be assumed that the same container of ENPs can be used over a long period of time, as ENP ageing is not a widely known or understood phenomenon. This report has found that changes in ENPs attributed to around 4 years ageing are highly significant and hence ageing should be considered in terms of ENP behaviour in toxicity experiments. The influence of these differences in particle properties was then investigated in terms of biological toxicity in the subsequent chapter.

7. EXAMINING THE TOXICITY OF ENGINEERED NANO-SCALE ZINC OXIDE IN PLANT AND BACTERIAL SYSTEMS AFTER AGEING IN AMBIENT CONDITIONS

7.1. Introduction

The potential of nanoparticle toxicity and physico-chemical behaviour is still poorly understood, and this, coupled with particle change due to ageing, leads to complications in terms of characterising impact and mechanisms of toxicity. Several papers published in physical and chemical journals describe physico-chemical changes as a result of nanomaterial ageing, but the effects on biological systems to date has received little attention (Buzea *et. al.*, 2007; Kim *et. al.*, 2009; Reidy *et. al.*, 2013).

Whether this ageing affect translates to a direct difference in toxicity to plants and bacteria is an important consideration, with minimal studies to date having been made on how these age-specific changes to the nanomaterials may impact on exposed organisms (Manier *et. al.*, 2014). There are potential differences to acute toxicity and bacteriostatic or bacteriotoxic behaviour as a result of age-related changes in particle chemistry. A recent study on ageing of nano-scale cerium dioxide (CeO_2) investigated artificially aged particles, which had been kept for 3 days in water under ambient light and slow magnetic stirring (Manier *et. al.*, 2014). The toxicity of these aged and non-aged particles on micro-algae was examined and it was found that there was a very slight difference between the two particles, with aged inhibiting growth slightly less than non-aged particles, however whether this difference was statistically significant was not mentioned. The slight difference in toxicity was attributed to greater agglomeration of aged particles as measured by DLS. In Chapter 6 of this project it was demonstrated that around 25 % of Old nZnO particles had a significantly larger mean hydrodynamic diameter than New nZnO particles as a result of

agglomeration and/or aggregation, which is concordant with results from the study by Manier *et. al.* (2014), which also revealed that aged particles had an increased tendency to aggregate. The work presented in Chapter 6 furthered this by including measurements of zeta potential which revealed that New nZnO had a greater zeta potential than Old nZnO therefore was less likely to agglomerate.

With increasing information on the types of changes that occur over time, converting this into useful data for impact studies requires studies in phytological and bacterial systems. This information will be useful for updating disposal and exposure guidelines, in case of unanticipated environmental release. In addition, by analysing the differences in behaviour of an aged form of nanoparticle compared to its non-aged form, it is possible to tease apart the mechanisms behind the toxicity, as the fundamental chemical compound is similar but subtle changes and differences in size, ROS release, dissolution and surface charge can impact on toxicity. It also provides information on whether current assumptions on toxicity are valid over time, i.e. with regards to particle ageing. A reduction in toxicity after ageing during storage without affecting the designed behaviour or engineered characteristics would be reassuring in terms of reducing impact of nanomaterials on the environment. Conversely, an increase in toxicity after ageing would suggest that disposal guidelines may need to consider particle age in the assessment of how hazardous the material may be. The work presented in this study aimed to determine plant and bacterial toxicity, using evaluation methods from previous Chapters to analyse the biological impact of nano-scale ZnO ageing.

7.1.1. Bacterial Toxicity

In this study the two whole-cell biosensors *E. coli HB101 lux* and *A. baylyi recA_lux* were employed as they were previously in Chapter 3 (pages 81 to 82) in order to test the hypothesis that there was a difference in acute and gene toxicity of New and Old ZnO

nanoparticles. The growth inhibition of *E. coli* by both particle types was also investigated to determine whether the two particles were differently bacteriostatic. *E. coli* are Gram-negative rod-shaped bacteria measuring approximately 0.5 to 2 μm (Kubitschek *et. al.*, 1990). This particular bacterium was chosen due to the ease of culturing *in vitro* as well as for having the potential for human pathogenicity (Baker, 2015).

In Chapter 6 it was demonstrated that there were slight differences in material characteristics between the two particle types; with Old nZnO particles being larger and able to release greater quantities of ROS, and having lower stability in water than the New nZnO particles. The solubility of the particles was similar in both water and Hoagland media hence any potential differences observed were likely the result of the other particle characteristics, rather than Zn^{2+} release. This comparison therefore was controlled for solubility when in DI water and Hoagland solution, and hence aimed to determine which other material characteristics were able to affect different types of toxicity.

7.1.2. Plant toxicity

The toxicity of the two particle types were examined in barley plants grown hydroponically in nanoparticle-containing Hoagland solution. The effect of treatment and concentration on plant dry biomass, and zinc uptake into root and shoot tissues was also investigated, as detailed in Chapter 5.

7.1.3. Barley Root Exudates

An investigation into whether root exudates taken from the hydroponic solutions of barley were able to affect growth of *E. coli* was undertaken. Plants release a mixture of organic chemical substances through their roots, allowing the plant a communication tool with their local environment and facilitating nutrient acquisition (Rico *et. al.*, 2011). In particular, microbes are maintained and selected in highly specific communities which is

dictated by individual plants and their species, suggesting a strong and closely-knit evolutionary link (Badri & Vivanco, 2009). This dynamic release of root exudates and their influence on nanomaterials must be better understood in order to further understanding of environmental fate and behaviour of nanoparticles in the rhizosphere.

During the Hydroponic studies in this study (section **5.2.3**) barley plants were grown in 20 % modified Hoagland solution; a liquid growth media containing micro and macro nutrients essential for plant life, as first developed by Hoagland and Arnon (Hoagland, 1938). Barley plants release a cocktail of exudates through their roots in order to interact with and influence the local root environment or rhizosphere, and during hydroponic growth these exudates mix with the liquid growth media. This produces a root-influenced solution which contains a mixture of organic compounds that could potentially interact with nanoparticles and affect their behaviour (Bais *et. al.*, 2006). Determining the potential of these root exudates to affect toxicity of nanomaterials is an important step in assessing the real-world effect of plant and microbe exposure to nanoparticles, differentiating toxicity from in-vitro water-based assays (Raliya *et. al.*, 2014).

To investigate the interaction between root secretions, bacteria and nanoparticles, *E. coli* was grown in the presence of the root exudates from the hydroponically grown barley plants, including post-treatment root exudates from plants that had been treated with New 50 nm nZnO particles at 500 mg/L. This assay provided information on whether a) root exudates were inhibitory or stimulatory to growth of *E. coli*, b) this inhibition or stimulation was affected by root exudates from plants which had undergone nanoparticle treatment, and c) nanoparticles were made more or less inhibitory by the presence of root exudates. The treatment of barley plants with nZnO particles, as described in Chapter 5, elicited a visible stress response as observed by chlorosis of the leaves and diminished biomass as compared with the control. Determining whether this stress response led to a change in ability of root

exudates to affect microbial growth provided information as to the dynamic microbiological effect of plant-nZnO treatment.

Root exudates are highly dynamic in their composition and have been shown to be affected by essential metal deficiency stress (Dakora & Phillips, 2002, Henry *et. al.*, 2007, and Carvalhais *et. al.*, 2010) and toxicity stress (Mariano *et. al.*, 2005). It has also been demonstrated that changes in rhizosphere chemistry of *Hordeum vulgare* (barley) were able to influence the microbial community structure as a result of changes in iron availability (Yang & Crowley, 2008). In the reported study it was found that around 40 % of bacterial community variation was attributed to the iron nutritional status. This, along with the change in root exudate chemistry as a result of nutritional stresses, demonstrated how knowledge of toxicity of these root exudates, as modified by nanoparticle exposure, would be of great use in further understanding the environmental implications of nanoparticle release (Berg *et. al.*, 2009).

Few studies have been made on the interactions between nanoparticles and organic substances (Biswas *et. al.,* 2005; Bojeong *et. al.*, 2010; Lowry *et. al.*, 2012). Potential interactions include adsorption of molecules on the particle surface, leading to changes in zeta potential and stability. In Chapter 6 it was demonstrated that root exudate influence in both water and Hoagland solution increased the zeta potential of both Old and New nZnO, hence increasing nanoparticle stability. It is hypothesized that the significantly different zeta potential values of the two different particles in DI water would affect toxicity, with the near zero value of Old nZnO hypothesized to be less bioavailable and therefore less toxic than New nZnO particles when tested in DI water.

7.1.4. Chapter Aims

The model bacterial species *E. coli,* two whole-cell biosensors and barley plants were challenged with two 50 nm nZnO particles; 'New' and 'Old'; to ascertain whether particle ageing affects toxicity in biological systems. The main aims in summary were: 1) to determine whether there was a significant difference in growth inhibition by Old and New nZnO to *E. coli*, 2) to determine whether root exudates altered nanoparticle inhibition of *E. coli*, 3) to examine Zn uptake in barley after Old and New nZnO treatment, and 4) to relate any observed differences in bacterial and plant systems to the material characteristics of the two particles.

7.2. Materials and Methods

7.2.1. Bacterial Toxicity Assays

Three complementary methods of determining the toxicity of nanoparticles to bacteria were employed; bacterial growth inhibition as measured by optical density (non-luminescent *E. coli*), and bioluminescence relating to acute toxicity (*E. coli* HB101) and genotoxicity (*A. baylyi* ADP1) as previously detailed in Chapter 3.

These assays were designed to determine whether there were any differences in growth inhibition and acute toxicity between Old and New nZnO. Furthermore, they offered information on how root exudates affected growth inhibition from nZnO, which could then be linked to the zeta potential, size and ROS data of the two particles in different media as collected in section **5.2.4.** All reads of luminescence and optical density were made using a BioTek Synergy HT microplate reader (BioTek Corporation, UK).

7.2.1.1. Acute toxicity of Old and New nZnO Using Whole-Cell Biosensor *E. coli* HB101

The luminescent ATP-linked biosensor *E. coli* HB101_pUCD607_ *lux* was challenged with both Old and New 50 nm nZnO particles to establish differences in acute toxicity between the two particles over a concentration range. Methodology followed that described in section **3.2.1** with 30 minutes exposure to 4 concentrations (10 to 1000 mg/L) of Old and New particles.

7.2.1.2. Growth Inhibition of Model Bacterium *E. coli* Challenged With New and Old nZnO

The growth of *E. coli* was investigated after 24 hours of treatment with New and Old nZnO particles using the optical density growth method as described in section **3.3.1**. Concentrations of nanoparticles were continually halved by use of a multi-channel pipette in a 96-well microplate with nutrient broth and *E. coli* inoculum to give a final concentration range of 500 mg/L to 0.488 mg/L in triplicate. Optical density measured at 630 nm of *E. coli* was recorded every 20 minutes for 24 hours using the microplate reader. Results were presented in the form of mean 24-hour optical density as well as temporal growth curves for comparison. Twenty-four hours of growth was chosen as in order to compare particle inhibition to the control after a sufficient period of growth. The term carrying capacity was defined as the maximum bacterial density after 24 hours growth. (Kim *et. al.*, 2007).

Particle turbidity was controlled for by subtracting particle absorbance values obtained at 630 nm by UV-visible spectroscopy (section **6.3.4**) from the total absorbance. Use of very low concentrations of substances containing essential elements such as zinc has previously been linked with bacterial growth stimulation (Brayner *et. al.*, 2006), and hence a low concentration range was included in order to investigate this phenomenon in *E. coli*.

7.2.1.3. Growth of Non-Luminescent *E. coli* with Root Exudates and nZnO

In order to investigate the inhibitory or stimulatory nature of root exudates to *E. coli*, bacterial cells were cultured for 24 hours with water and Hoagland solution as controls, and root exudate solutions as test substances. To determine how these different media affected inhibition of *E. coli* by the Old and New nZnO particles, to each media combination was added 100 mg/L New and Old 50 nm nZnO particles, and $ZnSO_4 \bullet 7H_2O$. Hence, the ability for nZnO to inhibit growth was examined with and without the presence of plant root exudates.

The particles were suspended in filtered Hoagland solution containing barley root exudates. This solution was collected from barley plants grown hydroponically for 27 days, with 7 days treatment at 500 mg/L with 50 nm New nZnO, compared with root exudate taken from the control, Hoagland solution and DI water (for collection methods used see section **5.2.4**). All suspensions were then sonicated for one hour prior to use.

New and Old nZnO particles were made into suspension in each of the test media at a concentration of 200 mg/L in order to have a nominal concentration of 100 mg/L when pipetted 50:50 into each well of a 96 well plate with nutrient broth. Suspensions were sonicated for one hour as previously described. One hundred microliters of nanoparticle suspension and 100 µl of sterile nutrient broth were pipetted under aseptic technique into each well of a 96 well plate. A multichannel pipette was used to inoculate 2 µl of overnight culture of *E. coli* into each well. Combinations were repeated in triplicate. Control wells contained each of the three test media without nanoparticles however were still subjected to the same technique including one hour sonication for consistency of method. Optical density was used as a measure of bacterial growth at a wavelength of 630 nm after 24 hours exposure, and plates were incubated at 30 ºC with continuous shaking.

7.2.1.4. Genotoxicity of Old and New nZnO to Whole-Cell Biosensor *A. baylyi* ADP1

The genotoxicity of both particle types was investigated using the whole-cell genotoxic biosensor *A. baylyi* ADP1_*recA_lux* utilising the same method as described in section **3.2.2**. Particle concentrations of 50 mg/L and 250 mg/L were chosen to investigate whether Old and New nZnO particles were differently genotoxic over 6 hours.

7.2.2. Barley Assays

Biomass and zinc uptake data was obtained after 27 days hydroponic growth of barley as described in section **5.2.3**. A minimum of eight plants for each treatment were equilibrated in 20% Hoagland solution in hydroponic containers prior to treatment at an age of 20 days with particle suspensions. Treatment with zinc-containing test compounds lasted for 7 days before plants were harvested and analysed using an Atomic Absorption Spectrophotometer (AAS) as previously described in section **5.2.6**. Measurements of root and shoot biomass and zinc content within tissues were taken to establish whether New and Old nZnO resulted in any differences in barley physiology and zinc uptake. Photographs of treated plants were taken in order to make visual comparisons according to plant height and leaf colour changes indicating chlorosis (Supplementary S3).

7.2.3. Statistical Analyses

Graphs were constructed using data means, and error bars described one standard deviation above and below the mean. Statistical significance was determined by comparing to the control using either a Student's t-test or a one-way ANOVA to compare differences between the group means with results yielding a p value of below 0.05 considered significant at a 95 % confidence level.

7.3. Results and Discussion

7.3.1. Bacterial Assays

Four types of bacterial assays were conducted. Acute toxicity of both particles was determined using a whole cell biosensor *E. coli* HB101 lux, and inhibition of growth to non-luminescent *E. coli* was examined using optical density. In addition, growth of non-bioluminescent *E. coli* in the presence of root exudates, both particles, and a combination thereof was investigated to see what effect root exudates had on particle toxicity. Finally, genotoxicity of the two particles was examined using biosensor *A. baylyi* ADP1.

7.3.1.1. Acute Toxicity of Old and New nZnO to ATP-Linked Luminescent Biosensor

Acute toxicity of the two particles suspensions in DI water (**Figure 7.1 A**) and 20 % Hoagland solution (**Figure 7.1 B**) to *E. coli* lux biosensor was examined after 30 minutes exposure and expressed as a percentage of luminescence relative to the control. In both DI water and 20 % Hoagland solution, a significant reduction in ATP linked luminescence was detected at all concentrations from 10 mg/L to 1000 mg/L as a result of treatment from both particles. For DI water suspended treatment (**Figure 7.1 A**), at the lowest concentration of 10 mg/L, around 67 % reduction was observed for Old nZnO particle types and 59 % reduction with New nZnO, the difference between which was statistically significant (p = 0.020). This showed that New nZnO was significantly less toxic than Old nZnO at the lowest concentration, the reverse of which was true for higher concentrations, where Old nZnO was significantly more acutely toxic than New nZnO. This may have been due to the increased toxicity at low concentrations causing slight simulation of metabolic activity in a stress response (Stuart *et. al.*, 2005).

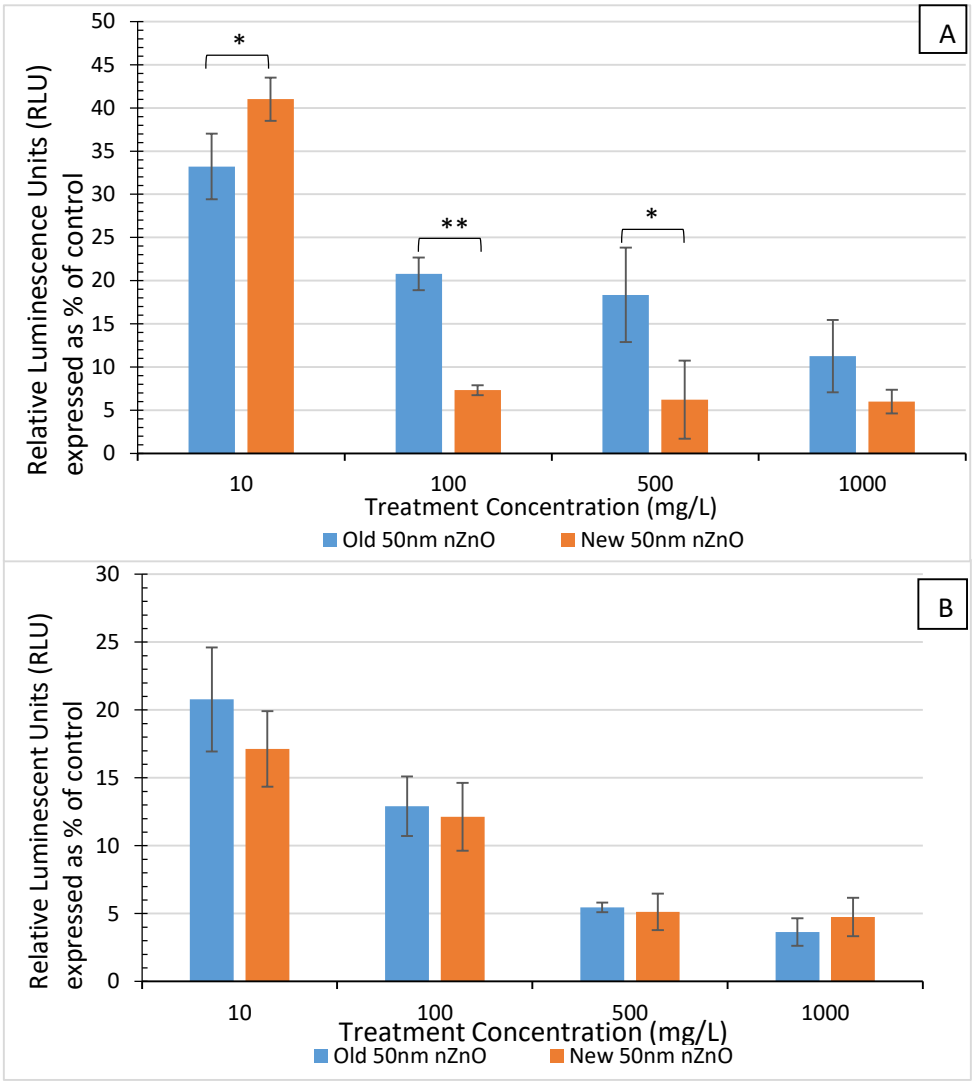


Figure 7.1 A & B: Bioluminescence of *E. coli* HB101_pUCD607_*lux* after 30 minutes treatment with New and Old 50 nm nZnO suspensions in DI water (A) and 20% Hoagland Solution (B) at four concentrations. Values expressed as a percentage of the control with standard deviations of three technical and biological replicates. Asterisks represent statistical significance at alpha value 0.05 (*) or 0.005 (**).

In DI water at increasing concentrations of 100 and 500 mg/L, particle toxicities were statistically different ($p < 0.001$, and $p = 0.021$ respectively) with New nZnO having caused a greater reduction in luminescence than old nZnO relative to the control. At the highest concentration of 1000 mg/L treatments were not found to be significantly different ($p = 0.054$), however the same trend was observed with New nZnO causing greater decrease in luminescence than Old nZnO relative to the control. Non significance at high concentrations

may have been due to high concentrations of particles leading to large acute toxicity and/or shielding the luminescence signal. Particles had previously been tested at the same setting as used for luminescence quantification and demonstrated to give an insignificant reading for luminescence at any concentration, however their turbid nature could be reducing the output luminescent value at the highest concentration of 1000 mg/L by shielding the signal.

Bioluminescence was also examined after treatment with both particle types suspended in Hoagland solution (**Figure 7.1 B**). Luminescence decreased as concentration increased, with around 79 % reduction from the control with Old nZnO and around 82 % reduction with New nZnO. Neither of the two treatments were determined to be statistically different from one another at any given concentration, as opposed to when particles were dispersed in DI water as above. At the highest two concentrations of 500 and 1000 mg/L, a reduction of around 95 % from the control was detected for both particle types, which showed high acute toxicity of particles at high concentration and was comparable to that observed from 1000 mg/L when the New nZnO particles were dispersed in DI water. This may have been due to the increased toxicity of components in Hoagland solution, as discussed in Chapter 3.

The results from this assay were then related to the zeta potential values obtained in section **6.2.2.3**. In water, Old and New nZnO values were −2.74 mV and +23.83 mV respectively, the difference between which was highly statistically different. In Hoagland solution they were −16.4 mV and −15.2 mV respectively, the difference between which was determined not to be statistically significant. This was reflected in the different results obtained for acute toxicity in Hoagland solution and in DI water; as in the former there was no statistical difference between the two particles, which correlated with the non-significant difference between the zeta potential values. These zeta potential results showed that the particles were similarly stable in Hoagland solution and hence had a similar bioavailability.

In water however, the Old nZnO particles had zeta potential values of near zero, which demonstrated their very low stability, as opposed to New nZnO particles which had a significantly higher zeta potential value of +23.83 mV. This correlated with toxicity, with more stable particles having caused greater acute toxicity than less stable particles.

7.3.1.2. Growth of *E. coli* Challenged with Old and New nZnO Particles

The growth of *E. coli* as determined by optical density after 24 hours exposure to the two nanoparticles was displayed in **Figure 7.2**, with values plotted against concentration transformed by $\log_{10}$.

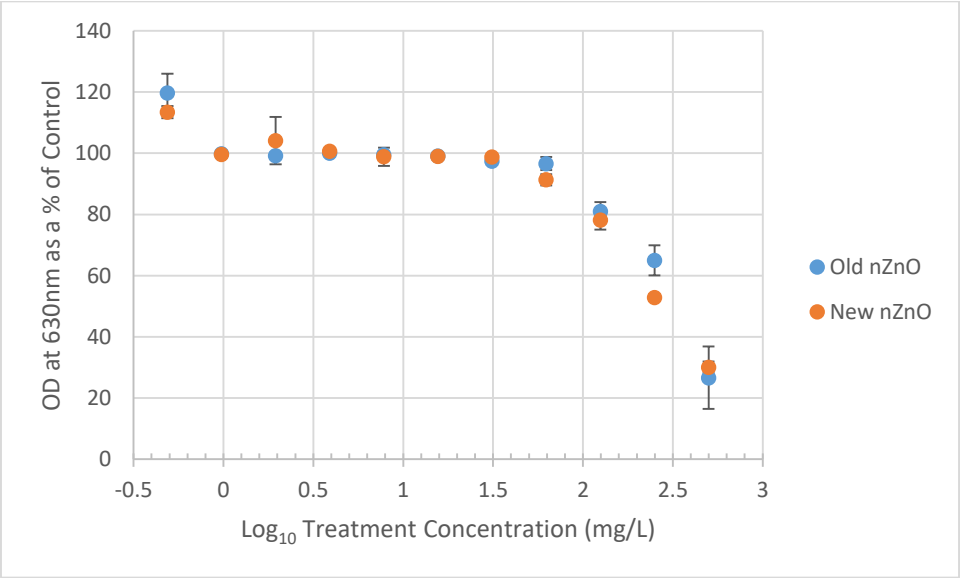


Figure 7.2: Optical density of *E. coli* bacteria expressed as a percentage of the DI water control, demonstrating 24 h growth in the presence of Old and New nZnO particles over a range of concentrations transformed by $\log_{10}$. Error bars denote one standard deviation above and below the mean (n = 3).

The results demonstrated that inhibition positively correlated with concentration. A slight stimulation in growth was detected at the lowest concentration of 0.488 mg/L for both particles. There was no inhibition of growth relative to the control detected at concentrations of 15.6 mg/L and below. There was no significant difference in inhibition between the two

particle types at almost all concentrations, with a significant difference detected only at a concentration of 62.5 mg/L ($p < 0.05$) and 250 mg/L ($p < 0.01$) where New nZnO was significantly more inhibitory than Old nZnO. This indicated that although the inhibition of growth by the two particles was similar overall, the New nZnO were more inhibitory than the Old nZnO particles at concentrations between 62.5 mg/L and 250 mg/L. At 125 mg/L the difference was non-significant ($p = 0.072$) however the trend continued of New nZnO being slightly more inhibitory than Old nZnO. This may have been a result of the higher zeta potential values of New nZnO in water, which would indicate greater dispersal in the media and hence greater contact, particularly at the higher concentrations, as they involve substantially more particles and hence the probability of a collision between particles, and also of particles with bacteria, is greater.

This was further investigated by plotting the growth of *E. coli* over time at each concentration, as displayed in in **Figures 7.3 A** & **B.**

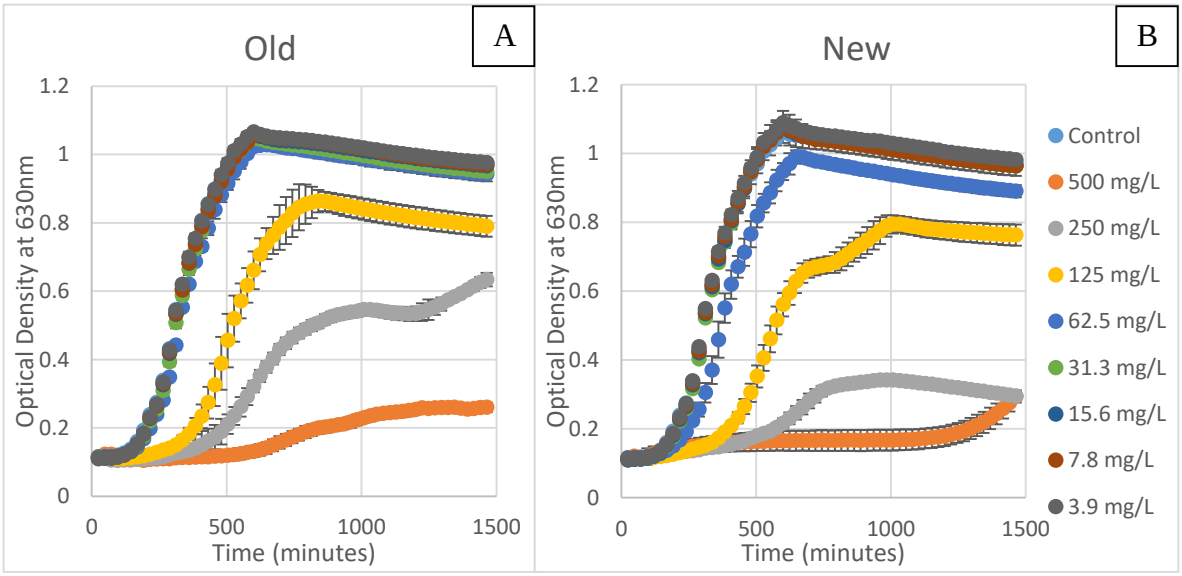


Figure 7.3 A & B: Growth curves of *E. coli* challenged with A) Old and B) New nZnO particles over 24 hours. Error bars denote one standard deviation of triplicates.

The growth curves demonstrated the effect of particle treatment on the lag, log and stationary phases of bacterial growth, in addition to the final carrying capacity after 24 hours particle exposure as discussed above. It was revealed that New nZnO was slightly more inhibitory than Old nZnO, most notably at a concentration of 62.5 mg/L which for New nZnO was significantly different to the curves at all of the lower concentrations ($p < 0.05$ at all the time points after 250 minutes) which was not the case for Old nZnO. It was also possible to detect an increase in the lag phase as a result of treatments above 125 mg/L for both particle types. This demonstrated that the bacteria were in lag phase for a longer period of time when in contact with the NPs before they were able to enter the exponential growth phase. Furthermore, the difference between the two particles at 250 mg/L was likely a result of particles being in high enough density and hence near enough to one another to overcome the electrostatic repulsion and agglomerate, hence at the highest concentration of 500 mg/L there was no significant detectable difference between the two particle types. This demonstrated the balance between concentration, zeta potential and inhibition.

7.3.1.3. Growth of *E. coli* Challenged with Old and New nZnO Particles in Root-Exudate Solutions

The growth of *E. coli* was examined by analysing optical density after 24 hours exposure to a fixed concentration of 100 mg/L nanoparticles suspended in four different media to determine whether a) root exudates were inhibitory or stimulatory, b) there was an ameliorative effect of root exudates on nanoparticle toxicity and c) exudates were more or less toxic from plants treated with 50 nm nZnO (**Figure 7.4**). The comparison of the two particles with $ZnSO_4$ allowed an insight into particle versus ionic toxicity, and how root exudates were able to influence this. For statistical analysis, growth after 24 hours was analysed using Student's t-test.

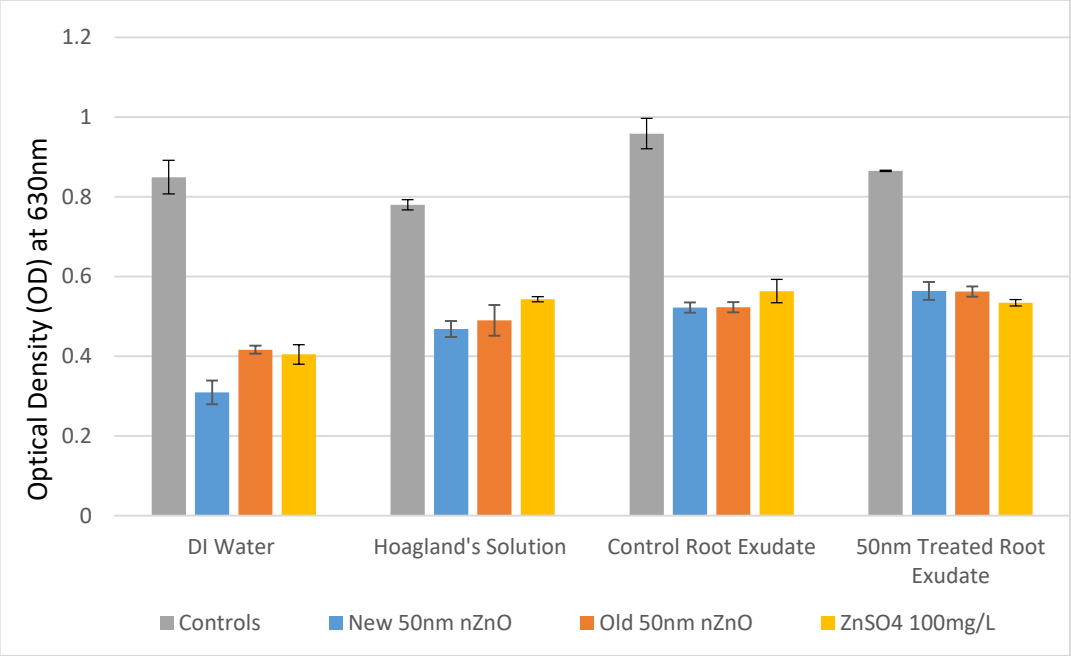


Figure 7.4: Optical density of *E. coli* at 630 nm as an indicator of growth after 24 hours exposure to 100 mg/L of Old 50 nm nZnO and New 50 nm nZnO suspended in water, Hoagland solution and root exudates. Exudates taken post-treatment from hydroponic barley grown for 27 days with 7 days treatment at 500 mg/L with 50 nm New nZnO, compared with root exudate taken from the control, Hoagland solution and DI water (controls shown). Samples performed in triplicate, error bars denote one standard deviation above and below the mean.

Growth of *E. coli* after 24 hours varied according to the 4 different media used. Hoagland solution significantly reduced growth when compared to DI water (p = 0.017), whereas control root exudate significantly stimulated growth (p = 0.015). This showed that the presence of barley root exudates, as collected from the control barley hydroponic experiment, increased growth significantly when compared to all other media controls. Hence, barley root exudates in Hoagland solution from 27 day old, untreated barley plants were deemed to be stimulatory to *E. coli* growth after 24 hours. After the hydroponically grown barley had been challenged with 50 nm nZnO, the stimulatory effect of the root exudates was not significantly different to the growth in DI water (p = 0.269). This may have been either due to the solution still containing nZnO particles from treatment, solubilized Zn^{2+} or a change in root exudate composition as a result of stress from treatment. The exact cause of the decreased stimulatory effect of the post treatment root exudates could be investigated in a future project, however this complex solution was not significantly different to DI water alone in terms of growth despite this which is an interesting result in itself. The results demonstrated that both particles were most inhibitory to *E. coli* when suspended in DI water as opposed to all the other media tested. The difference between Old and New nZnO in DI water was significant (p = 0.006) however in all other media there was no significant difference between the two particles ($p > 0.05$). This was again reflected in the zeta potential data, where in water New nZnO was more stable than Old nZnO, whereas in other media tested there was no significant difference in stability.

The control root-exudate containing solution resulted in 12.8% more growth than the water control. This was most likely due to the supplementary organics within the root exudate solution which the bacteria were able to utilise as an additional carbon source. The increase in growth in the presence of the Old and New nanoparticles when suspended in the control root exudate solution however was greater than when in water; with a 25.6 % and

68.9 % increase in growth respectively. This revealed that there may have been an ameliorative effect of the root exudate solution on the nanoparticle toxicity, with a detected increase greater than just the additional growth from the root exudate alone. When this was compared with the increase in growth between particles suspended in water and Hoagland solution, the differences were 17.7 % and 51.6 % for Old and New respectively, despite growth in Hoagland solution being 8.2 % lower than in DI water alone. The inclusion of 100 mg/L $ZnSO_4$ in the comparison demonstrated that a high dissolved Zn^{2+} concentration (22 mg/L) did not contribute to significantly lower optical density.

7.3.1.4. Genotoxicity of Old and New nZnO to *A. baylyi* ADP1_*recA*_*lux*

The bioluminescence of *A. baylyi* was recorded over time and displayed in **Figure 7.5**. An increase in luminescence corresponded to the upregulation of *recA* gene to produce the RecA protein involved in DNA repair, thus indicating gene damage. At the concentration of 50 mg/L it was demonstrated that an increase in genotoxicity relative to the control occurred after approximately 2.5 hours of exposure. It was detected that there was no significant difference between particle types at both 50 mg/L and 250 mg/L concentrations up to approximately 3.5 hours, after which point Old nZnO stimulated a significantly higher bioluminescent signal than New nZnO ($p < 0.05$ at each timepoint). The solubility of both particle types had previously been shown to be similar, whereas Old nZnO had produced more ROS than New nZnO as detected by the coumarin assay in section **6.3.5**. The higher concentration of 250 mg/L lead to a substantially lower signal, which indicated that the concentration was too high and had led to cell damage, as was also revealed in Chapter 3 at this concentration for nZnO compared with the bulk ZnO and $ZnSO_4$ treatments.

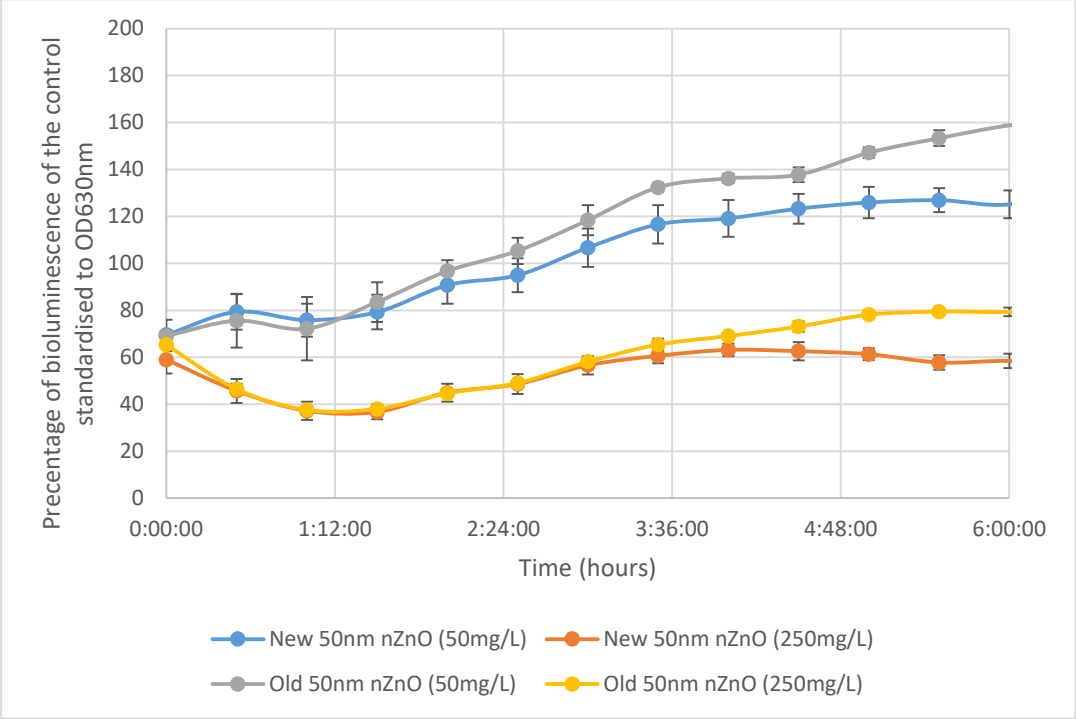


Figure 7.5: Bioluminescence of genotoxicity biosensor *A. baylyi* over time after exposure to 50 mg/L and 250 mg/L of both Old and New nZnO particles. Values expressed as a percentage of the negative control and standardised to optical density as measured at 630 nm to control for bacterial growth. Error bars represent standard deviation of triplicates.

7.3.2. Plant Assays

7.3.2.1. Barley Biomass

The biomass of root and shoot tissues of barley post-treatment with Old and New nZnO over a range of concentrations was displayed in **Figure 7.6**. The total biomass of each plant was significantly lower than the control at all concentrations of all treatments ($p < 0.05$ for all treatments). Both root and shoot biomasses were negatively affected by treatment, with a decrease in both tissue types observed. This demonstrated that treatment with both New and Old 50 nm nZnO particles caused a decrease in root and shoot biomass of barley relative to the control, from the lowest concentration of 10 mg/L up to 500 mg/L.

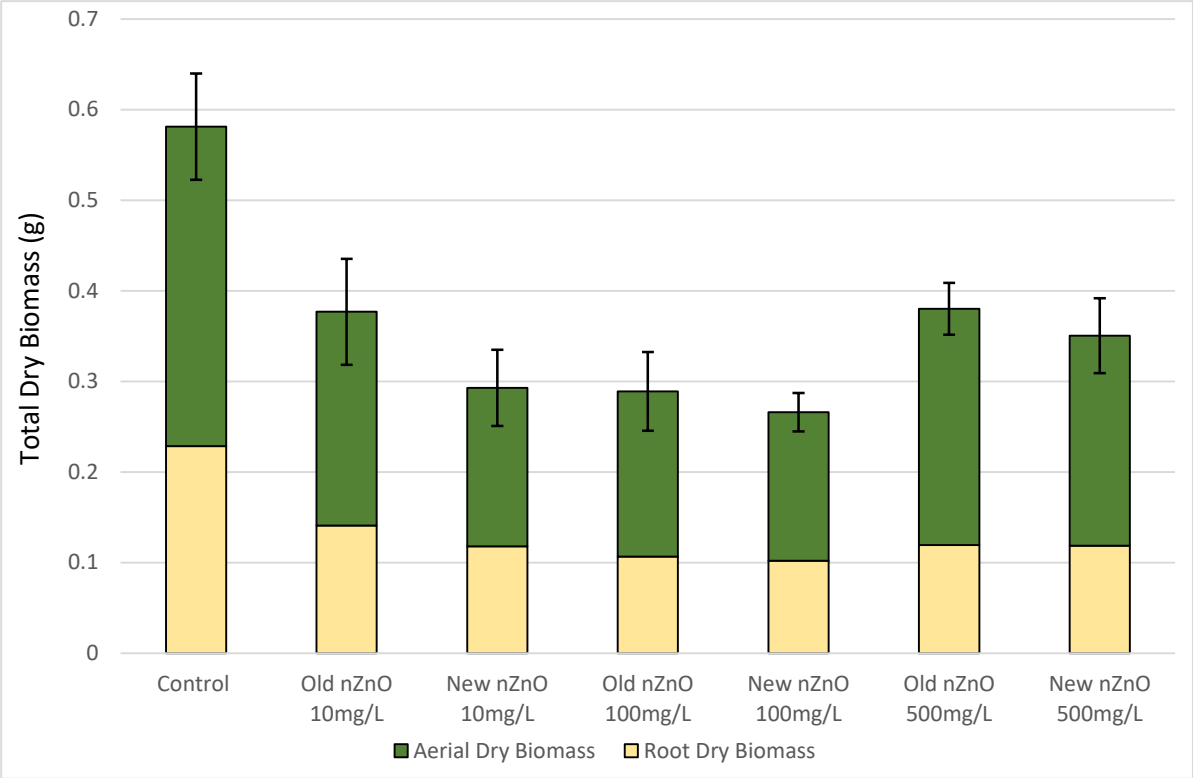


Figure 7.6: Total dry biomass of 27 day old barley treated with Old 50 nm nZnO and New 50 nm nZnO for 7 days. Top bars (green) depict aerial biomass and lower bars (yellow) depict root biomass. Error bars denote one standard deviation above and below the mean (*n* = 8).

Root mass of each plant remained relatively constant across all zinc-containing treatments and concentrations, ranging between 0.10 g and 0.14 g per plant; around half the root mass of the control. At the highest concentration of 500 mg/L, the total biomass was significantly higher than after 100 mg/L treatment for both particle types. This was contrary to expectations as it was hypothesised that the highest concentration of treatment would lead to the largest reduction in biomass, however the converse was true.

This may be due to the proximity of particles to one another when in a high concentration situation; particles are physically closer to one another and the reduced distance between them may overcome the repulsion from surface charge, as measured by

zeta potential, and lead to attraction by Van der Waals. This would in turn lead to agglomeration of particles and cause individual particles to crash out of suspension and become less bioavailable. In turn, as fewer particles would be available to the roots in suspension, there would have been decreased interaction and hence less of an effect on biomass post-treatment. The difference between the two particle types was not significant at any given concentration, however there was a trend for the biomass to be slightly lower for New nZnO particles at each concentration.

7.3.2.2. Zinc uptake into Barley tissues

Hydroponically grown barley plants were challenged with Old and New nZnO particles at 3 different concentrations for 7 days before being harvested and analysed using AAS for zinc concentration per gram of tissue subsequent to nitric acid digestion and dilution, with results displayed in **Figure 7.7**.

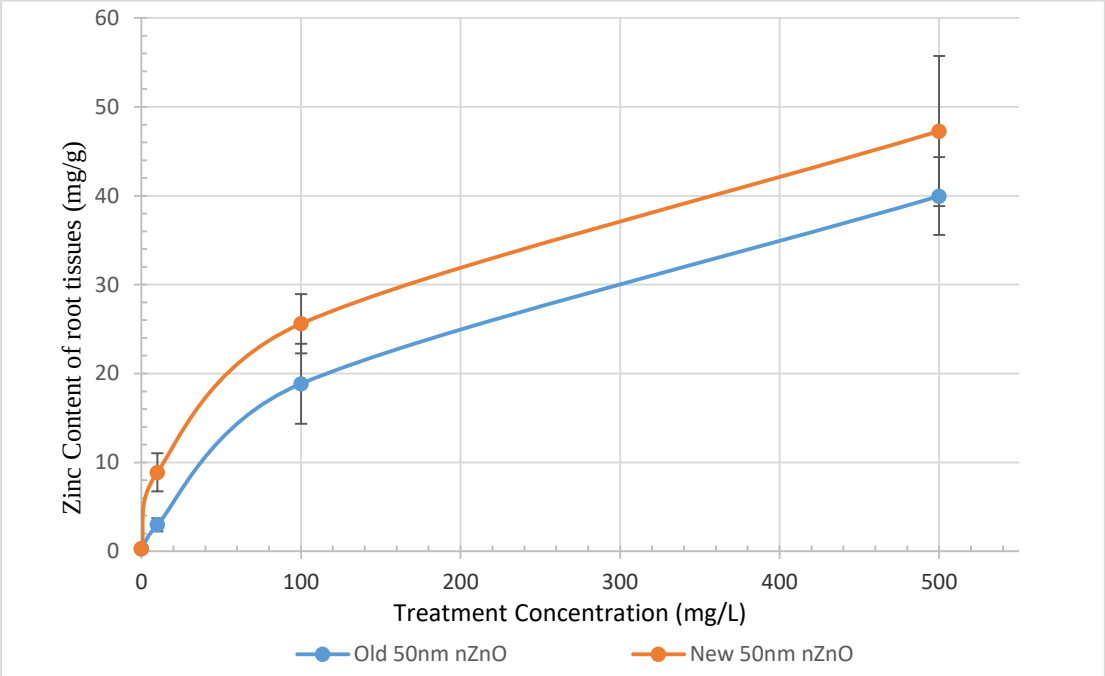


Figure 7.7: Zinc uptake into root tissues from barley hydroponically grown in 3 different concentrations of Old and New 50 nm nZnO particles. Zinc quantified per gram of plant material by nitric acid digestion and AAS analysis. Error bars denote one standard deviation above and below the mean (*n* = 3).

As the concentration of New and Old 50 nm nZnO treatment increased, the zinc content of root tissues also increased. At the lowest concentration of 10 mg/L and also at 100 mg/L, the zinc uptake as a result of New nZnO treatment was significantly greater than that as a result of Old nZnO treatment (p = 0.005 and p = 0.05 respectively). At each concentration, the zinc content of tissues was greatest as a result of New nZnO treatment, suggesting increased ability of barley to sequester zinc from the New nZnO suspensions. At the highest concentration of 500 mg/L, there was no significant difference in Zinc uptake as a result of treatment with both particle types (p = 0.127).

The zinc content of the shoot tissues according to treatment was displayed in **Figure 7.8**. The relationship between zinc content of shoot tissue and treatment concentration was found to be different than for the root tissue above. Although there was a concentration dependent response in terms of tissue zinc content as a result of increased treatment concentration, at the highest concentration of 500 mg/L there was a decreased level of internalised zinc as a result of both types of treatment. At this concentration, there was no significant difference between the two particle types (p = 0.269). At both the lowest concentration of 10 mg/L and the middle concentration of 100 mg/L there was a highly significant difference between the two particle types (p = 0.001 and p = 0.006 respectively). This difference was highly significant and demonstrated that approximately twice as much zinc was able to enter the shoot tissues from the New nZnO particles than from the Old nZnO. As their solubility in Hoagland solution and DI water was similar this was likely a result of the greater stability of New nZnO particles as revealed by their higher zeta potential. Better dispersed particles would allow greater interaction with roots and root exudates, and hence facilitate solubilisation and uptake.

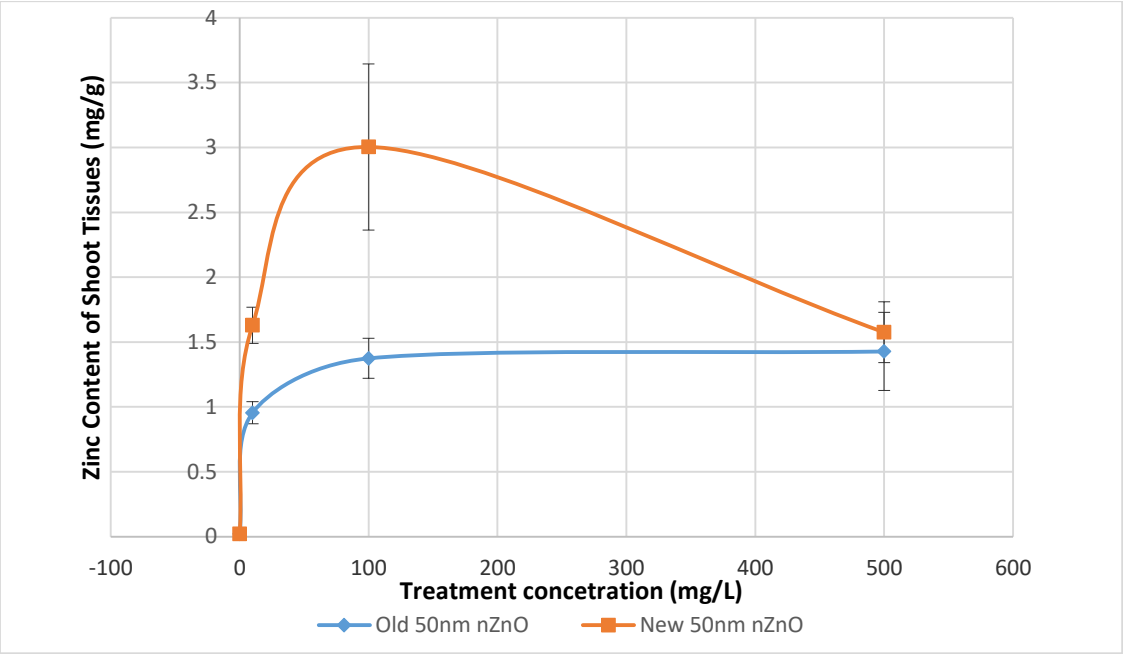


Figure 7.8: Zinc content of shoot tissues from barley hydroponically grown in 3 different concentrations of Old and New 50 nm nZnO particles. Zinc content quantified per gram of plant material by nitric acid digestion and AAS analysis. Error bars denote one standard deviation above and below the mean (*n* = 8).

7.4. Discussion and Conclusions

7.4.1. Acute Toxicity to *E. coli* lux Depended on Dispersal Media

The acute toxicity of Old and New particles to luminescent biosensor *E. coli* lux was examined in order to determine whether short-term treatment of Old and New nZnO particles impacted on metabolic activity in *E. coli*. Results demonstrated that the acute toxicity of the particles depended on the media in which they were dispersed. There was no significant difference between toxicity of the two particles when they were dispersed in Hoagland solution, whereas New nZnO was significantly more acutely toxic than Old nZnO when dispersed in DI water. This can be linked with information gathered on the zeta potential in both media; the zeta potentials of Old nZnO and New nZnO were not significantly different in Hoagland solution, however there was a significant difference when in DI water, with Old nZnO significantly lower in zeta potential than New nZnO. This meant

that Old nZnO was less stable in suspension than New nZnO when in DI water, and hence was more likely to agglomerate over time. This reduced the bioavailability of particles in the solution, as they were more likely to have agglomerated due to Van der Waals attraction due to insufficient electrostatic charge to repel particles. In Hoagland solution, the zeta potential of both particles was not significantly different hence they were both equally likely to agglomerate, which was reflected in the non-significant difference in acute toxicity to *E. coli* lux. Where these zeta potential values were significantly different in each media, the acute toxicity was demonstrated to be too.

As this was a short term exposure time of 30 minutes, very few ROS were likely to have been released within this time, as demonstrated in section **6.3.5** where the coumarin dye was not able to detect ROS until after 3 days of exposure. The osmotic pressure was higher in Hoagland solution than in DI water due to containing solutes, and this provided a protective effect on bacteria, reducing osmotic shock (Lloret *et. al.*, 1995). However the nanoparticle toxicity was higher in the medium with greater osmotic potential. This indicated that neither the differing osmotic potential of the two solutions nor the ROS release was likely to be a main driver for differences in acute toxicity.

7.4.2. *E. coli* Growth Inhibition was Similar for New and Old nZnO

The growth inhibition of *E. coli* was measured using optical density measurements at 630 nm after 24 h exposure to increasing concentrations of Old and New nZnO particles. Both forms of 50 nm nZnO caused inhibitory effects, with significantly greater growth inhibition detected from New nZnO than Old nZnO at only two concentrations.

It has previously been revealed that nano-scale ZnO was more antibacterial than its bulk counterpart, however the ageing effect of the nanoparticles has not been considered, and through bulk-nano comparisons, the mechanisms of action were not clear (Zhang *et. al.*,

2007). It was theorised that the antibacterial activity of nZnO is due to physical contact and surface chemistry (Nair *et. al.*, 2009). This is of particular interest when looking at the Gram-negative *E. coli* cells which have an additional outer lipopolysaccharide layer to Gram positive species (Li *et. al.*, 2011). The results of this study were concordant with the single-species test on *E. coli* by Brayner *et. al.*, 2006, who demonstrated that lower concentrations of nZnO (~10 nm) did not induce cell damage. Higher concentrations however led to inhibited growth. This was found to be due to Gram-negative membrane disruption as visualised with TEM, where the triple layer membrane and cell wall structure was disorganised and increased in permeability. This study also found that the low concentration of 0.488 mg/L resulted in a stimulation of growth relative to the control, which was most likely a result of the essential nature of low quantities of zinc to bacterial growth (Dhas *et. al.*, 2014).

Further work to measure the zeta potential of such particles over a range of concentrations would be of great interest, as currently a fixed concentration of 100 mg/L is recommended for analysing particles (Malvern, 2013), however this value may change as the concentration increases due to the increased probability of a collision. When the presence of bacterial cells together with the particles is considered, the overall concentration of particulates (including both cells and nanoparticles) is again increased, resulting in a large change of a collision and hence an interaction. It has been demonstrated that certain nanoparticles may be able to bind to bacterial surfaces via surface biomolecules such as lipopolysaccharide (Jiang, 2011). Hence, the stability of particles was likely to be an important factor in toxicity, as greater stability increases the chance of an interaction and therefore increases the likelihood of this binding to occur. Furthermore, close particle-cell proximity is required for OH radicals to affect cells, as these ROS can only travel a distance of approximately 5 nm (Lesser, 2006).

7.4.3. Growth Inhibition of *E. coli* by nZnO was Affected by Root Exudate Solution

In this chapter the growth of *E. coli* was measured in the presence of Old and New nZnO particles suspended in DI water, 20 % Hoagland solution, and Hoagland modified by barley root exudates from barley grown hydroponically in Chapter 5. It was demonstrated that New nZnO was more inhibitory than Old nZnO when in water, however there was no statistical difference between Old and New when the particles were dispersed in the other media.

The release of root exudates by plants serves to allow an adaptive and dynamic chemical communication with biotic and abiotic factors (Berg & Smalla, 2009; Bertin *et. al.*, 2003). Root exudates contain factors which are able to manipulate bacterial populations (Badri & Vivanco, 2009). The root exudates from the 27 day old barley used in this study were demonstrated to stimulate bacterial growth, with an increase in 24 hour growth of approximately 13 % as compared to the water control, and 23 % compared to Hoagland solution alone. This is likely due to increased carbon able to be utilised by the bacteria (TOC value was ~52 mg/L). Furthermore, when the particles were suspended in the root exudate, the growth of *E. coli* increased, with final values reflecting greater increase in growth than from the root exudates alone. This suggested that the root exudates were able to reduce the toxicity of the nZnO particles. Considering that the zeta potential values for Old nZnO when in root exudate in Chapter 6 were substantially greater than in DI water, this decrease in toxicity was unexpected, and may indicate that stimulatory compounds outweigh the increase in nZnO toxicity from the increase in zeta potential. This may have been due to organics binding to the surface which altered the surface chemistry and reduced toxicity, as has been suggested to occur in soil due to natural organic matter (Lowry *et. al.*, 2012).

The work presented in this study demonstrated that growth inhibition was likely to have been due to the product of zeta potential and additional substances within the root exudates. This analysis therefore revealed that in vitro assays of inhibition undertaken solely in DI water do not reflect the toxicity when the nanoparticles are in contact with root exudates. Hence, it is likely that environmental toxicity of the particles would be lower than suggested by water-based studies. Previous researchers have concluded that particles dispersed in soil bind to natural organic matter and become less available, reducing environmental toxicity (Biswas *et. al.,* 2005). When the results of this study are considered in conjunction with these findings, it is likely that environmental toxicity of nZnO would be significantly lower than *in vitro* studies in water suggest, as a result of adsorption to soil and contact with plant root exudates. Although Hoagland solution is not itself representative of environmental conditions, it does however add an additional level of complexity in terms of analysing nanoparticle behaviour and toxicity in root exudate solution.

7.4.4. Zinc Uptake in Barley was Greater as a Result of New nZnO than of Old nZnO Treatment

Barley plants were grown for 27 days in hydroponic systems containing New and Old nZnO particles in the liquid Hoagland media. Treatment with New nZnO lead to significantly greater uptake of zinc into plant tissues, despite the solubilities of both particle types in both water and Hoagland solution having been demonstrated not to be significantly different (section **6.3.6**). The results of the root and shoot zinc concentration analyses indicated that the quantities of cellular incorporated zinc from nZnO treatment were different for the two types of tissue. The uptake of water containing solubilised nutrients by the root cells is a passive process facilitated by low xylem pressure. Uptake into the xylem is controlled by the casparian strip, which prevents the solution from directly entering the xylem through the apoplastic pathway (between cells) without first passing through a

selectively permeable membrane into the symplastic (within cells) pathway. It was not possible to determine whether the nanoparticles were small enough to be able to traverse this barrier or whether zinc was solely in ionic form from this assay, however the presence of zinc in the shoot tissues demonstrated the ability of zinc to enter both tissue types from the nanoparticle treatment. When the 'clearing' phenomenon observed in Chapter 4 is considered, whereby the particles suspended in agar were able to be dissolved around the root, it is possible that the nanoparticles in the hydroponic assay were dissolved at the root interface, as a result of the low pH and presence of organic chelating molecules. The concentration of such root exudate compounds would be considerably higher at the boundary layer than was possible to measure in bulk solution, hence it was possible that particles were solubilised at the interface, prior to ionic and chelated zinc being uptaken and entering into the root and shoot tissues via the xylem.

7.4.5. Conclusions

In terms of establishing the effect that particle ageing had on the plant toxicity of nZnO it was determined that New nZnO was more inhibitory to barley plant growth than Old nZnO. Furthermore, New nZnO treatment resulted in greater zinc uptake into barley tissues. This, combined with the decrease in biomass from New nZnO treatment indicated that New nZnO posed a greater threat to barley than the Old nZnO.

For bacteria, it was demonstrated that the when the particles were dispersed in water, the New nZnO was more acutely toxic and inhibitory than the Old nZnO, however in different media which rendered the particle stabilities the same, there were no detectable differences between the two particle types. When the genotoxicity of both particle types was evaluated it was revealed that Old nZnO was able to cause greater gene damage than the New nZnO particles, however this did not translate into a difference in growth over 24 hours

hence it is likely that the difference, although significant, was quite slight. In conclusion, the two particles behaved similarly in biological media whereas New nZnO was more inhibitory and acutely toxic in water-based assays.

The results from this study indicated that plant zinc uptake from nZnO was likely to have been a factor of the interaction with root exudates. The acute toxicity of the two nanoparticles to bacteria was likely to have been the result of the zeta potential, as there was no significant difference between treatments when the zeta potential was the same, such as in Hoagland and root exudate solutions. Old nZnO caused greater genotoxicity to the whole-cell biosensor *A. baylyi*, which was potentially a result of the increased ROS released by Old nZnO as compared to New nZnO. Neither of the particles had a zeta potential value of above ± 30 mV (the threshold for long term stability), and the toxicity methods were undertaken over varying timescales, hence it is likely that the importance of zeta potential increased as the duration of the experiment increased. This was also the case for ROS, as these were detected by coumarin over the scale of days rather than hours. In conclusion, the results from this study demonstrated that as nZnO aged, it may have posed less of a concern to plants such as barley in terms of biomass and zinc uptake. In bacteria such as *E. coli*, there may have been little difference in terms of groth inhibition, however the ability of the particles to cause genetic damage may have increased over time.

8. DISCUSSION AND CONCLUSIONS

8.1. Discussion

Nanotechnology as a blanket term is one of the single most important areas of modern science, with production of novel materials increasing almost exponentially. The biological impact is potentially enormous, but there is very little research into the effects of nanomaterials in biological systems, especially in plants and bacteria.

Nanomaterials have existed for thousands of years, such as colloidal gold used by the Romans to produce red glass, nanoparticulate ash produced by volcanoes and nano-sized organic matter in soil (Stolpe & Hassellöv, 2007). Modern sources include mixed-compound nanoparticulates from vehicle exhausts (Uibel *et. al.*, 2012). Many chemical and physical processes produce nanoparticles and hence they are ubiquitous within the environment, however it is only recently in human history that we have begun to synthesise and engineer nanoparticles with specific properties (Mikrajuddin *et. al.*, 2001). These nanomaterials are different to those which are naturally occurring, as they can be designed to be more stable, more uniform and more toxic than those which are produced in nature. It is this engineering step which has been useful in so many aspects of human life, from energy storage, medical applications and water purification. It is for these reasons that nanotechnology is considered to be one of the most important modern technologies of the human era, with an enormous potential for solving pressing global issues. However, in order for this potential to be unlocked it is vital that we examine the potential impact such new technologies could have, particularly on complex biological systems. The evaluation of toxicity and consequences needs to keep up with the pace of the rapidly increasing global nanomaterial production.

The aim of this project was to identify the key nanomaterial characteristics that induced toxic responses in bacteria and plants. To date, research conducted in the field of

nanomaterial toxicity has focussed primarily on animal cells as opposed to plants or bacteria. Although this research is useful, particularly in the development of novel materials such as nano-based chemotherapeutics for the treatment of cancer, insufficient research has been conducted on the fate of engineered nanoparticles in the environment. This study sought to address the disparity between medical and environmental nanoparticle research by examining the toxicity of nano-scale ZnO particles in bacteria and plants.

8.2. Bacterial Toxicity

8.2.1. Whole-Cell Biosensors in Combination with *E. coli* cells Suggested the Mechanisms of nZnO Toxicity

The results from the bacterial assays of both the nano-bulk comparisons as well as the more subtle New-Old nZnO comparisons revealed that the likely mechanisms of toxicity for nZnO particles were: a) initial acute toxicity due to Zn^{2+} release and good dispersal (which enabled a greater number of interactions between particles and cells), and b) inhibition at low concentration, as a result of ROS-mediated gene damage. This increased the duration of the lag phase, as demonstrated in the genotoxicity and inhibition experiments. It was, however, demonstrated that a high concentration of 500 mg/L nZnO did not kill *E. coli* cells, nor increase the number of moribund, membrane-compromised cells. Hence it is proposed that the likely mode of action of nZnO particles was ROS release, which acted by reducing the rate growth by causing the cell to divert its energy towards gene repair rather than into accumulation of nutrients required for entering the exponential phase.

When the acute toxicity data was considered, the evidence pointed towards zeta potential being a key defining parameter in predicting toxicity, with the greater zeta potential values for the New 50 nm nZnO in water, as compared to the near-zero values of Old nZnO and Bulk ZnO leading to increased acute toxicity. This effect was eliminated when the

particles were tested in Hoagland solution, which modified the zeta potential of the particles to very similar values. This was reflected in the non-significant difference between acute toxicity when zeta potential values were similar. The inclusion of the Old versus New nZnO particles allowed zinc liberation to be eliminated as a key factor, as the release of Zn^{2+} from old and new particles was not significantly different in either DI water or Hoagland solution. This provided strong evidence that zeta potential was a key predictor in acute toxicity. This could be investigated further by testing particles suspended in a variety of different concentrations of Hoagland solution to produce a range of zeta potential values, and then testing these suspensions on the acute toxicity biosensor *E. coli* HB101 to determine if there is a direct correlation.

Particle size is also a factor to consider further, as this was linked to zeta potential due to the action of attractive forces forming larger particle agglomerates and aggregates. The lower zeta potential of Old nZnO particles than New nZnO particles coincided with Old particles having a larger mean diameter. Whether size or zeta potential was the key parameter in this project is difficult to determine due to their intrinsically linked characteristics. The data from this study suggested that acute toxicity may be predicted for nZnO particles by measuring their zeta potential and size in the media of concern, hence of particular interest may be soil pore water to better understand potential nZnO behaviour in the environment (Chaudri *et. al.*, 1999). The ability to predict acute toxicity based on just one or two factors could be of great use in estimating potential impact of environmental nZnO release.

8.2.2. Plant Root Exudates May Reduce nZnO Toxicity

The results presented in Chapter 7 demonstrated that root exudates may reduce the inhibitory effects of nZnO particles on the growth of *E. coli* bacteria. While focus has started

to occur on the achievement of maximal dispersion of nanoparticles for in vitro studies (Bihari *et. al.*, 2008) it is highly unlikely that these optimal states of dispersion are reached in the environment in the case of nZnO, with interactions with numerous organic and inorganic molecules modifying the surface chemistry, stability and availability of particles (Lowry *et. al.*, 2012).

Zeta potential data revealed that biological media, including root exudates, affected surface charge of different particles. Particle behaviour and toxicity in different chemical environments to different organisms provided information which could be used to predict behaviour in the natural environment. Current studies on nanoparticle uptake in plants have not considered root exudates and their effect on ENPs, which may strongly interact with the particles and change their properties such as surface charge and solubility. It is possible that plant root exudates increase the solubility of nZnO particles, as plants are frequently zinc limited and hence have evolved efficient mechanisms to increase the bioavailability of such metals by releasing chelating agents and reducing the pH around the root (Dakora *et. al.*, 2002). As opposed to dissolving the nZnO and releasing a large quantity of free Zn^{2+}, plants release phyto-metallophores; chelating complexes able to bind to specific ions and be absorbed directly (Tolay *et. al.*, 2001; Erenoglu *et. al.*, 2000). This property could reduce the bacterial toxicity of the nZnO particles by 'mopping up' free Zn^{2+} ions. In Chapter 3 however, it was revealed that Zn^{2+} was likely to have been a key factor in acute toxicity rather than in growth inhibition. Hence, it is possible that the other properties of the root exudate solution such as the carbon content, increased osmotic potential as compared to water, and stimulatory compounds which may instead have been responsible for the decrease in growth inhibition.

8.3. Plant Toxicity

8.3.1. A Novel Agar-Based Phytotoxicity Method Suggested Particle Contact was a Key Parameter in Root Inhibition; Not Solubility

The results from Chapter 4 revealed that there were differences in root and stem length after treatment according to whether the plant was a monocotyledon or dicotyledon. It was revealed that overall, the inhibition of root growth was greater in dicotyledons than monocotyledons for all treatments. Furthermore, the results indicated that there may be a particle specific effect, as particles were suspended in agar which maintained them in an artificially homogenous state of suspension. $ZnSO_4$ was less toxic than bulk or the nano ZnO despite its significantly higher solubility.

The conclusions drawn from this study were that mechanical abrasion of roots from the particulate treatments contributed to a greater inhibition of root length across the species. The higher solubility of nZnO when in contact with chelators contained in the root exudate explained the lower root inhibition caused by nZnO compared to bulk ZnO treatment. These results indicated that solubility was a key parameter in toxicity, though not as a result of Zn^{2+} release, but rather the increased solubility of nZnO led to a decrease in toxicity, as it involved the solubilisation of particles and hence reduced the root-particle contact. Whether the contact caused toxicity due to ROS release, physical abrasion or a combination is not clear. This was, however, a novel observation and could be further investigated by employing inert particles such as kaolinite in the same agar plate system, in order to determine whether particle abrasion of roots alone is sufficient to cause the root inhibition observed in this study.

8.3.2. Greater Quantities of Zinc were able to be Taken-Up by Barley Plants from nZnO than from Bulk or Ionic Treatments.

The findings of Chapter 5 demonstrated that zinc was able to be taken-up by barley from all of the zinc-containing treatments, with greater uptake as a result of nZnO treatment. At the lowest concentration, 103 % more zinc was detected in shoot tissues than from the bulk treatment, and 315 % more was detected in shoot tissues after treatment with the fully soluble $ZnSO_4$ treatment. Furthermore, in Chapter 7 it was discovered that greater quantities of zinc were able to enter shoot tissues as a result of New nZnO than Old nZnO. The solubility of the two particles was not significantly different in either water or Hoagland solution, however the zeta potential was significantly greater for the New nZnO than the Old. This, when combined with the results of the bulk and nano-scale comparison, revealed that zeta potential was key in determining zinc uptake. This was logical, as the better the particles were dispersed, the more likely it was that they would make contact with the plant roots. The clearing phenomenon in Chapter 3 demonstrated that plant root exudates may be able to solubilise nZnO particles when in close proximity to the root surface. Hence, the better dispersed the particles, the more likely they were to make contact with the root surface (the origin of exudate secretion) and hence to be solubilised and taken up in ionic form.

Studies reported here revealed that the translocation of zinc from the root to the shoot was lower as a result of nZnO treatment. This demonstrated that the majority of zinc remained in the root tissues. The high solubility of nZnO in 0.1 M EDTA solution revealed that it was unlikely that any nZnO could remain on the surfaces of the root after the EDTA washing step, hence it was likely that the measured root zinc content was within the tissues. It could not be determined whether uptake was in particulate or ionic form, however the results indicated that it was possible that the particles were solubilised when in contact with

the root surface. This could be further investigated by sectioning the roots after treatment and analysing with TEM.

8.4. Overall Biological Toxicity

8.4.1. Key Parameters Identified Could be Used to Aid Engineered Nanoparticle Design to Modify Toxicity in Biological Systems

Throughout this study, zeta potential and size have been identified as key parameters in nZnO toxicity to plants and bacteria. For plants, the solubility of the particles was also identified as an important factor in toxicity. Modern engineered nano-scale particles are frequently designed to be highly dispersed, and stable in suspension (Brayner et. al., 2006; Fernández-Garcia & Rodriguez, 2009). The physically smaller size of the particles resulted in greater solubility as a result of greater surface to volume ratio. Results from this study suggested that both of these properties were likely to increase toxicity in biological systems. It may be possible for manufacturers to consider these properties during the design of the particles, in order to reduce toxicity at end of life while maintaining the desired function, such as by engineering coatings which bind readily to natural organic matter (NOM) in the soil. It may in fact be that nature has already developed the mechanisms to reduce nanoparticle toxicity, as demonstrated in Chapters 6 and 7, where it was found that barley root exudates decreased the inhibitory action of nZnO despite maintaining the particles in a high zeta potential. Whether this is a property unique to barley should be investigated further, however it is unlikely as root exudates contain similar compounds across many species, and so it is possible that many plant root exudates would have this function in determining nanoparticle behaviour (Badri & Vivanco, 2009). The results from this study have emphasised the importance of media in determining toxicity, with comparisons between zeta potential and solubility of particles in DI water and Hoagland illustrating the potential for high and low solubility and dispersion states (**Figure 8.1).** The results of this

study generally suggested that toxicity was highest when particles were highly dispersed and highly soluble, and lowest where dispersal and solubility were low.

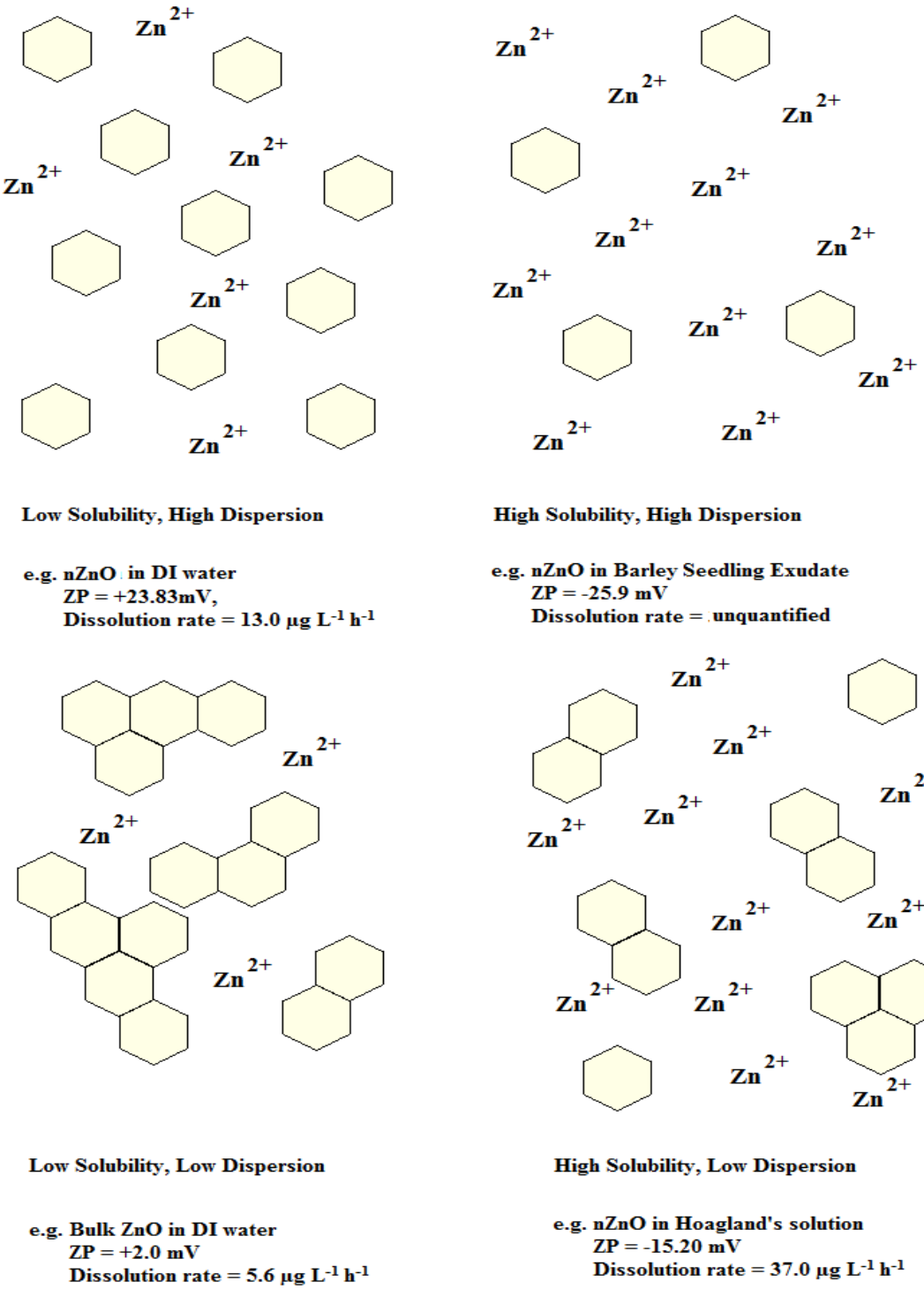


Figure 8.1: Illustration of the potential dispersion and solubility states of ZnO particles

8.5. Future Work

In order to further elucidate the potential impact of nZnO on environmental bacteria, microbial consortia from soil samples could be used as test organisms. By examining the potential shift in community structure and post-exposure recovery the long and short term effects of environmental nZnO could be established. This study identified that root exudates stimulated the growth of *E. coli* and decreased the inhibition as a result of nZnO treatment, so whether this occurs in natural soil communities would be of great interest in ascertaining the impact of nZnO exposure to soil bacteria in the exudate-modified vicinity of plant roots. In addition, a more specific study investigating the impact of nZnO on plant symbiotic species like mycorrhizal fungi and endophytic bacteria could help further in establishing the impact on plants and microbes simultaneously. As the majority of plants are colonised by mycorrhizal fungi (Smith & Read, 1996), determining whether nZnO affects this relationship would be an important consideration in how plants may be indirectly affected as a consequence of nZnO contact.

This study has focussed on the media-root mode of exposure as nZnO is most likely to encounter plant root systems from the water fraction of soil, as opposed to aerial exposure (Osmond & McCall, 2010). In the case of its use as a UV-blocking agent in creams and coatings it is incorporated into a liquid based product and as such does not pose an aerosol risk. It is unlikely to be released into the environment in powder form except perhaps in the case of accidental release directly from the manufacturing plant or suppliers of the dry particles, but plants may be exposed to other metal oxide particles such as CeO and Al_2O_3 from the air through sources such as vehicle exhausts.

A larger scale hydroponic assay of multiple important crop species treated with nZnO, bulk and ionic Zn^{2+} could be used to ascertain whether there is a pattern of uptake at

different concentration between species. There is then the potential for a model plant species to be identified as representative for mainstay crops exposed to nZnO. In addition, a multitude of nano-scale metal oxides could be compared for relative toxicity and perhaps to identify key characteristics of the particles and metal ions they release in terms of toxicity, biomass and uptake. With this information, mathematical models could be derived in order to predict nano-scale metal oxide toxicities in order to aid particle manufacturers in particle design to limit environmental toxicity as a consequence of end of life disposal.

Recently, the concept of 'green' synthesised nanomaterials has gained popularity, employing leaf extracts as a precursor in synthesis (Gnaanansangeetha *et. al.,* 2013). An investigation as to whether these nanomaterials are differently toxic to standard lab synthesised particles from purified chemical precursors would be useful, as should they exhibit reduced toxicity, then this, combined with their more eco-friendly nature, could be of use in producing the next generation of nanomaterials and maintaining positive public perception.

8.6. Conclusion

The experiments conducted throughout this project covered a wide breadth of methods in order to determine which measurable properties of the nanoparticles were most useful in terms of predicting toxicity to plants and bacteria. Zeta potential was identified as having a key role in toxicity across the domains. In bacteria, different material characteristics led to different forms of toxicity, however the overall finding was that nZnO was not more toxic to *E. coli* than the bulk form. In barley, the decrease in biomass and uptake into root and shoot tissues was greater as a result of nZnO treatment, and furthermore was greater with New nZnO exposure as opposed to Old nZnO treatment. This was again linked to the dispersal state of the particles, as the solubility was similar. These results suggested that

plant exposure to nZnO may have a greater consequence than bacterial exposure, however under environmental conditions in soil, as opposed to liquid media *in vitro*, it is likely that the actual toxicity would be lower, as a result of particle interaction with organics contained within the soil and released in plant root exudates.

The concern with emerging technologies such as nanotechnology is that environmental impact and toxicological studies are frequently insufficient in number or broad enough before the technology is adopted on a global scale. Hence, the implications of the technology may not be realised before detrimental effects are discovered, and promising methods could be stopped in their tracks. Research into the biological implications of exposure to nanoparticles is crucial to help shape the future developments of the technology (not least the actual design of the materials). Understanding the ecological impact now, by investigating the mechanisms of plant and bacterial toxicity of particles, can direct future design and considerations of engineered technologies.

REFERENCES

Aiken, A. M., Allegranzi, B., Scott, J. A., Mehtar, S., Pittet, D., Grundmann, H., (2014) 'Antibiotic resistance needs global solutions' *The Lancet Infectious Diseases,* 14 (7) pp 550-551

Alkahlout, A., Al Dahoudi, N., Grobelsek, I., Jilavi, M., and W. de Oliveria, P., (2014). 'Synthesis and Characterisation of Aluminium Doped Zinc Oxide Nanostructures via Hydrothermal Route'. *Journal of Materials.* Vol 2014, Article ID 235638

Al-Kaysi, R. O., Muller, M. A., Ahn, T-S., Lee, S., and Bardeen, C. J., (2005) 'effects of sonication on the size and crystallinity of stable zwitterionic organic nanoparticles formed by reprecipitation in water' *Langmuir* 21 (17) pp 7990-7994

Alscher R. G., Erturk N., Heath L. S., (2002). "Role of superoxide dismutases (SODs) in controlling oxidative stress in plants". *Journal of Experimental Botany* 53 (372) pp1331–41.

Atkins, P., and De Paula, J., (2010) Physical Chemistry (9th ed) Oxford, OUP

Atkinson, N. J., and Urwin, P. E., (2012) 'The interaction of plant biotic and abiotic stresses: from genes to the field' *Journal of Experimental Botany* 63 (1) pp 3523-3543

Bais, H. P., Weir, T. L., Perry, L. G., Gilroy, S., and Vivanco, J. M., (2006) 'The Role of root exudates in rhizosphere interactions with plants and other organisms.' *Annu. Rev. Plant Biol.* 57, pp 233-66

Baker, K. S., 'Demistifying *Escherichia coli* pathovars' (2015) *Nature Reviews Microbiology* 13 (5) p 1

Battke F, Leopold K, Maier M, Schmidhalter U, Schuster M. (2009) 'Palladium exposure of barley: uptake and effects' *Plant Biology* 10:272–6.

Bauer, A., C.V. Eberlein, J.W. Enz, and C. Fanning. 1984. Use of Growing-Degree Days to Determine Spring Wheat Growth Stages. North Dakota State University Extension Bulletin 37.

Becker-Ross, H., Florek, S., Heitmann, U., and Weisse, R., (1996) 'Influence of the spectral bandwidth of the spectrometer on the sensitivity using continuum source AAS' *Fresenius Journal of Analytical Chemistry,* 355 pp 300-303

Berg, G., and Smalla, K., (2009) 'Plant species and soil type cooperatively shape the structure and function of microbial communities in the rhizosphere' *FEMS Microbiology Ecology* 68 (1) pp 1-13

Berney, M., Hammes, F., Bosshard, F., Weilenmann, H-U., and Egli, T., (2007) 'Assessment and interpretation of bacterial viability by using the live/dead BacLight kit in combination with flow cytometry' *Applied environmental microbiology* 73 (10) pp 3283-3290

Bertin, C., Yang, X., and Weston, L. A., (2003) 'The role of root exudates and allelochemicals in the rhizosphere' *Plant and Soil* 256, pp 67-83

Berube, D. M., Cummings, C. L., Frith J. H., Binder A. R., and Oldendick, R., (2011) 'Comparing nanoparticle risk perceptions to other known EHS risks' *Journal of Nanoparticle Research*, 13, (8) pp 3089-3099

Bhattacharyya, J., Read, D., Amos. S., Dooley, S., Killham, K., Paton, G. I., (2005) 'Biosensor-based diagnostics of contaminated groundwater – assessment and remediation strategy' *Environmental Pollution*, 134 (3) pp 485-492

Bihari, P., Vippola, M., Schultes, S., Praetner, M., Khandoga, A. G., Reichel, C. A., Coester, C., Tuomi, T., Rehberg, M., and Krombach, F., (2008) 'Optimised dispersion of nanoparticles for biological in vitro and in vivo studies' *Particle and fibre toxicology* 5 (18)

Birbaum, K., Brogioli, R., Schellenberg, M., Martinoia, E., Stark, W. J., Gunther, D. and Limbach, L. K. (2010) "No Evidence for Cerium Dioxide Nanoparticle Translocation in Maize Plants" *Environmental Science & Technology*, 44, pp8718–8723

Biswas, P., and Wu, C-Y. (2005) 'Nanoparticles and the Environment' *Air & Water Management Association* 55, pp708–746

Bojeong, K., Park, C., Murayama, M., and Hochella, M. F., (2010) 'Discovery and characterization of silver sulphide nanoparticles in final sewage sludge products' *Environmental Science & Technology*, 44, pp7509-7514

Brayner, R., Ferrari-Iliou, R., Brivois, N., Djediat, S., (2006) 'Toxicological impact studies based on Escherichia coli bacteria in ultrafine ZnO nanoparticles colloidal medium' *Nano Letters* 6 pp 866-870.

Brock, T. D., (1999) 'Milestones in Microbiology 1546-1940' ASM press, ISBN 1555811426,

Brudzynski, K., Abubaker, K., St-Martin, L., and Castle, A., (2011) 're-examining the role of hydrogen peroxide in bacteriostatic activities of honey' Frontiers in Microbiology 2, 213

Buzea, C. I., Pacheco, K., Robbie, A. (2007) 'Nanomaterials and Nanoparticles: sources and toxicity' *Biointerphases* 2, 17-172

Campbell, N. A. and Reece J. B., (2005) Biology, 7th ed., Benjamin Cummings, San Francisco

Cao, Y., Ran, R., Wu, X., Zhao, B., Wan, J., and Weng, D., (2013). 'Comparative study of ageing condition effects on Pd/Ce0.5Zr0.5O2 and Pd/Al_2O_3 catalysts: Catalytic activity, palladium nanoparticle structure, and Pd-support interactions' *Applied Catalysis A: General* 457 pp 52-61

Chan, A. C., Ager, D., Thompson, I. P., (2013) 'Resolving the mechanism of bacterial inhibition by plant secondary metabolites employing a combination of whole-cell biosensors' *Journal of Microbiological Methods,* 93 (3) pp 209-217

Chen, K. J., Fang, T. H., Hung, F. Y., Jib, L. W., Chang, S. J., Young, S. J., and Hsiao, Y. J. (2008) 'The crystallisation and physical properties of Al-doped ZnO nanoparticles' *Applied Surface Chemistry* 254, (18) pp5791-5795

Chen, W., (2013) 'What is Zeta Potential?' Filtration media: American Filtration and Separations Society (afssociety.org).

Cho, W-S., Duffin, R., Thielbeer, F., Bradley, M., Megson, I. L., MacNee, W., Poland, C. A., Tran, C. L., and Donaldson, K., (2012) 'Zeta potential and solubility to toxic ions as mechanisms of lung inflammation caused by metal/metal-oxide nanoparticles' *Toxicological Sciences,* 10, 1093 pp 1-31

Chu, B., and Liu, T., (2000) 'Characterisation of nanoparticles by scattering techniques' *Journal of nanoparticle research* 2 (1) pp 29-41

Connolly, J., Valdramidis, V. P., Byrne, E., Karatzas, K. A., Cullen, P. J., Keener, K. M., and Mosnier, J. P., (2013) 'Characterization and antimicrobial efficacy against *E. coli* of a helium/air plasma at atmospheric pressure created in a plastic package' *Journal of Physics D: Applied Physics* 46 (3) 035401 pp 1-12

Cooke, M. S., Evans, M. D., Dizdaroglu, M., and Lunec, J., (2003) 'Oxidative DNA damage: mechanisms, mutation and disease' *The FASEB Journal* 17 (10) pp 1195-1214

Cooper, G. M., (2000) 'The Cell: A Molecular Approach' 2nd Ed., Sinauer Associates, Sunderland, Boston University, ISBN 0878931066

Cronholm, P., Midander, K., Karlsson, H. L., Elihn, K., Wallinger, I. O., and Moller, L., (2011) 'Effect of sonication and serum proteins on copper release from copper nanoparticles and the toxicity towards lung epithelial cells' *Nanotoxicology* 5 (2) pp 269-28

Dakora, F. D., & Phillips, D. A. (2002) Root exudates as mediators of mineral acquisition in low-nutrient environments. *Plant and Soil* 245: 35–47

Darlington, T. K., Neigh, A. M., Spencer, A. M., Nquyen, O. T., and Oldenburg, S. J., (2009) 'Nanoparticle characteristics affecting environmental fate and transport through soil' *Environmental Toxicology and Chemistry* 28 (6) pp 1191-1199

Das, M., Saxena, N., Dwivedi, P. D., (2009) 'Emerging trends of nanoparticles application in food technology: safety paradigms' *Nanotoxicology* 3 pp 10-18

Davey, H. M., and Kell, D. B., (1996) 'Flow cytometry and cell sorting of heterogenous microbial populations; importance of single-cell analyses' *Microbiology and molecular biology reviews* 60 (4) pp 641-696

Davis, T. M., Drews, T. O., Ramanan, H., He, C., Dong, J., Schnablegger, H., Katsoulakis, M. A., Kokkoli, E., McCormick, A. V., Penn, R. L., and Tsapatsis, M., (2006) 'Mechanistic principles of nanoparticle evolution to zeolite crystals' *Nature Materials* 5 pp 400-408

DeJong, J. T., Soga, K., Banwart, S. A., Whalley, R., Ginn, T. R., Nelson, D. C., Mortensen, B. M., Martinez, B. C., and Barkouki, T., (2010) 'Soil engineering in vivo: harnessing natural biogeochemical systems for sustainable, multi-functional engineering solutions' *Journal of the Royal Society Interface* doi: 10.1098/rsif.2010.0270

Dhas, S. P., Shiny, P. J., Khan, S., Mukherjee, A., Chandrasekaren, N., (2014) 'Toxic behaviour of silver and zinc oxide nanoparticles on environmental microorganisms' *Journal of Basic Microbiology* 54 (9) pp 916-927

Durieux, R. P., Bartless, R. J., and Magdoff, F. R., (1995) 'Separate mechanisms of aluminium toxicity for nitrate uptake and root elongation' *Plant and Soil* 172 pp 229-234

Dutta, R. K., Nenavathu, B. P., Gangishetty, M. K., Reddy, A. V. R., (2012) 'Studies on antibacterial activity of ZnO nanoparticles by ROS induced lipid peroxidation' *Colloids and surfaces B: Biointerfaces 94* pp 143-150

Eisenberger, I., Nentwich, M., Fiedeler, U., Gazsó, A., and Simkó, M., (2010) 'Nano Regulation in the European Union', *Nano Trust Dossiers* No. 017en

El-Temsah, Y. S., and Joner, E. J., (2012) 'Impact of Fe and Ag nanoparticles on seed germination and differences in bioavailability during exposure in aqueous suspension and soil.' (2012) *Environ, Toxicol*. 27(1) 42:9

European Commission (2009) 'ENRHES (Engineered Nanoparticles; Review of Health and Environmental Safety' Community Reseach and Development Information Service (CORDIS) Project Reference: 218433

Everett, D.H. (1994) Basic Principles Of Colloid Science, The Royal Society of Chemistry, UK

Fang, Y., Wang, T-J., Wu, H-X, and Jon, H., (2008) 'Surface Chemical modification of nanosized oxide particles with a titanate coupling reagent in isopropanol' *Industrial Engineering and Chemistry Research* 47, pp 1513-1517

Fang, Y., Wang, L., Xin, Z., Zhao, X-A., and Hu, Q., (2008) 'Effect of foliar application of zinc application of Zinc, Selenium, and Iron fertilisers on nutrient concentration and yield of rice grain in China' *J. Agric. Food chem*, 56 (6) pp2079-2084

FAOSTAT, 2015 Food and Agriculture Organisation of the United Nations, http://faostat.fao.org/site/567/DesktopDefault.aspx?PageID=567#ancor

FDA (U.S. Food and Drug Administration) (2006) 'Database of Select Committee on GRAS substances (SCOGS) Reviews; Zinc Oxide' ID Code: 1314-13-2; CFR Section 182.8991

Federal Register (1998) USA, Vol 63 No. 204

Fernández-Garcia, M., and Rodriguez, J. A. (2009) 'Metal Oxide Nanoparticles' *Encyclopedia of Inorganic Chemistry*

Glander, H. J., and Schaller, J., (1999) 'Binding of Annexin V to plasma membranes of human spermatozoa; a rapid assay for detection of membrane changes after cryostorage' *Molecular human reproduction,* 5 (2) pp 109-115

Gnanansangeetha, D., and SaralaThambacani, D., (2013) 'One Pot Synthesis of Zinc Oxide Nanoparticles via Chemical and Green Method' *Research Journal of Material Sciences,* 1 (7) pp 1-8

Goh, E. G., Xu, X., and McCormick, P. G., (2014) 'Effect of Particle size on the UV absorbance of Zinc Oxide nanoparticles' *Scripta Materialia* 78-79 pp 49-52

Grassian, V. H., O'Shaughnessy, P. T., Adamcakova-Dodd, A., Pettibone, J. M., and Thorne, P. S., (2007) 'Inhalation exposure study of titanium dioxide nanoparticles with a primary particle size of 2-5nm' *Environmental Health Perspectives* 115 (3) pp 397-402

Grasso, D., Subramaniam, K., Butkus, M., Strevett, K., Bergendahl, J., (2002) 'A review of non-DLVO interactions in environmental colloidal systems' *Review of Environmental Science and Biotechnology* 1 pp 17-38

Griffiths, P., and De Hasseth, J. A., (2007) 'Fourier Transform Infrared Spectrometry' *Wiley-Blackwell,* ISBN 0471194042

Grotz, N., Fox, T., Connolly, E., Park, W., Guerinot, M. L., and Eide, D., (1998) 'Identification of a family of zinc transporter genes from Arabidopsis that respond to zinc deficiency' *PNAS* 95, 12 pp7220-7224

Guo, L., Ji, Y. L., Xu, G., Simon, P., Wu, Z., (2002) 'Regularly shaped, singal-crystalline ZnO nanorods with wurtzite structure' *Journal of the American Chemical Society,* 124 (50) pp 14864-14865

Gupta, S., Zhang, Q., Emrick, T., Balazs, A. C., and Russell, T. P., (2006) 'Entropy-driven segregation of nanoparticles to cracks in multi-layered composite polymer structures' *Nature Materials* 5, pp 229-233

Guzman, M., Dille, J., and Godet, S., (2012) 'Synthesis and antibacterial activity of silver nanoparticles against gram-positive and gram-negative bacteria' *Nanomedicine: Nanotechnology, Biology and Medicine*. 8, pp 37-45

Hackley, V. A., ,and Clogston, J. D., (2011) 'Measuring the hydrodynamic size of nanoparticles in aqueous media using batch-mode dynamic light scattering' *Methods in molecular biology* 697 pp 35-52

Hambidge, M., (2000) 'Human Zinc Deficiency' *Journal of nutrition*, 130 pp 1344-1349

Hambidge, M., & Walravens, P. A., (1982) 'Disorders of mineral metabolism' *Clinical Gastroenterology* 11 pp 87-118

Handy, R.D., Owen, R., Valsami-Jones, E., (2008). 'The ecotoxicology of nanoparticles and nanomaterials: current status, knowledge gaps, challenges, and future needs'. *Ecotoxicology* 17, pp 315–325.

Hanley, C., Thurber, A., Hanna, C., Punnoose, A., Zhang, J., and Winget, D.G. (2009). 'The influences of cell type and ZnO nanoparticle size on immune cell cytotoxicity and cytokine induction'. *Nanoscale Research Letters*. 4, pp 1409-1420.

He, L., Liu, Y., Mustapha, A., and Lin, M., (2011) 'Antifungal activity of Zinc oxide nanoparticles against Botrytis cinerea and Penicillium expansum' Microbial Research 166 (3) pp 207-215

Heim, A., Brunner, I., Frey, B., Frossard, E., Luster, J., (2001) 'Aluminium resistance of Norway spruce: Root exudation versus immobilization in roots' *Plant Nutrition – developments in Plant and Soil Sciences* 92 pp 450-451

Heinlaan, M., Ivask, A., Blinova, I., Dubourguier, H.-C., and Kahru, A., (2008). 'Toxicity of nanosized and bulk ZnO, CuO and TiO2 to bacteria *Vibrio fischeri* and crustaceans *Daphnia magna* and *Thamnocephalus platyurus*'. *Chemosphere*, 71, 1308-1316.

Heisler, M. G., Ohno, C., Das, P., Sieber, P., Reddy, G. V., Long, J. A., Meyerowitz, E. M., (2005) 'Patterns of auxin transport and gene expression during primordium development revealed by live imaging of the Arabidopsis inflorescence meristem. *Curr Biol.* 8;15(21) pp1899-1911.

Henry, A., Doucette, W., Norton, J., and Bugbee, B., (2007) 'Changes in crested wheatgrass root exudation caused by flood, drought and nutrient stress' *Journal of Environmental Quality*, 26 pp 904-912

Hewitt C. J., and Nebe-Von-Caron, G., (2004) 'The application of multi-parameter flow cytometry to monitor individual microbial cell physiological state' *Advances biochemical engineering and Biotechnology* 89 pp 197-223

HGCA Recommended Lists database, (2012)

Honary, S., and Zahir, F., (2013) 'Effect of Zeta potential on the properties of N delivery systems – A review (Part 1) *Tropical Journal of Pharmaceutical Research* April 1596-5996

Hong, F. S.; Zhou, J.; Liu, C.; Yang, F.; Wu, C.; Zheng, L.; Yang, P. (2005) Effect of nano-TiO2 on photochemical reaction of chloroplasts of spinach. *Biol. Trace Elem. Res.* 105, pp 269–279.

Horst, Angela K. (2009) 'Antimicrobial Effects of Metal Oxide Nanoparticles' *NNIN REU Research Accomplishments, Biological Applications* 12-13

Hospital Management, (2010) 'Battling MRSA – superdrug for the superbug' http://www.hospitalmanagement.net/features/feature111217/feature111217-1.html

Huang, P. M., (2008) ‘Soil Physicochemical and Biological Interfactial interactions in the rhizosphere: impacts on food security and ecosystem integrity’ *Journal of Soil Sciences, Plant Nutrition* v8, pp 23-27

Hunter, R. J., (1986) ‘Zeta potential in colloid science: principles and applications’ Academic Press Limited, London ISBN 0-12-361960

Hussain, S. M., Braydich-Stolle, L. K., Schrand, A. M., Murdock, R. C., Yu, K. O., Mattie, D. M., Schlager, J. J., and Terrones, M., ‘Toxicity evaluation for safe use of nanomaterials: recent achievements and technical challenges’ *Advanced Materials* 21 pp 1549-1559

Ishibashi, K-I., Fujishima, A., Watanabe, T., Hashimoto, K., (2000) ‘Detection of active oxidative species in TiO2 photocatalysis using the fluorescence technique’ Electrochemistry communications 2, 3 pp 207-210

Jain, A., Bhargava, R., and Poddar, P., (2013) ‘Probing interaction of Gram-positive and Gram-negative bacterial cells with ZnO nanorods’ *Materials Science and Engineering: C* 33, (3) pp 12-47-1253

James, A. E., and Driskell, J. D., (2013) ‘Monitoring gold nanoparticle conjugation and analysis of biomolecular binding with nanoparticle tracking analysis (NTA) and dynamic light scattering (DLS)’ *Analyst* 138 pp 1212-1218

Jiang, J., Oberdorster, G., and Biswas, P., (2009) ‘Characterisation of size, surface charge, and agglomeration state of nanoparticle dispersions for toxicological studies’ *Journal of Nanoparticle Research* 11 pp 77-89

Jiang, W., (2011) ‘Bacterial toxicity of oxide nanoparticles and their effects on bacterial surface biomolecules’ University of Massachusetts – Amherst, Dissertations, paper 386

Johnson, A. C., Bowes, M. J., Crossley, A., Jarvie, H. P., Jurkschat, K., Jurgens, M. D., Lawlor, A. J., Park, B., Rowland, P., Spurgeon, D., Svedsen, C., Thompson, I. P., Barnes, R. J., Williams, R. J., and Xu, N. (2011) ‘An assessment of the fate behaviour and environmental risk associated with sunscreen TiO2 nanoparticles in UK field scenarios’ *Science of the Total Environment* 409 (13) pp 2503-2510

Juang, W., Mashayekhi, H., and Xing, B., (2009) ‘Bacterial toxicity comparison between nano- and micro-scaled oxide particles’ *environmental pollution* 157 pp 1619-1625

Kang, M. A., So, E-y., Simons, A. L., Spitz, D. R., and Ouchi, T., (2012) ‘DNA damage induces reactive oxygen species generation through the H2AX-Nox1/Rac1 pathway’ *Cell Death & Disease* 3 (1) pp 249

Kaprelyants, A. S., and Kell, D. B., (1992) ‘Rapid assessment of bacterial viability and vitality by rhodamine 123 and flow cytometry’ *Journal of applied bacteriology* 72 pp 410-422

Kasemets, K., Ivask, A., Dubourguier, H-C., K, A. (2009) Toxicity of nanoparticles of ZnO, CuO and TiO2 to yeast *Saccharomyces cerevisiae*. *Toxicology in Vitro* 23, 6, pp 1116–1122

Kimoto-Nira, H., Aoki, R., Mizumachi, K., Sasaki, K., Naito, H., Sawada, T., Suzuki, C. (2012) 'Interaction between Lactococcus lactis and Lactococcus raffinolactis during growth in milk: development of a new starter culture' *Journal of Dairy Science* 96 (4) pp 2176-2185

Kjelleberg, S., (1993) 'Starvation in Bacteria' Plenum Press, New York ISBN 0-30644430-5

Korayem, A. M., (1993), 'Effect of zinc fertilisation on rice plants and on the population of the rice-root nematode 'hirschmanniella oryzae'; *Anzeiger für Schädlingskunde* 66, 1 pp18-21

Koshkin, V. M., and Slezov, V. V. (2004) 'Doping Nanoparticles' *Technical Physics Letters*, 30, 5 pp 367-369

Kuchibhatla, S. V. N. T., Karakoti, A. S., Baer, D. R., Samudrala, S., Engelhard, M/ H., Amonette, J. E., Thevuthasan, S., and Seal, S. (2012) 'Influence of Aging and Environment on Nanoparticle chemistry – Implication to Confinement Effects in Nanoceria' *Journal of Physical Chemistry C. Nanomater Interfaces* 116(26): pp 14109-14114

Kurepa, J., Paunesku, T., Vogt, S., Arora, H., Rabatic, B. M., Lu, J., Wanzer, M. B., Woloschak, G. E., Smalle, J. A., (2011) 'Uptake and distribution of ultrasmall anatase TiO_2 alizarin red S nanoconjugates in *Arabidopsis thaliana*.' Nano Letters, 10 (7) pp 2296-2302

Kuzyakov, Y., & Domanski, G., (2000) 'Carbon input by plants into the soil: review'. *Journal of Plant Nutrition. Soil Sciences*. 163, pp 421–431.

Labouriau, L. G., (1970) 'On the physiology of seed germination in Vicia graminea'. *Sm. I. Anais da Academia Brasileira de Ciencias*, 42 pp 235-262

Landowne, D., (2006) 'Cell Physiology' McGraw Hill Medical Publishing Division, Miami, Florida (USA)

Lee, W-M., Kim, S. W., Kwak, J. I., Nam, S-H., Shin, Y-J., and An, Y-J. (2010) 'Research Trends of Ecotoxicity of Nanoparticles in Soil Environment' *Toxicological Research* 26(10) pp 253-359

Lee, W-M., Kwak, J. I., An, Y-J. (2012) 'Effect of silver nanoparticles in crop plants phaseolus radiates and sorghum bicolor; media effect on phytotoxicity' *Chemosphere* 86 pp 491-499

Lei, Y., Chen, W., and Mulchandani, A., (2006) 'Microbial Biosensors' *Analytica Chimica Acta* 568 pp 200-210

Lena, M., Quero, G. M., Santovito, E., Verran, J., Angelis, M. D., Fusco, V., (2015) 'A selective medium for isolation and accurate enumeration of lactobacillus casei-group lactobacilli in probiotic milks and dairy products' *International Dairy Journal* (In Press)

Lesser, M. P., (2006) ‘Oxidative stress in marine environments: biochemistry and physiological ecology’ *Annual Reviews in Physiology* 68 pp 253-78.

Li, N., Sioutas, C., Cho, A., Schmitz, D., Misra, C., Sempf, J., Wang, M., Oberley, T., Froines, J., Nel, A., (2003) 'Ultrafine particulate pollutants induce oxidative stress and mitochondrial damage' *Environmental Health Perspective* 111, pp 455-460

Li, Y., Zhang, W., Nium, J., and Chen, Y., (2012) ‘mechanism of photogenerated reactive oxygen species and correlation with the antibacterial properties of engineered metal-oxide nanoparticles’ *ACS Nano* 6 (6) pp 5164-5173

Lin, D., and Xing, B., (2007) 'Phytotoxicity of Nanoparticles: Inhibition of seed germination and root growth' *Environmental Pollution*, 150, 2 pp 243-250

Lin, D., and Xing, B., (2008) ‘Root uptake and Phytotoxicity of ZnO nanoparticles’ *Environmental Science & Technolology*, 42, pp 5580-5585

Lin, K-F., Cheng, H-M., Hsu, H-C., Lin, L-J., Hsieh, W-F., (2005) ‘Band gap variation of size-controlled ZnO quantum dots synthesised by sol-gel method’ *Chemical Physics Letters* 409, 208-211

Lin, S., Reppert, J., Hu, Q., Hudson, J. S., Reid, M. L., Ratnikova, T. A., Rao, A. M., Luo, H., Ke, P. C., (2009) ‘Uptake, translocation, and transmission of carbon nanomaterials in rice plants’ *Small* 5 (10)

Lines-Kelly, R., (2005) ‘The Rhizosphere’ *Profitable and Sustainable Primary Industries*

Liu, Q.; Chen, B.; Wang, Q.; Shi, X.; Xiao, Z.; Lin, J.; Fang, X. (2009) ‘Carbon Nanotubes as Molecular Transporters for Walled Plant Cells’. *Nano Letters* 9, pp 1007–1010.

Liu, Y., He, L., Mustapha, A., Li, H., Hu, Z. Q., and Lin, M., (2009) ‘Antibacterial activites of zinc oxide nanoparticles against Escherichia coli O157:H7’ *Journal of Applied Microbiology* 107 (4) pp 1193-1201

Liu, Y., and Hu, J., (2005) ‘Pd nanoparticle aging and its implications in the Suzuki cross-coupling reaction’ *Langmuir* 21 (6) pp 2121-2123

Liu, Y., and Yan, B., (2011) ‘Characterizing the Surface Chemistry of Nanoparticles: An Analogy to Solid-Phase Synthesis Samples’ *Combinatorial Chemistry & High Throughput Screening*, 14 pp 191-197

Lloret, J., Bolanos, L., Mercedes Lucas, M., Peart, J. M., Bewin, N. J., Bonilla, I., and Rivilla, R., (1995) ‘Ionic stress and osmotic pressure induce different alterations in the lipopolysaccharide of a *Rhizobium meliloti* strain’ Applied and environmental microbiology, pp 3701-3704

Louis, D., Foley, S., Cabillic, J., Coffigny, H., Taran, D., Valleix, A., Renault, P., and Pin, S., (2004) ‘The reaction of coumarin with the oh radical revisited: hydroxylation product analysis determined by fluorescence and chromatography’ *Radiation Physics and Chemistry*,

72 (2-3) pp 119-124

Lowry, G. V., Gregory, K. B., Apte, S. C., and Lead, J. R., (2012) 'Transformations of nanomaterials in the environment' Environmental science and technology 46 pp 6893-6899

Luna, E., Pastor, V., Robert, J., Flors, V., Mauch-Mani, B., and Ton, J., (2011) 'Callose deposition: a multifaceted plant defense response' *Molecular Plant-Microbe Interactions* 24 2 pp 183-193

L'vov, B. V., (2005) 'Fifty years of atomic absorption spectrophotometry' *Journal of Analytical Chemistry* 60 pp 382-392

Ma, H., Wallis, L. K., Diamond, S., Li, S., Canas-Carrell, J., Parra, A., (2014) 'Impact of solar UV radiation on toxicity of ZnO nanoparticles through photocatalytic reactive oxygen species (ROS) generation and photo-induced dissolution' *Environmental Pollution 193* pp 165-172

Ma, X., Geiser-Lee, J., Deng, Y., and Kolmakov, A., (2010) 'Interactions between engineered nanoparticles (ENPs) and plants: Phytotoxicity, uptake and accumulation' *Science of the Total Environment*, 408, 16 pp 3053-3061

Madigan, M. T., Martinko, J. M., Stahl, D. A., and Clark, D. P., (2011), 'Brock Biology of Microorganisms' Pearson Education 13th ed. ISBN 032173551X

Madler, L., Stark, W. J., and Pratsinis, S. E., (2002) 'Rapid synthesis of stable ZnO quantum dots' Journal of Applied Physics 92, 11 pp 6537-6540

Mahajan, P., Dhoke, S. K., and Khanna, A. S., (2011) 'Effect of nano-ZnO particle suspension on growth of mung (*vigna radiate*) and gram (*cicer arietinum*) seedlings using plant agar method' *Journal of Nanotechnology* 2011 pp 1-7

Malvern, (2013) 'Zeta Potential – an introduction in 30 minutes' Technical note, Malvern Instruments, MRK654-01, Worcestershire, UK,

Marczac, R., Segets, D., Voigt, M., Peukert, W., (2010) 'Optimum between purification and colloidal stability of ZnO Nanoparticles' *Advanced Powder Technology*, The Society of Powder Technology, Japan, 21, 1 pp 41-49

Mariano, E. D., Jorge, R. A., Keltjens, W. G., and Menossi, M., (2005) 'Metabolism and root exudation of organic acid anions under aluminium stress' Brazilian Journal Plant Physiology 17, pp 157-172

Marin, P., Israel, M., Glowinski, J., and Premond, J. (2000). 'Routes of zinc entry in mouse cortical neurons: a role in zinc-induced neurotoxicity' *European Journal of Neuroscience.* 12 pp8-18.

Mauseth, J. D., (2014) 'Botany – An Introduction to Plant Biology' Jones & Bartlett Publishers, ISBN 1284068854

Mendes, R. G., Koch, B., Bachmatiuk, A., El-Gendy, A. A., Krupskaya, Y., Springer, A., Klingeler, R., Schmidt, O., Buchner, B., Sanchez, S., Rummeli, M. H., (2014) 'Synthesis and toxicity characterization of carbon coated iron oxide nanoparticles with highly defined size distributions' *Biochimica et Biophysica Acta – general subjects* 1840 (1) pp 160-169

Mikrajuddin, F. I., Okuyama, K., and Shi, F. G., (2001) 'Stable Photoluminescence of Zinc Oxide Quantum Dots in Silica Nanoparticles Matrix Prepared by the Combined Sol-Gel and Spray Dry Method' *Journal of Applied Physics*, 89, pp 6431-4

Mitchnick, M. A., Fairhurst, D., and Pinnel, S. R., (1999) 'Microfine Zinc Oxide (Z-cote) as a photostable UVA/UVB sunblock agent' J*ournal of the American Academy of Dermatology*, 40, pp 85-90

Moghaddam, M. R. B. and Ende, W. V., (2012) 'Sugars and plant innate immunity' *Journal of Experimental* Botany pp 1-10

Molina, R., Al Salama, Y., Jurkschat, K., Dobson, P. J., Thompson, I. P., (2011) 'Potential environmental influence of amino acids on the behavior of ZnO nanoparticles' Chemosphere, 83, 4 pp 545-551

Moos, P. J., Chung, K., Woessner, D., Honeggar, M., Cutler, N. S., and Veranth, J. M. (2010) ZnO particulate matter requires cell contact for toxicity in human cancer cells) Chem. Res. Toxicol, 23 (4) pp 733-739

Morkoc, H., and Ozgur, U., (2009) 'Zinc oxide: fundamentals, materials and device technology' Wiley-CVH, Weinheim ISBN: 978-3-527-40813-9

Murdock, R. C., Braydich-Stolle, L., Schrand, A. M., Schlager, J. J., and Hussain, S. M., (2007) 'characterisation of nanomaterial dispersion in solution prior to in vitro exposure using dynamic light scattering technique' *Toxicological sciences* 101 (2) pp 239-253

Navarro, E., Baun, A., Behra, R., Hartmann, N. B., Filser,J., Miao, A-J., Quigg, A., Santschi, P. H., and Sigg, L. (2008) 'Environmental behavior and ecotoxicity of engineered nanoparticles to algae, plants, and fungi' *ecotoxicology* 17 (5) pp 372-386

Nelson, T., and Dengler, N., (1997) 'Leaf vascular pattern formation' *Plant Cell* 9 (7) pp 1121-1135

OECD, (2008) Annual Report (http://www.oecd.org/newsroom/40556222.pdf)

OECD, (2011) Nanosafety at the OECD – The First Five Years 2006-2010 http://www.oecd.org/science/nanosafety/47104296.pdf

Osmond, M. J., and McCall, M. J., (2010) 'Zinc oxide nanoparticles in modern sunscreens: an analysis of potential exposure and hazard' *Nanotoxocology* 4(1) pp 15-41

Paterson, A. H., Bowers, J. E., Chapman, B. A., Peterson, D. G., Rong, J., Wicker, T. M., (2004) 'Comparative genome analysis of monocots and dicots, toward characterisation of angiosperm diversity' *Current opinion in biotechnology* 15 (2) pp 120-125

Phe, M. H., Dossot, M., Guilloteau, H., Block, J. C., (2005) 'Nucleic acid fluorochromes and flow cytometry prove useful in assessing the effect of chlorination on drinking water bacteria' *Water Research* 39 (15) pp 3618-3628

Pinnell, S. R., Fairhurst, D., Gillies, R., Mitchnick, M. A., Kollias, N., (2000) 'Microfine Zinc oxide is a superior sunscreen ingredient to microfine titanium dioxide' *Dermatol Surg* 26, pp 309-314

Pouran, H. M., Martin, F. L., and Zhang, H., (2014) 'Measurement of ZnO nanoparticles using diffusive gradients in thin films: binding and diffusional characteristics' *Analytical Chemistry* 96 (2) pp 5906-5913

Prasad, M. N. V., (2004) 'Heavy metal stress in plants – From biomolecules to ecosystems' Springer Verlag, Berlin, Heidelberg, ISBN 978-3-540-40131-5

Provder, T., (1991) 'Particle size distribution II; assessment and characterization' American Chemical Society, Washington, USA ISBN 0-8412-2117-0

Raychaudhuri, S., Deng,X., (2008). "The Role of Superoxide Dismutase in Combating Oxidative Stress in Higher Plants". *The Botanical Review* 66 (1): pp 89–98.

Reed, B., (2008) 'Plant cryopreservation - a practical guide' New York, Springer ISBN 9780387722764

Reed, R., Ladner, D. A., Higgins, C. P., Westerhoff, P., and Ranville, J. F. (2012) Solubility of nano-zinc oxide in environmentally and biologically important matrices' *Environmental Toxicology and Chemistry*, Vol. 31, No. 1, pp 93–99

Rendueles, O., Travier, L., Latour-Lamber, P., Fontaine, T., Magnus, J., Denamur, E., and Ghigo, J-M (2014) 'Screening of *Escherichia coli* species biodiversity reveals new biofilm associated anti-adhesion polysaccharides' *mBio* 2 (3) pp 1-6

Riahi-Madvar, A., Rezaee, F., and Jalali, V., (2012) 'Effects of alumina nanoparticles on morphological properties and antioxidant system of *Triticum aestivum' Iranian journal of Plant Physiology* 3 (1) pp 595-565

Rico, C. M., Majumdar, S., Duarte-Gardea, M., Peralta-Videa, J. R., Gardea-Torresdey, J. L., (2011) 'Interaction of Nanoparticles with Edible Plants and Their Possible Implications in the Food Chain' Journal of Agricultural and Food Chemistry, 59 pp 3485-3498

Rothen-Rutishauser, B.M., Schirch, S., Haenni, B., Kapp, N., and Gehr, P. (2006) 'Interaction of Fine Particles and Nanoparticles with Red Blood Cells Visualized with Advanced Microscopic Techniques' *Environ. Sci. Technol.*, 40 (14), pp 4353-4359.

RCEP (Royal Commission on Environmental Pollution) (2008) 'Novel Materials in the Environment: The case of Nanotechnology' 27th Report

Royal Society, (2004), ‘Nanoscience and Nanotechnologies: Opportunities and Uncertainties’ http://royalsociety.org/policy/publications/2004/nanoscience-nanotechnologies/).

Russell, R. S., (1977) ‘Plant root systems: their function and interaction with the soil’ McGraw-Hill Book Company (Maidenhead, UK) ISBN 0070840687

Sadiq, I. M., Chowdhury, B., Chandrasekaran, N., Mukherjee, A., (2009) ‘Antimicrobial sensitivity of E. coli to alumina nanoparticles’ *Nanomedicine* 5 (3) pp 282-286

Sauve, S., Hendershot, W., and Allen, H. E., (2000) ‘Solid-solution partitioning of metals in contaminated soils: dependence on pH total metal burden and organic matter’ environmental science and technology, 34 (7) pp 1125-1131

Sawai, J., (2003) ‘Quantitative evaluation of antibacterial activities of metallic oxide powders (ZnO, MgO and CaO) by conductimetric assay’ *Journal of microbiological methods* 54 (2) pp 177-182

Schulze, C., Kroll, A, Lehr, C-M., Schafer, U. F., Becker, K., Schnekenburger, J., Isfort, C. S., Landsiedel, R., and Wohlleben, W., (2008) ‘Not ready to use – overcoming pitfalls when dispersing nanoparticles in physiological media’ *Nanotoxicology* 2 (2) pp 51-61

Shaw, D.J. (1992) Introduction to Colloid And Surface Chemistry, Butterworth Heinemann, UK

Shi, J., Abid, A. D., Kennedy, I. M., Hristova, K. R., and Silk, W. K., (2011) ‘To duckweeds (landoltia punctata) nanoparticulate copper oxide is more inhibitory than the soluble copper in the bulk solution’ *Environmental pollution* 159 pp 1277-1282

Singer, A. C., Bell, T., Heywood, C. A., Smith, J. A. C., Thompson, I. P., (2007) ‘Phytoremediation of mixed-contaminated soil using the hyperaccumulator plant *Alyssum lesbiacum:* Evidence of histidine as a measure of phytoextractable nickel’ *Environmental Pollution* 177 (1) pp 74-82

Singer, V. L., Lawlor, T. E., Yue, S., (1999) ‘Comparison of SYBR Green I Nucleic acid gel stain mutagenicity and ethidium bromide mutagenicity in the salmonella/mammalian microsome reverse mutation assay (Ames test) *Mutation Research* 439 (1) pp 37 – 47

Skebo, J. E., Grabinski, C. M., Schrand, A. M., Schlager, J. J., and Hussain, S. M. (2007) 'Assessment of Metal Nanoparticle Agglomeration, Uptake, and Interaction using High Illuminating System' *International Journal of Toxicology* 26, 2 pp 135-141

Smart, L. E., and Moore, E. A., (2005). *State Chemistry: An Introduction* pp 165–171.

Smirnoff, N., (1993). "The role of active oxygen in the response of plants to water deficit and desiccation". Tansley Review No. 52, *Plant Phytology* 125.

Smith, J. L., Burritt, D. J., and Bannister, P. (2000) ‘Shoot Dry Weight, Chlorophyll and UV-B-absorbing Compounds as Indicators of a Plant's Sensitivity to UV-B Radiation’. *Annals of Botany* 86: 1057±1063

Smith, S. E., and Read, D. J., (1996) ‘Mycorrhizal symbiosis’ Academic Press 2nd Ed. ISBN 0080537197

Song, Y., Li, G., Thornton, S. F., Thompson, I. P., Banwart, S. A., Lerner, D. N., and Huang, W., (2009) ‘Optimization of bacterial whole cell bioreporters for toxicity assay of encironmental samples’ Environmental Science and Technology, 43 (20) pp 7931-7938

Song, W., Zhang, J., Guo, J., Zhang, J., Ding, F., Li, L., Sun, Z., (2010) ‘Role of the dissolved zinc ion and reactive oxygen species in cytotoxicity of ZnO nanoparticles’ *Toxicology Letters* 199 pp 389-397

Stampoulis, D., Sinha, S. K., and White, J. C., (2009) ‘Assay-dependent phytotoxicity of nanoparticles to plants’ *Environmental Science and Technology* 43 (24) pp 9473-9479

Stuart, E. J., Madden, R., Paul, G., Taddei, F., (2005) ‘Aging and death in an organism that reproduces by morphologically symmetric division’ *PLoS biology* 3 (2) e45 pp 295-300

Stolpe, B., and Hesselov, M., (2007) ‘Changes in size distribution of fresh water nanoscale colloidal matter and associated elements on mixing in seawater, *Geochimica et Cosmochimica Acta*, 71 pp 3292-3301

Sunkar, R., Kapoor, A., and Zhu, J-K., (2006) 'Posttranscriptional induction of two Cu/Zn superoxide dismutase genes in Arabidopsis is mediated by downregulation of miR398 and Important for Oxidative stress tolerance' *The Plant cell*, 18 pp 2051-2065

Sutton, S., (2011) ‘Measurement of Microbial Cells by Optical Density’ Microbiology Topics; *Journal of Validation Technology* pp 46-49

Taurozzi, J. S. and Hackley, V. A., (2012) ‘Preparation of nanoparticle dispersions from powdered material using ultrasonic disruption’ US Dept. of Commerce, NIST Special Publication pp 1200-2

Taylor, L. L., Leake, J. R., Quirk, J., Hardy, K., Banwart, S. A. and Beerling, D. J., (2009) ‘Biological weathering and the long-term carbon cycle: integrating mycorrhizal evolution and function into the current paradigm’, *Geobiology* 7, pp 171–191

Thill, A., Zeyons, O., Spalla, O., Chauvat, F., Rose, J., Auffan, M., Flank, A. M., (2006) ‘Cytotoxicity of CeO2 nanoparticles for Escherichia coli. Physico-chemical insight of the cytotoxicity mechanism’ *Environmental Science and Technology* 1; 40 (19) pp 6151-6156

Threes S. G., Stanislav, P. (2011) ‘Titanium dioxide and zinc oxide nanoparticles in sunscreens: focus on their safety and effectiveness’ *Nanotechnology, Science and Applications* 4, pp 95–112

Toolabi, A., and Khanhani, N., (2013) 'Evaluating the toxicity of zinc oxide nanoparticles on the dominant bacteria in the sludge of wastewater treatment facilities' *Advances in Environmental Biology* 7 (4) pp 812-816

Torney, F., Trewyn, B. G., Lin, V. S.-Y., and Wang, K., (2007) 'Mesoporous silica nanoparticles deliver DNA and chemicals into plants; *Nature Nanotechnology* 2, pp 295-300

Townley, H. E., Rapa, E., Wakefield, G., Dobson, P. J., (2011) 'Nanoparticle augmented radiation treatment decreases cancer cell proliferation' Nanomedicine: nanotechnology, biology and medicine 8 (4) pp 526-536

Turner, A., Wilson, G., & Kaube, I., (1987) 'Biosensors: fundamentals and applications' Oxford, UK: Oxford University Press (OUP)

Uibel, S., Takemura, L., Mueller, D., Quarcoo, D., Klingelhoefer, D., and Groneberg, D. A., (2012) 'Nanoparticles and cars - analysis of potential sources' *Journal of Occupational Medicine and Toxicology* 7 (13)

Uren, N. C., (2000) 'Types, amounts and possible functions of compounds released into the rhizosphere by soil-grown plants' In the Rhizosphere: Biochemistry and organic substances at the soil plant interface pp 19-40

Vieira, F. C. S., and Nahas, E., (2005) 'Comparison of microbial numbers in soils by using various culture media and temperatures' *Microbiological research* 160 (2) pp 197-202

Visiola, G., Conti, F. D., Gardi, C., and Menta, C., (2014) 'Germination and root elongation bioassays in siz different plant species for testing Ni contamination in soil' *Bulletin of Environmental Contamination and Toxicology* 92 (4) pp 490-496

Walker, T. S., Bais, H. P., Grotewold, E., and Vivanco, J. M., (2003) 'Root exudation and Rhizosphere Biology' *Plant Physiology*, 132, 1 pp 44-51

Wang, C., Liu, L-L., Zhang, A-T., Xie, P., Lu, J-J., and Zou, X-T., (2012) 'Antibacterial effects of zinc oxide nanoparticles on *Escherichia coli* K88' *African Journal of Biotechnology* 11 (44) pp 10248-10254

Warheit, D. B., (2008) 'How Meaningful are the Results of Nanotoxicity Studies in the Absence of Adequate Material Characterization?' *Toxicological Sciences* 101(2) pp 183-185

Wasternack, C., and Hause, B., (2013). 'Jasmonates: biosynthesis, perception, signal transduction and action in plant stress response, growth and development' *Annals of Botany* 111 pp 1021-1058

Welz, B., Becker-Ross, H., Florek, S., Heitmann, U., (2005) 'High resolution continuum source AAS, Wiley-VCH, Weinheim, Germany ISBN 3527307362

Welz, B., and Sperling, (1999) 'Atomic Absorption Spectrometry, Wiley-VCH Weinheim, Germany ISBN 3527285717

Wiseman, H., and Halliwell, (1996) ‘Damage to DNA by reactive oxygen and nitrogen species: role in inflammatory disease and progression to cancer’ *Biochemistry Journal* 313 pp 17-29

Whitman, B., Coleman, D., Wiebe, W. J., (1998) ‘Prokaryotes: the unseen majority’ Perspective - *Proceedings of the National Academy of Science, USA* 95 pp 6578-6583

Wilkinson, K. J. & Lead, J. R., (2007) Environmental Colloids and Particles; Behaviour, Separation and Characterisation. Vol. 10. IUPAC, John Wiley & Sons ltd, UK,

Xiong, D., Fang, T., Yu, L., Sima, and X., Zhu, W., (2011) ‘Effects of nano-scale TiO_2, ZnO and their bulk counterparts on zebrafish: Acute toxicity, oxidative stress and oxidative damage’ *Science of The Total Environment* 409, 8 pp 1444–1452

Xu, J., Futakuchi, M., Alexander, D. B., Fukamachi, K., Numano, T., Suzui, M., Tsuda, H. (2014). ‘Nanosized zinc oxide particles do not promote DHPN-induced lung carcinogenesis but cause reversible epithelial hyperplasia of terminal bronchioles’, *Archives of Toxicology*, *88*(1), pp 65–75.

Yamamoto, O., (2001) ‘Influence of particle size on the antibacterial activity of zinc oxide’ *International journal of inorganic materials* 3 (7) pp 643-646

Yang, L., and Watts, D. J., (2005) ‘Particle surface characteristics may play an important role in phytotoxicity of alumina nanoparticles’ *Toxicology letters* 158 (2) pp 122-132

Yang, Z., and Xie, C. (2006) ‘Zn2+ release from zinc and zinc oxide particles in simulated uterine solution’ *Colloids and Surfaces B: Biointerfaces*, 47, 2 pp 140-145

Yu, L., Chen, W., & Mulchandani, A., (2006) ‘Review: Microbial biosensors’ *Analytica Chimica Acta*, 568 pp 200-210

Yu, Y., Xin, H., Hovden, R., Wang, D., Rus, E., Mundy, J., Muller, D., and Abruna, H., (2012) ‘Three-dimensional tracking and visualisation of hundreds of Pt-Co fuel cell nanocatalysts during electrochemical aging’ *Nano Letters* 12 (9) pp 4417-4423

Zang, W-X., and Karn, B. (2005) 'Nanoscale Environmental Science and Technology: Challenges and Opportunities' *Environmental Science & Technology*, 39 (5) pp 94A-95A

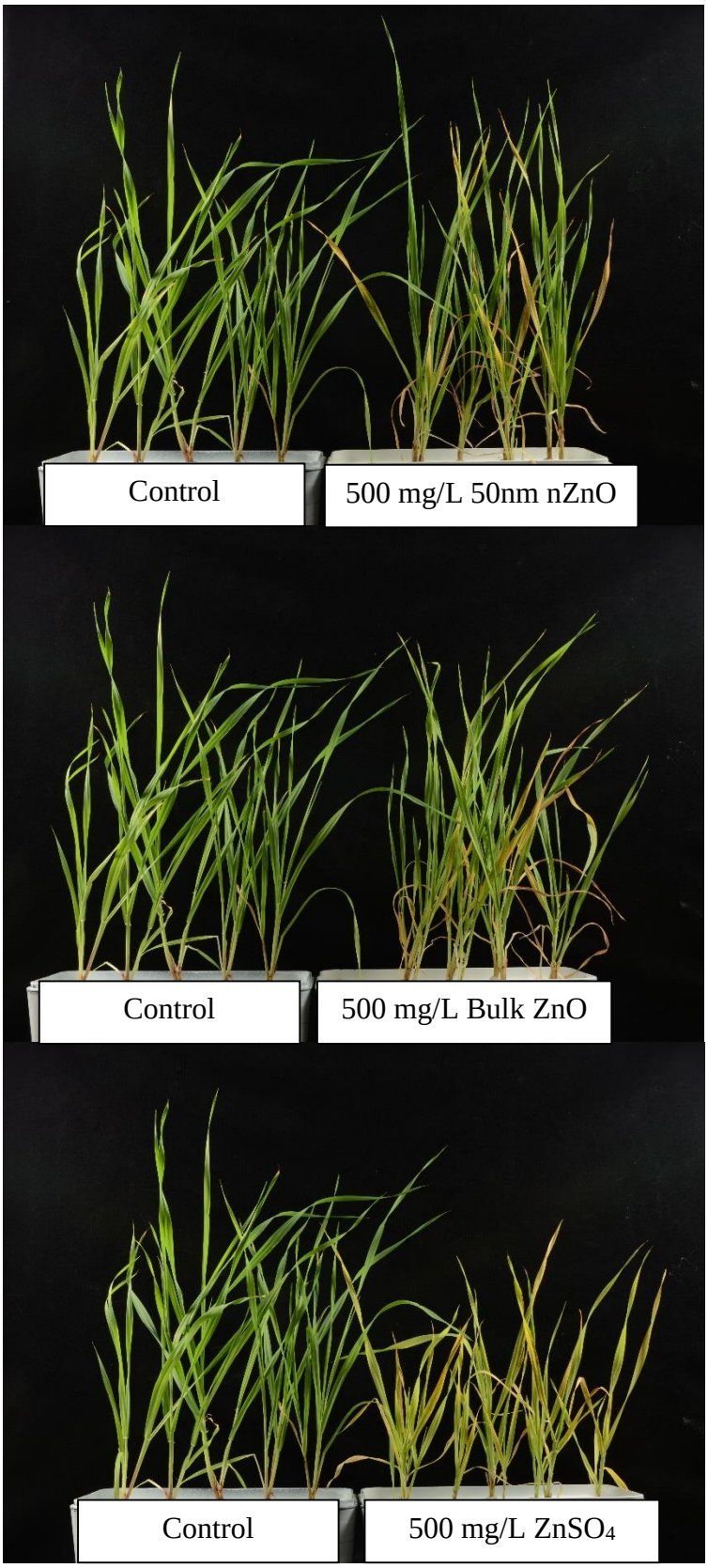
Zhang, F., & Keasling, J., (2011) ‘Biosensors and their applications in microbial metabolic engineering’ *Trends in Microbiology, 19* (7), pp 323-329.

Zhang, Q., Leoo, J., Yang, J., Boothroyd, C., and Zhang, J., (2007) ‘Size and composition tunable Ag-Au nanoparticles by replacement reactions’ *Nanotechnology* 18 pp 1-8

Zhu, H., Han, J., Xiao, J. Q., and Jin, Y., (2008) ‘Uptake, translocation and accumulation of manufactured iron oxide nanoparticles by pumpkin plants’ *Journal of environmental monitoring*, 10, 6 pp 685-784

SUPPLEMENTARY INFORMATION

S1: Photographs of 27 day old barley plants after 7 days treatment at the highest concentration, 500 mg/L, with 50nm nZnO, bulk-sized ZnO and $ZnSO_4$



S2: **Photographs of MicroTom tomato plants after growth for A) 5 weeks; B) 6 weeks and 3 days; and C) 18 weeks, in the presence of 100 mg/L bulk and 50nm zinc oxide particles.**



S3: **Photographs of 27 day old barley plants after 7 days treatment at the highest concentration, 500 mg/L, with Old and New 50nm nZnO particles.**

